



Max-Planck-Institut für Metallforschung
Stuttgart

Experimental and Computational Phase Studies of the ZrO₂-based Systems for Thermal Barrier Coatings

Chong Wang

Dissertation
an der
Universität Stuttgart

Bericht Nr. 189
September 2006

Experimental and Computational Phase Studies of the ZrO₂- based Systems for Thermal Barrier Coatings

Dissertation

Von der Fakultät Chemie der Universität Stuttgart

zur Erlangung der Würde eines

Doktors der Naturwissenschaften (Dr. rer. nat.)

genehmigte Abhandlung

Vorgelegt von

Chong Wang

Aus Jingmen, Hubei, China

Hauptberichter : Prof. Dr. rer. nat. Fritz Aldinger

Mitberichter : Prof. Dr. rer. nat. Dr. hc. mult. Günter Petzow

Mitpruefer und Prüfungsvorsitzender : Prof. Dr. Eric. J. Mittemeijer

Tag der mündlichen Prüfung : 19.09.2006

Institut für Nichtmetallische Anorganische Materialien der Universität Stuttgart

Max-Planck-Institut für Metallforschung, Stuttgart

Pulvermetallurgisches Laboratorium / Abteilung Aldinger

Stuttgart 2006

Acknowledgements

I owe my current research to many contributors' help and suggestion. Without their patience and intelligence, I undoubtedly cannot present this thesis.

First of all, my sincere gratitude should go first and foremost to my supervisor, Prof. Dr. F. Aldinger, who has been giving me the most decisive and effective support and encouragement. His valuable instructions and constructive suggestions have always inspired me to carry on this study, so that I can finish my PhD thesis smoothly. He always brings people comfortable feeling during talking and discussion. I really learned a lot from him not only on the attitude of academic research, but also on the art of making good relationship with people.

Deeply sincere gratitude is also delivered to my good group leader, Dr. M. Zinkevich, who gave me great contribution on the research work from very beginning. Without his guidance on both experimental work and computations in my thesis, I could not grow into an experienced person in my research field. Importantly, I learned from him on how to independently organize my research work.

The financial support from the program of international research collaboration between Europe Commission (GRD2-200-30211) and the National Science Foundation (DMR-0099695), and the Max-Planck-Society are greatly acknowledged.

I am much obliged to Prof. Dr. G. Petzow and Prof. Dr. E. J. Mittemeijer for agreeing to be the co-examiners of my PhD examination.

My endless thanks would be presented to all those individuals who have assisted in the development of my present research. Among them special thanks go to Prof. Zhanpeng Jin in Central South University who is and will still be the most important person in my academic career. His active spirits in both life and scientific research always promote me to go ahead. All of his students make up of a large family, in which we always help each other without any hesitation. Especially, I am very grateful to Prof. Yong Du for his recommendation for my PhD position, and his diligence is really impressive to me. At the same time, I would like to acknowledge Dr. Xiaogang Lu for his help during my application of this position.

It is my great pleasure to have extensive discussions with Dr. O. Fabrichnaya, and really benefit much and appreciate for her help on my work. Dr. B. Wu makes the opportunity for us to talk thermodynamics in Chinese, and I am happy to learn the knowledge of ab initio calculation from him. The other students in our group: N. Solak, V. Manga Rao, S. Geupel, M. Cancarevic and D. Djurovic also gave me much help, and made lots of discussions with me.

I would like to extend my great appreciation to Prof C. G. Levi who helped me much and gave me suggestion on the work of my thesis in University of California at Santa Barbara from Jan. to Mar. in 2004. It was also my pleasure to get known his postdocs and PhD students N. R. Rebollo Franco, A. S. Gandhi, R. Leckie et al. I thank them for their great help.

Ms. Klink and Ms. Paulsen are appreciated for their great help on both my life and study since I was in Stuttgart. I thank those technicians for their important technical assistance on my experiments: Mr. Labizke and Ms. Predel for SEM, Ms. Haug for EPMA, Ms. Thomas for XRD, Ms. Shafer for ceramography, Mr. Kumer for DTA, Mr. Mager, Mr. Kaiser, Mr. Meyer, Mr. Werner for ICP–OES analysis, Mr. Schweizer, Ms. Hofer for Pt crucible and many other people who are not mentioned here. Dr. F. M. Morales in Prof. M. Ruhle department is also appreciated for his TEM analysis. Thank Dr. N. Dupin for sending her thesis so that I could write program to solve the equations for order-disorder modeling.

I enjoyed my office time with Shijun Jia, Ravi Kumar, S. H. Lee, Y. Qiu and S. F. Du in past several years. Furthermore, I owe much gratitude to some Chinese who brought me much happiness in Stuttgart: Longjie Zhou and his wife, Hong Peng and her husband, Jianyun Shuai, Pengxiang Qian, Youping Huang, Hanlin Li, and some other Chinese who played table tennis with me. The memory from those people will stay forever in my life. I am also pleased to know Prof. Hui Gu and Prof. Wenqing Zhang in Shanghai Ceramic Institute, and grateful to them for interesting discussions and nice care when I was in Shanghai.

A special word of gratitude also should be said to aunt Deng and uncle Wang who have been taking care of me since I was in Changsha.

Last but not the least, my parents, my sister and her boyfriend always gave me great encouragement and understanding in past years. I would like to dedicate this thesis to my family and share my happiness with them at this moment.

Chong Wang, June-2006, Stuttgart

Table of Contents

Acknowledgements	1
Abstract	1
1. Introduction	4
1.1. TBC for high temperature gas turbine engines	4
1.2. Phase transformations in ZrO ₂ -based systems and their implications on TBC	5
1.2.1. Phase transformation phenomena in doped zirconia	5
1.2.2. Implications on TBC	7
1.3. Scope of the present work	7
2. Experimental procedures and thermodynamic modeling	9
2.1. Sample preparation	9
2.2. Sample treatment and characterization	9
2.3. Thermodynamic modelling of phases	10
2.3.1. Introduction	10
2.3.1.1. The CALPHAD approach	10
2.3.1.2. Pure elements	12
2.3.1.3. Thermodynamic models for the solution phases	12
2.3.2. Pure components	17
2.3.3. The gas phase	17
2.3.4. The liquid phase	17
2.3.4.1. The Hf – Zr – O system	17
2.3.4.2. The ZrO ₂ – REO _{1.5} systems	17
2.3.5. The <i>bcc</i> and <i>hcp</i> phase	18
2.3.6. The ZrO ₂ (HfO ₂)-based solid solution phases	19
2.3.6.1. The Hf – Zr – O system	19
2.3.6.2. The ZrO ₂ – REO _{1.5} systems	20
2.3.7. The RE ₂ O ₃ -based phases	21
2.3.8. The pyrochlore phase	23
2.3.8.1. The model (Zr ⁺⁴ , RE ⁺³) ₂ (RE ⁺³ , Zr ⁺⁴) ₂ (O ⁻² , Va) ₆ (O ⁻²) ₁ (Va, O ⁻²) ₁	25
2.3.8.2. The splitting model (Zr ⁺⁴ , RE ⁺³) ₂ (RE ⁺³ , Zr ⁺⁴) ₂ (O ⁻² , Va) ₈	30
2.3.9. The RE ₄ Zr ₃ O ₁₂ (δ) phase	32

3. Experimental study and thermodynamic modeling of the Zr – O, Hf – O and ZrO₂ – HfO₂ systems -----	35
3.1. Literature review -----	35
3.1.1. The Zr – O system-----	35
3.1.2. The Hf – O system -----	38
3.1.3. The ZrO ₂ – HfO ₂ system -----	40
3.2. Experimental results and discussion-----	41
3.3. Thermodynamic assessments and calculations-----	44
3.3.1. Pure zirconia -----	44
3.3.2. The Zr – O system-----	46
3.3.3. Pure hafnia -----	50
3.3.4. The Hf – O system -----	52
3.3.5. The ZrO ₂ – HfO ₂ system -----	55
4. Experimental study and thermodynamic modeling of the ZrO₂ – LaO_{1.5} system -----	62
4.1. Literature review -----	62
4.1.1. Phase equilibria -----	62
4.1.2. Thermodynamic data-----	64
4.2. Experimental results and discussion-----	65
4.3. Selected experimental data for optimization -----	66
4.3.1. Phase diagram data -----	66
4.3.2. Thermodynamic data-----	67
4.4. Optimization procedure -----	67
4.5. Calculated results and discussion -----	68
5. Experimental study and thermodynamic modeling of the ZrO₂ – NdO_{1.5} system -----	73
5.1. Literature review -----	73
5.1.1. Phase equilibria -----	73
5.1.2. Thermodynamic data-----	74
5.2. Experimental results and discussion-----	75
5.2.1. The as-pyrolysed state -----	75
5.2.2. The tetragonal + fluorite phase equilibrium-----	76
5.2.3. The fluorite + pyrochlore phase equilibrium-----	76
5.2.4. The fluorite + A-Nd ₂ O ₃ and pyrochlore + A-Nd ₂ O ₃ phase equilibria -----	78

5.3. Selected experimental data for optimization -----	79
5.4. Optimization procedure -----	79
5.5. Calculated results and discussion -----	79
6. Experimental study and thermodynamic modeling of the ZrO₂ – SmO_{1.5} system -----	84
6.1. Literature review -----	84
6.1.1. Phase equilibria -----	84
6.1.2. Thermodynamic data -----	85
6.2. Experimental results and discussion -----	85
6.2.1. The as-pyrolysed state -----	85
6.2.2. The tetragonal + fluorite phase equilibrium -----	86
6.2.3. The fluorite + pyrochlore phase equilibrium -----	86
6.2.4. The fluorite + B-Sm ₂ O ₃ phase equilibrium -----	88
6.3. Selected experimental data for optimization -----	89
6.4. Optimization procedure -----	89
6.5. Calculated results and discussion -----	90
7. Experimental study and thermodynamic modeling of the ZrO₂ – GdO_{1.5} system -----	94
7.1. Literature review -----	94
7.1.1. Phase equilibria -----	94
7.1.2. Thermodynamic data -----	96
7.2. Experimental results and discussion -----	96
7.2.1. The as-pyrolysed state -----	96
7.2.2. The fluorite / pyrochlore phase transition -----	96
7.2.3. The fluorite + C-Gd ₂ O ₃ and C-Gd ₂ O ₃ + B-Gd ₂ O ₃ phase equilibria -----	102
7.2.4. The martensitic transformation temperatures of the tetragonal phase -----	103
7.3. Selected experimental data for optimization -----	103
7.3.1. Phase diagram data -----	103
7.3.2. Thermodynamic data -----	104
7.4. Optimization procedure -----	104
7.5. Calculated results and discussion -----	104
7.5.1. The phase diagram without pyrochlore ordering -----	104
7.5.2. Calculated results by the pyrochlore model (Zr ⁺⁴ ,Gd ⁺³) ₂ (Gd ⁺³ ,Zr ⁺⁴) ₂ (O ⁻² ,Va) ₆ (O ⁻²) ₁ (Va,O ⁻²) ₁ -----	106

7.5.3. Calculated results by the pyrochlore model $(\text{Zr}^{+4}, \text{Gd}^{+3})_2(\text{Gd}^{+3}, \text{Zr}^{+4})_2(\text{O}^{-2}, \text{Va})_8$ -----	107
7.5.4. Thermodynamic properties-----	110
8. Experimental study and thermodynamic modeling of the $\text{ZrO}_2 - \text{DyO}_{1.5}$ system-----	114
8.1. Literature review -----	114
8.2. Experimental results and discussion-----	115
8.2.1. The as-pyrolysed state -----	115
8.2.2. The tetragonal + fluorite phase equilibrium-----	115
8.2.3. The martensitic transformation temperatures of the tetragonal phase -----	116
8.2.4. The fluorite + C- Dy_2O_3 phase equilibrium-----	117
8.3. Selected experimental data for optimization -----	118
8.4. Optimization procedure -----	118
8.5. Calculated results and discussion -----	118
9. Experimental study and thermodynamic modeling of the $\text{ZrO}_2 - \text{YbO}_{1.5}$ system -----	123
9.1. Literature review -----	123
9.2. Experimental results and discussion-----	124
9.2.1. The as-pyrolysed state -----	124
9.2.2. The tetragonal + fluorite phase equilibrium-----	125
9.2.3. The phase equilibria involving δ and C- Yb_2O_3 -----	126
9.3. Selected experimental data for optimization -----	127
9.4. Optimization procedure -----	128
9.5. Calculated results and discussion -----	128
10. Experimental study and calculation of the $\text{ZrO}_2 - \text{GdO}_{1.5} - \text{YO}_{1.5}$ system -----	133
10.1. Calculations and experimental results -----	133
10.2. Discussion -----	135
11. Characteristic changes in the $\text{ZrO}_2 - \text{REO}_{1.5}$ systems-----	136
11.1. The evolutions of the phase relations in the $\text{ZrO}_2 - \text{REO}_{1.5}$ systems -----	136
11.2. The evolutions of the thermodynamic properties in the $\text{ZrO}_2 - \text{REO}_{1.5}$ systems-----	139
11.3. The mechanism of the pyrochlore ordering -----	141
Zusammenfassung -----	144

Appendix: The thermodynamic parameters obtained in this work -----	147
References -----	154
Curriculum Vitae -----	170

List of symbols and abbreviations:

TBC: Thermal Barrier Coatings

XRD: X-ray diffraction

HTXRD: high-temperature X-ray diffraction

SEM: Scanning electron microscopy

EDX: Energy dispersive X-ray

TEM: Transmission electron microscopy

DTA: Differential thermal analysis

DSC: Differential scanning calorimetry

ND: Neutron diffraction

RS: Raman scattering

M: Monoclinic

T: Tetragonal

F: Fluorite

A: A-type RE₂O₃

B: B-type RE₂O₃

C: C-type RE₂O₃

H: H-type RE₂O₃

X: X-type RE₂O₃

L: Liquid

P: Pyrochlore

δ: RE₄Zr₃O₁₂

Abstract

The ZrO₂-based materials are practically important as the thermal barrier coatings (TBC) for high temperature gas turbines, due to their low thermal conductivity, high temperature thermal stability and excellent interfacial compatibility. Studies of the phase equilibria, phase transformation, and thermodynamics of the ZrO₂-based systems can provide the necessary basic knowledge to develop the next generation TBC materials.

In the thesis, the systems ZrO₂ – HfO₂, ZrO₂ – LaO_{1.5}, ZrO₂ – NdO_{1.5}, ZrO₂ – SmO_{1.5}, ZrO₂ – GdO_{1.5}, ZrO₂ – DyO_{1.5}, ZrO₂ – YbO_{1.5} and ZrO₂ – GdO_{1.5} – YO_{1.5} were experimentally studied. The samples were prepared by the chemical co-precipitation method, with aqueous solutions Zr(CH₃COO)₄, HfO(NO₃)₂, and RE(NO₃)₃·xH₂O (RE=La, Nd, Sm, Gd, Dy, Yb) as starting materials. Various experimental techniques, X-ray diffraction (XRD), scanning electron microscopy (SEM), electron probe microanalysis (EPMA), transmission electron microscopy (TEM), differential thermal analysis (DTA), and high temperature calorimetry were employed to study the phase transformation, phase equilibria between 1400 and 1700°C, heat content and heat capacity of the materials. A lot of contradictions in the literature were resolved and the phase diagrams were reconstructed.

Firstly, the thermodynamic transformation temperatures (T_0 , where the Gibbs energies of monoclinic and tetragonal phases are identical) were reviewed and extrapolated for pure ZrO₂ (1367 ± 5 K) and HfO₂ (2052 ± 5 K) from the DTA study of ZrO₂ – HfO₂ system. The temperatures (A_s , A_f , M_s , M_f) on the martensitic transformation of the materials in ZrO₂ – HfO₂ system directly obtained by DTA measurements show well consistent behavior together with the calculated T_0 temperatures. Based on the present DTA results and literature information on transformation temperatures of monoclinic ↔ tetragonal, tetragonal ↔ cubic and cubic ↔ liquid, as well as the thermodynamics of different structures, the thermodynamic parameters of the pure ZrO₂ and HfO₂ were assessed, and the ZrO₂ – HfO₂ phase diagram was calculated without any fitting parameter.

Within the scope of the thesis, the tetragonal + fluorite (or the tetragonal + pyrochlore for RE=La) two-phase region, the phase equilibria between disordered fluorite and ordered pyrochlore (or the δ phase for RE=Yb), and the phase equilibria between fluorite and REO_{1.5} terminal solutions were well established for ZrO₂ – REO_{1.5} (RE=La, Nd, Sm, Gd, Dy, Yb) systems, and the enthalpy increments of the materials with 30 mol% REO_{1.5}, and 50 mol% REO_{1.5} (57.14 mol% for RE=Yb) were determined in the temperature range 200-1400°C.

Furthermore, the isothermal sections of $\text{ZrO}_2 - \text{GdO}_{1.5} - \text{YO}_{1.5}$ system at 1200-1600°C were experimentally investigated by XRD measurements.

Based on the experimental data obtained in this work and literature, the systems $\text{Zr} - \text{O}$, $\text{Hf} - \text{O}$, $\text{ZrO}_2 - \text{REO}_{1.5}$ ($\text{RE}=\text{La, Nd, Sm, Gd, Dy, Yb}$) were thermodynamically optimized using the CALPHAD (CALculation of PHase Diagram) approach. Most of the experimental data were well reproduced, and the self-consistent thermodynamic parameters were derived for all the systems. Since the experimental isothermal sections on the $\text{ZrO}_2 - \text{GdO}_{1.5} - \text{YO}_{1.5}$ system could be reproduced well only by the extrapolation from binary systems, no any further optimization was done.

Finally, based on the present experiments and calculations, some clear characteristic evolutions with the change of the ionic radius of doping element RE^{+3} can be concluded and applied also for those $\text{ZrO}_2 - \text{REO}_{1.5}$ systems which are not studied in this work:

1). The solubility of $\text{REO}_{1.5}$ in the tetragonal phase increases almost linearly with decreasing the radius of RE^{+3} . At the same time, the homogeneity range of fluorite phase enlarges towards ZrO_2 . Those changes result in a narrower tetragonal + fluorite two-phase region for the $\text{ZrO}_2 - \text{REO}_{1.5}$ system with smaller RE^{+3} .

2). It is confirmed that the pyrochlore structure is only stable when the ionic radius of RE^{+3} is larger than that of Dy^{+3} . The homogeneity range of the pyrochlore phase gradually increases from $\text{RE}=\text{La}$ to Gd , while the fluorite \leftrightarrow pyrochlore transformation temperature decreases. There is no any detectable ordered compound in the system $\text{ZrO}_2 - \text{DyO}_{1.5}$. For the $\text{ZrO}_2 - \text{YbO}_{1.5}$ system, the ordered structure of fluorite is δ ($\text{RE}_4\text{Zr}_3\text{O}_{12}$) phase. It is reasonable to deduce that the δ phase is only stable when the ionic radius of RE^{+3} is smaller than that of Dy^{+3} , and the $\delta \leftrightarrow$ fluorite transformation temperature increases with reducing the ionic radius of RE^{+3} .

3). The enthalpy of formation of the fluorite phase has more negative value for the system with smaller RE^{+3} , while that of the ordered pyrochlore phase presents the opposite tendency. Those evolutions result in the smaller energetic differences between fluorite and pyrochlore for the system with smaller RE^{+3} , and thus the narrower fluorite + pyrochlore two-phase region.

4). The complete ordering of the pyrochlore phase with ZrO_2 excess may take very long time, especially for the systems with smaller RE^{+3} , while the ordering of pyrochlore with $\text{REO}_{1.5}$ excess is much more easily approached, because less oxygen atoms take part in the

process. The XRD results show that the samples in ZrO₂-rich region of the ZrO₂ – NdO_{1.5} system distinctly separate into fluorite + pyrochlore two-phase structure after the heat treatment of 1700°C for 36h, while samples heat treated at lower temperatures do not. No any separation of the XRD peaks of fluorite and pyrochlore was found for the samples with ZrO₂ excess in the ZrO₂ – SmO_{1.5} and ZrO₂ – GdO_{1.5} systems. Those observations reveal that the fluorite ⇌ pyrochlore phase transformation in materials with ZrO₂ excess is a long kinetic process, and may be initially of second-order, and then of first order only when a critical configurational state of the ordered structure is reached to offer enough driving force for the long distance diffusion.

Chapter 1

Introduction

1.1. TBC for high temperature gas turbine engines

Nowadays, the development of the novel Thermal Barrier Coatings (TBC) for the new generation high temperature gas turbine engines is increasingly promoted. The crucial ZrO₂-based TBC or “top coat” plays an important role for improving the performance and lifetime of gas turbine engines, by creating a large temperature gradient (100-300°C) from the surface of the layer of the TBC to the coated alloy components. Such benefit allows increasing the hot gas temperature around the engines, and improving the efficiency, without change of the Ni-based superalloy components. On the one hand, modern turbine engines can be operated at temperatures above the melting point (~1300°C) of the superalloys with the protection of the TBC. On the other hand, TBC can lower the temperature on the superalloy surface, to improve the durability and performance of the engines [2002Pad].

A thermal barrier system generally consists of four different layers as shown in Fig. 1-1. The TBC is the top layer of the system, and directly contacts with the high temperature hot gas stream. The most widely adopted material for TBC is the yttria-stabilized zirconia (YSZ, ~8 mol % YO_{1.5}), which is manufactured by air-plasma spraying (APS) or electron-beam physical vapour deposition (EB-PVD) technology. To prevent the oxidation of the alloy components, a thin layer of dense thermally grown oxide (TGO) is very critical between TBC and alloys. Generally, the main component of the TGO is Al₂O₃. To produce this TGO and modify the surface between TBC and the superalloy, a “bond coat” is essential for the thermal barrier system. The single β -(Ni, Pt)Al (B2) phase and overlay two phase (γ' + β/γ) MCrAlY alloys are the two groups of bond coat materials which are practically used [2004Lev]. The superalloy is generally the Ni-based alloy.

Worldwide, a lot of efforts have been put into the development of alternative ceramics for TBC other than state-of-the-art YSZ (yttria-stabilized zirconia), aiming to lower thermal conductivity and/or to improve high temperature performance and durability [2004Lev], so that larger temperature gradients can be established through the TBC without excessive augmentation of its thickness. Co-doping of YSZ by rare earths such as Gd is of interest in thermal barrier systems because of concomitant benefits to the thermal insulating efficiency [2002Nic, 2003Zhu]. Some rare earth zirconates have been proposed to reduce the thermal conductivity of TBC by as much as 30% of current levels without the change of the thermal stability [2000Vas, 2002Wu]. At the same time, the TBC/Al₂O₃ (TGO) interface can maintain

good thermochemical compatibility and stability at high temperatures without losing the reliability of TBC. Especially, the pyrochlore phases in some ZrO_2 -based systems containing rare earth oxides are paid much more attention in recent years because they combine lower thermal conductivity with enhanced microstructural stability upon high temperature exposure [2001Mal, 2002Wu, 2004Lev, 2005Lec].

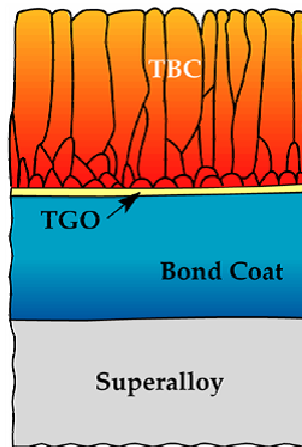


Figure 1-1. The schematic of the thermal barrier system (with the permission from C. G. Levi at University of California, Santa Barbara).

1.2. Phase transformations in ZrO_2 -based systems and their implications on TBC

1.2.1. Phase transformation phenomena in doped zirconia

It is well known that the phase transformation behaviour in doped ZrO_2 presents large complexity. There are three structural modifications for the pure ZrO_2 at ambient pressure [1986Abr]: the cubic structure with the fluorite type ($Fm\bar{3}m$) at high temperatures, the tetragonal structure ($P4_2/nmc$) at intermediate temperatures, and the monoclinic structure ($P2_1/c$) at low temperatures. Many experimental studies confirmed that the monoclinic \leftrightarrow tetragonal phase transformation is of displacive martensitic type [1974Sub]. The transformation between cubic and tetragonal phases may be not the regular first order transition [1991Hil].

The solubility of rare earths in the monoclinic ZrO_2 phase is negligible, while the tetragonal phase can dissolve considerable amounts of rare earth elements depending on the radius of cations. The tetragonal ZrO_2 phase cannot be stabilized to low temperature due to the diffusionless martensitic transformation. Since about 8% volume change is associated with this transformation, cracks can form at the grain boundaries, what is detrimental to the materials.

The tetragonal \leftrightarrow monoclinic athermal phase transformation occurs martensitically with a temperature hysteresis loop near 1373 K [1995And] for pure ZrO_2 . The hysteresis loop extends about 200 K for ZrO_2 . Generally, the transformation temperatures on heating and cooling are referred as A_s (starting) and A_f (finishing), and as M_s (starting) and M_f (finishing). For thermodynamic studies, the transformation temperature T_0 (where the Gibbs energies of monoclinic and tetragonal phases are identical) is undoubtedly important. Due to the experimental difficulty in the direct measurement of the T_0 temperature, it is customary to calculate it empirically by the equation [1995Yas]

$$T_0 = \frac{A_s + M_s}{2} \quad (1-1)$$

or

$$T_0 = \frac{A_f + M_f}{2} \quad (1-2)$$

In the literature [1995Yas] it was already confirmed that the results obtained by these two equations are quite similar. However, mostly equation (1-1) is preferred, because A_s and M_s can be determined more precisely from the results of DTA or dilatometry methods than A_f and M_f .

The high temperature cubic fluorite-type structure can be stabilized to lower temperatures by doping with certain amounts of rare earth elements, so that the destructive tetragonal \leftrightarrow monoclinic transition can be avoided. Nevertheless, in some composition range, even the cubic phase is not quenchable due to a diffusionless transformation from cubic to another kind of tetragonal phase T' [1992She, 1996Yas]. Such diffusionless transformation occurs near the stable cubic + tetragonal two-phase region, within a certain temperature hysteresis during heating and cooling as the martensitic tetragonal \leftrightarrow monoclinic transformation. Unlike the equilibrium tetragonal phase, the T' phase is kinetically non-transformable into the equilibrium phase assemblage at low temperatures due to its smaller axis ratio c/a than that of equilibrium tetragonal phase, although it is thermodynamically metastable.

Another tetragonal phase T'' was also found as the transformation product of the cubic phase, where the axis ratio c/a is nearly 1 [1996Yas].

1.2.2. Implications on TBC

(1). Due to the destructive tetragonal-to-monoclinic phase transition, the composition of the TBC must satisfy the demand to avoid this transformation. The TBC are often partially

stabilized zirconia, i.e. the metastable supersaturated T' phase, which is the most preferred TBC material of practical interest because of its higher cyclic lives [2004Lev]. However, it can transform into the stable tetragonal and fluorite phases during the long-term thermal cycling, and thus brings the risk of failure due to the destructive martensitic transformation. To select the composition and thermal cycling temperature range (operating temperature limits), it is very important to understand the equilibrium phase diagrams, so that the formation of stable tetragonal phase can be avoided, and the appropriate operating temperature limits can be determined to prevent the destructive transformation. In recent study it was found that the 8YSZ TBC partly transforms into stable tetragonal phase at 1425°C [2005Lug]. It is reasonable to believe that the upper temperature limits are different for the materials with different compositions or doping elements according to the phase diagrams of different systems.

(2). A possible failure of thermal barrier system occurs at the TBC/TGO interface, if the TGO is not thermodynamically stable and reacts with TBC. As an example, the pyrochlore phases of some $ZrO_2 - RE_2O_3$ (RE=Rare Earth Element) systems are very promising TBC materials for their lower thermal conductivity and high temperature stability, however, they react with Al_2O_3 . The phase diagram calculations can give the answer if TBC reacts with TGO. Furthermore, the limits of doping and the temperature range in which TBC can stably coexist with TGO can be determined [2004Fab]. For example, compositions with more than ~32 mol % $GdO_{1.5}$ are not thermochemically compatible with the underlying alumina layer in the coating system [2005Lec, 2006Lak] and tend to form interphases at high temperature, with significantly active kinetics at ~1100°C and above [2005Lec]. An approach to circumvent the problem is to add an interlayer of YSZ between $Gd_2Zr_2O_7$ and the underlying alumina [2004Lev]. It is undoubted that precise phase diagrams and thermodynamic data are very helpful tools to study the interfacial stabilities in thermal barrier system.

1.3. Scope of the present work

Basic system $ZrO_2 - YO_{1.5} - AlO_{1.5}$ was already assessed by O. Fabrichnaya [2004Fab]. In order to evaluate the full potential of $ZrO_2 - REO_{1.5} - AlO_{1.5}$ (RE=Rare earth elements) and $ZrO_2 - YO_{1.5} - REO_{1.5} - AlO_{1.5}$ systems, it is the object of this work to study phase equilibria, phase transformation, and thermodynamics of some zirconia-based systems. Although there are numerous literature works on zirconia, most of them are concentrated on the materials properties. Phase equilibria or phase transformation studies mainly concern the

ZrO₂ – Y₂O₃, ZrO₂ – CeO₂, ZrO₂ – CaO, and ZrO₂ – MgO systems. As for the ZrO₂ – RE₂O₃ systems except RE=Y, only very limited phase equilibria and thermodynamic investigations are available in literature, despite the importance of such systems. Additionally, the martensitic transformation temperatures are affected by many factors such as particle size, impurities, stress and thermal history of materials, the literature data present large discrepancies, and no quantitative analysis has been done yet on how these factors can affect the transformation temperatures.

Therefore, some critical experiments had to be done in this work to offer reliable results for thermodynamic calculations. In summary, present work covers the following issues related to phase equilibria and thermodynamics of ZrO₂-based thermal barrier coating systems:

(1). Careful literature reviews on the phase transformation temperatures and thermodynamic properties of ZrO₂ and HfO₂, on the phase equilibria and thermodynamic information for the systems ZrO₂ – REO_{1.5} (RE=La, Nd, Sm, Gd, Dy, Yb).

(2). Experimental investigations on the phase relations, phase transformation, and thermodynamic properties of the ZrO₂ – HfO₂, ZrO₂ – REO_{1.5} (RE=La, Nd, Sm, Gd, Dy, Yb) and ZrO₂ – GdO_{1.5} – YO_{1.5} systems by means of XRD, SEM, EPMA, TEM, DTA, and high temperature calorimetry.

(3). Assessment of the thermodynamic parameters of pure ZrO₂ and HfO₂, and self-consistent thermodynamic modelling and calculations on Zr – O, Hf – O, ZrO₂ – REO_{1.5} (RE=La, Nd, Sm, Gd, Dy, Yb), and ZrO₂ – GdO_{1.5} – YO_{1.5} systems based on the experimental results obtained in this work and those reported in literature.

Chapter 2

Experimental procedures and thermodynamic modeling

2.1. Sample preparation

The zirconium acetate solution, $Zr(CH_3COO)_4$ (99.99 %, Sigma-Aldrich), rare earth nitrate hydrate, $RE(NO_3)_3 \cdot xH_2O$ [$Dy(NO_3)_3 \cdot 5H_2O$: 99.99 %, Alfa Aesar; $Gd(NO_3)_3 \cdot 6H_2O$: 99.99 %, Strem Chemicals; $La(NO_3)_3 \cdot 6H_2O$: 99.99 %, Alfa Aesar; $Nd(NO_3)_3 \cdot 6H_2O$: 99.9 %, Alfa Aesar; $Sm(NO_3)_3 \cdot 6H_2O$: 99.99 %, Sigma-Aldrich; $Y(NO_3)_3 \cdot 6H_2O$: 99.9 %, Alfa Aesar; $Yb(NO_3)_3 \cdot 5H_2O$: 99.9 %, Sigma-Aldrich] and the hafnium dinitrate oxide, $HfO(NO_3)_2$ (99.9%, 10% W/V aqueous solution, Alfa Aesar) were adopted as the starting chemicals. The $RE(NO_3)_3 \cdot xH_2O$ was dissolved in the water as the first step. After the determination of the oxide yield of different solutions, they were mixed according to the given ratios. Thus obtained precursor solution was dropped from the buret at a low speed (around $1 \text{ ml} \cdot \text{min}^{-1}$) into a big beaker containing about 500 ml of deionized water, while maintaining the pH value above 9.0 by adding ammonium hydrate. The precipitation occurred during dropping and stirring. The precipitate was then filtered and dried at 75°C . Finally, the white powder was obtained after pyrolysis of the dried precipitate at 700°C for 3h or 1000°C for 1h in air.

2.2. Sample treatment and characterization

The pyrolysed powder was isostatically pressed into cylindrical pellets and sintered in air at temperatures ranging from 1400 to 1700°C to obtain the equilibrium microstructure (Pt-crucible, heating and cooling rate of $10 \text{ K} \cdot \text{min}^{-1}$). The duration of heat treatments was 10 days at 1400°C , 5 days at 1500°C , 3 days at 1600°C , and 36 h at 1700°C . The samples were then analyzed by XRD, SEM, EPMA, TEM, DTA and high temperature calorimetry.

The XRD patterns of powdered specimens were recorded on Siemens diffractometer D5000 ($\text{CuK}\alpha_1$ radiation, $\lambda = 0.15406 \text{ nm}$, 2θ range $10\text{-}80^\circ$). Precise measurements of lattice parameters were carried out using silicon or alumina powder as internal standard.

The microstructures of sintered samples were examined by SEM (Zeiss DSM 982 GEMINI operating at 20 kV and 10 nA) and the energy dispersive X-ray spectroscopy (EDX, Oxford-Instrument ISIS 300) was employed to obtain the compositions of phases ($\pm 1 \text{ mol}\%$ $\text{REO}_{1.5}$) in equilibrium state. Furthermore, the electronic probe microanalyser (EPMA, SX-100, Cameca) was also employed for the precise composition analysis.

Specimens of the $\text{ZrO}_2 - \text{GdO}_{1.5}$ system for TEM studies were prepared using mechanical thinning and Ar^+ ion milling in a Gatan Precision Ion Polishing System (PIPS). Conventional TEM was performed in JEOL 2000FX and JEOL 4000FX electron microscopes equipped with EDX detector (HPGe, Voyager, Noran Instruments), which allowed high spatial resolution (< 20 nm). Selected area electron diffraction (SAED) experiments were accomplished in both microscopes. The EDX spectra were carefully collected from electron-transparent thin areas of single grains and then analyzed by the software “Flame”. Standardless quantitative analysis was carried out, and theoretical k-factors were used for converting intensity ratios into composition ratios [1996Wil]. Each grain was measured at least five times and the standard deviation was estimated as 2 mol% $\text{GdO}_{1.5}$.

The heat contents of the compositions ZrO_2 -30 mol% $\text{REO}_{1.5}$ (RE=Nd, Sm, Gd, Dy), ZrO_2 -30 mol% $\text{REO}_{1.5}$ (RE= Nd, Sm, Gd, Dy, Yb), and ZrO_2 -57.14 mol% $\text{YbO}_{1.5}$, were determined by high temperature drop calorimetry (SETARAM, Pt crucible air atmosphere) in the temperature range 200°C-1400°C. Before measurement, the samples were heat treated at 1600°C for 72 h, and then ground into small pellets in the range 10-60mg.

The heat capacity of the pyrochlore sample with the composition of 50 mol% $\text{GdO}_{1.5}$ was measured in the temperature range 100-1400°C by using high-temperature DSC (SETARAM, heating and cooling rate 5 K/min; He + 20 vol.% O_2 ; Pt crucible). The sample was heat treated at 1400°C for 240h, and then ground into fine powder.

The samples in the $\text{ZrO}_2 - \text{HfO}_2$ system and those with ZrO_2 -rich in the $\text{ZrO}_2 - \text{GdO}_{1.5}$ and $\text{ZrO}_2 - \text{DyO}_{1.5}$ systems were studied by DTA up to 1700°C (Bähr, heating and cooling rate 5 K/min, Al_2O_3 crucible). The uncertainty of the measurements is estimated to be ± 5 K.

2.3. Thermodynamic modelling of phases

2.3.1. Introduction

2.3.1.1. The CALPHAD approach

It is easy to accept that the combination of thermodynamics and visualized phase diagrams can be very efficient to describe and analyze the phase equilibria and phase transformation under both equilibrium and non-equilibrium conditions. The CALPHAD (CALculation of PHase Diagram) approach is a method which was developed originally for the calculation of phase diagram and now as the powerful tool for materials design. It is an approach of coupling the phase diagram with thermochemistry. Fig. 2-1 schematically presents how the CALPHAD method works.

There are three critical factors in the CALPHAD approach [1992Nis]:

1). The input data. Because CALPHAD is an approach strongly based on the experimental data, it is very important that all possible input data are collected before the work is started. The experimental data include the crystal structure information, stable and metastable phase equilibria, thermodynamic properties such as enthalpy and Gibbs energy of phases and changes of these quantities during phase formation, structural transformations and change of temperatures, the absolute value of heat capacity and entropy, vapour pressure, various partial molar properties for multicomponent systems. Nowadays, with the development of the theoretical models and computer technology, the first principle calculations can offer very important data on the enthalpy of formation at ground state, which is comparable to the standard enthalpy of formation at 298.15K, when the experimental data are not available yet. All the original experimental and theoretical data should be carefully evaluated in order that the selected data are reasonable and consistent.

2). The model for phases. Appropriate thermodynamic model has to be adopted to describe the energetic behavior of phases. Reasonably, only the model based on the structural and physical realities can truly reproduce the thermodynamic behavior of different phases. The model is composed of a series of parameters, which are optimized from the input experimental data. Some thermodynamic models have already been constructed to reflect the real interactions between different atoms with good generalization. For example, the sublattice model can describe both the substitutional solid solution formed by the atoms with similar properties, and the interstitial solid solution formed by the atoms with largely different properties and the high temperature liquid phases.

3). The method of computation. Both the assessment of the model parameters and calculation of the phase diagram must be carried out by computer program. Since H. L. Lukas [1977Luk] developed the first software LUKAS, a lots of commercial software based on different mathematical methods and computer languages have been developed for scientific and industrial users, (e.g. Thermo-Calc, www.thermocalc.com; Pandat, www.computherm.com; MTDATA, www.npl.co.uk/mtdata; FactSage, www.factsage.com).

All the optimizations and calculation in this thesis were carried out by the Thermo-calc software package [1985Sun]. To derive the thermodynamic parameters of different phases, appropriate thermodynamic models have to be selected based on their structures.

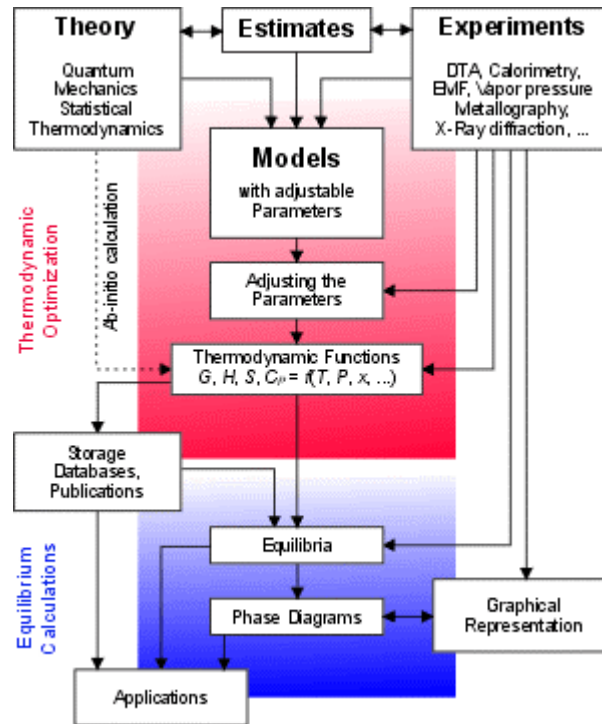


Figure 2-1. The schematic diagram for the CALPHAD approach.

2.3.1.2. Pure elements

The Gibbs energy of an element or a stoichiometric substance at the ambient pressure can be expressed by:

$$G = A + BT + CTLnT + DT^2 + ET^{-1} + \dots \quad (2-1)$$

where A, B, C, D, E, ... are the parameters which can be optimized from the experimental heat capacity, heat content and entropy data.

The equation (2-1) actually is valid only in a certain temperature range, and generally phases have different Gibbs energy functions in different temperature ranges. At the interval limits, the Gibbs energies are continuous. Because only the thermodynamic properties above room temperature (298.15 K) are of practical interest, it is supposed that the enthalpy of stable structure of any element at 298.15 K and 1 bar is equal to zero, and this assumption is set to be the reference state of elements. This reference state has already been widely accepted, and SGTE (Scientific Group Thermodata Europe: www.sgte.com) has optimized the lattice stabilities of all elements with this principle.

2.3.1.3. Thermodynamic models for the solution phases

- (1). Substitutional solution

The solution formed by components which can substitute randomly is called substitutional solution. The thermodynamic properties of substitutional solution (gas, some liquid and solid solution phases) are referred to the ideal solution. The molar Gibbs energy of substitutional solution α phase is generally expressed by the following equation:

$$G_m^\alpha = \sum_i x_i {}^0G_i^\alpha + {}^M G_m^\alpha \quad (2-2)$$

where x_i means the mole fraction of component i . ${}^0G_i^\alpha$ is the Gibbs energy of component i with the same structure of α , and ${}^M G_m^\alpha$ is called the Gibbs energy of mixing which is composed of two parts:

$${}^M G_m^\alpha = -T {}^M S_m^{ideal} + {}^E G_m^\alpha \quad (2-3)$$

in which $-T {}^M S_m^{ideal}$ is the part from the contribution of ideal mixing, and ${}^E G_m^\alpha$ is the excess Gibbs energy. For the ideal mixing, because no any heat effect is produced, and thus only the entropy makes contribution to the Gibbs energy of mixing. ${}^E G_m^\alpha$ reflects how large the mixing behavior deviates from the ideal case, and how it varies with composition.

For example, the Gibbs energy of a solution phase which is composed of two components A and B can be formulated by:

$$G_m^\alpha = x_A {}^0G_A^\alpha + x_B {}^0G_B^\alpha + RT(x_A \ln x_A + x_B \ln x_B) + {}^E G_m^\alpha \quad (2-4)$$

$x_A {}^0G_A^\alpha + x_B {}^0G_B^\alpha$ is the part of Gibbs energy of mechanical mixing, and $RT(x_A \ln x_A + x_B \ln x_B)$ is the part of Gibbs energy associated with the entropy of mixing. The sum of these two parts is the Gibbs energy function of ideal mixing. For the ideal case, the bond energies of A-A, A-B, and B-B are equal, and the atoms of A and B mix randomly without the production of heat. For the nonideal substitutional solution, ${}^E G_m^\alpha$ can be expressed by some polynomials, for example the Redlich-Kister polynomial [1948Red]:

$${}^E G_m^\alpha = x_A x_B \sum_j I_j (x_A - x_B)^j \quad (2-5)$$

in which x_A and x_B are the mole fraction of atoms A and B, respectively, and the I_j is called the interaction parameter in the order of j . In case of $j=0$, the equation (2-5) is simplified to be:

$${}^E G_m^\alpha = X_A X_B I_0 \quad (2-6)$$

Such case is called regular solution. In regular solution, the bond energies of A-A, A-B and B-B are not equal. Suppose v is the energy to form a A-B or B-A atom bond by destroying a A-A and a B-B bonds ($2v=2\varepsilon_{A-B}-\varepsilon_{A-A}-\varepsilon_{B-B}$, ε means the bond energy), N is the number of atoms, and Z is the coordination numbers of A and B, then the numbers of A-B and B-A

bonds will be $NZX_A X_B$. Therefore, the excess Gibbs energy will be $vNZX_A X_B$, and the interaction parameter is:

$$I_0 = vNZ \quad (2-7)$$

The I_0 is related to the solution status after the mixing of A and B atoms, and thus explicitly its physical meanings are described as follows:

(a). $I_0 = 0$. This means $\epsilon_{A-B} = (\epsilon_{A-A} + \epsilon_{B-B})/2$, which corresponds to the ideal mixing. The atoms of A and B can substitute and arrange randomly.

(b). $I_0 > 0$. This means $\epsilon_{A-B} > (\epsilon_{A-A} + \epsilon_{B-B})/2$, which corresponds to less stable A-B and B-A bonds than A-A and B-B bonds. Different kinds of atoms are repulsive to each other, and the same atoms can form clusters or order in some short range. In case of large positive I_0 , the solution phase may separate into two isostructural compositions, which forms the miscibility gap.

(c). $I_0 < 0$. This means $\epsilon_{A-B} < (\epsilon_{A-A} + \epsilon_{B-B})/2$, which corresponds to more stable A-B and B-A bonds than A-A and B-B bonds. The formation of A-B and B-A bonds is a spontaneous process, by decreasing the Gibbs energy of the system after mixing.

However, the regular solution model treats the solution by assuming the atoms always distribute randomly without the consideration of the influence of the different atoms surroundings. Actually, the atoms surroundings can make the thermodynamic properties of solution more complicated than those of regular mixing. To describe the more complicated cases, sometimes the sub-regular solution model ($j=1$) or the sub-sub-regular solution model ($j=2$) has to be used.

(2). Compound energy formalism

The compound energy formalism developed by M. Hillert et al. [2001Hil] can be applied to the most of solution phases, which have separate crystallographic sublattices. It is called formalism because it includes a large variety of thermodynamic models.

Compound energy formalism was developed from the sublattice model for the reciprocal quaternary system [2001Hil]. It assumes that in crystals different atomic species occupy separate (the stoichiometric compounds) or same sublattices (the phases with composition range). A certain sublattice can be occupied by the intrinsic atoms, anti-site atoms, interstitial atoms, vacancies and electrons. The compound energy formalism can be thought as the substitutional model applied for the case of phase with two or more sublattices. This generalized formalism can be used to describe different solution phases with substitutional and interstitial species, charged species, ordering behavior, etc. The

construction of the sublattices should be exactly based on the structure information of phases, so that the model has a physical meaning.

The compound energy formalism applied in different cases is shortly reviewed in the following paragraphs.

(a). General case

The model for a solution phase can be expressed with the formula $(A,B,\dots)_k(C,D,\dots)_l(\dots)_{\dots}$, in which A, B, C, D,... are the constituents, and k, l, ... are called stoichiometric coefficients. The division on sublattices is made according to the phase structures, and in principle there are no limitation on the numbers of sublattices. The Gibbs energy function of generalized model is given by:

$$G_m = \sum \prod y_J^S {}^0G_{end} + RT \sum \sum n^S y_J^S \ln(y_J^S) + {}^E G_m \quad (2-8)$$

in which n^S is stoichiometric coefficient of sublattice S, and y_J^S is the site fraction of constituent J in the sublattice S. ${}^0G_{end}$ is the Gibbs energy of end members which are the stoichiometric compounds formed by the constituents when each sublattice is only occupied by only one species, e.g. $A_k C_l \dots$. The excess Gibbs energy ${}^E G_m$ is expressed by:

$${}^E G_m = \prod y_J^S \sum y_B^t L_{A,B,C:D\dots} + \prod y_J^S \sum \sum y_B^t y_D^u L_{A,B,C,D:E\dots} + \dots \quad (2-9)$$

where the commas in the subscripts separate different constituents in the same sublattice, and the colons separate the species in different sublattices. In the first group of terms, the interaction parameter $L_{A,B,C:D\dots}$ describes the interactions in a certain sublattice while each of the other sublattices is only occupied by a single constituent. In the second group of terms, the interaction parameter $L_{A,B,C,D:E\dots}$ describes the interactions occurred in two sublattices at a same time while each of the other sublattices is only occupied by a single constituent, and this interaction parameter is called ‘‘reciprocal parameter’’. All these interaction parameters can be expanded as the Redlich-Kister polynomials.

(b). Ionic crystals

For the ionic crystals, the constituents are charged ions, and the sublattices are distinguished by cation and anion sublattices. The model is given by the formula $(A^{+m}, B^{+n}, \dots)_a (C^{+i}, D^{+j}, \dots)_b (E^{-k}, F^{-l}, \dots)_c (\dots)_{\dots}$. Some of these end members could be not electroneutral, and thus the occupations of constituents in certain sublattice are not always independent on the occupations of constituents in other sublattices so that the model can

maintain the electroneutrality. The equation (2-8) can also be applied for the Gibbs energy function of ionic crystal phase, and the only difference is that the constraint on the electroneutrality can affect the site fractions of constituents in sublattices.

(c). Ionic melts

For the melted ionic crystals, its long range ordering disappears, and the atoms do not have their fixed lattice positions by reaching disordered state. However, due to the interactions between the atoms with opposite charges, it can still be assumed that there are one cation and one anion sublattices in a short distance range. To maintain the electroneutrality of the phase, the assumption is made that the numbers of the cation and anion sublattices are changeable, what is consistent with the real structure of ionic liquid. If we use the model $A_P B_Q$, in which A, B are the cation and anion sublattices respectively, and P, Q are the stoichiometric coefficients, and can be calculated by:

$$P = \sum y_j (-\gamma_j) \quad (2-10)$$

$$Q = \sum y_i \gamma_i \quad (2-11)$$

where γ is the valence, and y is the site fraction of species in sublattices. Subscripts i and j represent the different components in sublattices. The Gibbs energy of two-sublattice ionic solution model is given by:

$$G_m = \sum_{ij} y_i y_j {}^0G_{i,j} + PRT \sum_i y_i \ln(y_i) + QRT \sum_j y_j \ln(y_j) + {}^E G_m \quad (2-12)$$

${}^0G_{i,j}$ is the Gibbs energy of formation of the substance formed by cation species i and anion species j . $PRT \sum_i y_i \ln(y_i)$ is the entropy of mixing by the species in cation sublattice, and

$QRT \sum_j y_j \ln(y_j)$ is the entropy of mixing by the species in anion sublattice. The excess

Gibbs energy ${}^E G_m$ can be expressed by equation (2-9).

(d). The stoichiometric phases

A limiting case of the model $(A,B,\dots)_k(C,D,\dots)_l(\dots)_m$ is that each sublattice is only occupied by different single species, which are also components of the system. This means that the different components have their own fixed crystal lattices, without the variation of the stoichiometry. Such phase is called stoichiometric compound. The Gibbs energy of such compound can be simply described by the format of equation (2-1) if there are enough thermodynamic data on heat capacity, enthalpy increment, or entropy. However, for the case

that such thermodynamic data are not available, the Gibbs energy function can be simply expressed by Neumann-Kopp rule [1998Hil]:

$$G_m = \sum_i x_i {}^0G_i + A + BT \quad (2-13)$$

where the x_i and 0G_i are the mole fraction and Gibbs energy of component i , respectively. A and B are the parameters to be determined and can be thought as the enthalpy and entropy of formation of the compound from the components. In the case of lacking thermodynamic data, A and B can be optimized from phase equilibria data.

2.3.2. Pure components

In this work, the lattice stability functions of the pure elements are taken from SGTE database [1991Din]. The Gibbs energy functions for stoichiometric ZrO₂ and HfO₂ are assessed in this thesis, while those for rare earth oxides are taken from the recent evaluation [2006Zin].

2.3.3. The gas phase

The gas phase in the Hf – Zr – O system (Zr – O and Hf – O systems in this work) is treated as ideal mixture of species O, O₂, O₃, ZrO, ZrO₂, Zr, Zr₂, Hf, HfO, and HfO₂ according to the SGTE substance database [Version 1997, SGTE, Gernoble, France, 1997]. All the parameters for these species are also taken from SGTE database. The Gibbs energy function can be formulated by:

$$G_m = \sum_i x_i {}^0G_i + RT(x_i \ln x_i) + RT \ln\left(\frac{P}{P_0}\right) \quad (2-14)$$

in which x_i is the mole fraction of constituent i , and 0G_i is Gibbs energy of substance i in gas state. P_0 is the standard pressure of 1 bar (101325 Pa).

2.3.4. The liquid phase

2.3.4.1. The Hf – Zr – O system

The two-sublattice model for partially ionic liquids within the compound formalism [2001Hil] is used to describe the liquid phase of the Hf – Zr – O system. For simplicity, the model (Hf⁺⁴, Zr⁺⁴)_P(O⁻², Va⁻⁴)_Q without the O species in the anion sublattice is selected in this work. The stoichiometry coefficients P and Q can be represented as follows:

$$P = 2y_{O^{-2}} + 4y_{Va^{-4}} \quad (2-15)$$

$$Q=4y_{Hf^{+4}} + 4y_{Zr^{+4}} \quad (2-16)$$

in which the y_i is the site fraction of constituent in certain sublattice. Accordingly, the Gibbs energy function for the liquid phase can be given by:

$$\begin{aligned} G_m^L &= y_{Hf^{+4}} y_{O^{2-}} {}^0G_{Hf^{+4};O^{2-}}^L + y_{Hf^{+4}} y_{Va^{4-}} {}^0G_{Hf^{+4};Va^{4-}}^L \\ &+ y_{Zr^{+4}} y_{O^{2-}} {}^0G_{Zr^{+4};O^{2-}}^L + y_{Zr^{+4}} y_{Va^{4-}} {}^0G_{Zr^{+4};Va^{4-}}^L \\ &+ PRT(y_{Hf^{+4}} \ln y_{Hf^{+4}} + y_{Zr^{+4}} \ln y_{Zr^{+4}}) + QRT(y_{O^{2-}} \ln y_{O^{2-}} + y_{Va^{4-}} \ln y_{Va^{4-}}) \\ &+ y_{O^{2-}} y_{Va^{4-}} [{}^0L + (y_{O^{2-}} - y_{Va^{4-}}) {}^1L] \end{aligned} \quad (2-17)$$

where ${}^0G_{Hf^{+4};O^{2-}}^L$, ${}^0G_{Hf^{+4};Va^{4-}}^L$, ${}^0G_{Zr^{+4};O^{2-}}^L$ and ${}^0G_{Zr^{+4};Va^{4-}}^L$ represent the Gibbs energies of end-members in the liquid state, respectively. 0L and 1L are the interaction parameters to be optimized.

2.3.4.2. The ZrO₂ – REO_{1.5} systems

The liquid phase of the ZrO₂ – REO_{1.5} system is also described with the two-sublattice model for ionic liquids [2001Hil] (RE⁺³, Zr⁺⁴)_P(O²⁻)_Q but without vacancies in the anion sublattice. The stoichiometry coefficients P and Q are formulated by:

$$P=2 \quad (2-18)$$

$$Q=3 y_{RE^{+3}} + 4 y_{Zr^{+4}} \quad (2-19)$$

where $y_{RE^{+3}}$ and $y_{Zr^{+4}}$ are the site fractions of the RE⁺³ and Zr⁺⁴ in cation sublattice, respectively. The Gibbs energy function for the liquid phase can be given by:

$$\begin{aligned} G_m^L &= y_{RE^{+3}} y_{O^{2-}} {}^0G_{RE^{+3};O^{2-}}^L + y_{Zr^{+4}} y_{O^{2-}} {}^0G_{Zr^{+4};O^{2-}}^L \\ &+ PRT(y_{RE^{+3}} \ln y_{RE^{+3}} + y_{Zr^{+4}} \ln y_{Zr^{+4}}) \\ &+ y_{RE^{+3}} y_{Zr^{+4}} [{}^0L + (y_{RE^{+3}} - y_{Zr^{+4}}) {}^1L] \end{aligned} \quad (2-20)$$

where the ${}^0G_{RE^{+3};O^{2-}}^L$ and ${}^0G_{Zr^{+4};O^{2-}}^L$ are the Gibbs energies of end components ZrO₂ and REO_{1.5} in liquid state, respectively. The 0L and 1L in equation (2-20) are the interaction parameters, which are lineally temperature dependent, and to be optimized in the work.

2.3.5. The bcc and hcp phase

The bcc and hcp phases are Zr- or Hf-based solid solutions in the Zr – O and Hf – O systems. In this work, the model of hcp phase is selected to be (Hf, Zr)₁(O, Va)_{0.5} according to the standard thermodynamic database of SGTE. The bcc phase however is described by a model (Hf, Zr)₁(O, Va)₁ suggested in a recent work of the Ce – O system [2006Zin1], rather than the traditional model (Hf, Zr)₁(O, Va)₃ due to the limited homogeneity range of bcc

phases in both Zr – O and Hf – O systems. The general expression of the Gibbs energies of bcc and hcp can be given by:

$$\begin{aligned}
 G_m^\alpha &= y_{Zr} y_O {}^0G_{Zr:O}^\alpha + y_{Zr} y_{Va} {}^0G_{Zr:Va}^\alpha \\
 &+ y_{Hf} y_O {}^0G_{Hf:O}^\alpha + y_{Hf} y_{Va} {}^0G_{Hf:Va}^\alpha \\
 &+ RT(y_{Zr} \ln y_{Zr} + y_{Hf} \ln y_{Hf}) + xRT(y_O \ln y_O + y_{Va} \ln y_{Va}) \\
 &+ {}^E G_m^\alpha
 \end{aligned} \tag{2-21}$$

in which α denotes hcp or bcc solution, and y_i is the site fraction of species i in different sublattices. x is 0.5 for hcp phase and 1 for bcc phase, and ${}^E G_m^\alpha$ is the excess Gibbs energy, which can be formulated by the expression (2-9).

2.3.6. The ZrO₂ (HfO₂)-based solid solution phases

2.3.6.1. The Hf – Zr – O system

The ZrO₂ or HfO₂-based solutions with structures of cubic fluorite, tetragonal and monoclinic in the Zr – O and Hf – O system are described by the model (Hf⁺², Zr⁺², Hf⁺⁴, Zr⁺⁴)₁(O⁻², Va)₂ in this work according to [2004Wan]. The Gibbs energy is formulated by:

$$\begin{aligned}
 G_m^{ZrO_2-Solution} &= y_{Hf^{+2}}^I y_{O^{-2}}^{II} {}^0G_{Hf^{+2}:O^{-2}}^{ZrO_2-Solution} + y_{Zr^{+2}}^I y_{O^{-2}}^{II} {}^0G_{Zr^{+2}:O^{-2}}^{ZrO_2-Solution} \\
 &+ y_{Hf^{+2}}^I y_{Va}^{II} {}^0G_{Hf^{+2}:Va}^{ZrO_2-Solution} + y_{Zr^{+2}}^I y_{Va}^{II} {}^0G_{Zr^{+2}:Va}^{ZrO_2-Solution} \\
 &+ y_{Hf^{+4}}^I y_{O^{-2}}^{II} {}^0G_{Hf^{+4}:O^{-2}}^{ZrO_2-Solution} + y_{Zr^{+4}}^I y_{O^{-2}}^{II} {}^0G_{Zr^{+4}:O^{-2}}^{ZrO_2-Solution} \\
 &+ y_{Hf^{+4}}^I y_{Va}^{II} {}^0G_{Hf^{+4}:Va}^{ZrO_2-Solution} + y_{Zr^{+4}}^I y_{Va}^{II} {}^0G_{Zr^{+4}:Va}^{ZrO_2-Solution} \\
 &+ 2RT(y_{Hf^{+2}}^I \ln y_{Hf^{+2}}^I + y_{Zr^{+2}}^I \ln y_{Zr^{+2}}^I + y_{Hf^{+4}}^I \ln y_{Hf^{+4}}^I + y_{Zr^{+4}}^I \ln y_{Zr^{+4}}^I) \\
 &+ 4RT(y_{O^{-2}}^{II} \ln y_{O^{-2}}^{II} + y_{Va}^{II} \ln y_{Va}^{II}) + {}^E G_m^{ZrO_2-Solution}
 \end{aligned} \tag{2-22}$$

in which the ${}^0G_{a:b}^{ZrO_2-Solution}$ are the Gibbs energies of end-members, and I and II mean the different sublattice. The excess Gibbs energy in (2-22) can be expressed by:

$$\begin{aligned}
 {}^E G_m^{ZrO_2-Solution} &= y_{Hf^{+2}}^I y_{O^{-2}}^{II} y_{Va}^{II} \left[{}^0L_{Hf^{+2}:O^{-2},Va} + (y_{O^{-2}}^{II} - y_{Va}^{II}) {}^1L_{Hf^{+2}:O^{-2},Va} \right] \\
 &+ y_{Zr^{+2}}^I y_{O^{-2}}^{II} y_{Va}^{II} \left[{}^0L_{Zr^{+2}:O^{-2},Va} + (y_{O^{-2}}^{II} - y_{Va}^{II}) {}^1L_{Zr^{+2}:O^{-2},Va} \right] \\
 &+ y_{Hf^{+4}}^I y_{O^{-2}}^{II} y_{Va}^{II} \left[{}^0L_{Hf^{+4}:O^{-2},Va} + (y_{O^{-2}}^{II} - y_{Va}^{II}) {}^1L_{Hf^{+4}:O^{-2},Va} \right] \\
 &+ y_{Zr^{+4}}^I y_{O^{-2}}^{II} y_{Va}^{II} \left[{}^0L_{Zr^{+4}:O^{-2},Va} + (y_{O^{-2}}^{II} - y_{Va}^{II}) {}^1L_{Zr^{+4}:O^{-2},Va} \right] \\
 &+ y_{Hf^{+2}}^I y_{Hf^{+4}}^I y_{O^{-2}}^{II} \left[{}^0L_{Hf^{+2},Hf^{+4}:O^{-2}} + (y_{Hf^{+2}}^I - y_{Hf^{+4}}^I) {}^1L_{Hf^{+2},Hf^{+4}:O^{-2}} \right] \\
 &+ y_{Zr^{+2}}^I y_{Zr^{+4}}^I y_{O^{-2}}^{II} \left[{}^0L_{Zr^{+2},Zr^{+4}:O^{-2}} + (y_{Zr^{+2}}^I - y_{Zr^{+4}}^I) {}^1L_{Zr^{+2},Zr^{+4}:O^{-2}} \right] \\
 &+ y_{Hf^{+2}}^I y_{Hf^{+4}}^I y_{Va}^{II} \left[{}^0L_{Hf^{+2},Hf^{+4},Va} + (y_{Hf^{+2}}^I - y_{Hf^{+4}}^I) {}^1L_{Hf^{+2},Hf^{+4},Va} \right] \\
 &+ y_{Zr^{+2}}^I y_{Zr^{+4}}^I y_{Va}^{II} \left[{}^0L_{Zr^{+2},Zr^{+4},Va} + (y_{Zr^{+2}}^I - y_{Zr^{+4}}^I) {}^1L_{Zr^{+2},Zr^{+4},Va} \right]
 \end{aligned} \tag{2-23}$$

where the interaction parameters 0L and 1L are to be optimized from the experimental data.

2.3.6.2. The $ZrO_2 - REO_{1.5}$ systems

Three kinds of ZrO_2 -based solid solutions with cubic fluorite, tetragonal and monoclinic structures are treated with same model, $(RE^{+3}, Zr^{+4})_2(O^{2-}, Va)_4$ in this work. The Gibbs energies of these phases are given by:

$$\begin{aligned} G_m^{ZrO_2-Solution} &= y_{RE^{+3}}^I y_{O^{2-}}^{II} {}^0G_{RE^{+3};O^{2-}}^{ZrO_2-Solution} + y_{Zr^{+4}}^I y_{O^{2-}}^{II} {}^0G_{Zr^{+4};O^{2-}}^{ZrO_2-Solution} \\ &+ y_{RE^{+3}}^I y_{Va}^{II} {}^0G_{RE^{+3};Va}^{ZrO_2-Solution} + y_{Zr^{+4}}^I y_{Va}^{II} {}^0G_{Zr^{+4};Va}^{ZrO_2-Solution} \\ &+ 2RT(y_{RE^{+3}}^I \ln y_{RE^{+3}}^I + y_{Zr^{+4}}^I \ln y_{Zr^{+4}}^I) + 4RT(y_{O^{2-}}^{II} \ln y_{O^{2-}}^{II} + y_{Va}^{II} \ln y_{Va}^{II}) \\ &+ {}^E G_m^{ZrO_2-Solution} \end{aligned} \quad (2-24)$$

where ${}^0G_{RE^{+3};O^{2-}}^{ZrO_2-Solution}$, ${}^0G_{Zr^{+4};O^{2-}}^{ZrO_2-Solution}$, ${}^0G_{RE^{+3};Va}^{ZrO_2-Solution}$, and ${}^0G_{Zr^{+4};Va}^{ZrO_2-Solution}$ are the Gibbs energies of the end members formed between species in different sublattices, and I and II represent the different sublattice. The composition square composed by these end members is shown in Fig. 2-2. RE_2O_3 in Fig. 2-2 represents the hypothetical compound of pure RE_2O_3 with the structure of zirconia.

For the fluorite phase, the functions of the Gibbs energies of ${}^0G_{Zr^{+4};O^{2-}}^{ZrO_2-F}$ and ${}^0G_{Zr^{+4};Va}^{ZrO_2-F}$ are given as follows:

$${}^0G_{Zr^{+4};O^{2-}}^{ZrO_2-F} = 2 \cdot GZrO_2F \quad (2-25)$$

$${}^0G_{Zr^{+4};Va}^{ZrO_2-F} = 2 \cdot GZrO_2F - 4 \cdot GHSEROO \quad (2-26)$$

The Gibbs energy of compound RE_2O_3 with cubic fluorite-type structure is modified from that of the stable structure at low temperatures:

$$GRE_2O_3F = GRE_2O_3C + A + BT + C \ln T \quad (2-27)$$

where A , B and C are the parameters to be optimized. The parameter C is used to assess the experimental heat capacity data when it is necessary. According to the composition square, a relation is obtained:

$$GRE_2O_3F = \frac{3}{4} {}^0G_{RE^{+3};O^{2-}}^{ZrO_2-F} + \frac{1}{4} {}^0G_{RE^{+3};Va}^{ZrO_2-F} + 4RT \left(\frac{3}{4} \ln \frac{3}{4} + \frac{1}{4} \ln \frac{1}{4} \right) \quad (2-28)$$

By combining with the constraint of the reciprocal reaction:

$${}^0G_{RE^{+3};O^{2-}}^{ZrO_2-F} + {}^0G_{Zr^{+4};Va}^{ZrO_2-F} - {}^0G_{RE^{+3};Va}^{ZrO_2-F} - {}^0G_{Zr^{+4};O^{2-}}^{ZrO_2-F} = 0 \quad (2-29)$$

The following equations is obtained:

$${}^0G_{RE^{+3};O^{2-}}^{ZrO_2-F} = GRE_2O_3F + GHSEROO + 18.702165T \quad (2-30)$$

$${}^0G_{RE^{+3};Va}^{ZrO_2-F} = GRE_2O_3F - 3 \cdot GHSEROO + 18.702165T \quad (2-31)$$

Likewise, very similar results can be obtained for the tetragonal phase, by only replacing the $GZrO_2F$ with $GZrO_2T$, and replacing GRE_2O_3F with GRE_2O_3T which represents the Gibbs energy of the RE_2O_3 with tetragonal structure. The function of GRE_2O_3T is arbitrarily given by:

$$GRE_2O_3T = GRE_2O_3F + 10000 \quad (2-32)$$

since there are no any available thermodynamic data concerning the tetragonal solid solution phase.

The Gibbs energy of RE_2O_3 with the monoclinic structure is simply modified from the RE_2O_3 phase by adding a positive constant which will be determined from the experimental T_0 data for tetragonal + monoclinic equilibrium.

${}^E G_m^{ZrO_2-Solution}$ in equation (2-24) is the excess Gibbs energy, which is expressed as follows:

$$\begin{aligned} {}^E G_m^{ZrO_2-Solution} = & y_{RE^{+3}}^I y_{O^{-2}}^{II} y_{Va}^{II} \left[{}^0 L_{RE^{+3}, O^{-2}, Va} + (y_{O^{-2}}^{II} - y_{Va}^{II}) {}^1 L_{RE^{+3}, O^{-2}, Va} \right] \\ & + y_{Zr^{+4}}^I y_{O^{-2}}^{II} y_{Va}^{II} \left[{}^0 L_{Zr^{+4}, O^{-2}, Va} + (y_{O^{-2}}^{II} - y_{Va}^{II}) {}^1 L_{Zr^{+4}, O^{-2}, Va} \right] \\ & + y_{RE^{+3}}^I y_{Zr^{+4}}^I y_{O^{-2}}^{II} \left[{}^0 L_{RE^{+3}, Zr^{+4}, O^{-2}} + (y_{RE^{+3}}^I - y_{Zr^{+4}}^I) {}^1 L_{RE^{+3}, Zr^{+4}, O^{-2}} \right] \\ & + y_{RE^{+3}}^I y_{Zr^{+4}}^I y_{Va}^{II} \left[{}^0 L_{RE^{+3}, Zr^{+4}, Va} + (y_{RE^{+3}}^I - y_{Zr^{+4}}^I) {}^1 L_{RE^{+3}, Zr^{+4}, Va} \right] \end{aligned} \quad (2-33)$$

in which the ${}^0 L$ and ${}^1 L$ are the interaction parameters to be optimized. In order to simplify the optimization, some assumptions are given to reduce the numbers of parameters:

$${}^0 L_{RE^{+3}, O^{-2}, Va} = {}^0 L_{Zr^{+4}, O^{-2}, Va} = 0 \quad (2-34)$$

$${}^1 L_{RE^{+3}, O^{-2}, Va} = {}^1 L_{Zr^{+4}, O^{-2}, Va} = 0 \quad (2-35)$$

$${}^0 L_{RE^{+3}, Zr^{+4}, O^{-2}} = {}^0 L_{RE^{+3}, Zr^{+4}, Va} = D + ET \quad (2-36)$$

$${}^1 L_{RE^{+3}, Zr^{+4}, O^{-2}} = {}^1 L_{RE^{+3}, Zr^{+4}, Va} = F + GT \quad (2-37)$$

where D , E , F and G are the parameters to be optimized. For the fluorite phase, both ${}^0 L$ and ${}^1 L$ are used for optimization due to its existence in a wide composition and temperature range. Only one parameter without temperature dependence is adopted for the tetragonal phase. For simplicity, the interaction parameter is not given to the monoclinic phase, since its homogeneity range is negligible.

2.3.7. The RE_2O_3 -based phases

In the RE_2O_3 -rich region, there are five polymorphic structures named A, B, C, H, and X in literature [2006Zin]. From La to Nd, the stable structure of RE_2O_3 at room temperature is

A-type, while from Sm to Yb, the stable structure of RE₂O₃ at room temperature is C-type. The phases with solubility range are described with the three-sublattice model (RE⁺³, Zr⁺⁴)₂(O⁻²)₃(O⁻², Va)₁ in this work according to the suggestion by O. Fabrichnaya et al. [2004Fab]. Thus, the Gibbs energy function can be expressed by:

$$\begin{aligned}
 G_m^{RE_2O_3-Solution} &= y_{RE^{+3}}^I y_{O^{2-}}^{II} y_{O^{2-}}^{III} {}^0G_{RE^{+3};O^{2-};O^{2-}}^{RE_2O_3-Solution} + y_{Zr^{+4}}^I y_{O^{2-}}^{II} y_{O^{2-}}^{III} {}^0G_{Zr^{+4};O^{2-};O^{2-}}^{RE_2O_3-Solution} \\
 &+ y_{RE^{+3}}^I y_{O^{2-}}^{II} y_{Va}^{III} {}^0G_{RE^{+3};O^{2-};Va}^{RE_2O_3-Solution} + y_{Zr^{+4}}^I y_{O^{2-}}^{II} y_{Va}^{III} {}^0G_{Zr^{+4};O^{2-};Va}^{RE_2O_3-Solution} \\
 &+ 2RT(y_{RE^{+3}}^I \ln y_{RE^{+3}}^I + y_{Zr^{+4}}^I \ln y_{Zr^{+4}}^I) + RT(y_{O^{2-}}^{III} \ln y_{O^{2-}}^{III} + y_{Va}^{III} \ln y_{Va}^{III}) \\
 &+ {}^E G_m^{RE_2O_3-Solution}
 \end{aligned} \tag{2-38}$$

In above equation, the ${}^0G_{RE^{+3};O^{2-};O^{2-}}^{RE_2O_3-Solution}$, ${}^0G_{Zr^{+4};O^{2-};O^{2-}}^{RE_2O_3-Solution}$, ${}^0G_{RE^{+3};O^{2-};Va}^{RE_2O_3-Solution}$ and ${}^0G_{Zr^{+4};O^{2-};Va}^{RE_2O_3-Solution}$ are the Gibbs energies of the end members formed between species in different sublattices. The superscripts *I*, *II* and *III* denote the different sublattice, while $y_{O^{2-}}^{II}$ always equal to 1. The composition square is given in Fig. 2-3. The dashed line corresponds to all the available electroneutral combinations. The two terminals of the neutral line are RE₂O₃ and ZrO₂ with the same structure.

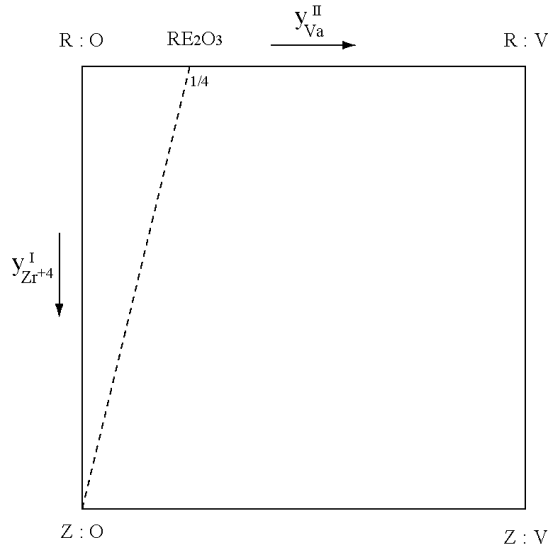


Figure 2-2. The composition square of the ZrO₂-rich phases with the model (RE⁺³, Zr⁺⁴)₂(O⁻², Va)₄. The dashed line means the combinations with electroneutrality. (R, Z, O, V represent the species RE⁺³, Zr⁺⁴, O⁻², Va respectively. $y_{Zr^{+4}}^I$ and y_{Va}^{II} mean the Zr⁺⁴ species in first sublattice and vacancy in second sublattice, respectively).

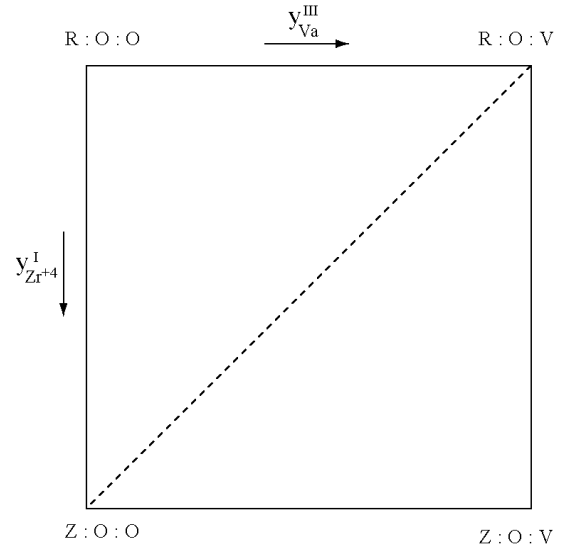


Figure 2-3. The composition square of the RE₂O₃-rich phases with the model (RE⁺³, Zr⁺⁴)₂(O⁻²)₃(O⁻², Va)₁. The dashed line means the combinations with electroneutrality. (R, Z, O, V denote the species RE⁺³, Zr⁺⁴, O⁻², and Va. $y_{Zr^{+4}}^I$ and y_{Va}^{III} mean the Zr⁺⁴ species in first sublattice and vacancy in third sublattice, respectively).

As an example, for the C-RE₂O₃ phase, the Gibbs energies of the four end members are given as follows:

$${}^0G_{RE^{+3},O^{-2},Va}^{C-RE_2O_3} = GRE_2O_3C \quad (2-39)$$

$${}^0G_{RE^{+3},O^{-2},O^{-2}}^{C-RE_2O_3} = GRE_2O_3C + GHSEROO \quad (2-40)$$

$${}^0G_{Zr^{+4},O^{-2},O^{-2}}^{C-RE_2O_3} = GZRO_2F + 5000 \quad (2-41)$$

$${}^0G_{Zr^{+4},O^{-2},Va}^{C-RE_2O_3} = GZRO_2F + 5000 - GHSEROO \quad (2-42)$$

The Gibbs energies of the four end members for other RE₂O₃ phases can be given by similar functions. The excess Gibbs energy ${}^E G_m^{Gd_2O_3-Solution}$ is given with following formula:

$$\begin{aligned} {}^E G_m^{RE_2O_3-Solution} = & y_{RE^{+3}}^I y_{O^{-2}}^{III} y_{Va}^{III} \left[{}^0L_{RE^{+3},O^{-2},O^{-2},Va} + (y_{O^{-2}}^{III} - y_{Va}^{III}) {}^1L_{RE^{+3},O^{-2},O^{-2},Va} \right] \\ & + y_{Zr^{+4}}^I y_{O^{-2}}^{III} y_{Va}^{III} \left[{}^0L_{Zr^{+4},O^{-2},O^{-2},Va} + (y_{O^{-2}}^{III} - y_{Va}^{III}) {}^1L_{Zr^{+4},O^{-2},O^{-2},Va} \right] \\ & + y_{RE^{+3}}^I y_{Zr^{+4}}^I y_{O^{-2}}^{III} \left[{}^0L_{RE^{+3},Zr^{+4},O^{-2},O^{-2}} + (y_{RE^{+3}}^I - y_{Zr^{+4}}^I) {}^1L_{RE^{+3},Zr^{+4},O^{-2},O^{-2}} \right] \\ & + y_{RE^{+3}}^I y_{Zr^{+4}}^I y_{Va}^{III} \left[{}^0L_{RE^{+3},Zr^{+4},O^{-2},Va} + (y_{RE^{+3}}^I - y_{Zr^{+4}}^I) {}^1L_{RE^{+3},Zr^{+4},O^{-2},Va} \right] \end{aligned} \quad (2-43)$$

where 0L and 1L are the interaction parameters for optimization. Like the case of ZrO₂-rich phases, some simplifications also made. Only the interaction parameters ${}^0L_{RE^{+3},Zr^{+4},O^{-2},Va}$ and ${}^1L_{RE^{+3},Zr^{+4},O^{-2},Va}$ are adopted in the optimization, and the other are simply fixed to be zero because of their lower significance for the phase diagram. For the other structures of RE₂O₃ except C-type phase, only one interaction parameter without temperature dependence is adopted, due to their limited composition or temperature range.

2.3.8. The pyrochlore phase

The pyrochlore phase is the ordered structure of the fluorite phase at low temperatures. A detailed description of the pyrochlore structure has been given elsewhere [2000Min, 2002Sta]. The crystal structures of the fluorite and pyrochlore phases are shown in Fig. 2-4. The general formula of the pyrochlore structure can be written as A₂B₂O₆O'. There are four crystallographically unique atom positions for the stoichiometric phase, and the space group is $Fd\bar{3}m$. The pyrochlore structure of stoichiometric A₂B₂O₇ can be derived from the fluorite structure by doubling the fluorite cell edge, placing the large A⁺³ ions at 16*d* site, the smaller B⁺⁴ ions at 16*c*, and the O⁻² ions at 48*f* and 8*b*, leaving the fluorite position 8*a* vacant. The A⁺³ cations are eight-fold coordinated with six 48*f* oxygen atoms (O1) and two 8*b* oxygen atoms (O2), and the B⁺⁴ cations are coordinated with six 48*f* oxygen atoms, while the O1 anions in 48*f* site are coordinated with two A⁺³ and two B⁺⁴ cations, and O2 anions in 8*b* site are

coordinated with four A^{+3} cations. The substitution between A^{+3} and B^{+4} or introducing point defects into the pyrochlore-type structure (vacancies or interstitials) results in formation of the nonstoichiometric phases $A_{2-x}B_{2+x}O_{7+0.5x}$.

There is a lot of information on the occupancies of different lattice sites by oxygen and vacancies in nonstoichiometric pyrochlore. Generally, it is accepted that excess oxygen will enter into the $8a$ site, while the $16d$ sublattice site will be partially occupied by Zr^{+4} species. However, in the modeling work [1985Dij], the authors found that the oxygen interstitials would preferably occupy the $8a$ site, and a new $32e$ site. This $32e$ site occupation was also reported by [1999Tho] in their study of the oxygen excess pyrochlore, and additionally they reported that both $8b$ and $8a$ sites were not fully occupied in this case. The existence of oxygen interstitial in $32e$ site was later confirmed by Blundred et al. [2004Blu] even in the oxygen deficient pyrochlores. Furthermore, they also stated that preferential loss of oxygen anions occurs from $48f$ site rather than $8b$ site, because the B^{+4} species were not directly bound to the O_2 in the $8b$ site. This is in agreement with most of investigations [1998Wil, 1999Wil, 2001Pir, 2001Wil, 2004Pan] that for the case of Zr^{+4} deficiency the oxygen vacancy for the pyrochlore forms more easily at the $48f$ site rather than $8b$ site. The nonstoichiometry in $A_2B_2O_7$ pyrochlore was simulated by Stanek et al. [2002Sta]. They proposed two preferential ways for the BO_2 excess: one is the cation vacancy mechanism in the A^{+3} sublattice, and another is the oxygen interstitials mechanism in the $8a$ site while additional B^{+4} species have to enter into $16d$ site to compensate the electroneutrality, and in the stable pyrochlores, the A^{+3} cation vacancy mechanism is predicted to be more favorable. For the A_2O_3 excess case, the predicted most favorable way is the formation of oxygen vacancies in $48f$ site. Taking all the literature information into account, it is not possible to find the general occupancy rules for the defect pyrochlore, because it seems that the case partly depends on the radius of A^{+3} and B^{+4} cations, and the samples in different experimental works with different ordering degree may also cause the discrepancies. In this work, based on the principle to adopt simplified model, the $32e$ site and the vacancy in cation sublattice are not considered, and only two general and simple cases for defect pyrochlore are accepted. For the oxygen excess case, additional oxygen species enter into the $8a$ sites, and excess B^{+4} species enter into $16d$ site. For oxygen deficiency case, vacancies are formed in $48f$ site, and additional A^{+3} species enter into $16c$ site. In both cases, the $8b$ site is fully occupied by oxygen. These two cases produce the nonstoichiometry of pyrochlore. At the stoichiometric composition, the $48f$ site is completely occupied by oxygen, and the $8a$ site is fully vacant. Thus, a model can be created to describe the pyrochlore phase with five sublattices (Zr^{+4} ,

$\text{RE}^{+3})_2(\text{RE}^{+3}, \text{Zr}^{+4})_2(\text{O}^{-2}, \text{Va})_6(\text{O}^{-2})_1(\text{Va}, \text{O}^{-2})_1$, in which the fourth sublattice is fully occupied by oxygen.

As it was already pointed out [2005Zin], the transition between fluorite and pyrochlore in the $\text{ZrO}_2 - \text{GdO}_{1.5}$ system shows a hybrid character, and it is not clear yet whether it is of first or second order. Thus, except the model proposed in above paragraph, further efforts are also put to model it as a second-order phase transition in this work. The thermodynamic model to describe the order-disorder transitions in metallic systems has been developed by Ansara et al. [1988Ans, 1997Ans], and makes it possible to describe the ordered and disordered phases within the single splitting sublattice model. By this way, the Gibbs energies of the ordered and disordered phases can be expressed by a continuous function, which is the sum of two terms, a disordered part and an ordered part. Examples could be found in literature for the $\text{fcc} \leftrightarrow \text{L1}_2$ first-order transition [1997Ans] and $\text{bcc_A2} \leftrightarrow \text{bcc_B2}$ second-order transition [1999Dup]. Generally, mathematical constraints are needed for parameters to ensure that the Gibbs energy always has an extremum at the disordered state. Currently, the applications of this model are mainly concerning the metal alloy systems. For the case of pyrochlore phase, what is different from the metallic system is that the ordering occurs independently at both cation sublattice and anion sublattice. According to the crystal structure information, the pyrochlore phase can be described with the model $(\text{Zr}^{+4}, \text{RE}^{+3})_2(\text{RE}^{+3}, \text{Zr}^{+4})_2(\text{O}^{-2}, \text{Va})_6(\text{O}^{-2}, \text{Va})_1(\text{Va}, \text{O}^{-2})_1$. The phase becomes completely disordered when $y_i^1 = y_i^2$ ($i = \text{RE}^{+3}, \text{Zr}^{+4}$), and $y_j^3 = y_j^4 = y_j^5$ ($j = \text{O}^{-2}, \text{Va}$). However, the commercial softwares such as Thermo-Calc are not available to simultaneously treat the orderings in both cation and anion sublattices for this model yet. Very recently, Ohtani et al. [2005Oht] applied the model $(\text{Zr}^{+4}, \text{Nd}^{+3})_{0.5}(\text{Nd}^{+3}, \text{Zr}^{+4})_{0.5}(\text{O}^{-2}, \text{Va})_2$ to study the order-disorder transition between fluorite and pyrochlore phase for $\text{ZrO}_2 - \text{Nd}_2\text{O}_3$ system. The model proposed there is also accepted in this work with the formula $(\text{Zr}^{+4}, \text{RE}^{+3})_2(\text{RE}^{+3}, \text{Zr}^{+4})_2(\text{O}^{-2}, \text{Va})_8$ to describe the second-order transition in the $\text{ZrO}_2 - \text{GdO}_{1.5}$ system, without considering the ordering of the oxygen and vacancies.

For the first model $(\text{Zr}^{+4}, \text{RE}^{+3})_2(\text{RE}^{+3}, \text{Zr}^{+4})_2(\text{O}^{-2}, \text{Va})_6(\text{O}^{-2})_1(\text{Va}, \text{O}^{-2})_1$, it is impossible to give appropriate values for all end members without any constraints. The derivation of all the parameters for this model takes several steps. Fig. 2-5 gives the composition space of this model, where the dashed triangles and parallelogram represent the compositional possibilities of electroneutrality.

2.3.8.1. The model $(\text{Zr}^{+4}, \text{RE}^{+3})_2(\text{RE}^{+3}, \text{Zr}^{+4})_2(\text{O}^{-2}, \text{Va})_6(\text{O}^{-2})_1(\text{Va}, \text{O}^{-2})_1$

(1). The stoichiometric pyrochlore

The homogeneity range of the pyrochlore phase is ignored in the first step, with the model $(Zr^{+4}, RE^{+3})_2(RE^{+3}, Zr^{+4})_2(O^{-2})_6(O^{-2})_1(Va)_1$. In the ideally ordered stoichiometric pyrochlore structure, the first sublattice (*16c* site) is fully occupied by Zr^{+4} , and the second sublattice (*16d* site) is completely occupied by RE^{+3} . In Fig. 2-5, all the available stoichiometric compositions are on the electroneutral line which connects the end members $Zr^{+4}:RE^{+3}:O^{-2}:O^{-2}:Va$ (ZROOV) and $RE^{+3}:Zr^{+4}:O^{-2}:O^{-2}:Va$ (RZOOV) if only the substitution of cation species is taken into account. The Gibbs energy function of stoichiometric pyrochlore thus can be given by:

$$G_m^{pyrochlore} = y_{RE^{+3}}^1 y_{RE^{+3}}^2 y_{O^{-2}}^3 y_{O^{-2}}^4 y_{Va}^5 {}^0G_{RE^{+3}:RE^{+3}:O^{-2}:O^{-2}:Va}^{pyrochlore} + y_{RE^{+3}}^1 y_{Zr^{+4}}^2 y_{O^{-2}}^3 y_{O^{-2}}^4 y_{Va}^5 {}^0G_{RE^{+3}:Zr^{+4}:O^{-2}:O^{-2}:Va}^{pyrochlore} + y_{Zr^{+4}}^1 y_{RE^{+3}}^2 y_{O^{-2}}^3 y_{O^{-2}}^4 y_{Va}^5 {}^0G_{Zr^{+4}:RE^{+3}:O^{-2}:O^{-2}:Va}^{pyrochlore} + y_{Zr^{+4}}^1 y_{Zr^{+4}}^2 y_{O^{-2}}^3 y_{O^{-2}}^4 y_{Va}^5 {}^0G_{Zr^{+4}:Zr^{+4}:O^{-2}:O^{-2}:Va}^{pyrochlore} + 2RT(y_{RE^{+3}}^1 \ln y_{RE^{+3}}^1 + y_{Zr^{+4}}^1 \ln y_{Zr^{+4}}^1) + 2RT(y_{Zr^{+4}}^2 \ln y_{Zr^{+4}}^2 + y_{RE^{+3}}^2 \ln y_{RE^{+3}}^2) \quad (2-44)$$

where the superscripts 1 to 5 denote the different sublattices, respectively. The Gibbs energy function for the ideal stoichiometric pyrochlore $Zr^{+4}:RE^{+3}:O^{-2}:O^{-2}:Va$ can be assessed from the experimental data of heat capacity, enthalpy increment, and enthalpy of formation, i.e.,

$${}^0G_{Zr^{+4}:RE^{+3}:O^{-2}:O^{-2}:Va}^{pyrochlore} = a + bT + cT \ln T + dT^{-1} + eT^2 \quad (2-45)$$

The Gibbs energy of inverse pyrochlore $RE^{+3}:Zr^{+4}:O^{-2}:O^{-2}:Va$ is expressed by adding an arbitrary large positive value to the ${}^0G_{Zr^{+4}:RE^{+3}:O^{-2}:O^{-2}:Va}^{pyrochlore}$:

$${}^0G_{RE^{+3}:Zr^{+4}:O^{-2}:O^{-2}:Va}^{pyrochlore} = {}^0G_{Zr^{+4}:RE^{+3}:O^{-2}:O^{-2}:Va}^{pyrochlore} + VI \quad (2-46)$$

in which *VI* is the cationic anti-site energy. The end member $Zr^{+4}:Zr^{+4}:O^{-2}:O^{-2}:Va$ (ZZOOV) can be treated as pyrochlore-type $(ZrO_2)_4$ with the deficiency of one oxygen species. Firstly, the Gibbs energy of the end member $Zr^{+4}:Zr^{+4}:O^{-2}:O^{-2}:O^{-2}$ (ZZOOO) is assumed to be:

$${}^0G_{Zr^{+4}:Zr^{+4}:O^{-2}:O^{-2}:O^{-2}}^{pyrochlore} = 4 \cdot GZRO_2F + V2 + V3T \quad (2-47)$$

where the $GZRO_2F$ is the Gibbs energy of fluorite-type ZrO_2 , and *V2* and *V3* are the parameters to be optimized. Then the Gibbs energy of the $Zr^{+4}:Zr^{+4}:O^{-2}:O^{-2}:Va$ is given by:

$${}^0G_{Zr^{+4}:Zr^{+4}:O^{-2}:O^{-2}:Va}^{pyrochlore} = {}^0G_{Zr^{+4}:Zr^{+4}:O^{-2}:O^{-2}:O^{-2}}^{pyrochlore} - GHSEROO \quad (2-48)$$

where the GHSEROO is the Gibbs energy of 1/2 mole of oxygen gas. A constraint is then given for this reciprocal system to obtain the function of ${}^0G_{RE^{+3}:RE^{+3}:O^{-2}:O^{-2}:Va}^{pyrochlore}$:

$${}^0G_{Zr^{+4}:Zr^{+4}:O^{-2}:O^{-2}:Va}^{pyrochlore} + {}^0G_{RE^{+3}:RE^{+3}:O^{-2}:O^{-2}:Va}^{pyrochlore} - {}^0G_{RE^{+3}:Zr^{+4}:O^{-2}:O^{-2}:Va}^{pyrochlore} - {}^0G_{Zr^{+4}:RE^{+3}:O^{-2}:O^{-2}:Va}^{pyrochlore} = \Delta G1 \quad (2-49)$$

in which the energy difference $\Delta G1$ is set to zero to simplify the modeling.

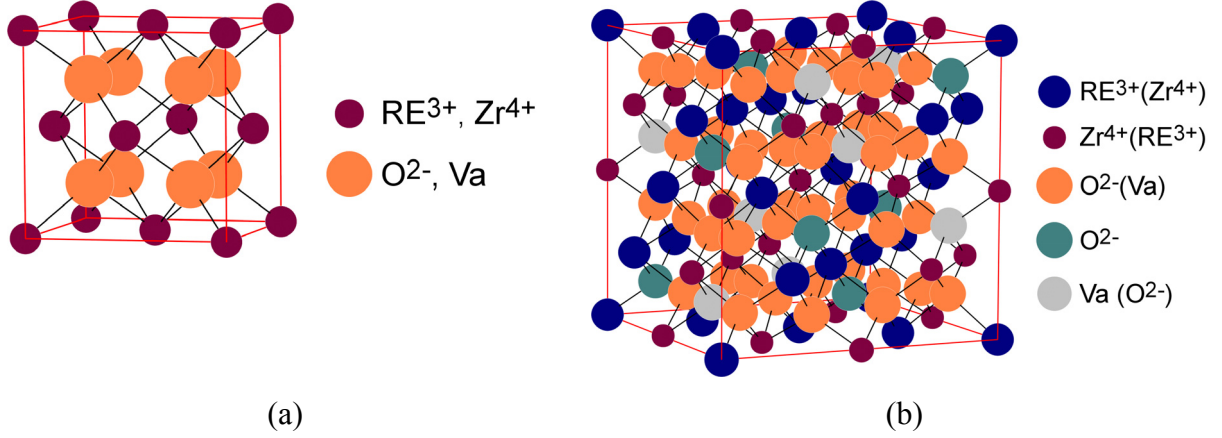


Figure 2-4. The visualized crystal unit cells for the fluorite (a) and pyrochlore (b) phases.

(2). The oxygen excess pyrochlore

The excess of oxygen in the fifth sublattice is accompanied by the additional Zr^{+4} species in the second sublattice. This case can be expressed by the model $(Zr^{+4}, RE^{+3})_2(RE^{+3}, Zr^{+4})_2(O^{2-})_6(O^{2-})_1(Va, O^{2-})_1$, which can be seen as the middle cube in Fig. 2-5. Totally the parameters of eight end members are to be determined according to this model. The available compositional combinations with electroneutrality are denoted by the dashed triangle ZROOV-RZOOV-ZZOOO. The Gibbs energies of five end members ${}^0G_{Zr^{+4}:Zr^{+4}:O^{2-}:O^{2-}:Va}^{pyrochlore}$,

${}^0G_{RE^{+3}:RE^{+3}:O^{2-}:O^{2-}:Va}^{pyrochlore}$, ${}^0G_{RE^{+3}:Zr^{+4}:O^{2-}:O^{2-}:Va}^{pyrochlore}$, ${}^0G_{Zr^{+4}:RE^{+3}:O^{2-}:O^{2-}:Va}^{pyrochlore}$ and ${}^0G_{Zr^{+4}:Zr^{+4}:O^{2-}:O^{2-}:O^{2-}}^{pyrochlore}$ are already determined in the first step, and the three others ${}^0G_{Zr^{+4}:RE^{+3}:O^{2-}:O^{2-}:O^{2-}}^{pyrochlore}$, ${}^0G_{RE^{+3}:Zr^{+4}:O^{2-}:O^{2-}:O^{2-}}^{pyrochlore}$ and

${}^0G_{RE^{+3}:RE^{+3}:O^{2-}:O^{2-}:O^{2-}}^{pyrochlore}$ can be determined by the equations:

$${}^0G_{Zr^{+4}:Zr^{+4}:O^{2-}:O^{2-}:Va}^{pyrochlore} + {}^0G_{Zr^{+4}:RE^{+3}:O^{2-}:O^{2-}:O^{2-}}^{pyrochlore} - {}^0G_{Zr^{+4}:RE^{+3}:O^{2-}:O^{2-}:Va}^{pyrochlore} - {}^0G_{Zr^{+4}:Zr^{+4}:O^{2-}:O^{2-}:O^{2-}}^{pyrochlore} = \Delta G2 \quad (2-50)$$

$${}^0G_{Zr^{+4}:RE^{+3}:O^{2-}:O^{2-}:Va}^{pyrochlore} + {}^0G_{RE^{+3}:RE^{+3}:O^{2-}:O^{2-}:O^{2-}}^{pyrochlore} - {}^0G_{Zr^{+4}:RE^{+3}:O^{2-}:O^{2-}:O^{2-}}^{pyrochlore} - {}^0G_{RE^{+3}:RE^{+3}:O^{2-}:O^{2-}:Va}^{pyrochlore} = \Delta G3 \quad (2-51)$$

$${}^0G_{RE^{+3}:Zr^{+4}:O^{2-}:O^{2-}:O^{2-}}^{pyrochlore} + {}^0G_{RE^{+3}:RE^{+3}:O^{2-}:O^{2-}:Va}^{pyrochlore} - {}^0G_{RE^{+3}:Zr^{+4}:O^{2-}:O^{2-}:Va}^{pyrochlore} - {}^0G_{RE^{+3}:RE^{+3}:O^{2-}:O^{2-}:O^{2-}}^{pyrochlore} = \Delta G4 \quad (2-52)$$

$\Delta G2$, $\Delta G3$, and $\Delta G4$ are the reciprocal energies to be determined in this work.

The ZrO_2 excess can be approached if only $y_{O^{2-}}^3 + 1/6y_{O^{2-}}^5 > 1$ is reached. It must be noted that this composition space cannot give all the available combinations for the ZrO_2 excess. The description of all the available cases for the ZrO_2 excess involves the substitution of species in the four sublattices, which cannot be visualized simply in a three dimensional space.

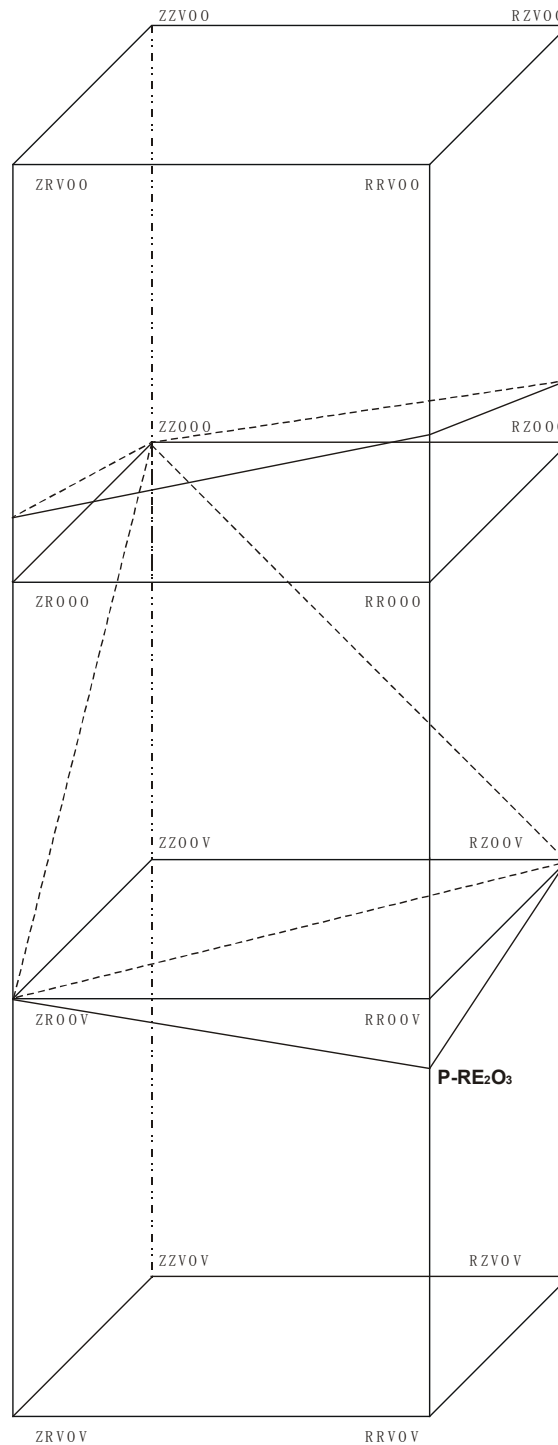


Figure 2-5. The composition space for the pyrochlore structure (R, Z, O, V denote the species RE^{+3} , Zr^{+4} , O^{-2} , and Va.)

(3). The oxygen deficient pyrochlore

The oxygen deficiency in the third sublattice is accompanied by the additional RE^{+3} in the cation sublattice. This causes the Zr^{+4} deficiency in the pyrochlore structure, which can be seen in the bottom cube in Fig. 2-5, and it can be expressed by the model $(Zr^{+4}, RE^{+3})_2(RE^{+3}, Zr^{+4})_2(O^{-2}, Va)_6(O^{-2})_1(Va)_1$. The electroneutrality triangle is shown by the dashed line. The

pyrochlore structure with the composition of pure RE₂O₃ is denoted by **P-RE₂O₃**, and its Gibbs energy function can be derived from the equation:

$$G(\mathbf{P-RE}_2\mathbf{O}_3)$$

$$=2 \cdot \text{GRE}_2\text{O}_3\text{C} + V4 + V5T$$

$$= \frac{5}{6} {}^0G_{\text{RE}^{+3}:\text{RE}^{+3}:\text{O}^{-2}:\text{O}^{-2}:\text{Va}}^{\text{pyrochlore}} + \frac{1}{6} {}^0G_{\text{RE}^{+3}:\text{RE}^{+3}:\text{Va}:\text{O}^{-2}:\text{Va}}^{\text{pyrochlore}} + 6RT \left[\frac{5}{6} \ln \frac{5}{6} + \frac{1}{6} \ln \frac{1}{6} \right] \quad (2-53)$$

where GRE₂O₃C is the Gibbs energy function for the cubic RE₂O₃, and the V4, V5 are the parameters to be assessed. With this equation, ${}^0G_{\text{RE}^{+3}:\text{RE}^{+3}:\text{Va}:\text{O}^{-2}:\text{Va}}^{\text{pyrochlore}}$ can be determined:

$$\begin{aligned} & {}^0G_{\text{RE}^{+3}:\text{RE}^{+3}:\text{Va}:\text{O}^{-2}:\text{Va}}^{\text{pyrochlore}} \\ &= 6 \cdot G(\mathbf{P-RE}_2\mathbf{O}_3) - 5 \cdot {}^0G_{\text{RE}^{+3}:\text{RE}^{+3}:\text{O}^{-2}:\text{O}^{-2}:\text{Va}}^{\text{pyrochlore}} - 36RT \left[\frac{5}{6} \ln \frac{5}{6} + \frac{1}{6} \ln \frac{1}{6} \right] \\ &= 12 \cdot \text{GRE}_2\text{O}_3\text{C} + 6V4 + 6V5T - 5 \cdot {}^0G_{\text{RE}^{+3}:\text{RE}^{+3}:\text{O}^{-2}:\text{O}^{-2}:\text{Va}}^{\text{pyrochlore}} + 134.8548T \end{aligned} \quad (2-54)$$

Subsequently, three constraints can be made for the end members on the bottom of the composition space:

$${}^0G_{\text{Zr}^{+4}:\text{RE}^{+3}:\text{Va}:\text{O}^{-2}:\text{Va}}^{\text{pyrochlore}} + {}^0G_{\text{RE}^{+3}:\text{RE}^{+3}:\text{O}^{-2}:\text{O}^{-2}:\text{Va}}^{\text{pyrochlore}} - {}^0G_{\text{RE}^{+3}:\text{RE}^{+3}:\text{Va}:\text{O}^{-2}:\text{Va}}^{\text{pyrochlore}} - {}^0G_{\text{Zr}^{+4}:\text{RE}^{+3}:\text{O}^{-2}:\text{O}^{-2}:\text{Va}}^{\text{pyrochlore}} = \Delta G5 \quad (2-55)$$

$${}^0G_{\text{Zr}^{+4}:\text{Zr}^{+4}:\text{Va}:\text{O}^{-2}:\text{Va}}^{\text{pyrochlore}} + {}^0G_{\text{Zr}^{+4}:\text{RE}^{+3}:\text{O}^{-2}:\text{O}^{-2}:\text{Va}}^{\text{pyrochlore}} - {}^0G_{\text{Zr}^{+4}:\text{RE}^{+3}:\text{Va}:\text{O}^{-2}:\text{Va}}^{\text{pyrochlore}} - {}^0G_{\text{Zr}^{+4}:\text{Zr}^{+4}:\text{O}^{-2}:\text{O}^{-2}:\text{Va}}^{\text{pyrochlore}} = \Delta G6 \quad (2-56)$$

$${}^0G_{\text{RE}^{+3}:\text{Zr}^{+4}:\text{Va}:\text{O}^{-2}:\text{Va}}^{\text{pyrochlore}} + {}^0G_{\text{RE}^{+3}:\text{RE}^{+3}:\text{O}^{-2}:\text{O}^{-2}:\text{Va}}^{\text{pyrochlore}} - {}^0G_{\text{RE}^{+3}:\text{RE}^{+3}:\text{Va}:\text{O}^{-2}:\text{Va}}^{\text{pyrochlore}} - {}^0G_{\text{RE}^{+3}:\text{Zr}^{+4}:\text{O}^{-2}:\text{O}^{-2}:\text{Va}}^{\text{pyrochlore}} = \Delta G7 \quad (2-57)$$

(4). The model (Zr⁺⁴, RE⁺³)₂(RE⁺³, Zr⁺⁴)₂(O⁻², Va)₆(O⁻²)₁(O⁻²)₁: The oxygen deficiency in the third sublattice with the fifth sublattice occupied by oxygen.

Except the cases mentioned above, another case of electroneutrality can be reached when the vacancies enter into third sublattice partly while the fifth sublattice is fully occupied by oxygen species. This case is shown by the parallelogram which intercepts the top rectangle in the Fig. 2-5. According to the structural information, for both oxygen excess and oxygen deficiency in the pyrochlore phase, such case is not physically preferable. The following constraints are made to determine the parameters of the four end members ZRVOO, RZVOO, ZZVOO, and RRVOO:

$${}^0G_{\text{Zr}^{+4}:\text{RE}^{+3}:\text{Va}:\text{O}^{-2}:\text{O}^{-2}}^{\text{pyrochlore}} + {}^0G_{\text{Zr}^{+4}:\text{RE}^{+3}:\text{O}^{-2}:\text{O}^{-2}:\text{Va}}^{\text{pyrochlore}} - {}^0G_{\text{Zr}^{+4}:\text{RE}^{+3}:\text{O}^{-2}:\text{O}^{-2}:\text{O}^{-2}}^{\text{pyrochlore}} - {}^0G_{\text{Zr}^{+4}:\text{RE}^{+3}:\text{Va}:\text{O}^{-2}:\text{Va}}^{\text{pyrochlore}} = \Delta G8 \quad (2-58)$$

$${}^0G_{\text{Zr}^{+4}:\text{RE}^{+3}:\text{O}^{-2}:\text{O}^{-2}:\text{O}^{-2}}^{\text{pyrochlore}} + {}^0G_{\text{RE}^{+3}:\text{RE}^{+3}:\text{Va}:\text{O}^{-2}:\text{O}^{-2}}^{\text{pyrochlore}} - {}^0G_{\text{Zr}^{+4}:\text{RE}^{+3}:\text{Va}:\text{O}^{-2}:\text{O}^{-2}}^{\text{pyrochlore}} - {}^0G_{\text{RE}^{+3}:\text{RE}^{+3}:\text{O}^{-2}:\text{O}^{-2}:\text{O}^{-2}}^{\text{pyrochlore}} = \Delta G9 \quad (2-59)$$

$${}^0G_{\text{Zr}^{+4}:\text{Zr}^{+4}:\text{Va}:\text{O}^{-2}:\text{O}^{-2}}^{\text{pyrochlore}} + {}^0G_{\text{Zr}^{+4}:\text{RE}^{+3}:\text{O}^{-2}:\text{O}^{-2}:\text{O}^{-2}}^{\text{pyrochlore}} - {}^0G_{\text{Zr}^{+4}:\text{Zr}^{+4}:\text{O}^{-2}:\text{O}^{-2}:\text{O}^{-2}}^{\text{pyrochlore}} - {}^0G_{\text{Zr}^{+4}:\text{RE}^{+3}:\text{Va}:\text{O}^{-2}:\text{O}^{-2}}^{\text{pyrochlore}} = \Delta G10 \quad (2-60)$$

$${}^0G_{\text{RE}^{+3}:\text{Zr}^{+4}:\text{Va}:\text{O}^{-2}:\text{O}^{-2}}^{\text{pyrochlore}} + {}^0G_{\text{Zr}^{+4}:\text{Zr}^{+4}:\text{O}^{-2}:\text{O}^{-2}:\text{O}^{-2}}^{\text{pyrochlore}} - {}^0G_{\text{RE}^{+3}:\text{Zr}^{+4}:\text{O}^{-2}:\text{O}^{-2}:\text{O}^{-2}}^{\text{pyrochlore}} - {}^0G_{\text{Zr}^{+4}:\text{Zr}^{+4}:\text{Va}:\text{O}^{-2}:\text{O}^{-2}}^{\text{pyrochlore}} = \Delta G11 \quad (2-61)$$

For the complete description $(Zr^{+4}, RE^{+3})_2(RE^{+3}, Zr^{+4})_2(O^{-2}, Va)_6(O^{-2})_1(Va, O^{-2})_1$, the Gibbs energy of the pyrochlore phase is formulated by

$$\begin{aligned}
 G_m^{pyrochlore} = & y_{RE^{+3}}^1 y_{RE^{+3}}^2 y_{O^{-2}}^3 y_{O^{-2}}^4 y_{O^{-2}}^5 {}^0 G_{RE^{+3}:RE^{+3}:O^{-2}:O^{-2}:O^{-2}}^{pyrochlore} + y_{RE^{+3}}^1 y_{RE^{+3}}^2 y_{O^{-2}}^3 y_{O^{-2}}^4 y_{Va}^5 {}^0 G_{RE^{+3}:RE^{+3}:O^{-2}:O^{-2}:Va}^{pyrochlore} + \\
 & y_{RE^{+3}}^1 y_{RE^{+3}}^2 y_{Va}^3 y_{O^{-2}}^4 y_{O^{-2}}^5 {}^0 G_{RE^{+3}:RE^{+3}:Va:O^{-2}:O^{-2}}^{pyrochlore} + y_{RE^{+3}}^1 y_{RE^{+3}}^2 y_{RE^{+3}}^3 y_{O^{-2}}^4 y_{Va}^5 {}^0 G_{RE^{+3}:RE^{+3}:Va:O^{-2}:Va}^{pyrochlore} + \\
 & y_{RE^{+3}}^1 y_{Zr^{+4}}^2 y_{O^{-2}}^3 y_{O^{-2}}^4 y_{O^{-2}}^5 {}^0 G_{RE^{+3}:Zr^{+4}:O^{-2}:O^{-2}:O^{-2}}^{pyrochlore} + y_{RE^{+3}}^1 y_{Zr^{+4}}^2 y_{O^{-2}}^3 y_{O^{-2}}^4 y_{Va}^5 {}^0 G_{RE^{+3}:Zr^{+4}:O^{-2}:O^{-2}:Va}^{pyrochlore} + \\
 & y_{RE^{+3}}^1 y_{Zr^{+4}}^2 y_{Va}^3 y_{O^{-2}}^4 y_{O^{-2}}^5 {}^0 G_{RE^{+3}:Zr^{+4}:Va:O^{-2}:O^{-2}}^{pyrochlore} + y_{RE^{+3}}^1 y_{Zr^{+4}}^2 y_{Zr^{+4}}^3 y_{O^{-2}}^4 y_{Va}^5 {}^0 G_{RE^{+3}:Zr^{+4}:Va:O^{-2}:Va}^{pyrochlore} + \\
 & y_{Zr^{+4}}^1 y_{RE^{+3}}^2 y_{O^{-2}}^3 y_{O^{-2}}^4 y_{O^{-2}}^5 {}^0 G_{Zr^{+4}:RE^{+3}:O^{-2}:O^{-2}:O^{-2}}^{pyrochlore} + y_{Zr^{+4}}^1 y_{RE^{+3}}^2 y_{O^{-2}}^3 y_{O^{-2}}^4 y_{Va}^5 {}^0 G_{Zr^{+4}:RE^{+3}:O^{-2}:O^{-2}:Va}^{pyrochlore} + \\
 & y_{Zr^{+4}}^1 y_{RE^{+3}}^2 y_{Va}^3 y_{O^{-2}}^4 y_{O^{-2}}^5 {}^0 G_{Zr^{+4}:RE^{+3}:Va:O^{-2}:O^{-2}}^{pyrochlore} + y_{Zr^{+4}}^1 y_{RE^{+3}}^2 y_{Va}^3 y_{O^{-2}}^4 y_{Va}^5 {}^0 G_{Zr^{+4}:RE^{+3}:Va:O^{-2}:Va}^{pyrochlore} + \\
 & y_{Zr^{+4}}^1 y_{Zr^{+4}}^2 y_{O^{-2}}^3 y_{O^{-2}}^4 y_{O^{-2}}^5 {}^0 G_{Zr^{+4}:Zr^{+4}:O^{-2}:O^{-2}:O^{-2}}^{pyrochlore} + y_{Zr^{+4}}^1 y_{Zr^{+4}}^2 y_{O^{-2}}^3 y_{O^{-2}}^4 y_{Va}^5 {}^0 G_{Zr^{+4}:Zr^{+4}:O^{-2}:O^{-2}:Va}^{pyrochlore} + \\
 & y_{Zr^{+4}}^1 y_{Zr^{+4}}^2 y_{Va}^3 y_{O^{-2}}^4 y_{O^{-2}}^5 {}^0 G_{Zr^{+4}:Zr^{+4}:Va:O^{-2}:O^{-2}}^{pyrochlore} + y_{Zr^{+4}}^1 y_{Zr^{+4}}^2 y_{Va}^3 y_{O^{-2}}^4 y_{Va}^5 {}^0 G_{Zr^{+4}:Zr^{+4}:Va:O^{-2}:Va}^{pyrochlore} + \\
 & 2RT(y_{RE^{+3}}^1 \ln y_{RE^{+3}}^1 + y_{Zr^{+4}}^1 \ln y_{Zr^{+4}}^1) + 2RT(y_{Zr^{+4}}^2 \ln y_{Zr^{+4}}^2 + y_{RE^{+3}}^2 \ln y_{RE^{+3}}^2) \\
 & + 6RT(y_{O^{-2}}^3 \ln y_{O^{-2}}^3 + y_{Va}^3 \ln y_{Va}^3) + RT(y_{Va}^5 \ln y_{Va}^5 + y_{O^{-2}}^5 \ln y_{O^{-2}}^5) + \\
 & E G_m^{pyrochlore}
 \end{aligned} \tag{2-62}$$

where y_j^n represents the site fraction of species j in the sublattice n , and ${}^0 G_{a:b:c:d:e}^{pyrochlore}$ are the Gibbs energies of the end members of this model. Totally there are 16 combinations, which are determined so far in the previous steps. The excess Gibbs energy $E G_m^{pyrochlore}$ is set to be zero in the present optimization, to avoid too many independent adjustable parameters for such a complicated model.

2.3.8.2. The splitting model $(Zr^{+4}, RE^{+3})_2(RE^{+3}, Zr^{+4})_2(O^{-2}, Va)_8$

According to the suggestion by I. Ansara et al. [1988Ans], a splitting model can be applied for both disordered and ordered phases, by dividing the Gibbs energy into contributions of a disordered and an ordered states by the following equation:

$$G_m^\Phi = G_m^\phi(x_i) + \Delta G_m^{ord}(y_i^s) \tag{2-63}$$

in which $G_m^\phi(x_i)$ is the Gibbs energy of the disordered phase ϕ , and $\Delta G_m^{ord}(y_i^s)$ is the Gibbs energy part contributed by the ordering of sublattices, which is given by the equation:

$$\Delta G_m^{ord}(y_i^s) = G_m(y_i^s) - G_m(y_i^s = x_i) \tag{2-64}$$

where $G_m(y_i^s = x_i)$ represents the disordered part which is corresponding to the case that the site fraction of species i in sublattice s is equal to the mole fraction x_i . As long as the $y_i^s \neq x_i$, the phase becomes ordered, and then its Gibbs energy is expressed by $G_m(y_i^s)$, so that the

Gibbs energy difference $\Delta G_m^{ord}(y_i^s)$ in (2-64) is the Gibbs energy of ordering with respect to the disordered state. Finally, the Gibbs energy can be represented by the equation:

$$\begin{aligned}
 G_m^{pyrochlore} = & y_{RE^{+3}} y_{RE^{+3}} y_{O^{2-}} {}^0 G_{RE^{+3}, RE^{+3}, O^{2-}}^{pyrochlore} + y_{Zr^{+4}} y_{RE^{+3}} y_{O^{2-}} {}^0 G_{Zr^{+4}, RE^{+3}, O^{2-}}^{pyrochlore} \\
 & + y_{RE^{+3}} y_{Zr^{+4}} y_{O^{2-}} {}^0 G_{RE^{+3}, Zr^{+4}, O^{2-}}^{pyrochlore} + y_{Zr^{+4}} y_{Zr^{+4}} y_{O^{2-}} {}^0 G_{Zr^{+4}, Zr^{+4}, O^{2-}}^{pyrochlore} + \\
 & y_{RE^{+3}} y_{RE^{+3}} y_{Va} {}^0 G_{RE^{+3}, RE^{+3}, Va}^{pyrochlore} + y_{Zr^{+4}} y_{RE^{+3}} y_{Va} {}^0 G_{Zr^{+4}, RE^{+3}, Va}^{pyrochlore} \\
 & + y_{RE^{+3}} y_{Zr^{+4}} y_{Va} {}^0 G_{RE^{+3}, Zr^{+4}, Va}^{pyrochlore} + y_{Zr^{+4}} y_{Zr^{+4}} y_{Va} {}^0 G_{Zr^{+4}, Zr^{+4}, Va}^{pyrochlore} + \\
 & + 2RT(y_{RE^{+3}} \ln y_{RE^{+3}} + y_{Zr^{+4}} \ln y_{Zr^{+4}}) + 2RT(y_{Zr^{+4}} \ln y_{Zr^{+4}} + y_{RE^{+3}} \ln y_{RE^{+3}}) \\
 & + 8RT(y_{O^{2-}} \ln y_{O^{2-}} + y_{Va} \ln y_{Va}) + {}^E G_m^{pyrochlore}
 \end{aligned} \tag{2-65}$$

where ${}^0 G_{a:b:c}^{pyrochlore}$ denotes the Gibbs energy of end members, and y is the site fraction of constituent in a certain sublattice. ${}^E G_m^{pyrochlore}$ is the excess Gibbs energy, which can be given by the equation:

$$\begin{aligned}
 {}^E G_m^{pyrochlore} = & y_{RE^{+3}}^1 y_{Zr^{+4}}^1 y_{Zr^{+4}}^2 y_{O^{2-}}^3 L_{RE^{+3}, Zr^{+4}, Zr^{+4}, O^{2-}} + y_{RE^{+3}}^1 y_{Zr^{+4}}^1 y_{RE^{+3}}^2 y_{O^{2-}}^3 L_{RE^{+3}, Zr^{+4}, RE^{+3}, O^{2-}} \\
 & + y_{RE^{+3}}^1 y_{Zr^{+4}}^1 y_{Zr^{+4}}^2 y_{Va}^3 L_{RE^{+3}, Zr^{+4}, Zr^{+4}, Va} + y_{RE^{+3}}^1 y_{Zr^{+4}}^1 y_{RE^{+3}}^2 y_{Va}^3 L_{RE^{+3}, Zr^{+4}, RE^{+3}, Va} \\
 & + y_{RE^{+3}}^1 y_{Zr^{+4}}^2 y_{RE^{+3}}^2 y_{O^{2-}}^3 L_{RE^{+3}, Zr^{+4}, RE^{+3}, O^{2-}} + y_{Zr^{+4}}^1 y_{Zr^{+4}}^2 y_{RE^{+3}}^2 y_{O^{2-}}^3 L_{Zr^{+4}, Zr^{+4}, RE^{+3}, O^{2-}} \\
 & + y_{RE^{+3}}^1 y_{Zr^{+4}}^2 y_{RE^{+3}}^2 y_{Va}^3 L_{RE^{+3}, Zr^{+4}, RE^{+3}, Va} + y_{Zr^{+4}}^1 y_{Zr^{+4}}^2 y_{RE^{+3}}^2 y_{Va}^3 L_{Zr^{+4}, Zr^{+4}, RE^{+3}, Va} \\
 & + y_{RE^{+3}}^1 y_{Zr^{+4}}^2 y_{O^{2-}}^3 y_{Va}^3 L_{RE^{+3}, Zr^{+4}, O^{2-}, Va} + y_{Zr^{+4}}^1 y_{Zr^{+4}}^2 y_{O^{2-}}^3 y_{Va}^3 L_{Zr^{+4}, Zr^{+4}, O^{2-}, Va} \\
 & + y_{RE^{+3}}^1 y_{RE^{+3}}^2 y_{O^{2-}}^3 y_{Va}^3 L_{RE^{+3}, RE^{+3}, O^{2-}, Va} + y_{Zr^{+4}}^1 y_{RE^{+3}}^2 y_{O^{2-}}^3 y_{Va}^3 L_{Zr^{+4}, RE^{+3}, O^{2-}, Va} \\
 & + y_{RE^{+3}}^1 y_{Zr^{+4}}^1 y_{Zr^{+4}}^2 y_{RE^{+3}}^2 y_{O^{2-}}^3 L_{RE^{+3}, Zr^{+4}, Zr^{+4}, RE^{+3}, O^{2-}} \\
 & + y_{RE^{+3}}^1 y_{Zr^{+4}}^1 y_{Zr^{+4}}^2 y_{RE^{+3}}^2 y_{Va}^3 L_{RE^{+3}, Zr^{+4}, Zr^{+4}, RE^{+3}, Va}
 \end{aligned} \tag{2-66}$$

in which y_j^n means the site fraction of species j in the sublattice n , and L are the interaction parameters. When $y_{Zr^{+4}}^1 = y_{Zr^{+4}}^2 = x_{Zr^{+4}}$, the pyrochlore phase is completely disordered into the fluorite structure, and its Gibbs energy can be expressed by the equation (2-24). It must be emphasized that the contribution by the disordering should be subtracted from the $G_m^{pyrochlore}$ and ${}^E G_m^{pyrochlore}$ in above equations.

The model thus works with two splitting parts, in which one part describes the disordered state, and another part describes the ordered part. Because the disordering can always be stable before ordering occurs, a constraint must be made so that the Gibbs energy surface always has a minimum at the composition where $y_{Zr^{+4}}^1 = y_{Zr^{+4}}^2 = x_{Zr^{+4}}$ when the first and second sublattices merge into a single one. This constraint can be realized when the derivative of the $G_m^{pyrochlore}$ with respect to the $y_{Zr^{+4}}^1$ or $y_{Zr^{+4}}^2$ is zero:

$$\left[dG = \frac{\partial G}{\partial y_{Zr^{+4}}^1} dy_{Zr^{+4}}^1 + \frac{\partial G}{\partial y_{Zr^{+4}}^2} dy_{Zr^{+4}}^2 \right]_{x_{Zr^{+4}}} = 0 \quad (2-67)$$

By using suitable mathematical software and taking the relationship $dx_{Zr^{+4}} = dy_{Zr^{+4}}^1 + dy_{Zr^{+4}}^2 = 0$ into account, the above equation can be solved to find the relations of different parameters. Generally, there are many solutions which can fit this equation, thus some assumptions are necessary. In this work, the final constraints are given as follows:

$${}^0G_{Zr^{+4};RE^{+3};O^{-2}}^{pyrochlore} = u1 \quad {}^0G_{RE^{+3};Zr^{+4};O^{-2}}^{pyrochlore} = u2$$

$${}^0G_{Zr^{+4};RE^{+3};Va}^{pyrochlore} = u3 \quad {}^0G_{RE^{+3};Zr^{+4};Va}^{pyrochlore} = u4$$

$$L_{Zr^{+4};Zr^{+4};RE^{+3};O^{-2}} = L_{Zr^{+4};Zr^{+4};RE^{+3};Va} = L_{RE^{+3};Zr^{+4};RE^{+3};O^{-2}} = L_{RE^{+3};Zr^{+4};RE^{+3};Va} = u5$$

$$L_{RE^{+3};Zr^{+4};O^{-2};Va} = L_{Zr^{+4};Zr^{+4};O^{-2};Va} = L_{RE^{+3};RE^{+3};O^{-2};Va} = L_{Zr^{+4};RE^{+3};O^{-2};Va} = u6$$

$$L_{Zr^{+4};RE^{+3};RE^{+3};Zr^{+4};O^{-2}} = L_{Zr^{+4};RE^{+3};RE^{+3};Zr^{+4};Va} = u7$$

$$L_{Zr^{+4};RE^{+3};Zr^{+4};O^{-2}} = u5 + u1 - u2$$

$$L_{Zr^{+4};RE^{+3};Zr^{+4};Va} = u5 + (8u1 - 8u2 + u3 - u4)$$

$$L_{Zr^{+4};RE^{+3};RE^{+3};O^{-2}} = u5 + (-5u1 + 5u2 - u3 + u4)/2$$

$$L_{Zr^{+4};RE^{+3};RE^{+3};Va} = u5 + (9u1 - 9u2 + u3 - u4)/2$$

where $u1-u7$ are the parameters to be evaluated from experimental data. Further assumptions are $u1 = u2 = u3 = u4$ to simplify the modeling in case of very limited experimental information, and $u6$ and $u7$ are set to be zero since they are not related to the other parameters.

2.3.9. The $RE_4Zr_3O_{12}$ (δ) phase

The δ phase is also a kind of ordered superstructures of fluorite at low temperatures when the ionic radius of the doping element RE^{+3} is smaller than that of Dy^{+3} [1991Red]. The crystal structure of this phase has been described in literature [1970Tho, 1976Ros, 1977Sco, 2002Lop]. It can be derived from the defective fluorite structure by the ordering of oxygen vacancies to produce a rhombohedral cell. There are two different cation positions: one is the single site at the origin which is octahedrally coordinated with anions, and another are the six equivalent sites which are coordinated by anions on seven of the eight vertices of a slightly distorted cube. For the ideally ordered δ phase, the position $3a$ is fully occupied by Zr^{+4} , and the other cationic sites $18f$ are occupied by RE^{+3} ions and the residual Zr^{+4} ions, while the

oxygen ions occupy two anion *18f* positions. The anion vacancies are on the position of *6c* according to the references [1976Ros, 1991Red].

Based on crystal structure information, in this work the δ phase is described with the four-sublattice model $(Zr^{+4})_1(RE^{+3}, Zr^{+4})_6(O^{-2}, Va)_{12}(Va, O^{-2})_2$ and its Gibbs energy function of δ phase is given by:

$$\begin{aligned}
 G_m^\delta = & y_{Zr^{+4}}^1 y_{RE^{+3}}^2 y_{O^{-2}}^3 y_{O^{-2}}^4 {}^0G_{Zr^{+4};RE^{+3};O^{-2};O^{-2}}^\delta + y_{Zr^{+4}}^1 y_{Zr^{+4}}^2 y_{O^{-2}}^3 y_{O^{-2}}^4 {}^0G_{Zr^{+4};Zr^{+4};O^{-2};O^{-2}}^\delta \\
 & + y_{Zr^{+4}}^1 y_{RE^{+3}}^2 y_{O^{-2}}^3 y_{Va}^4 {}^0G_{Zr^{+4};RE^{+3};O^{-2};Va}^\delta + y_{Zr^{+4}}^1 y_{Zr^{+4}}^2 y_{O^{-2}}^3 y_{Va}^4 {}^0G_{Zr^{+4};Zr^{+4};O^{-2};Va}^\delta \\
 & + y_{Zr^{+4}}^1 y_{RE^{+3}}^2 y_{Va}^3 y_{O^{-2}}^4 {}^0G_{Zr^{+4};RE^{+3};Va;O^{-2}}^\delta + y_{Zr^{+4}}^1 y_{Zr^{+4}}^2 y_{Va}^3 y_{O^{-2}}^4 {}^0G_{Zr^{+4};Zr^{+4};Va;O^{-2}}^\delta \\
 & + y_{Zr^{+4}}^1 y_{RE^{+3}}^2 y_{Va}^3 y_{Va}^4 {}^0G_{Zr^{+4};RE^{+3};Va;Va}^\delta + y_{Zr^{+4}}^1 y_{Zr^{+4}}^2 y_{Va}^3 y_{Va}^4 {}^0G_{Zr^{+4};Zr^{+4};Va;Va}^\delta \\
 & + 6RT(y_{RE^{+3}}^2 \ln y_{RE^{+3}}^2 + y_{Zr^{+4}}^2 \ln y_{Zr^{+4}}^2) + 12RT(y_{O^{-2}}^3 \ln y_{O^{-2}}^3 + y_{Va}^3 \ln y_{Va}^3) \\
 & + 2RT(y_{O^{-2}}^4 \ln y_{O^{-2}}^4 + y_{Va}^4 \ln y_{Va}^4) + {}^E G_m^\delta
 \end{aligned} \tag{2-68}$$

where y_j^n means the site fraction of the species j in the sublattice n . ${}^0G_{a:b:c:d}^\delta$ is the Gibbs energy of the end member. The excess Gibbs energy ${}^E G_m^\delta$ is simply set to zero in this work, because the available thermodynamic data are scarce.

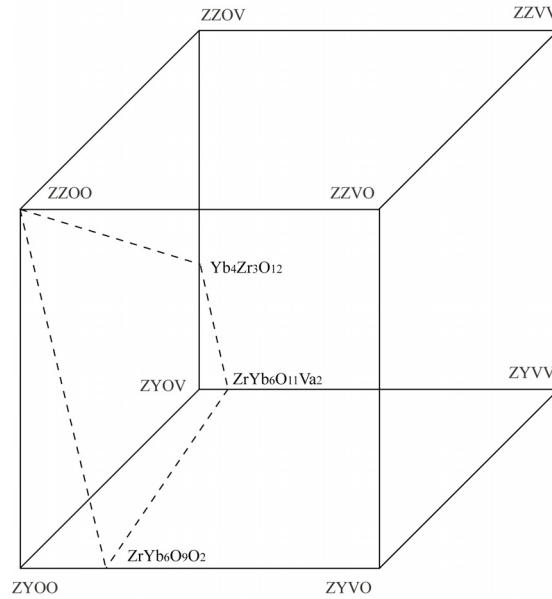


Figure 2-6. The composition space for the model of δ ($Yb_4Zr_3O_{12}$). The dashed plane represents the compositional possibilities with the electroneutrality (Y, Z, O, V denote the species Yb^{+3} , Zr^{+4} , O^{-2} , and Va.).

Fig. 2-6 gives the composition space for the δ phase, and the combinations with the electroneutrality are shown by the dashed plane, where $Yb_4Zr_3O_{12}$ is the stable phase, and $ZrYb_6O_{11}Va_2$ and $ZrYb_6O_9O_2$ are two compounds with oxygen deficiency. According to the

structural information, the oxygen species prefer the third sublattice, and $ZrYb_6O_9O_2$ will be less stable than the compound $ZrYb_6O_{11}Va_2$, thus the nonstoichiometry can be reached by changing the compositions along the lines $ZZOO-Yb_4Zr_3O_{12}$ and $Yb_4Zr_3O_{12}-ZrYb_6O_{11}Va_2$. Totally there are eight end members in this model. The Gibbs energies of $ZZOO$, $ZZOV$ and the compounds $Yb_4Zr_3O_{12}$ and $ZrYb_6O_{11}Va_2$ can be as:

$${}^0G_{Zr^{+4},Zr^{+4},O^{-2},O^{-2}}^{\delta} = 7 \cdot GZRO2F + V6 + V7T \quad (2-69)$$

$${}^0G_{Zr^{+4},Zr^{+4},O^{-2},Va}^{\delta} = 7 \cdot GZRO2F - 2 \cdot GHSEROO + V6 + V7T \quad (2-70)$$

$$G(Yb_4Zr_3O_{12}) = 2 \cdot GYB2O3C + 3 \cdot GZRO2F + V8 + V9T \quad (2-71)$$

$$G(ZrYb_6O_{11}Va_2) = 3 \cdot GYB2O3C + GZRO2F + V10 + V11T \quad (2-72)$$

where $V6$ to $V11$ are the parameters to be determined from the experimental data.

Accordingly, the Gibbs energies of the end members ${}^0G_{Zr^{+4},Yb^{+3},O^{-2},Va}^{\delta}$ (ZYOV) and

${}^0G_{Zr^{+4},Yb^{+3},Va}^{\delta}$ (ZYVV) are derived by the following equations:

$$G(Yb_4Zr_3O_{12}) = \frac{2}{3} {}^0G_{Zr^{+4},Yb^{+3},O^{-2},Va}^{\delta} + \frac{1}{3} {}^0G_{Zr^{+4},Zr^{+4},O^{-2},Va}^{\delta} + 6RT \left[\frac{2}{3} \ln \frac{2}{3} + \frac{1}{3} \ln \frac{1}{3} \right] \quad (2-73)$$

$$G(ZrYb_6O_{11}Va_2) = \frac{11}{12} {}^0G_{Zr^{+4},Yb^{+3},O^{-2},Va}^{\delta} + \frac{1}{12} {}^0G_{Zr^{+4},Yb^{+3},Va}^{\delta} + 12RT \left[\frac{11}{12} \ln \frac{11}{12} + \frac{1}{12} \ln \frac{1}{12} \right] \quad (2-74)$$

and the following relations are obtained:

$${}^0G_{Zr^{+4},Yb^{+3},O^{-2},Va}^{\delta} = 1.5 \cdot G(Yb_4Zr_3O_{12}) - 0.5 \cdot {}^0G_{Zr^{+4},Zr^{+4},O^{-2},Va}^{\delta} + 47.6278T \quad (2-75)$$

$${}^0G_{Zr^{+4},Yb^{+3},Va}^{\delta} = 12 \cdot G(ZrYb_6O_{11}Va_2) - 11 \cdot {}^0G_{Zr^{+4},Yb^{+3},O^{-2},Va}^{\delta} + 343.4046T \quad (2-76)$$

To determine the Gibbs energies of other four end members, four independent reciprocal reactions are given:

$${}^0G_{Zr^{+4},Zr^{+4},O^{-2},O^{-2}}^{\delta} + {}^0G_{Zr^{+4},Yb^{+3},O^{-2},Va}^{\delta} - {}^0G_{Zr^{+4},Zr^{+4},O^{-2},Va}^{\delta} - {}^0G_{Zr^{+4},Yb^{+3},O^{-2},O^{-2}}^{\delta} = \Delta G_a \quad (2-77)$$

$${}^0G_{Zr^{+4},Zr^{+4},O^{-2},Va}^{\delta} + {}^0G_{Zr^{+4},Yb^{+3},Va}^{\delta} - {}^0G_{Zr^{+4},Yb^{+3},O^{-2},Va}^{\delta} - {}^0G_{Zr^{+4},Zr^{+4},Va}^{\delta} = \Delta G_b \quad (2-78)$$

$${}^0G_{Zr^{+4},Zr^{+4},O^{-2},O^{-2}}^{\delta} + {}^0G_{Zr^{+4},Zr^{+4},Va}^{\delta} - {}^0G_{Zr^{+4},Zr^{+4},O^{-2},Va}^{\delta} - {}^0G_{Zr^{+4},Zr^{+4},O^{-2}}^{\delta} = \Delta G_c \quad (2-79)$$

$${}^0G_{Zr^{+4},Zr^{+4},Va}^{\delta} + {}^0G_{Zr^{+4},Yb^{+3},O^{-2},O^{-2}}^{\delta} - {}^0G_{Zr^{+4},Zr^{+4},O^{-2},O^{-2}}^{\delta} - {}^0G_{Zr^{+4},Yb^{+3},Va}^{\delta} = \Delta G_d \quad (2-80)$$

in which ΔG_a , ΔG_b , ΔG_c and ΔG_d are the reciprocal energies of the independent reactions, which are determined by the phase equilibria data concerning the δ phase. Finally, the Gibbs energies of all end members can be solved from the above equations.

Chapter 3

Experimental study and thermodynamic modeling of the Zr – O, Hf – O and ZrO₂ – HfO₂ systems

3.1. Literature review

3.1.1. The Zr – O system

A detailed review of the experimental phase equilibria and thermodynamic information for the Zr – O system was given by Abriata et al. [1986Abr].

According to the assessment [1986Abr], only one stable oxide i.e. zirconium dioxide (ZrO₂) exists in this system. A compilation of the literature information on the polymorphic transformations of ZrO₂ is given in Table 3-1. As indicated above, ZrO₂ has a monoclinic (M) structure below 1478 K, where it transforms into the intermediate tetragonal (T) structure, and at its stoichiometric composition at about 2650 K into cubic fluorite-type (F) modification. At sub-stoichiometric compositions the cubic modification is stable down to 1798 K at its eutectoid decomposition into the hcp solution of O in Zr and the tetragonal modification. The cubic phase was reported to melt congruently at about 2983 K. There is a eutectic reaction liquid \Leftrightarrow hcp-Zr + F at about 2338 K, 40 at.% O. The homogeneity range of the hcp solid solution of Zr extends to 35 at.% O. It reveals a congruent melting point at 2583 K, 25 at.% O, and is stable down to room temperature. A lower oxygen content the bcc structure will be formed by a peritectic reaction (liquid + hcp-Zr \Leftrightarrow bcc-Zr) at about 2243 K and 10 at.% O. Furthermore, many experimental investigations indicate that several ordered phases can exist at low temperature in the hcp-Zr phase region [1973Cla, 1974Hir, 1995Tsu1].

After the assessment by Abriata et al. [1986Abr], very few experimental works about the phase equilibria were reported, and only some experimental determinations of thermodynamic properties were published [1990Nev, 1995Tsu2, 1999Toj, 2003Deg, 2005Nav1, 2006Mor].

The temperature of the M \leftrightarrow T structural transformation has extensively been studied in the literature. There are large discrepancies, due to the experimental difficulties from martensitic nature of the M \leftrightarrow T transformation, and some other factors such as impurities in samples, the particle size of the powder, the experimental techniques, and the errors in experiments. In Table 3-1, the literature data obtained by thermal analysis, high-temperature X-ray diffraction, dilatometry and some other methods are compiled. The enthalpy of M \leftrightarrow T transformation was studied by [1950Cou, 1965Tsa, 1966Kir, 1979Che, 1995Yas, 2001Jer,

2003Sur, 2006Mor]. The value of $5941 \text{ J}\cdot\text{mol}^{-1}$, which was determined by [1950Cou], was accepted in the review work of Ackerman et al. [1975Ack]. Tsagareishvili and Gvelesiani [1965Tsa] reported a value of $5272 \text{ J}\cdot\text{mol}^{-1}$ at 1475 K. Subsequently, Kirillin et al. [1966Kir] and Chekhovskoi et al. [1979Che] reported the values of $7763 \text{ J}\cdot\text{mol}^{-1}$ and $8297 \text{ J}\cdot\text{mol}^{-1}$, respectively, which were higher than previous data. Yashima et al. [1995Yas] measured this enthalpy of transformation by DSC as $5640 \text{ J}\cdot\text{mol}^{-1}$ and evaluated the entropy of transformation as $4.07 \text{ J}\cdot\text{mol}^{-1}\cdot\text{K}^{-1}$ at around 1395 K. By using DTA method, Jerebtsov et al. [2001Jer] determined the enthalpy of $M \leftrightarrow T$ transformation in their experimental studies of phase diagram involving ZrO_2 systems, and obtained the value of $5175.24 \pm 616.1 \text{ J}\cdot\text{mol}^{-1}$ at about 1435 K. Suresh et al. [2003Sur] determined the enthalpy of $M \leftrightarrow T$ transformation for the ZrO_2 powder with different crystallite sizes, and obtained a plateau value of around $4313 \text{ J}\cdot\text{mol}^{-1}$ when the crystallite size was beyond 150 nm. This value was accepted in their work as the volumetric heat of transformation (ΔH_{vol}) although the reported temperature of the transformation was only 1286 K. Very recently, [2006Mor] carried out the measurement between 1000-1700 K by DSC. The determined enthalpy and entropy of the $M \leftrightarrow T$ transformation in their work were $5430 \pm 310 \text{ J}\cdot\text{mol}^{-1}$ and $3.69 \pm 0.21 \text{ J}\cdot\text{mol}^{-1}\cdot\text{K}^{-1}$, respectively, while the transformation occurred in the temperature range 1460~1480 K on heating, and in the temperature range 1325~1305 K on cooling.

The enthalpies of formation of cubic yttria-stabilized zirconia with different compositions were measured by high temperature solution calorimetry and oxide melt solution calorimetry [1998Mol, 2003Lee]. The enthalpy of $M \leftrightarrow F$ transformation was then extrapolated to be $13500 \pm 2200 \text{ J}\cdot\text{mol}^{-1}$ at 1043 K and $9700 \pm 1100 \text{ J}\cdot\text{mol}^{-1}$ at 973 K, respectively. However, Lee et al. [2003Lee] also got a modified result $9200 \pm 1200 \text{ J}\cdot\text{mol}^{-1}$ at 1043 K by using the original experimental data of [1998Mol]. Since there are no other experimental data available, the reliability of their extrapolated results cannot be assessed.

The literature data on the temperature of the $T \leftrightarrow F$ transformation are also included in the Table 3-1. Ackermann et al. [1975Ack] evaluated a value of $5564 \text{ J}\cdot\text{mol}^{-1}$ for the enthalpy of transformation, and the entropy of transition as $2.09 \text{ J}\cdot\text{mol}^{-1}\cdot\text{K}^{-1}$. [2005Nav1] measured the temperature and enthalpy for the $T \leftrightarrow F$ phase transformation by high temperature calorimeter in the temperature range 2000-2400°C, with the results of $2584 \pm 15 \text{ K}$, and $3400 \pm 3100 \text{ J}\cdot\text{mol}^{-1}$.

The melting point was reported by many groups (Table 3-1). Owing to the experimental uncertainties at such high temperatures, the data show some disagreement. Most of the authors accepted the value 2983 K or 2950 K. No any experimental data exist on the

enthalpy of $F \leftrightarrow L$ transformation. The assessed value given in JANAF compilation [1971JAN] is $87027 \text{ J}\cdot\text{mol}^{-1}$.

Many works contributed to the determination of the heat content of zirconia in a wide temperature range [1950Cou, 1950Art, 1963Pea, 1965Tsa1, 1966Kir, 1979Che]. The heat capacities were studied by [1950Art, 1990Nev, 1999Toj, 2001Tan, 2003Deg, 2006Mor].

The data of enthalpy of formation, entropy, and heat capacity of monoclinic ZrO_2 at 298 K reported in literature are compiled in Table 3-2.

Several groups contributed to the thermodynamic modeling of the Zr – O system due to its practical significance in the past several years [1998Che, 2001Lia, 2002Arr, 2004Che, 2004Chen, 2004Sun]. In these studies, however, various thermodynamic models, especially for the cubic zirconia were adopted, and so were the parameters for stoichiometric zirconia. The Gibbs energy parameters of ZrO_2 were reported in several papers [1992Du, 1998Che, 2001Lia, 2002Arr, 2004Chen]. Their data on the critical transformation temperatures, enthalpies, and entropies are also compiled in Table 3-1 and Table 3-2.

The different models so far used for the Zr – O system are summarized in Table 3-3.

Chevalier and Fischer [1998Che] adopted for the liquid an associate solution model (O, ZrO_2 , Zr), and for the cubic ZrO_2 phase a two-sublattice model $(\text{Zr},\text{Va})(\text{O},\text{Va})_2$ in their assessment of the Zr – O system. The calculated phase diagram shows poor agreement with the experimental data. Very recently, they published an improved assessment [2004Che]. A better agreement between the experimental and calculated phase diagram was obtained. A revised model $(\text{Zr})(\text{O},\text{Va})_2(\text{Va},\text{O})$ was applied to the cubic zirconia.

Liang and co-workers [2001Lia] described the high temperature cubic ZrO_2 also with the two-sublattice model $(\text{Zr})(\text{O},\text{Va})_2$. For the liquid phase they used the partial ionic sublattice model $(\text{Zr}^{+4})_P(\text{O}^{-2},\text{Va},\text{O})_Q$, where P and Q are the site numbers of cation and anion sublattices, respectively. The oxygen and vacancy species can be neutrally substituted under the assumption of the model for cubic zirconia phase. The ordering of hcp-Zr phase at low temperature was taken into account in their description with the model $\text{Zr}_6(\text{O},\text{Va})_2(\text{Va},\text{O})_2$.

Arroyave and co-workers [2002Arr] treated the cubic ZrO_2 as pure ionic compound with the sublattice model $(\text{Zr}^{+4})(\text{O}^{-2},\text{Va}^{-2})_2$. However, this model is actually identical to that of reference [2001Lia], due to introducing the charged vacancy. The calculated bcc-Zr / bcc-Zr + hcp-Zr phase boundary shows large disagreement with the experimental data and the bcc phase is stable in the temperature range 4400-5000 K, and a broad gas + liquid two-phase region is presented compared with the result of Liang et al. [2001Lia].

A very recent work on this system is done by Chen and co-workers [2004Chen]. The authors introduced a neutral Zr species into the cation sublattice to obtain the electroneutrality with the model $(\text{Zr}, \text{Zr}^{+4})(\text{O}^{-2}, \text{Va})_2$. The phase diagram agrees well with most of the experimental data except small deviation between experimental and calculated F / F + hcp-Zr phase boundary at the temperatures near the eutectoid point of reaction $\text{F} \Leftrightarrow \text{hcp-Zr} + \text{T}$, and a higher congruent melting point obviously deviating from stoichiometric composition is obtained for the cubic ZrO_2 in comparison with the results of [2001Lia] and [2002Arr].

Sundman [2004Sun] recently modified the description of [2001Lia] in his work on the Zr – U – O system, by keeping all the parameters of [2002Lia], except that the cubic ZrO_2 was described with the model $(\text{Zr}^{+2}, \text{Zr}^{+4})(\text{O}^{-2}, \text{Va})_2$. The calculated phase diagram is very similar to that of [2001Lia].

3.1.2. The Hf – O system

The phase diagram of the Hf – O system was first established by Rudy and Stecher [1963Rud] by means of XRD, metallographic method and thermal analysis. Two eutectic reactions involving liquid phase were determined at high temperatures: liquid \Leftrightarrow bcc-Hf + hcp-Hf at $2000 \pm 30^\circ\text{C}$, and liquid \Leftrightarrow hcp-Hf + F (cubic fluorite-type HfO_2) at $2180 \pm 40^\circ\text{C}$, while the hcp-Hf phase melted at $2300 \pm 20^\circ\text{C}$ congruently. The temperature of the transition between the monoclinic and tetragonal phase was measured at around 1700°C . The solubility of oxygen in hcp-Hf extends to around 20 at.%.

[1965Dom] contributed to the phase equilibria study on this system later. They obtained 2500°C for the melting point of the hcp-Hf phase which was 200°C higher than the result of [1963Rud]. Moreover, the invariant reaction in the hafnium-rich part was reported as peritectic at 2250°C , while the temperature of 2200°C for the reaction liquid \Leftrightarrow hcp-Hf + F was quite consistent with the previous result.

In the later work [1973Ruh], the reaction of cubic F \Leftrightarrow hcp-Hf + T (tetragonal HfO_2) was carefully determined at 2125°C , which was very close to the temperature of the reaction liquid \Leftrightarrow hcp-Hf + F. The maximum oxygen deficiency was measured to be around 64 at.% in cubic HfO_2 .

Subsequently, [1976Rud] studied phase relation in the Hf-rich region. The reported solubility of oxygen in hcp-Hf was 20 at.% up to 2000°C , and that in bcc-Hf was less than 5 at.%. The temperature for the reaction liquid \Leftrightarrow hcp-Hf + F is $2100 \pm 20^\circ\text{C}$ according to their work.

In the hafnium-rich part, there are some reports concerning the ordering of the hcp-Hf phase at low temperatures. [1972Hir, 1973Hir] found the order-disorder transformations near the compositions $\text{HfO}_{1/6}$ by neutron diffraction, while [1995Kat1, 1997Kat] determined the temperatures of order-disorder transition by means of the low-temperature heat capacity measurements.

HfO_2 and ZrO_2 are thought as twin oxides, for their similarities in structural modifications, lattice constants, chemical and physical properties. Because of the higher temperature of the martensitic transformation of HfO_2 as compared to that of ZrO_2 , the literature data on the $M \leftrightarrow T$ transition are more limited and show some inconsistency. The temperature measured by thermal analysis, high-temperature XRD and some other methods are compiled in Table 3-4. The [2001Fuj] studied the phase transition of pure hafnia by using *in situ* Ultraviolet Raman scattering up to 2085 K. The monoclinic-to-tetragonal phase transition finished at around 2080 K on heating, and started at 2018 K on cooling. Since the A_f temperature is comparable to the temperature A_s , it can be seen in Table 3-4 that the result of [2001Fuj] is quite consistent with the works of [1965Sta, 1976Kuz, 1987She, 1991Gul]. For the start temperature of tetragonal-to-monoclinic transition, the result of [2001Fuj] also presents good agreement with those of [1965Sta, 1983Sen]. Stacy et al. [1972Sta] determined the variation of the lattice parameters of the monoclinic and tetragonal phase by using high-temperature XRD up to 2213 K, and derived an equilibrium temperature at 2023 ± 20 K. Coutures [1987Cou] obtained the same value with the same route, while Aldebert et al. [1975Ald] reported a value of 2038 K by measuring the lattice expansion with the neutron diffraction. All these results [1972Sta, 1975Ald, 1987Cou] are very close to the approximate T_0 temperature calculated from the data of Fujimori et al. [2001Fuj]. The results [1963Wol, 1963Bau, 1975Sta] obtained by HTXRD are questionable, because they present higher M_s temperatures than the A_s temperatures, and the other results of HTXRD [1954Cur, 1965Bog, 1968Ruh, 1976Ruh] reveal considerable deviation from the DTA, dilatometry and Raman scattering results are considered as less reliable in that respect.

The $T \leftrightarrow F$ transformation of HfO_2 was experimentally studied by only a few groups (Table 3-4). The existence of the cubic HfO_2 was firstly confirmed by Boganov et al. [1965Bog] using the HTXRD, and the $T \leftrightarrow F$ transformation was observed at around 2973 K. Other values obtained by thermal analysis and radiation pyrometry are between 2763 and 2873 K [1985She, 1987Cou, 1987She, 1988Sig, 1988Yam, 1997And] with a maximum discrepancy of 110 K. The works [1985She, 1987She, 1997And] were performed by same

group based on DTA measurements. On cooling a value of 2803 K was reported [1985She, 1997And], whereas on heating 2793 K was obtained [1987She].

Many data are available on the melting point. Most of the results are in the temperature range 3073-3105 K [1975Sta, 1977Sch, 1985She, 1986Yam, 1987She, 1988Sig, 1988Yam, 1997And], whereas the result 3123 K of Coutures [1987Cou] is slightly higher. There is also good agreement between cooling and heating curves of DTA measurements (3073 K) [1985She, 1987She, 1997And]. Earlier measurements [1932Cla, 1954Cur, 1966Nog] seem to be less reliable. The literature data are collected in Table 3-4.

[1963Sil] determined the partial molar Gibbs free energy of oxygen in hcp solid solution of Hf from 0 to 25 at.%O in the temperature range 968 to 1232 K by equilibrating samples with alkaline metal oxide-metal vapor combinations.

The enthalpy of formation of the hcp-Hf phase was obtained by [1974Kor] from the measurements of the heats of combustion at four HfO_x compositions.

With the help of the Tian-Calvet microcalorimetric method, [1984Bou] measured the partial molar enthalpy of mixing of oxygen (\bar{H}_{O_2}) in hafnium at 1232 K.

The standard enthalpy of formation of the monoclinic hafnia was experimentally determined by several groups [1932Rot, 1953Hum, 1968Hub, 1971Kor, 1974Pap, 1975Kor], ranging from $-1144.74 \text{ kJ}\cdot\text{mol}^{-1}$ [1968Hub] to $-1113.2 \text{ kJ}\cdot\text{mol}^{-1}$ [1953Hum]. Kornilov and Ushakova [1971Kor] first reported $-1117.128 \text{ kJ}\cdot\text{mol}^{-1}$, and shortly offered a very consistent value $-1117.630 \text{ kJ}\cdot\text{mol}^{-1}$ [1975Kor] in cooperation with Huber and Holley [1968Hum]. The result of this measurement [1975Kor] is thus thought to be the most reliable one. All of these data are summarized in Table 3-5.

[1953Tod] measured the heat capacity of HfO₂ at low temperatures (52.47-298.16 K) and determined the entropy of HfO₂ at 298.16 K (Table 3-5). The heat content of hafnia was studied in the temperature ranges 382.7-1803.6 K [1953Orr], and 650.4-2883.7 K [1963Pea].

Lee and Navrotsky determined the enthalpy of formation of the cubic solid solution in the system HfO₂ – YO_{1.5} by oxide melt solution calorimetry. The enthalpy of transition of monoclinic to cubic of pure hafnia was extrapolated to be $32.5 \pm 1.7 \text{ kJ}\cdot\text{mol}^{-1}$ [2004Lee]. However, this value is three times larger than the related value of ZrO₂ ($9.7 \pm 1.1 \text{ kJ}\cdot\text{mol}^{-1}$) [2003Lee] estimated by the same group. In view of the similarity of HfO₂ and ZrO₂, such difference seems to be too large.

3.1.3. The ZrO₂ – HfO₂ system

The difference of the lattice constants of both ZrO_2 and HfO_2 are very small, due to the equivalent valence and almost equivalent ionic radii of Zr^{+4} and Hf^{+4} . For this reason, the $ZrO_2 - HfO_2$ system can form continuous solutions, and it is only possible to distinguish the X-ray diffraction patterns of ZrO_2 , HfO_2 , and solid solutions of them by using extremely high resolution. Stansfield [1965Sta] firstly studied the thermal expansion of five solid solutions in the $ZrO_2 - HfO_2$ system by dilatometry measurement in the temperature range between 1173 and 2773 K, but did not give quantitative values. Ruh et al. [1968Ruh] determined the transformation temperatures of A_s , A_f , M_s , and M_f in the whole composition range by both the HTXRD and DTA. The results obtained by HTXRD showed a large disagreement with the DTA results, which however are consistent with the dilatometric study of Stansfield [1965Sta]. With the help of thermal analysis, the phase transformations $M \leftrightarrow T$ and $T \leftrightarrow F$ were studied in the temperature range 1373-3073 K by Shevchenko et al. [1987She]. But, in fact, only the A_s temperatures for the monoclinic-to-tetragonal transition were reported, and were misinterpreted as the monoclinic / tetragonal phase boundary data. [1993Yam] reported the temperatures of the $T \leftrightarrow F$ transformation using radiation pyrometry, and their data are well consistent with those from reference [1987She]. An additional solid-solid transformation peak was found by Yamada et al. [1993Yam] at temperatures higher than that of the $T \leftrightarrow F$ transformation, for which no explanation was given. Obolonchik et al. [1991Obo] reported two sets of tetragonal / monoclinic phase equilibria data in their work on the ternary $HfO_2 - ZrO_2 - Y_2O_3$ system.

Three groups [1968Ruh, 1987She, 1988Yam] measured the liquidus of the $ZrO_2 - HfO_2$ system. The two data sets [1987She, 1988Yam] are mutually consistent and lie almost on a straight line connecting the end members.

The activities of ZrO_2 and HfO_2 in the $ZrO_2 - HfO_2$ system at 2773 K derived from the vapor pressure data obtained from high temperature mass spectrometry were reported in the literature [1985Bel] with large errors. Both of the reported activities of ZrO_2 and HfO_2 presented some deviation from the ideal behavior.

3.2. Experimental results and discussion

The $ZrO_2 - HfO_2$ system was experimentally studied by DTA measurements. All the prepared compositions are given in Table 3-6. The XRD patterns of the sample No.8 before and after heat treatment are shown in Fig. 3-1. After the pyrolysis at 700°C for 3h, the structure is mainly monoclinic with a small amount of tetragonal phase. Since the particle size is quite small, the tetragonal phase is stabilized because of its lower surface energy than that

of the monoclinic phase [2005Pit]. There are no visible differences between the XRD patterns of different samples. After heat treatment at higher temperature, the XRD patterns show pure monoclinic structure.

The DTA curves for each sample reveal one peak on heating and one on cooling according to the transition between monoclinic and tetragonal phases. Fig. 3-2 shows the DTA curve of the sample No.5 as an example, where the temperatures A_s , A_f , M_s , and M_f are identified. All the transformation temperatures measured by DTA are included in Table 3-6, and plotted in Fig. 3-3 together with the data reported in references [1968Ruh, 1987She]. Compared with the literature data, the results of the present work are quite consistent. With the change of the composition, the present data of A_s , A_f , M_s , and M_f show a linear behavior in the whole composition range. By applying the linear relations, the A_s , A_f , M_s , and M_f temperatures can be fitted well against the composition ($x(\text{HfO}_2)$ =mole fraction). The functions obtained in this work are:

$$A_s = 1429.71 + 6.36181 * x(\text{HfO}_2) \quad (3-1)$$

$$A_f = 1473.93 + 6.60491 * x(\text{HfO}_2) \quad (3-2)$$

$$M_s = 1304.75 + 7.32675 * x(\text{HfO}_2) \quad (3-3)$$

$$M_f = 1263.66 + 7.19513 * x(\text{HfO}_2) \quad (3-4)$$

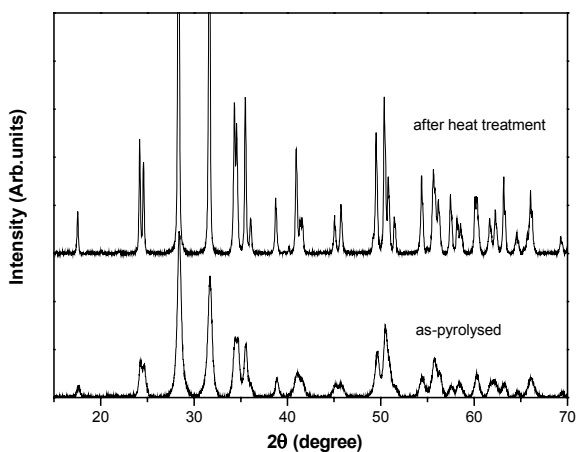


Figure 3-1. The XRD patterns of the sample No.8 in $\text{ZrO}_2 - \text{HfO}_2$ system after pyrolysis (700°C , 3h) and after heat treatment (1400°C , 48h).

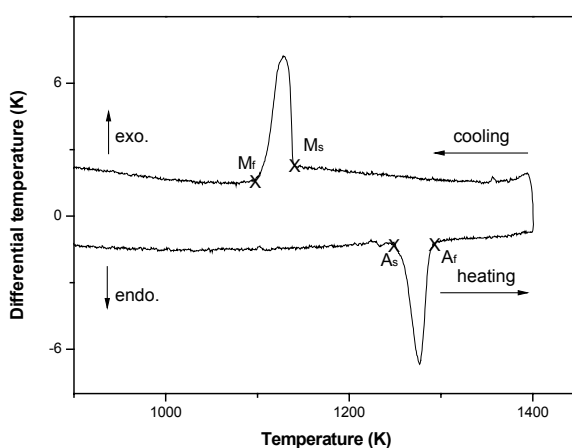


Figure 3-2. The DTA curve of the sample No.5 in $\text{ZrO}_2 - \text{HfO}_2$ system (The A_s , A_f , M_s , and M_f represent the starting and finishing temperatures on heating and cooling, respectively).

With increasing HfO₂ content, the temperature difference between A_s and A_f as well as between M_s and M_f do not change evidently. However, due to the higher slope of function (3-3) and (3-4), it can be seen that the difference between A_s and M_s for pure hafnia is much smaller than that for pure zirconia. In this work, the difference between A_s and M_s is 125 K for ZrO₂ and 28 K for HfO₂ which is quite consistent with the value reported by [1963Wol] (30 K). The A_s (1430 K), A_f (1474 K), M_s (1305 K), M_f (1264 K) of pure ZrO₂ obtained in this work show striking agreement with the results of Ruh et al. [1968Ruh] (A_s : 1433 K, A_f : 1488 K, M_s : 1311 K, M_f : 1266 K). Additionally, the current A_s of ZrO₂ is consistent with the literature data [1966Kir, 1968Ruh, 1973Mit, 1977Ruh, 1979Che, 1984Ruh, 1985Per, 1987She, 1990Fre, 1995And, 2001Jer] within the maximum deviation of 20 K, and the M_s obtained in this work for ZrO₂ presents maximum 32 K deviation with the data from references [1968Ruh, 1984Ruh, 1985Ada, 1985Per, 1987She, 1990Dur, 1995And, 1995Yas, 1997Kas, 1999Hay, 2003Sur, 2006Mor,]. For the HfO₂, though the literature data are scarce, present work still provides considerable consistency with the reported A_s temperatures [1976Kuz, 1975Sta, 1991Gul, 2001Fuj] and M_s temperatures reported by Senft and Stubican [1983Sen] and Fujimori et al. [2001Fuj].

The calculated T_0 temperatures for different compositions are also given in Table 3-6. They are calculated by two different ways which agree within a maximum discrepancy of 6 K. Fig. 3-4 shows the T_0 temperatures calculated using equation (1-1), together with the linear fit function and the literature data [1968Ruh]. The data of Ruh et al. [1968Ruh] agree well with the fitted function in both the ZrO₂ and HfO₂-rich region, but deviate in the composition range 20-50 mol% HfO₂. According to the fitted function:

$$T(T_0) = 1367.23 + 6.84428 * x(\text{HfO}_2) \quad (3-5)$$

for the two end members, T_0 are 1367 K and 2052 K, respectively. The uncertainties introduced by linear fit are estimated to be 5 K. The value of 1367 K for ZrO₂ is only 20 K lower than the value 1387 K suggested in the work of Yashima et al. [1996Yas] by extrapolating the T_0 data of the ZrO₂ – YO_{1.5} system, and agree well with most of literature data obtained by DTA or dilatometry, while the value of 2052 K for HfO₂ is also consistent with the experimental data of [1965Sta, 1972Sta, 1987Cou, 2001Fuj] within the limits of uncertainty.

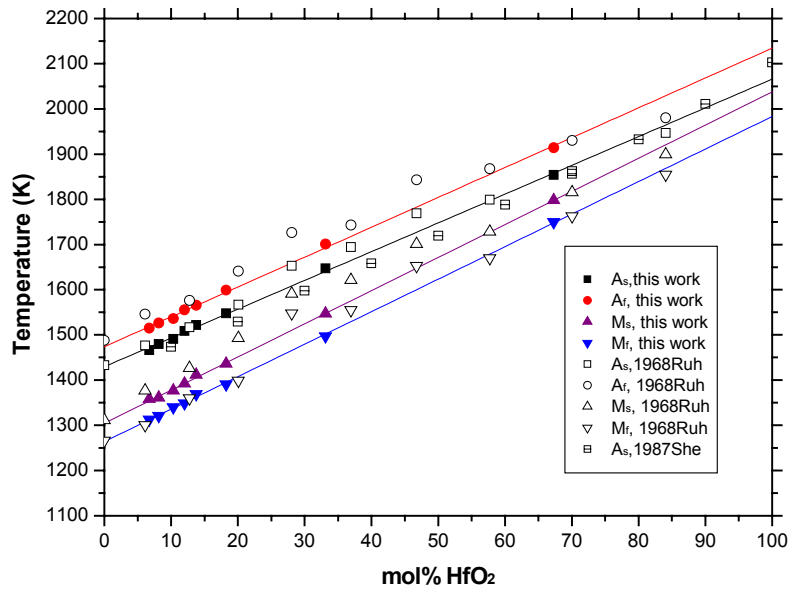


Figure 3-3. The measured A_s , A_f , M_s , and M_f temperatures in the $ZrO_2 - HfO_2$ system together with the fitting linear functions.

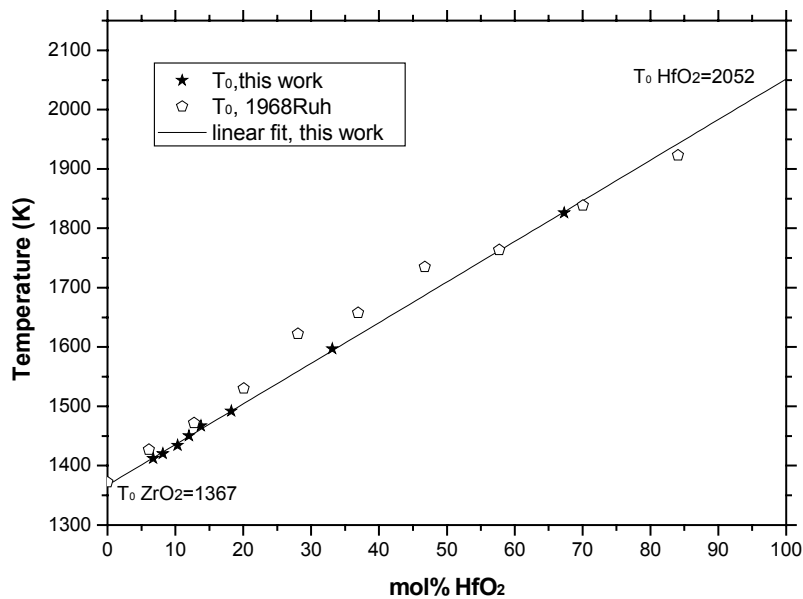


Figure 3-4. The calculated T_0 data for the $ZrO_2 - HfO_2$ system together with linear fit and literature data.

3.3. Thermodynamic assessments and calculations

3.3.1. Pure zirconia

The experimental data on the heat capacity [1950Art, 1990Nev, 1999Toj, 2001Tan, 2003Deg, 2006Mor] and heat content [1950Art, 1950Cou, 1965Tsa1, 1966Kir, 1979Che] are accepted for the optimization. The standard values at 298.15 K are taken for the enthalpy of formation from the references [1964Hub, 1967Kor], for the heat capacity and entropy from the reference [1999Toj].

For the M \leftrightarrow T transition, the value obtained in this work (1367 K) is taken. The most reliable data [1950Cou, 1965Tsa, 1995Yas, 2001Jer, 2006Mor] on the enthalpy of transformation (Table 3-1) are in the range of 5000-6000 J·mol⁻¹. All of the data were obtained at the A_s temperature on heating, and they could have slight differences compared with the results measured on cooling [1995Yas]. In this work, it is assumed that both enthalpy and entropy of transformation are independent on temperature. The entropy of transformation is selected as 4 J·mol⁻¹·K⁻¹, and the enthalpy of transformation as 5648 J·mol⁻¹, which both fall well among those literature data.

There is only one experimental report on the enthalpy of the T \leftrightarrow F phase transformation [2005Nav1]. Their data on the transformation temperature (2584 K) is accepted in this work, but the enthalpy value (3400 \pm 3100 J·mol⁻¹) is not taken for present optimization, partly due to the large experimental error. Moreover, it has been clear from several thermodynamic assessments [2004Jac, 2004Che, 2005Fab] that by accepting a low enthalpy of T \leftrightarrow F transformation, the F + T two-phase equilibrium boundaries in ZrO₂-based binary systems cannot be well reproduced. The lower the value which has been used, the worse was the F + T phase equilibrium of the phase diagram presented [2004Jac]. Actually, the T \leftrightarrow F transition may be of second-order type at high temperature, and the F + T two-phase region in ZrO₂-based binary systems could be a miscibility gap [1991Hil]. In this work, because it is modeled as a first-order transition, a relatively large value is selected. Compared with the M \leftrightarrow T transition, assuming the same entropy of transformation (4 J·mol⁻¹·K⁻¹) for the T \leftrightarrow F transition, the enthalpy of transformation 10336 J·mol⁻¹ is well consistent with the enthalpy of monoclinic-to-cubic transformation extrapolated from calorimetric experiments [2003Lee].

The temperature and enthalpy of transformation for F \leftrightarrow L transition are selected to be 2983 K, and 87027 J·mol⁻¹, as recommended in reference [1971JAN].

The calculated heat capacity and enthalpy increment ($H_T - H_{298}$) are shown in Fig. 3-5 and Fig. 3-6, together with experimental data. The calculated heat capacity, entropy, and enthalpy of formation of monoclinic ZrO₂ at 298.15 K are 56.26 J·mol⁻¹·K⁻¹, 49.76 J·mol⁻¹·K⁻¹ and -1100.56 kJ·mol⁻¹, respectively. All the experimental data are well reproduced. The assessed Gibbs energy parameters are given in **Appendix**.

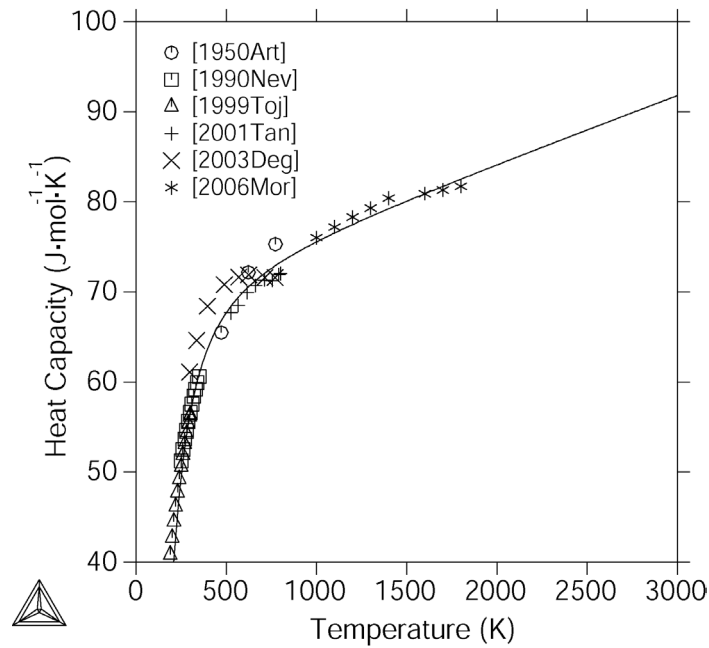


Figure 3-5. The calculated heat capacity of ZrO_2 together with experimental data.

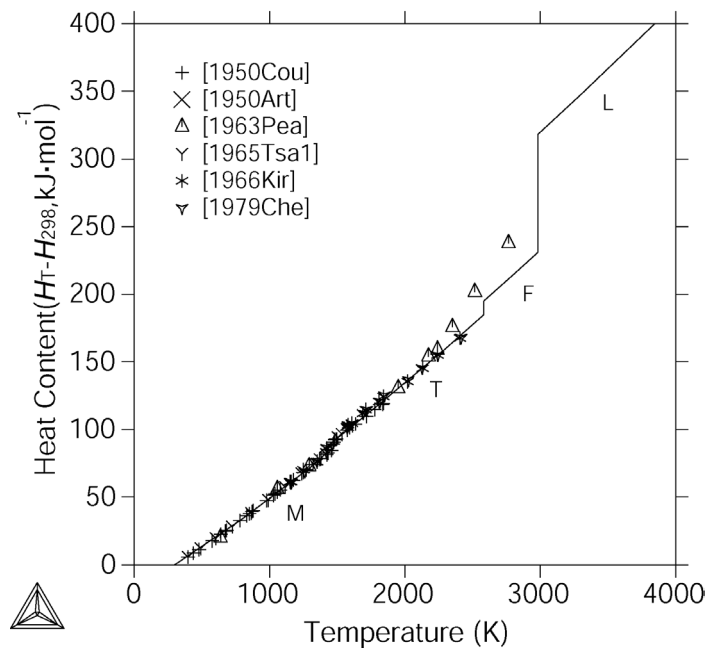


Figure 3-6. The calculated heat content ($H_T - H_{298}$) of ZrO_2 together with experimental data.

3.3.2. The Zr – O system

The phase equilibria in the Zr – O system were studied by [1954Dom, 1961Geb, 1961Hol, 1977Ack, 1978Ack, 1980Rau]. Most of the phase boundary data in these works are adopted for the optimization. The thermodynamic data reported by [1962Kom, 1974Bou, 1974Vas, 1979Ack, 1984Bou] are accepted as well for the assessment in this work. The data of invariant reactions reviewed by [1986Abr] are input in the optimization as the start values.

The phase diagram calculated in this work is shown in Fig. 3-7 together with the experimental data. The calculated invariant reactions are presented in Table 3-7 together with the assessed data [1986Abr]. It can be seen in Fig. 3-7 that the existing experimental data are reproduced very well within the experimental errors. The optimized parameters are listed in **Appendix**.

The congruent melting point of the hcp-Zr phase (2404 K) is calculated at 29 at.% O, which has to be compared with 25 at.% O given by [1986Abr]. However, the calculated value is rather consistent with the results of previous assessments [2001Lia, 2002Arr, 2004Che, 2004Chen]. Since many thermodynamic and phase boundary data for the hcp-Zr phase region are employed in the optimization, the calculated values seems to be more reasonable than the assessed one [1986Abr].

The calculated congruent melting point of cubic zirconia is at 65.78 at.% O and 3055 K, which is very similar to the result of [2004Chen]. Chevalier et al. [2004Che] and Liang et al. [2001Lia] obtained the results of 66.3 at.% O at 2993 K and 66 at.% O at 2983 K, respectively, and reproduced the L + F / F phase boundary very well. Both the results [2001Lia, 2004Che] present their efforts to obtain a stoichiometric congruent melting point. Compared to the results of this work and [2004Chen], the models with substitutional species adopted by [2001Lia] and [2004Che] are more workable to deal with the L + F phase equilibrium. However, the associated model in the work of [2004Che] produces a discontinuity in the slope of the liquidus. The phase diagram calculated by [2002Arr] presents a congruent melting point very close to the stoichiometric composition at 2950 K, but lacks the consistency with the experimental data for the phase boundary L + F / F at high temperatures. Because there is no any experimental data concerning the composition of the congruent melting point, it is impossible to judge which result is more valid. Since the experimental data can be reproduced well, the present results are thought to be acceptable.

The present thermodynamic dataset also gives reasonable predictions at high temperatures (Fig. 3-8) and a very similar result to that of [2002Arr] is obtained for the gas + liquid phase region.

The calculated partial molar Gibbs energy of O in the hcp phase region at 1100 K is shown in Fig. 3-9, together with the experimental data in the temperature range 1073-1273K [1962Kom]. Fig. 3-10 presents the experimental and calculated partial molar enthalpy of oxygen (\overline{H}_{O_2}) in the whole composition range. Fig. 3-11 shows the calculated partial pressure of the species Zr, ZrO, ZrO₂ and O over the saturated Zr + ZrO₂ two-phase region. In view of

the less reliability of such thermodynamic data, the agreements in Fig. 3-9, Fig. 3-10 and Fig. 3-11 are reasonable.

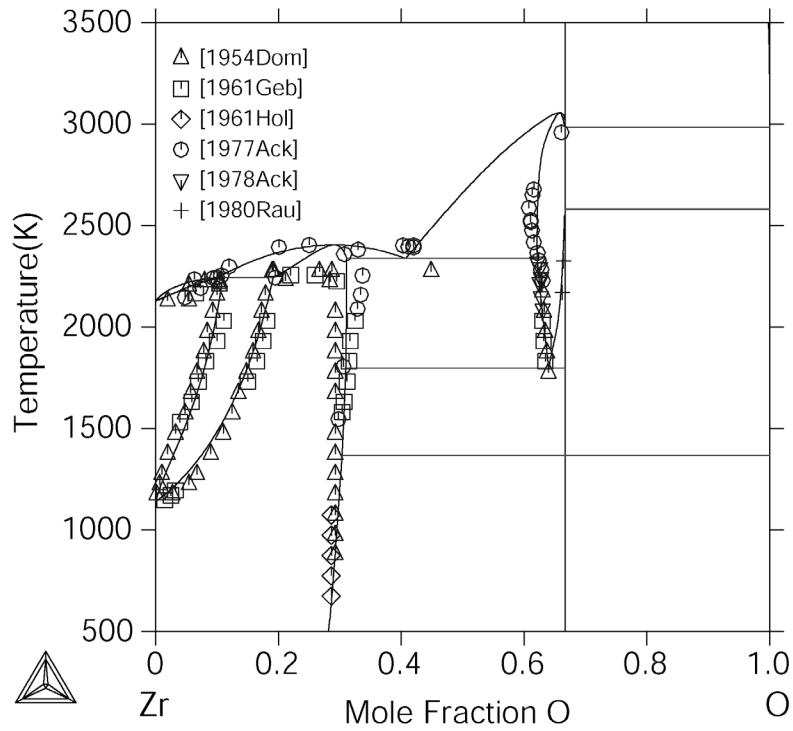


Figure 3-7. The calculated Zr – O phase diagram in this work together with experimental data.

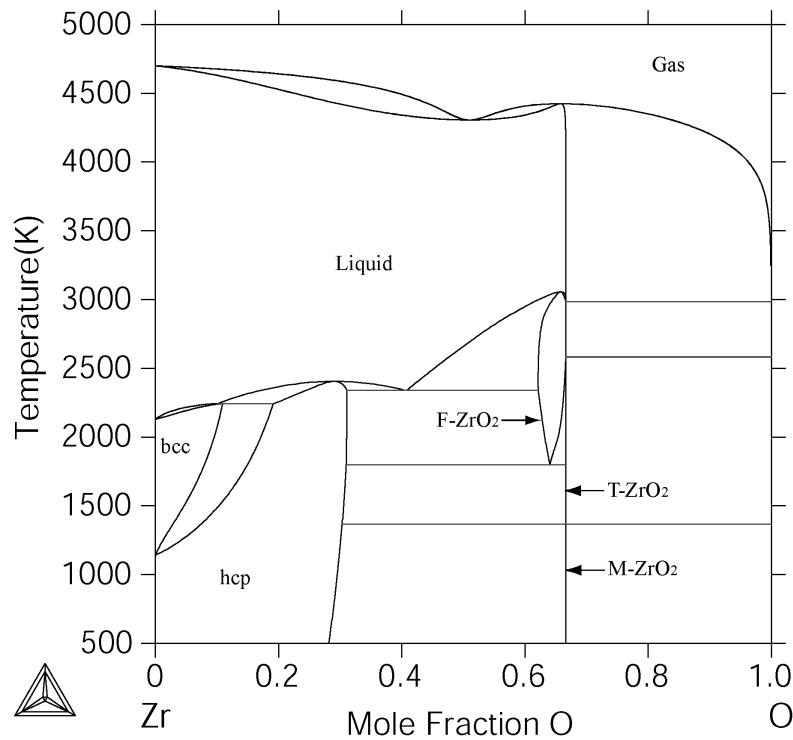


Figure 3-8. The Zr – O phase diagram calculated in this work at high temperatures.

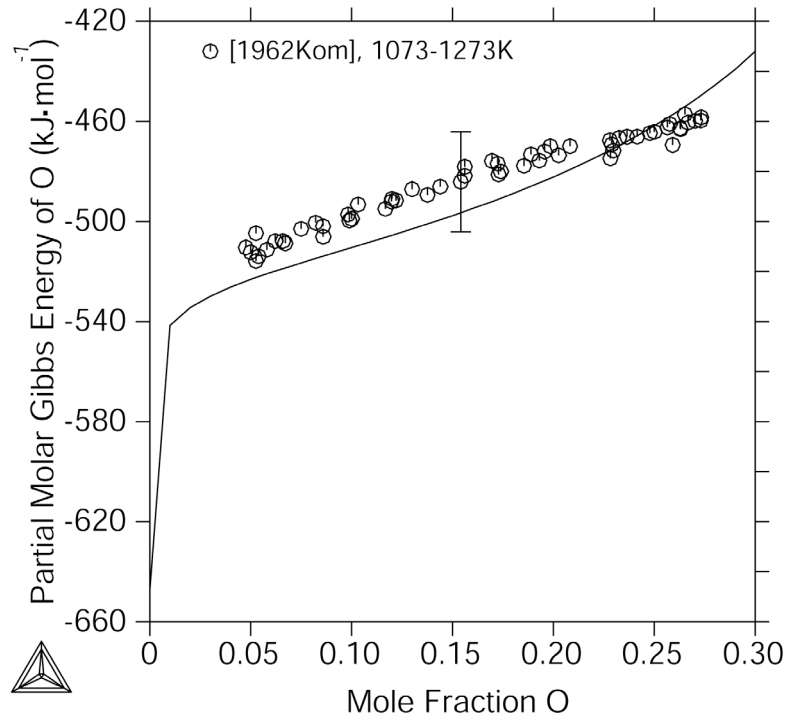


Figure 3-9. Calculated and experimental partial Gibbs energy of oxygen in the Zr – O system at 1100K, referred to pure O₂ at 1 bar.

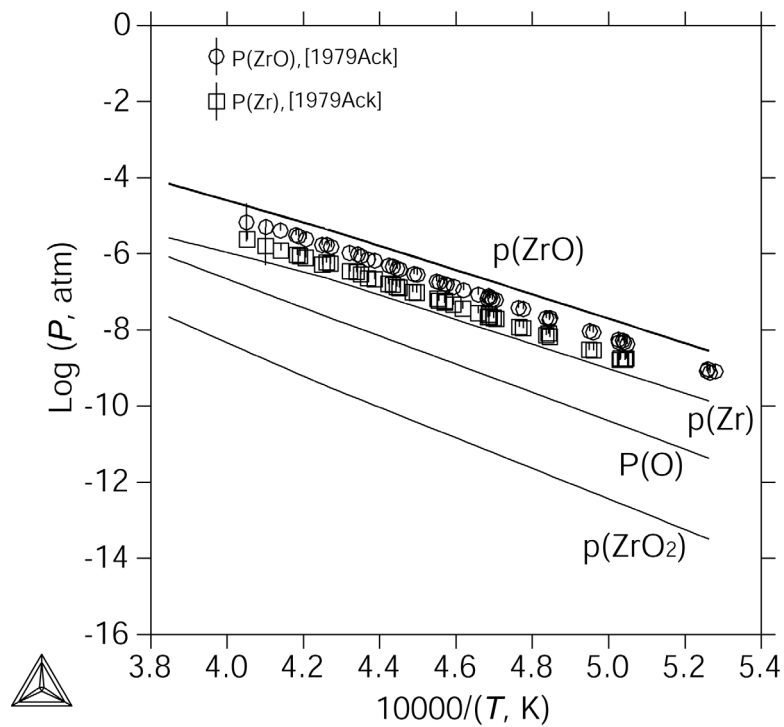


Figure 3-10. Calculated partial pressures of ZrO₂(g), ZrO(g), Zr(g) and O(g) over the saturated Zr + ZrO₂ two-phase region, together with experimental data.

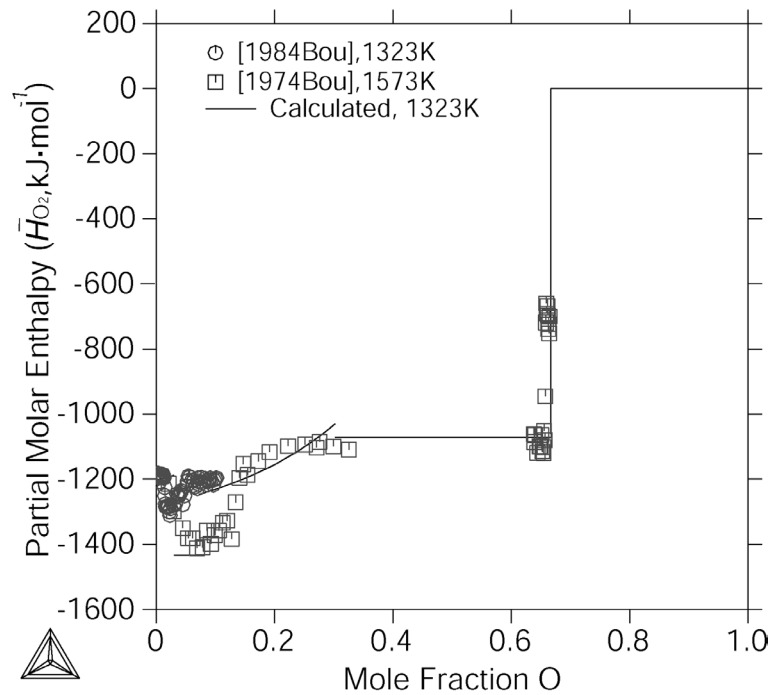


Figure 3-11. Calculated partial molar enthalpy as a function of the oxygen content in the Zr – O system together with experimental data.

3.3.3. Pure hafnia

The heat capacity and heat content data given in the literature [1953Tod, 1953Orr] are taken for the optimization. Since the heat content data of Pears and Osment [1963Pea] have been already confirmed to be incorrect for ZrO_2 , they are not used for optimization but only for comparison in this work. The standard enthalpy of formation data of Kornilov et al. [1975Kor] is accepted, while the heat capacity and entropy at 298.15 K reported by Todd [1953Tod] are selected as starting values. Due to the lack of the high temperature heat capacity data, the heat capacity of the solid phase at the melting point is taken as that of ZrO_2 .

There are not any experimental data on the enthalpy of transformation for the monoclinic \leftrightarrow tetragonal, tetragonal \leftrightarrow cubic, and cubic \leftrightarrow liquid transitions of HfO_2 . Owing to the similarity of HfO_2 and ZrO_2 , the same entropies of transformation as for ZrO_2 are adopted for HfO_2 . The present result of 2052 K is accepted for the temperature of monoclinic \leftrightarrow tetragonal transformation. For the temperature of the tetragonal \leftrightarrow cubic transformation, the result 2803 K obtained in the literature [1985She, 1997And] from the cooling curve of the DTA measurements is consistent with the results [1987She, 1988Sig] within a maximum discrepancy of 22 K, and is selected in this work. For the melting point, the reported temperatures 3073 K [1985She, 1987She, 1997And], 3076 K [1986Yam], and 3074 K [1988Yam] are in very good agreement, and the deviations with the most of other results

[1932Cla, 1975Sta, 1988Sig, 1977Sch] are within 30 K. Therefore, the value of 3073 K is accepted in this work. Thus, the enthalpies for the monoclinic \leftrightarrow tetragonal, tetragonal \leftrightarrow cubic, and cubic \leftrightarrow liquid transformation are $8208 \text{ J}\cdot\text{mol}^{-1}$, $11212 \text{ J}\cdot\text{mol}^{-1}$, and $89653 \text{ J}\cdot\text{mol}^{-1}$, respectively.

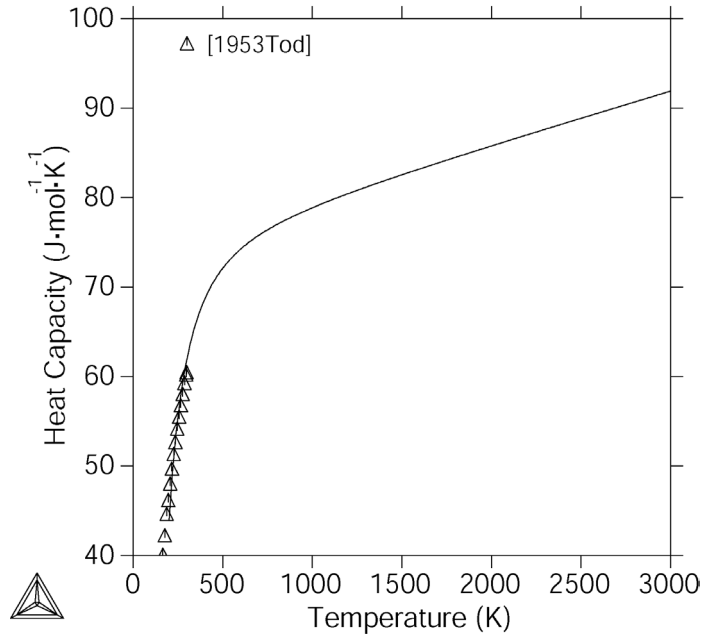


Figure 3-12. The calculated heat capacity of HfO_2 together with experimental data.

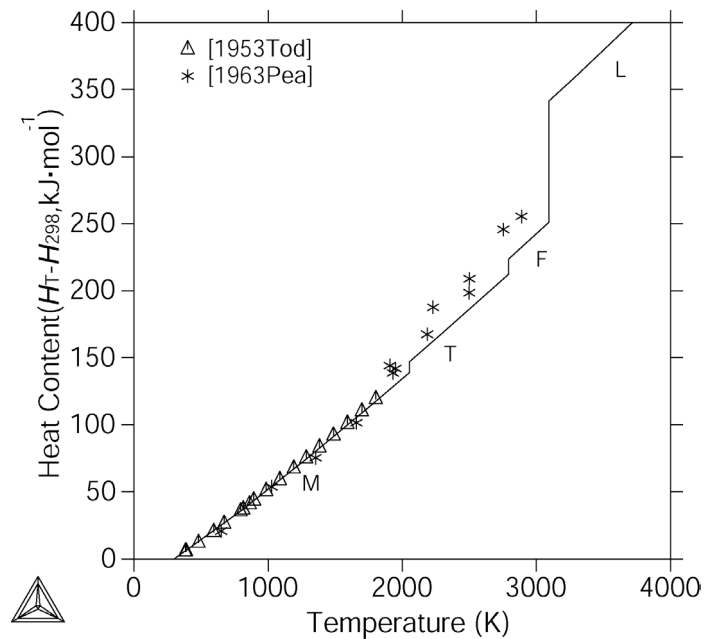


Figure 3-13. The calculated heat content ($H_T - H_{298}$) of HfO_2 together with experimental data.

The calculated heat capacity and heat content ($H_T - H_{298}$) are shown in Fig. 3-12 and Fig. 3-13, together with experimental data. The optimized parameters for the HfO_2 are included in **Appendix**.

3.3.4. The Hf – O system

Though [1963Rud] investigated the system in a wide composition range, their results present large deviation with those obtained by [1965Dom] in Hf-rich region. Compared to the Zr – O and Ti – O systems, a eutectic reaction liquid \Leftrightarrow bcc-Hf + hcp-Hf reported by [1963Rud] is probably less reasonable, because the reaction types involving these three phases are both peritectic for the Zr – O and Ti – O systems. Thus, the reaction liquid + hcp-Hf \Leftrightarrow bcc-Hf proposed by [1965Dom] is accepted together with the phase equilibria data for solid phases. However, with increasing the O content, the liquidus temperatures determined by [1965Dom] change very sharply, while the results of [1963Rud, 1976Rud] are well consistent. Therefore, the congruent melting temperature and the liquidus temperatures beyond 18 at.% O are taken from [1963Rud, 1976Rud], as well as the invariant reaction liquid \Leftrightarrow hcp-Hf + F. The results of the reaction F \Leftrightarrow hcp-Hf + T obtained by [1973Ruh] are also accepted as the starting values for optimization.

The thermodynamic data reported by [1963Sil, 1974Kor, 1984Bou] are all adopted for the assessment.

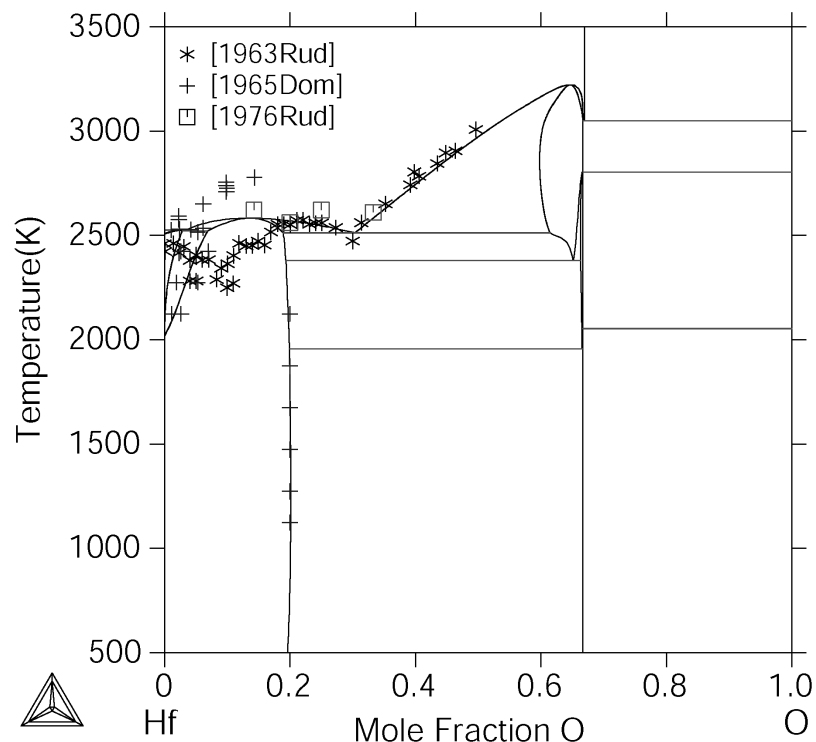


Figure 3-14. The Hf – O phase diagram calculated in this work together with experimental data.

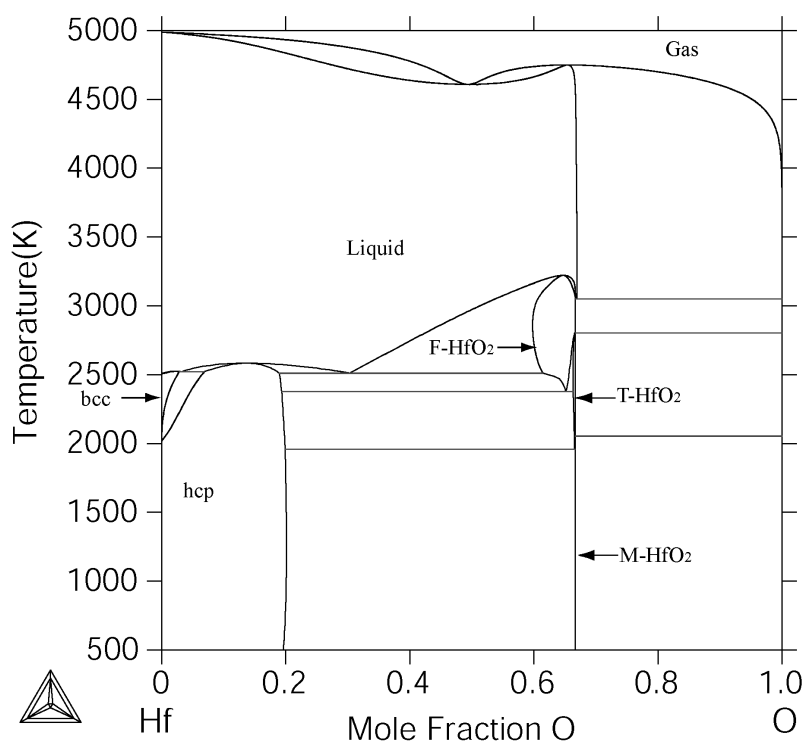


Figure 3-15. The Hf – O phase diagram calculated in this work at high temperatures.

A calculated Hf – O phase diagram together with experimental data is shown in Fig. 3-14. The calculated invariant reactions are presented in Table 3-8 together with the experimental data. At higher temperatures, a similar gas + liquid two-phase region to that of the Zr-O system is obtained, and shown in Fig. 3-15.

In the Hf-rich region, the calculated liquidus temperatures are between the results of [1963Rud] and [1965Dom], but agree well with that of [1976Rud]. The calculated invariant reaction involving liquid, hcp-Hf and bcc-Hf phases occurs at 2522 K, which is consistent with the value 2523 K reported by [1965Dom]. However, present calculation gives a eutectic type for this reaction rather than peritectic type, while the compositions of liquid and bcc-Hf are very close. In view of the large uncertainties in this region, the calculation is thought to be acceptable, but further experimental investigations are necessary. The congruent melting point of hcp-Hf phase calculated in this work is 2583 K, which is close to the results reported by [1963Rud] (2573 K). At the same time, like in the Zr – O system, the calculated composition (13.7 at.% O) for this congruent melting shifts to Hf-rich region, comparing to the experimental data (18 at.% O) of [1963Rud]. This is reasonable because it is optimized from both the liquidus data and the phase boundary data of the hcp-Hf phase.

The experimental liquidus data beyond 18 at.% O are considerably well reproduced by the calculations. The calculated invariant reaction liquid \leftrightarrow hcp-Hf + F is 2512 K, 30.4 at.%

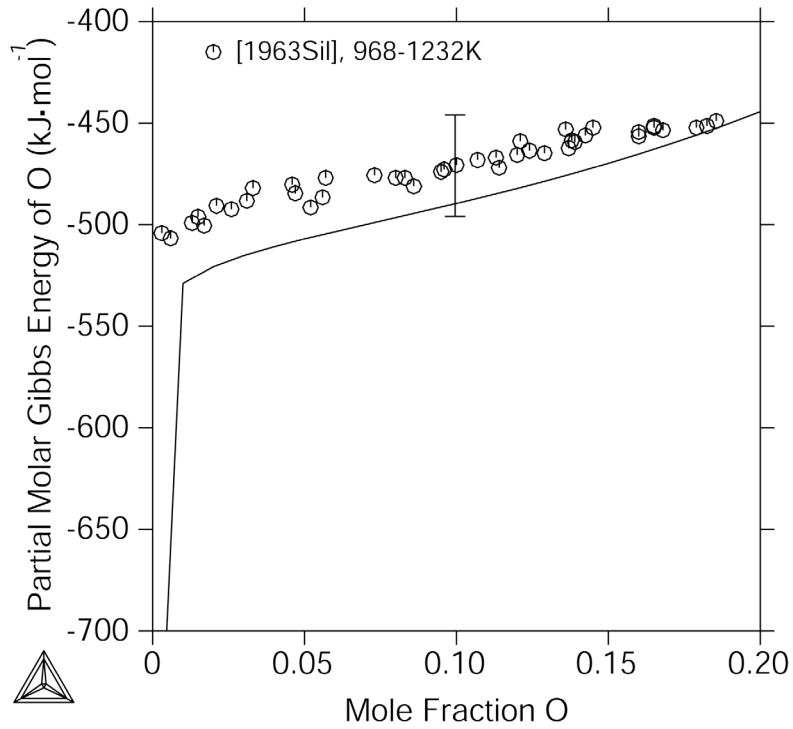


Figure 3-16. Calculated and experimental partial Gibbs energy of oxygen in the Hf – O system at 1100K, referred to pure O₂ at 1 bar.

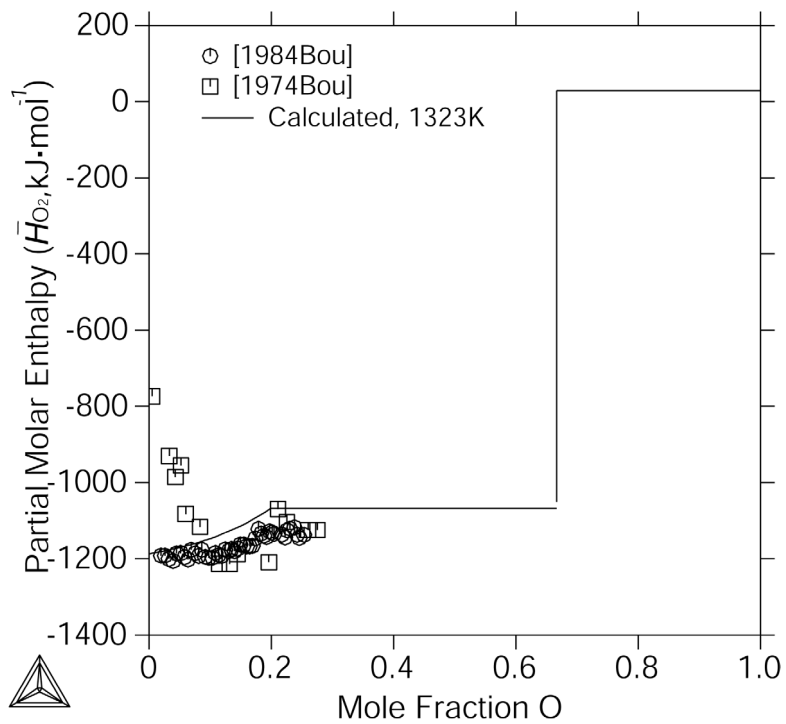


Figure 3-17. Calculated partial molar enthalpy of oxygen (O₂) in the Hf – O system together with experimental data.

O, and agrees with the composition reported by [1963Rud]. To obtain good agreement with the liquidus data, the calculated temperature for this reaction is slightly higher than the literature data [1963Rud, 1965Dom]. The temperature of 2398 K determined by [1973Ruh] for the reaction $F \rightleftharpoons \text{hcp-Hf} + T$ is difficult to be well reproduced, but the present result 2379 K, is accepted within the limits of experimental uncertainties. The calculated congruent melting point of HfO_2 deviates from the stoichiometric composition, and is highly elevated compared with the melting temperature of stoichiometric composition. This is similar to the case of the Zr – O system.

Fig. 3-16 and Fig. 3-17 give the calculated partial Gibbs energy as a function of the oxygen content at 1100 K, and the partial molar enthalpy of oxygen (\bar{H}_{O_2}) compared with the experimental data. Reasonable agreement is obtained in both cases.

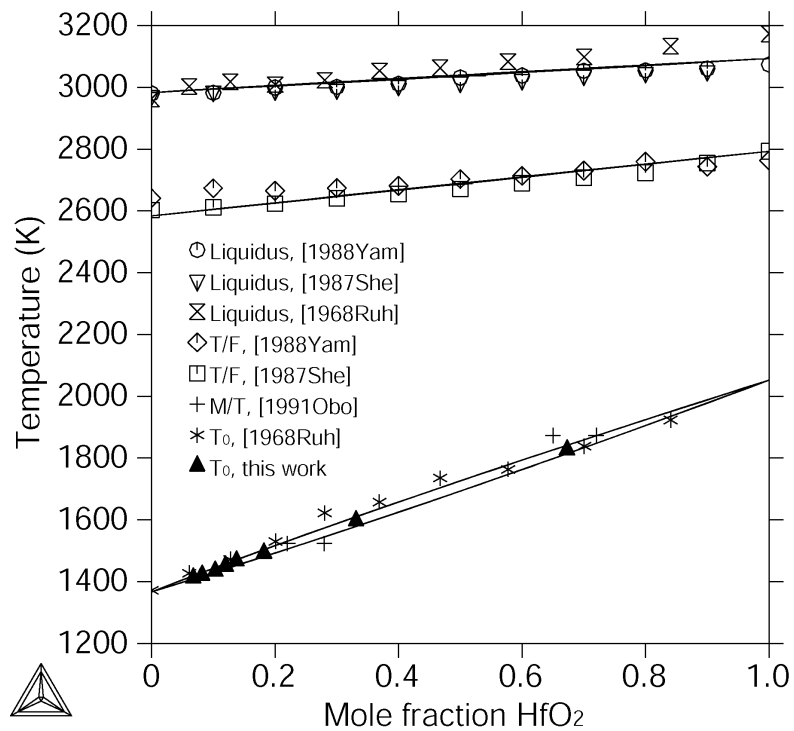


Figure 3-18. The calculated $\text{ZrO}_2 - \text{HfO}_2$ phase diagram compared with experimental data.

3.3.5. The $\text{ZrO}_2 - \text{HfO}_2$ system

All the phases in the $\text{ZrO}_2 - \text{HfO}_2$ system are modeled as ideal solutions. The calculated phase diagram is presented in Fig. 3-18. It shows a narrow monoclinic + tetragonal two-phase region, as a result of the similar thermodynamic properties of ZrO_2 and HfO_2 . The DTA data [1968Ruh, 1987She] and the phase boundary data [1991Obo] are in reasonable agreement with the calculation. The calculated high temperature T / F and F / L phase

equilibria are almost straight lines without visible two-phase regions, and consistent with the phase diagrams proposed by references [1968Ruh, 1987She, 1988Yam]. The liquidus shows some deviation with that of Ruh et al. [1968Ruh], because the melting point of HfO₂ which was taken in this work is based on the data of Shevchenko et al. [1987She] and Yamada et al. [1988Yam].

Table 3-1. Literature information on phase transition data of ZrO₂.

Transition	Reference	Temperature (K)			Enthalpy of transformation (J.mol ⁻¹)	Entropy of transformation (J.mol ⁻¹ . K ⁻¹)	Experimental method
		<i>A_s</i>	<i>M_s</i>	<i>T₀</i>			
M ↔ T	[1950Cou]	1478			5941	4.0	drop calorimetry
	[1963Bau]	1273	1243	1258			HTXRD
	[1963Wol]	1328	1183	1255.5			HTXRD
	[1965Tsa]	1475			5272 ± 544	3.56	calorimetry
	[1966Kir]	1420			7763		mixing method
	[1970Pat]	1373	1303	1338			HTXRD
	[1973Mit]	1433 ~1463	1343 ~1373	1388 ~1418			DTA
	[1974Sri]	1443					DTA
	[1977Ruh]	1429	1036	1232.5			DTA
	[1979Che]	1423			8297	5.836	mixing method
	[1984Ruh]	1425	1318	1371.5			DTA
	[1985Ada]	1452 1447	1321 1319	1386.5 1383			dilatometry
	[1985Per]	1343	1273	1308			RS
	[1986Ban]	1473	1213	1343			DTA
	[1986Yos]			1373 ± 100			dilatometry
	[1987She]	1423	1283	1353			DTA
	[1990Fre]	1450					ND
	[1990Dur]	1473	1273	1373			DTA
	[1991Boy]		1373				ND
	[1995And]	1446	1284	1365			DTA
	[1995Yas]	1477	1323	1400	5710 ± 290	4.07	DSC
	[1997Kas]	1469	1317	1393			dilatometry
	[1999Hay]	1454	1320	1387			dilatometry
	[2001Jer]	1438±7			5175		DTA
	[2003Sim]	~1380	~1390	~1385			ND
	[2003Sur]		1286		4312.80		DSC
	[2006Mor]	1461	1326	1393.5	5430 ± 310	3.69 ± 0.21	DSC

	[1975Ack]	1478			5941		assessed
	[1981Sub]	1443					assessed
	[1986Abr]	~1478					assessed
	[1992Du]			1454	6024		optimization
	[1998Che] [2004Che]			1478	8075		optimization
	[2001Lia]			1476	6441		optimization
	[2002Arr]			1478	5941		optimization
	[2004Chen]			1387	6000		optimization
	This work	1430	1305	1367	5468		DTA, extrapolated; optimization
T ↔ F	[1962Smi]	2558 ± 15					HTXRD
	[1963Wol]	2566					HTXRD
	[1965Vie]	2645 ± 50					HTXRD
	[1965Bog]	2573					HTXRD
	[1987She]	2603 ± 30					DTA
	[1993Yam]	2641 ± 25					pyrometer
	[2001Sch]				1450		molecular dynamics
	[2005Nav1]	2584 ± 15			3400 ± 3100		DTA
	[1975Ack]	2650			5564	2.09	assessed
	[1981Sub]	2643					assessed
	[1986Abr]	~2650					assessed
	[1992Du]	2642			5968		optimization
	[1998Che] [2004Che]	2650			13000		optimization
	[2001Lia]	2627			21699		optimization
	[2002Arr]	2641			6045		optimization
	[2004Chen]	2647			7500		optimization
This work	2584			10336		optimization	
F ↔ L *	[1925Hen]	2960					not reported
	[1932Cla]	2950 ± 20					not reported
	[1965Lam]	2983					not reported
	[1965Nog]	2979 ± 20					Solar furnace
	[1966Nog1]	2995 ± 20					Solar furnace
	[1966Nog2]	2972 ± 20					Solar furnace
	[1970Lat]	2953 ± 15					DTA
	[1977Ack]	2983 ± 15					pyrometry
	[1987She]	2973					DTA
	[1993Yam]	2980 ± 25					pyrometer
	[1971JAN]				87027		assessed
	[1981Sub]	2953					assessed
	[1992Du]	2983			87986.62		optimization
	[1998Che] [2004Che]	2985			87027		optimization
	[2001Lia]	2961			86313		optimization
	[2002Arr]	2950			87027		optimization
	[2004Chen]	2984			68600		optimization
This work	2983			87027		optimization	
M ↔ F	[1998Mol]	1043			13500±2200 9200±1200 (modified)		solution calorimetry

	[2003Lee]	973	9700±1100		solution calorimetry
--	-----------	-----	-----------	--	----------------------

*(at the stoichiometric composition for the optimized results)

Table 3-2. Experimental and optimized heat capacity, entropy and enthalpy of formation of monoclinic ZrO₂ at 298.15 K.

Reference	Heat capacity J·mol ⁻¹ ·K ⁻¹	Entropy J·mol ⁻¹ ·K ⁻¹	Enthalpy of formation kJ·mol ⁻¹
[1944Kel]	50.33 ± 0.33		
[1961Kel]		50.71	
[1964Hub]			-1100.919
[1967Kor]			-1100.559
[1990Nev]	56.50		
[1999Toj]	56.14	49.79	
[1992Du]	56.12	50.35	-1100.568
[2001Lia]	63.43	50.73	-1100.970
[2002Arr]	55.90	50.36	-1100.308
[2004Chen]	57.21	49.8	-1100.686
[1998Che]	56.04	50.35	-1100.568
[2004Che]			
This work	56.26	49.76	-1100.56

Table 3-3. List of models of the Zr – O system adopted in previous works.

Reference	Model	
	Liquid	Cubic ZrO ₂
[2004Che]	(O, ZrO ₂ , Zr)	(Zr)(O, Va) ₂ (Va, O)
[2001Lia]	(Zr ⁺⁴) _P (O ⁻² , Va ⁻⁴ , O) _O	(Zr)(O, Va) ₂
[2002Arr]	(Zr ⁺⁴) _P (O ⁻² , Va ⁻⁴) _O	(Zr ⁺⁴)(O ⁻² , Va ⁻²) ₂
[2004Chen]	(Zr ⁺⁴) _P (O ⁻² , Va ⁻⁴) _O	(Zr, Zr ⁺⁴)(O ⁻² , Va) ₂
[2004Sun]	(Zr ⁺⁴) _P (O ⁻² , Va ⁻⁴ , O) _O	(Zr ⁺² , Zr ⁺⁴)(O ⁻² , Va) ₂
This work	(Zr ⁺⁴) _P (O ⁻² , Va ⁻⁴) _O	(Zr ⁺² , Zr ⁺⁴)(O ⁻² , Va) ₂

Table 3-4. Literature information on the phase transition data of HfO₂.

Transition	Reference	Temperature (K)			Enthalpy of transformation (J·mol ⁻¹)	Entropy of transformation (J·mol ⁻¹ ·K ⁻¹)	Experimental method
		A _s	M _s	T ₀			
M ↔ T	[1954Cur]	1973					HTXRD
	[1963Wol]	1883	2013	1948			HTXRD
	[1963Bau]	1773	1823	1798			HTXRD
	[1965Sta]	2113	2063	2088			dilatometry
	[1965Bog]	2173					HTXRD
	[1968Ruh]			1893			HTXRD

	[1972Sta]			2023 ±20			HTXRD
	[1975Ald]			2038			ND
	[1975Sta]	2023	2073	2048			HTXRD
	[1976Ruh]	1863					HTXRD
	[1976Kuz]	2073					DTA
	[1983Sen]		2066 ±40				HTXRD
	[1987Cou]			2023 ±20			HTXRD
	[1987She]	2103	2083	2093			DTA
	[1991Gul]	2073					HTXRD
	[2001Fuj]	2080 (A _f)	2018				RS
	This work	2066	2038	2052	8208		DTA, extrapolated, optimization
T ↔ F	[1965Bog]		2973				HTXRD
	[1987Cou]		2873				DTA
	[1985She]		2803				DTA
	[1987She]		2793				DTA
	[1988Sig]		2825				DTA
	[1988Yam]		2763 ± 25				pyrometry
	[1997And]		2803				DTA
	This work		2803		11212		optimization
F ↔ L *	[1932Cla]		3047 ± 25				pyrometry
	[1954Cur]		3173				optical pyrometry
	[1966Nog1]		3026 ± 20				pyrometry
	[1975Sta]		3098				pyrometry
	[1977Sch]		3093 ± 40				microoptical pyrometry
	[1986Yam]		3076 ± 15				pyrometry
	[1985She]		3073				DTA
	[1987She]		3073				DTA
	[1987Cou]		3123				DTA
	[1988Sig]		3105				DTA
	[1988Yam]		3074 ± 25				pyrometry
	[1997And]		3073				DTA
	This work		3073		89653		optimization

*(at the stoichiometric composition for the optimized results)

Table 3-5. Experimental heat capacity, entropy and enthalpy of formation of monoclinic HfO₂ at 298.15 K.

Reference	Heat capacity (J·mol ⁻¹ ·K ⁻¹)	Entropy (J·mol ⁻¹ ·K ⁻¹)	Enthalpy of formation (kJ·mol ⁻¹)
[1932Rot]			-1135.956
[1953Hum]			-1113.195 ± 1.172
[1953Tod]	60.2496	59.33 ± 0.48	
[1968Hub]			-1144.742 ± 1.255
[1974Pap]			-1133.864 ± 6.276
[1975Kor]			-1117.630 ± 1.63
This work	61.76	59.43	-1117.628

Table 3-6. Sample compositions and the DTA results of the ZrO₂ – HfO₂ system.

Sample No.	Composition (mol%)HfO ₂	On heating		On cooling		$T_0, (A_s+M_s)/2$ (K)	$T_0', (A_f+M_f)/2$ (K)
		A_s (K)	A_f (K)	M_s (K)	M_f (K)		
1	6.7	1466	1515	1358	1313	1412	1414
2	8.2	1480	1526	1361	1321	1420.5	1423.5
3	10.3	1491	1536	1377	1340	1434	1438
4	12.0	1509	1555	1392	1349	1450.5	1452
5	13.8	1522	1566	1412	1369	1467	1467.5
6	18.2	1548	1599	1436	1391	1492	1495
7	33.1	1647	1701	1547	1497	1597	1599
8	67.3	1854	1914	1798	1750	1826	1832

Table 3-7. Comparison of the invariant reactions in the Zr – O system.

Reaction	Reference	Temperature (K)	Composition of phases (at.% O)		
L + hcp-Zr ⇌ bcc-Zr	[1986Abr]	2243 ± 10	10.0 ± 0.5	19.5 ± 2	10.5 ± 0.5
	This work	2242	10.05	19.1	10.95
L ⇌ hcp-Zr + F	[1986Abr]	2338 ± 5	40 ± 2	35 ± 1	62 ± 1
	This work	2337	40.7	31.1	62.15
F ⇌ hcp-Zr + T	[1986Abr]	1798	63.6 ± 0.4	31.2 ± 0.5	66.5 ± 0.1
	This work	1798	64.05	30.98	66.667
L ⇌ F	[1986Abr]	2983	66.6	66.6	–
	This work	3055	65.78	65.78	–
L ⇌ hcp-Zr	[1986Abr]	2403 ± 10	25 ± 1	25 ± 1	–
	This work	2404	29.05	29.05	–

Table 3-8. Comparison of the invariant reactions in the Hf – O system.

Reaction	Reference	Temperature (K)	Composition of phases (at.% O)		
L + hcp-Hf \leftrightarrow bcc-Hf	[1965Dom]	2523	1	3	8
	[1963Rud]	2273	8	5	12
	This work	2522	3.34	2.9	6.9
L \leftrightarrow hcp-Hf + F	[1965Dom]	2473	37	22	–
	[1963Rud]	2453	29	21	62
	This work	2512	30.4	19	61.5
F \leftrightarrow hcp-Hf + T	[1973Ruh]	2398	63.6	22	–
	This work	2379	65.2	19.4	66.3
L \leftrightarrow F	This work	3222	64.7	64.7	–
L \leftrightarrow hcp-Hf	[1965Dom]	2773	–	–	–
	[1963Rud]	2573	18	18	–
	This work	2583	13.7	13.7	–

Chapter 4

Experimental study and thermodynamic modeling of the $ZrO_2 - LaO_{1.5}$ system

4.1. Literature review

4.1.1. Phase equilibria

Many groups [1937War, 1955Bro, 1959Lef, 1962Per, 1963Lef, 1964Lin, 1968Rou3, 1971Rou, 1972Cab, 1973Pal, 1978Zoz, 1988Bas, 1990Zhe, 1995And, 1999Tab1, 2005Lak] contributed to the investigation of the phase equilibria of the $ZrO_2 - La_2O_3$ system.

[1937War] reported the liquidus temperature of six compositions with possible large experimental error. [1955Bro] firstly reported the phase relations for the $ZrO_2 - La_2O_3$ system. However, no any intermediate compound was found, and wrong structural modifications on both ZrO_2 and La_2O_3 were given. The reaction $T \Leftrightarrow M + F$ was measured at $930^\circ C$, and the reported solubility of both tetragonal and monoclinic phases were around 4 mol% La_2O_3 . Additionally, a wrong fluorite phase region was shown, which was actually the pyrochlore phase region according to the latter experimental reports of [1959Lef]. [1962Per] proposed that a compound with cubic CaF_2 -type structure existed in the La_2O_3 rich, and [1963Lef] presented a similar phase diagram with that of [1955Bro].

Lin and Yu [1964Lin] determined the phase relations above $1600^\circ C$, but didn't give quantitative results for the liquidus. The structural information on both ZrO_2 and La_2O_3 were wrong, and only the monoclinic ZrO_2 and hexagonal La_2O_3 were shown in their reported phase diagram. The ZrO_2 -based CaF_2 -type solid solution was reported to be only stable in a limited temperature and composition range. In their work, the existence of a very wide pyrochlore $La_2Zr_2O_7$ field was confirmed, but the compound reported by [1962Per] was not detected. The congruent melting point of $La_2Zr_2O_7$ (P) was measured at $2250^\circ C$. Four invariant reactions were determined in their study: Liquid \Leftrightarrow P + H- La_2O_3 at $1925 \pm 25^\circ C$, 82.5 \pm 2.5 wt.% La_2O_3 ; M + Liquid \Leftrightarrow F, at $2325 \pm 25^\circ C$; F \Leftrightarrow P + M, at $1775 \pm 25^\circ C$, 30 wt.% La_2O_3 ; Liquid \Leftrightarrow F + P, at $2125 \pm 25^\circ C$, 42.5 \pm 2.5 wt.% La_2O_3 .

Rouanet [1968Rou3, 1971Rou] studied this system and reported a detailed phase diagram above $1800^\circ C$ over the whole composition range. The correct stabilization region of the fluorite phase was given for the first time in their work. The solidus for the F / F + L and X- La_2O_3 / X- La_2O_3 + L were estimated according to the well-determined liquidus data by optical pyrometry. The solid-state phase transitions were determined by the HTXRD using a

Re ribbon under reducing conditions ($\text{He} + \approx 10\% \text{H}_2$). The pyrochlore $\text{La}_2\text{Zr}_2\text{O}_7$ was observed to melt congruently at 2280°C , and the eutectic reaction $\text{Liquid} \Leftrightarrow \text{F} + \text{P}$ was determined to be at 2220°C and 25 mol% La_2O_3 , which was very consistent with the result $2224 \pm 10^\circ\text{C}$ measured by [1972Cab]. The determined reaction $\text{F} \Leftrightarrow \text{P} + \text{T}$ was at 1950°C and 7 mol% La_2O_3 . At the La_2O_3 -rich, a eutectic reaction occurred at 2030°C and 62.5 mol% La_2O_3 , where the liquid phase transformed into X- La_2O_3 and a cubic Tl_2O_3 -type C_2 phase. However, due to the vaporization at high temperatures, the X phase could not be well studied, and its maximum solubility of ZrO_2 was around 30 mol% ZrO_2 at 1900°C . The temperature of the peritectic reaction $\text{Liquid} + \text{P} \Leftrightarrow \text{C}_2$ was not reported in their papers. The C_2 phase, which is stable in a very limited temperature and composition range, decomposes into $\text{La}_2\text{Zr}_2\text{O}_7$ and X- La_2O_3 phase at the temperature 1950°C , 52 mol% La_2O_3 . With decreasing the temperature, the eutectoid reaction $\text{X-La}_2\text{O}_3 \Leftrightarrow \text{P} + \text{H-La}_2\text{O}_3$ occurs at 1900°C . A possible invariant reaction for H- La_2O_3 , P and the A- La_2O_3 phases was not reported in Rouanet's work [1968Rou3, 1971Rou].

[1978Zoz] studied the solid phase formation at 1000 - 1900°C and in the composition range of 1-50 mol% La_2O_3 using XRD, IR spectroscopy, X-ray dilatometry, and crystal optics. The melting point of $\text{La}_2\text{Zr}_2\text{O}_7$ was also measured at $2230 \pm 20^\circ\text{C}$ by high temperature thermal analysis. They determined the homogeneity range of the pyrochlore phase at different temperatures by lattice constant measurements. With the rise of the temperature, the reported width of the nonstoichiometry was more than 10 mol% La_2O_3 which were comparable to the data determined by [1962Per, 1973Pal, 1990Zhe], but was argued by very recent work [1999Tab1] that the pyrochlore phase region should be considerably narrower and less than 2 mol% $\text{LaO}_{1.5}$ in width. The solubility of La_2O_3 in tetragonal ZrO_2 proposed by [1978Zoz] was less than 1 mol%.

[1988Bas] investigated the range of 0-15 mol% La_2O_3 using X-ray diffraction and thermal analysis. The eutectoid decomposition $\text{T} \Leftrightarrow \text{M} + \text{P}$ was determined to occur at 1100°C , 0.75 mol% La_2O_3 . [1995And] studied the $\text{T} \Leftrightarrow \text{M}$ transformation in the same composition range, the same reaction was determined at 1110°C , 0.75 mol% La_2O_3 , which was in good agreement with that of [1988Bas].

[2005Lak] reinvestigated some critical reactions involving the liquid phase by DTA: $\text{L} \Leftrightarrow \text{P}$ (2340°C), $\text{L} \Leftrightarrow \text{P} + \text{F}$ (2315°C), and $\text{L} \Leftrightarrow \text{P} + \text{X-La}_2\text{O}_3$ (1980°C). However, the same compositions of liquid phases for those reactions as the results of [1971Rou] were reported, and there were no more details on how many samples were studied.

Some general conclusions on the phase relation of the $\text{ZrO}_2 - \text{LaO}_{1.5}$ system can be made from review of the literature review outlined above:

(1). The high temperature fluorite phase cannot be stabilized to low temperature by the doping of La, and the solubility of La in the tetragonal phase is not clear.

(2). The pyrochlore phase melts congruently, but the homogeneity range is not clear yet due to the scattered experimental data.

(3). The high temperature invariant reactions are well determined. The existence of the C_2 phase reported by [1968Rou3, 1971Rou] was not confirmed by other works, and could be the fluorite phase, by taking account of the similarities of the many $\text{ZrO}_2 - \text{REO}_{1.5}$ systems.

The compilation of all the invariant reactions in literature is given in Table 4-1.

4.1.2. Thermodynamic data

[1971Kor] determined the enthalpy of formation of the stoichiometric pyrochlore phase by combustion in a bomb calorimeter.

Du et al. [1995Du] carried out a thermodynamic assessment on the $\text{ZrO}_2 - \text{La}_2\text{O}_3$ system based on all available phase diagram and thermodynamic data. They treated the fluorite phase and X- La_2O_3 phase as a miscibility gap, and adopted the substitutional solution models for all phases.

[1995Bol] measured the enthalpy of formation of the stoichiometric pyrochlore phase at 974K by using high-temperature solution calorimetry in molten lead borate, and then derived the standard enthalpy of formation at 298.15 K.

The heat capacity of $\text{La}_2\text{Zr}_2\text{O}_7$ was measured by [1997Bol] from 4 to 400 K by adiabatic calorimetry. By using drop calorimetry, they also measured the enthalpy increment relative to 298.15 K from 500 to 900 K. Some thermodynamic data are derived and smoothed from 4 to 1000 K.

[1998Jac] determined the Gibbs energy of formation of $\text{La}_2\text{Zr}_2\text{O}_7$ (with respect to monoclinic ZrO_2 and A-type $\text{LaO}_{1.5}$) by a solid-state galvanic cell involving composition-graded electrolyte ($x\text{LaF}_3 + (1-x)\text{CaF}_2$), in the temperature range of 870-1240 K. They reported a function of $-133800 - 10.32T$ for Gibbs energy of formation of the pyrochlore phase. The calculated enthalpy of formation from oxides was $-133.8 \pm 5 \text{ kJ.mol}^{-1}$ (per mole of compound). The standard entropy of formation from oxides was derived at $10.32 \text{ J.mol}^{-1}.\text{K}^{-1}$ (per mole of compound).

[2002Rog] also determined the standard molar Gibbs energy of formation of $\text{La}_2\text{Zr}_2\text{O}_7$ (with respect to monoclinic ZrO_2 and A-type $\text{LaO}_{1.5}$) by the e.m.f measurements in the

temperature range 1073-1273 K. The calculated enthalpy of formation was -134.3 ± 0.8 kJ.mol⁻¹ (per mole of compound), and the calculated standard entropy of formation was 10.54 ± 0.48 J.mol⁻¹.K⁻¹ (per mole of compound).

The enthalpy increment (H_T-H_{298}) for the pyrochlore phase La₂Zr₂O₇ was measured using drop calorimetry in a recent work of Sedmidubsky et al. [2005Sed] in the temperature range 888-1567 K. Combining the heat capacity data reported by [1995Bol], Sedmidubsky et al. derived the heat capacity function of the La₂Zr₂O₇ in the temperature range 298-1550 K.

In a more recent paper, [2005Nav] reported a less negative value (-22585 J.mol⁻¹, per mole of cations) for the enthalpy of formation of pyrochlore, without giving the detailed experimental method.

The literature data on the enthalpy of formation of the pyrochlore phase are compiled in Table 4-2.

4.2. Experimental results and discussion

Only two compositions in the ZrO₂ – LaO_{1.5} system with 25 mol% and 75 mol% LaO_{1.5} were prepared, to determine the phase equilibria of tetragonal + pyrochlore, and pyrochlore + A-La₂O₃. However, the A-La₂O₃ phase at 75 mol% LaO_{1.5} reacts with moisture in air in very short time so that it is difficult to obtain dense samples for SEM or EPMA analyses. Therefore, only the tetragonal + pyrochlore phase equilibrium data at 1400°C, 1600°C, and 1700°C were finally determined from the composition 25 mol% LaO_{1.5}.

The XRD results of the samples containing 25 mol% and 75 mol% LaO_{1.5} after the pyrolysis at 700°C for 3h are shown in Fig. 4-1, which indicates that the pyrolyzed powder is poorly crystallized with very fine particle. Fig. 4-2 gives the XRD results for the samples heat treated at 1600°C. The sample with 25 mol% LaO_{1.5} presents the pyrochlore + monoclinic structure, where the monoclinic phase formed from the tetragonal phase by cooling. The sample with 75 mol% LaO_{1.5} presents the pyrochlore + La(OH)₃ structure, in which La(OH)₃ formed from A-La₂O₃ and water. The SEM back scattered electron image ($\times 1000$) of the sample with 25 mol% LaO_{1.5} heat treated at 1600°C for 72h is shown in Fig. 4-3, where the grey areas are the monoclinic phase, and the white areas are pyrochlore. It can be seen that the sample is quite homogeneous, and many cracks in the sample are caused by the volume change of the martensitic tetragonal-to-monoclinic transformation during cooling. The measured content of LaO_{1.5} in both the tetragonal and pyrochlore phases at different temperatures are given in Table 4-3. The composition range of the pyrochlore phase is very narrow in the studied temperature range. At 1400°C it is almost a stoichiometric compound.

This is consistent with the conclusion of [1999Tab1] that the width of the pyrochlore field is less than 2 mol%. Due to the temperature limitation of the current experiments, it was not possible to confirm the composition range of the fluorite phase in ZrO_2 -rich region, and its possible existence in the $LaO_{1.5}$ -rich region.

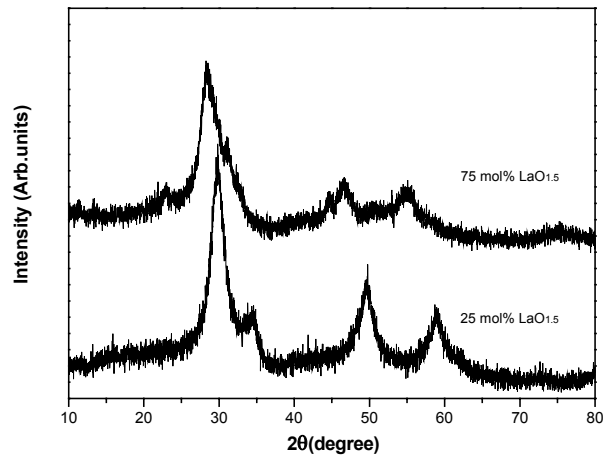


Figure 4-1. The XRD patterns of the as-pyrolysed $ZrO_2 - LaO_{1.5}$ samples at $700^\circ C$ for 3h.

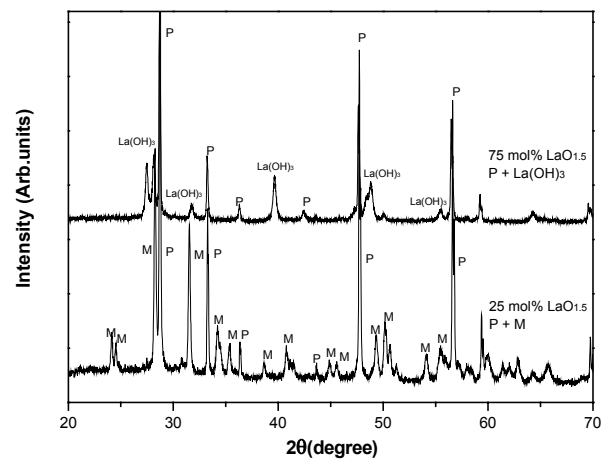


Figure 4-2. The XRD peaks of the samples after heat treatments at $1700^\circ C$ (The sample with 25 mol% $LaO_{1.5}$ presents the P + M structure. The sample with 75 mol% $LaO_{1.5}$ presents the P + $La(OH)_3$ structure).

4.3. Selected experimental data for optimization

4.3.1. Phase diagram data

The liquidus and high temperature phase equilibria data and invariant reactions reported by [1968Rou3, 1971Rou, 1972Cab, 2005Lak] are taken for the current assessment, together with the experimental data on the tetragonal + pyrochlore phase equilibrium obtained in this work. However, the C_2 phase reported by [1968Rou3, 1971Rou] is considered as the fluorite phase according to the experience from other systems. For the temperature of the

reaction $H\text{-La}_2\text{O}_3 \Leftrightarrow A\text{-La}_2\text{O}_3 + P$, a start value of 2073 K is arbitrarily given, due to the lack of experimental data. The solubility of ZrO_2 in the $A\text{-La}_2\text{O}_3$ phase is taken to be lower than 2 mol%, which is comparable to the result for the $A\text{-Nd}_2\text{O}_3$ phase. The homogeneity range of the pyrochlore phase is thought to be symmetric on both sides of the stoichiometric composition.

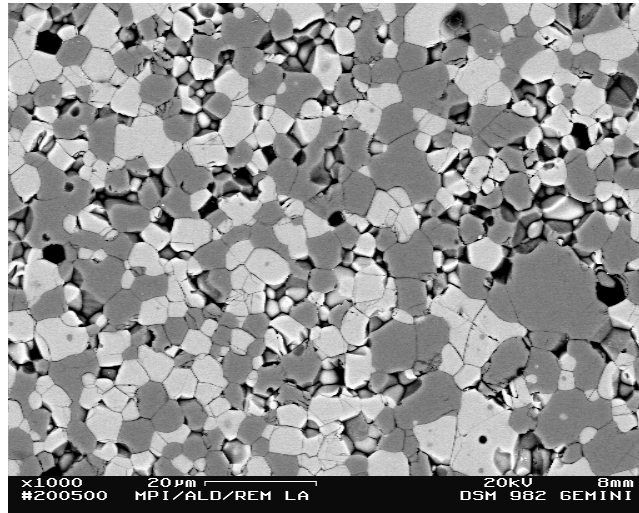


Figure 4-3. The SEM back scattered electron image ($\times 1000$) of the $\text{ZrO}_2\text{-25 mol\% LaO}_{1.5}$ sample heat treated at 1600°C for 72h (the grey areas are the monoclinic phase, and the white ones are pyrochlore).

4.3.2. Thermodynamic data

The data of the enthalpy of formation of the pyrochlore phase reported by [1971Kor, 1995Bol, 1998Jac, 2002Rog] show good agreement. They are more negative than the value reported by [2005Nav]. All of these data are considered, but not given a high weight for the assessment. The assessed result of the thermodynamic property ($CT\ln T + ET^{-1} + FT^2$ part of the Gibbs energy) of the pyrochlore phase given by [2005Sed] is accepted in this work.

4.4. Optimization procedure

The Gibbs energy parameters of the pyrochlore phase were preliminarily determined from the literature data on thermodynamic properties. Treating the pyrochlore phase as a stoichiometric compound, the phase diagram was roughly calculated by using the solid phase boundary and liquidus data, with only very limited number of parameters. Finally, a full optimization was carried out by taking the homogeneity range of pyrochlore into account. The parameters were adjusted simultaneously to fit all the selected experimental phase equilibria

and thermodynamic data. The thermodynamic parameters for all phases are summarized in **Appendix**.

4.5. Calculated results and discussion

The calculated $\text{ZrO}_2 - \text{LaO}_{1.5}$ phase diagram is shown in Fig. 4-4. Most of the selected experimental data are reasonably reproduced within the limits of experimental uncertainties. The optimized invariant reactions are included in Table 4-1.

The eutectic points for the reactions $\text{L} \Leftrightarrow \text{F} + \text{P}$ and $\text{L} \Leftrightarrow \text{F} + \text{X-La}_2\text{O}_3$ calculated in this work are 2529 K (39.6 mol% $\text{LaO}_{1.5}$) and 2288 K (77.5 mol% $\text{LaO}_{1.5}$) respectively, which fall well among the results of [1968Rou3, 1971Rou, 2005Lak]. The calculated liquidus presents some deviation from the experimental data of [1971Rou], because the work of [2005Lak] was considered in the optimization. Moreover, the sharp liquidus reported by [1971Rou] was also questioned by the previous review on this system [1998Ond]. For the melting point of the pyrochlore phase, the result of the present work (2556 K) is closer to the data of [1971Rou] than that of [2005Lak]. The results of [2005Lak] are not given a higher weight for assessment because no detailed information on the measurements is given. However, in a parallel work on the $\text{ZrO}_2 - \text{LaO}_{1.5} - \text{AlO}_{1.5}$ system, it has been proved that the optimized phase diagram without taking account of the data of [2005Lak] will have a worse agreement with the liquidus projection of the ternary phase diagram. In fact, because the experimental uncertainty of 100 K at such temperatures is normal for many systems, the present calculations are thought to be reasonable.

In the $\text{LaO}_{1.5}$ -rich region, the calculated data of the reactions $\text{L} + \text{P} \Leftrightarrow \text{F}$ (2309 K, 75.6 mol% $\text{LaO}_{1.5}$), $\text{F} \Leftrightarrow \text{P} + \text{X-La}_2\text{O}_3$ (2199 K, 69.1 mol% $\text{LaO}_{1.5}$) and $\text{X-La}_2\text{O}_3 \Leftrightarrow \text{P} + \text{H-La}_2\text{O}_3$ (2165 K, 86 mol% $\text{LaO}_{1.5}$) show reasonable agreements with the experimental results obtained by Rouanet [1971Rou], while the compositions of the solid phases could not be well fitted, because it was already accepted that the homogeneity range of the pyrochlore phase is not so wide, and the composition of $\text{X-La}_2\text{O}_3$ phase reported by [1971Rou] is also less reliable for their experimental difficulties at high temperatures. For the reaction $\text{H-La}_2\text{O}_3 \Leftrightarrow \text{P} + \text{A-La}_2\text{O}_3$, the present calculation reveals a value of 1994 K.

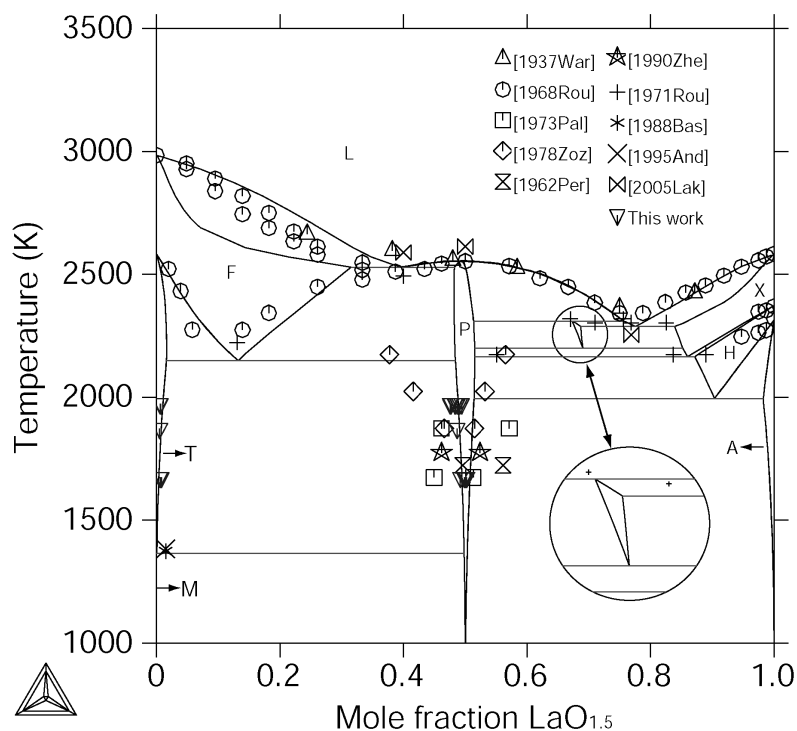


Figure 4-4. The calculated ZrO₂ – LaO_{1.5} phase diagram together with experimental data.

At the ZrO₂-rich side of the diagram, the experimental data on the P + T equilibrium obtained in this work are well reproduced. However, the calculated temperature of the invariant reaction $F \Leftrightarrow P + T$ cannot be fitted to value as high as 2223 K reported by [1971Rou], unless a very positive enthalpy of formation of the fluorite phase is used. Fig. 4-5 shows the calculated metastable ZrO₂ – LaO_{1.5} phase diagram without the pyrochlore phase. In this work, the enthalpy of formation of the fluorite phase at 50 mol% LaO_{1.5} with respect to the monoclinic ZrO₂ and A-type LaO_{1.5} is $-939 \text{ J}\cdot\text{mol}^{-1}$ at 298.15 K. A much more positive enthalpy of formation will make the fluorite phase only stable at high temperatures. Owing to the similarities of the ZrO₂ – REO_{1.5} systems, it is reasonable to assume that before ordering occurs, the fluorite phase is always stable at room temperature. Additionally, the calculated phase diagram in Fig. 4-5 presents a wide tetragonal + fluorite two-phase region, which is also consistent with the tendency that with increasing the ionic radius of RE⁺³, the tetragonal + fluorite two-phase region enlarges gradually. The calculated temperature of the reaction $T \Leftrightarrow P + M$ is 1363 K, which is only 4 K lower than the T_0 temperature for pure ZrO₂. Moreover, the calculated composition of the tetragonal phase for this reaction is only 0.13 mol% LaO_{1.5} which is consistent with present experimental result. The higher value 1.5 mol% LaO_{1.5} reported by [1988Bas, 1995And] is thought to be the composition at a nonequilibrium state.

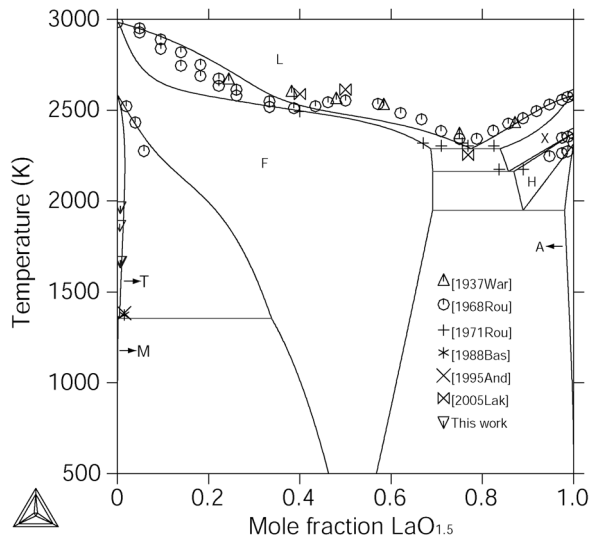


Figure 4-5. The calculated $ZrO_2 - LaO_{1.5}$ phase diagram without the pyrochlore phase together with experimental data.

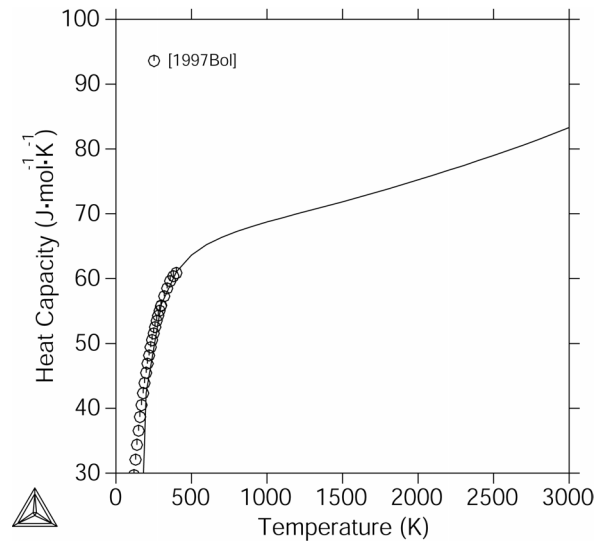


Figure 4-6. Calculated and experimental heat capacity of the stoichiometric pyrochlore phase (per mole of cations) in the $ZrO_2 - LaO_{1.5}$ system.

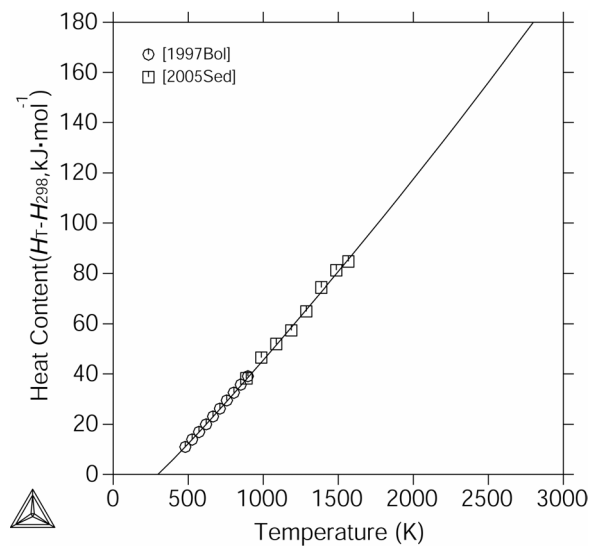


Figure 4-7. Calculated enthalpy increment ($H_T - H_{298}$) of the stoichiometric pyrochlore phase (per mole of cations) in the $ZrO_2 - LaO_{1.5}$ system together with experimental data.

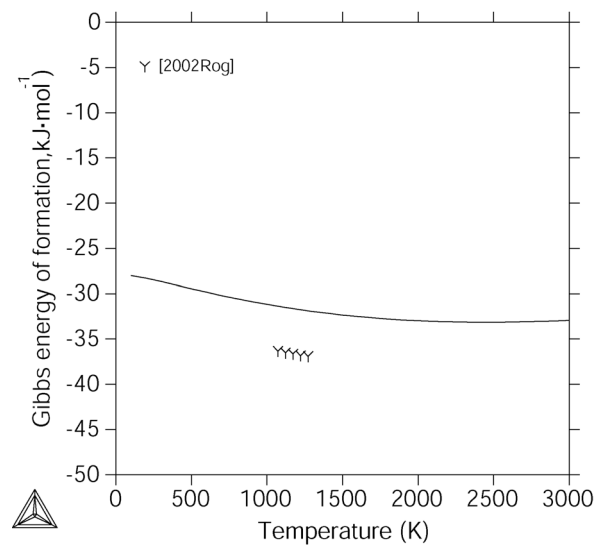


Figure 4-8. The calculated Gibbs energy of formation of the stoichiometric pyrochlore phase (per mole of cations) in the $ZrO_2 - LaO_{1.5}$ system together with experimental data.

Though the enthalpy of formation of the pyrochlore phase was experimentally measured by several groups [1971Kor, 1995Bol, 1998Jac, 2002Rog, 2005Nav], the result obtained in this work doesn't fit well any of them. A parallel work on the modeling of the $ZrO_2 - LaO_{1.5} - AlO_{1.5}$ system by Fabrichnaya et al. reveals that the values reported by

[1971Kor, 1995Bol, 1998Jac, 2002Rog] are too negative to reproduce the experimental tie-lines [2005Lak]. Finally, a value of $-27516 \text{ J.mol}^{-1}$ was obtained for the enthalpy of formation of pyrochlore in this work, which is slightly less stable than the data of [1971Kor, 1995Bol, 1998Jac, 2002Rog], but more negative than the value around $-22585 \text{ J.mol}^{-1}$ included in [2005Nav]. The calculated heat capacity and enthalpy increment ($H_T - H_{298}$) are plotted in Fig. 4-6 and Fig. 4-7 respectively, showing good agreement with the experimental data. In Fig. 4-8, owing to the more negative enthalpy of formation of the pyrochlore phase of the data [1998Jac, 2002Rog], some deviation also exists between the present calculated and their experimental Gibbs energies of formation of the pyrochlore phase.

Table 4-1. The invariant reactions in the $\text{ZrO}_2 - \text{LaO}_{1.5}$ system.

Reaction	Type	Reference	Temperature (K)	Composition of phases (mol% $\text{LaO}_{1.5}$)		
$L \Leftrightarrow F + P$	eutectic	[1971Rou]	2493	40	–	–
		[1972Cab]	2497 ± 10	–	–	–
		[2005Lak]	2588	40	–	–
		This work	2529	39.6	31.4	48.2
$F \Leftrightarrow T + P$	eutectoid	[1971Rou]	2223	13.1	–	–
		This work	2155	13.2	1.7	48.4
$T \Leftrightarrow M + P$	eutectoid	[1988Bas]	1373	1.5	–	–
		[1995And]	1383	1.5	–	–
		This work	1363	0.13	0.04	49.8
$L \Leftrightarrow P$	congruent	[1964Lin]	2523	–	50	–
		[1971Rou]	2553	–	50	–
		[1972Por]	2433 ± 50	–	50	–
		[1978Zoz]	2503 ± 20	–	50	–
		[2005Lak]	2613	–	50	–
		This work	2556	49.4	49.4	–
$L + P \Leftrightarrow F$	peritectic	[1971Rou]	2318	75.6	55	67
		This work	2309	75.6	51.4	67.4
$L \Leftrightarrow F + X$	eutectic	[1971Rou]	2303	76.9	71	82.4
		[2005Lak]	2253	76.9	–	–
		This work	2288	77.5	68.7	83.9
$F \Leftrightarrow P + X$	eutectoid	[1971Rou]	2223	68.4	55	83.7
		This work	2199	69.1	51.5	85.2

X \leftrightarrow P + H	eutectoid	[1971Rou]	2173	83.7	55	87.3
		This work	2165	86	51.5	87.2
H \leftrightarrow P + A	eutectoid	This work	1994	90.4	51.4	98.2

Table 4-2. The reported enthalpy of formation of the pyrochlore phase (ZrO_2 -50 mol% $\text{LaO}_{1.5}$, for one mole of cations, from the monoclinic ZrO_2 and A-type $\text{LaO}_{1.5}$).

Reference	Value ($\text{J}\cdot\text{mol}^{-1}$)	Temperature (K)
[1971Kor]	-31470 ± 1020	298.15
[1995Bol]	-33950 ± 1600	974
	-34025 ± 1600	298.15
[1998Jac]	-33450 ± 1250	298.15
[2002Rog]	-33575 ± 200	298.15
[2005Nav]	-22585	298.15
This work	-27515.6	298.15

Table 4-3. The measured phase composition data (mol% $\text{LaO}_{1.5}$) for the tetragonal + pyrochlore phase equilibria in the $\text{ZrO}_2 - \text{LaO}_{1.5}$ system at different temperatures.

Temperature (K)	T	P
1673	0.7 ± 0.3	49.9 ± 0.5
1873	0.6 ± 0.3	48.7 ± 0.5
1973	0.6 ± 0.3	48.4 ± 0.5

Chapter 5

Experimental study and thermodynamic modeling of the $\text{ZrO}_2 - \text{NdO}_{1.5}$ system

5.1. Literature review

5.1.1. Phase equilibria

The phase equilibria of the $\text{ZrO}_2 - \text{Nd}_2\text{O}_3$ system were experimentally studied by many groups [1955Bro, 1956Rot, 1965Dav, 1965Glu, 1970Rou, 1971Rou, 1981Gav1, 1982Gav, 1995And, 1995Kat].

[1955Bro] firstly constructed a phase diagram for the $\text{ZrO}_2 - \text{Nd}_2\text{O}_3$ system using X-ray diffraction. However, wrong structural modifications on both ZrO_2 and Nd_2O_3 sides were given. The compound $\text{Nd}_2\text{Zr}_2\text{O}_7$ was not reported, and a miscibility gap of the cubic phase was plotted in combination with an invariant reaction with the Nd_2O_3 -based solid solution at around 1100°C . This phase diagram was slightly modified by [1956Rot] by including pyrochlore $\text{Nd}_2\text{Zr}_2\text{O}_7$ (P). Later, [1962Per] reported a similar phase diagram to that of [1955Bro] by indicating the pyrochlore phase and a higher temperature for the invariant reaction $F \Leftrightarrow P + A\text{-Nd}_2\text{O}_3$.

[1965Dav, 1965Glu] studied the phase relations in the complete composition range up to 1700°C by using XRD measurements. In the ZrO_2 -rich region, the F + T two-phase region was determined, and the fluorite phase could be stabilized to very low temperature according to [1965Dav]. The minimum solubility of Nd_2O_3 in the fluorite phase was reported for different temperatures. According to both work, the tetragonal and monoclinic phases can dissolve as much as 2-4 mol% Nd_2O_3 . At the Nd_2O_3 -rich side, the low temperature hexagonal structure of the Nd_2O_3 solid solution coexists with the pyrochlore phase. Above 1500°C , a phase with Mn_2O_3 structure (C-type) forms between the Nd_2O_3 -rich hexagonal (H-type) and pyrochlore phases by a eutectoid reaction $C_2 \Leftrightarrow X\text{-Nd}_2\text{O}_3 + P$. The maximum solubility of Nd_2O_3 in pyrochlore is 40 mol% at $1500\text{-}1700^\circ\text{C}$. The maximum solubility of ZrO_2 in the H-type Nd_2O_3 was determined as 5 mol%.

[1970Rou, 1971Rou] measured the $\text{ZrO}_2 - \text{Nd}_2\text{O}_3$ phase diagram above 1400°C . The liquidus was determined by the cooling curve of the thermal analysis in the whole composition range, and the solidus was accordingly estimated. The solid-state phase transitions above 1800°C were observed by HTXRD using a Re ribbon under reducing conditions ($\text{He} + \sim 10\% \text{H}_2$). The pyrochlore phase was estimated to transform into fluorite at

around 2300° C, what is consistent with 2220°C reported by [1982Zoz], but does not agree with 2000°C reported by [1974Mic]. At high temperatures, Rouanet [1970Rou, 1971Rou] revealed two invariant reactions: $L \Leftrightarrow C_2 + X\text{-Nd}_2\text{O}_3$ (2100°C, L: 70 mol% Nd_2O_3 , C_2 : 60 mol% Nd_2O_3) and $X\text{-Nd}_2\text{O}_3 \Leftrightarrow H\text{-Nd}_2\text{O}_3 + C_2$ (2060°C, $H\text{-Nd}_2\text{O}_3$: 87 mol% Nd_2O_3 ; $X\text{-Nd}_2\text{O}_3$: 80 mol% Nd_2O_3 ; C_2 : 59 mol% Nd_2O_3). The X-type Nd_2O_3 -based solid solution was not well studied because of its high volatility, and a possible invariant reaction involving $H\text{-Nd}_2\text{O}_3$, $A\text{-Nd}_2\text{O}_3$, and the so-called Mn_2O_3 structured C_2 phase was not detected in their work. At 1440° C, the C_2 phase was found to decompose into pyrochlore and $A\text{-Nd}_2\text{O}_3$ using the X-ray diffraction, which is consistent with the work of [1965Glu].

[1972Por] measured the melting point of the composition $\text{Nd}_2\text{Zr}_2\text{O}_7$ to be 2320°C. The respective result of [1982Zoz] was $2280 \pm 20^\circ\text{C}$. Both studies revealed that the melting point was probably very close to the pyrochlore \Leftrightarrow fluorite transition temperature.

Gavriš et al. [1981Gav1, 1982Gav] studied the phase formation of the $\text{ZrO}_2 - \text{Nd}_2\text{O}_3$ system in the whole composition range between 1300 and 1900° C by X-ray diffraction and crystal-optical methods. However, some metastable phases were reported in their paper probably because the heat treatment was only done for a short time and not efficient to form the stable phases. They obtained same results on the phase relations as [1970Rou, 1971Rou] at high temperatures. The homogeneity range of the pyrochlore phase was found to be 30-33.3 mol% Nd_2O_3 at 1500°C, and increased to 20-55 mol% Nd_2O_3 at 1900°C. For the A-type Nd_2O_3 phase, the reported maximum solubility of ZrO_2 was around 10 mol%.

[1991Wit] studied the $\text{ZrO}_2 - \text{NdO}_{1.5}$ system using electron and XRD at 1600°C. The pyrochlore phase field was found to occur from 38 to 55 mol% $\text{NdO}_{1.5}$. In a study of the influence of the composition on the $T \Rightarrow M$ transformation, [1995And] derived the eutectoid point of the reaction $T \Leftrightarrow M + P$ at 880° C and 1.0 mol% Nd_2O_3 using DTA and dilatometry. The $F + T$ phase equilibrium was experimentally examined by [1995Kat], and the phase boundary data of both the fluorite and the tetragonal phase were determined at 1600, 1700, and 1800° C.

The invariant reactions reported in literature are collected in Table 5-1.

5.1.2. Thermodynamic data

[1971Kor] determined the enthalpy of formation of the stoichiometric pyrochlore phase (from oxides) by combustion in a bomb calorimeter and reported a value of $-27719 \text{ J}\cdot\text{mol}^{-1}$ (per mole of cations). However, [2005Nav] reported a less negative value of around $-16200 \text{ J}\cdot\text{mol}^{-1}$ (per mole of cations) recently.

Lutique et al. [2003Lut1, 2003Lut2] measured the heat capacity of stoichiometric $\text{Nd}_2\text{Zr}_2\text{O}_7$ from 300 K to 1600 K by differential scanning calorimetry and from 0.45 K to 400 K by adiabatic calorimetry and the hybrid adiabatic relaxation method.

The heat content ($H_T - H_{298}$) for the pyrochlore phase $\text{Nd}_2\text{Zr}_2\text{O}_7$ was measured using drop calorimetry in a recent work of Sedmidubsky et al. [2005Sed] in the temperature range 484-1487 K.

Very recently, [2005Oht] modeled the fluorite \Leftrightarrow pyrochlore order-disorder transition in this system with a model $(\text{Zr}^{+4}, \text{Nd}^{+3})_{0.5}(\text{Nd}^{+3}, \text{Zr}^{+4})_{0.5}(\text{O}^{-2}, \text{Va})_2$. Two miscibility gaps of fluorite were shown in their work, but poorly reasonable phase relationships were presented.

5.2. Experimental results and discussion

5.2.1. The as-pyrolysed state

Totally sixteen compositions were prepared for the study of the $\text{ZrO}_2 - \text{NdO}_{1.5}$ system. The XRD patterns of selected samples after the pyrolysis at 1000°C for 1h are shown in Fig. 5-1. Very clear peaks in all samples reveal that well-crystallized powders already can be obtained under these conditions compared with the poor crystallized samples after pyrolysis at 700°C for the other systems. For the samples less than 70 mol% $\text{NdO}_{1.5}$, the XRD patterns present mostly peaks of the tetragonal or fluorite phase, and above 70 mol% $\text{NdO}_{1.5}$, the existence of the A- Nd_2O_3 phase can be identified from the XRD peaks.

The phase identified together with the compositions of the samples are listed in Table 5-2.

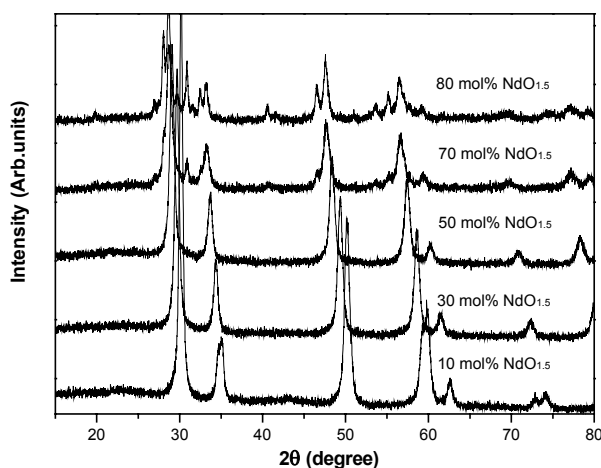


Figure 5-1. The XRD patterns of the as-pyrolysed $\text{ZrO}_2 - \text{NdO}_{1.5}$ samples at 1000°C for 1h.

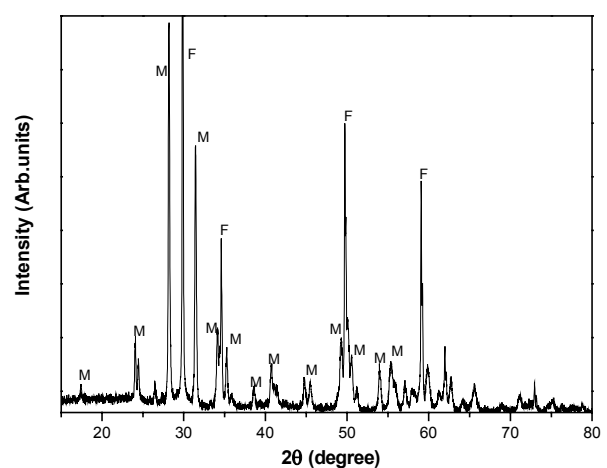


Figure 5-2. The XRD patterns for the ZrO_2 -10 mol% $\text{NdO}_{1.5}$ sample heat treated at 1600°C for 72h.

5.2.2. The tetragonal + fluorite phase equilibrium

The heat treated sample containing 10 mol% $\text{NdO}_{1.5}$ presents well-distributed monoclinic + fluorite structure according to the XRD patterns in Fig. 5-2. Fig. 5-3 shows the SEM back scattered electron image ($\times 1000$) of the same sample. The grey areas in Fig. 5-3 are the monoclinic phase formed from the tetragonal phase during cooling, and the white ones are the fluorite phase. Table 5-3 gives the determined compositions for the tetragonal and fluorite phases. A wide tetragonal + fluorite two-phase region can be derived according to the present experimental data, which are consistent with the data reported by [1995Kat]. The solubility of $\text{NdO}_{1.5}$ in the tetragonal phase is only around 2 mol% $\text{NdO}_{1.5}$ in the studied temperature range.

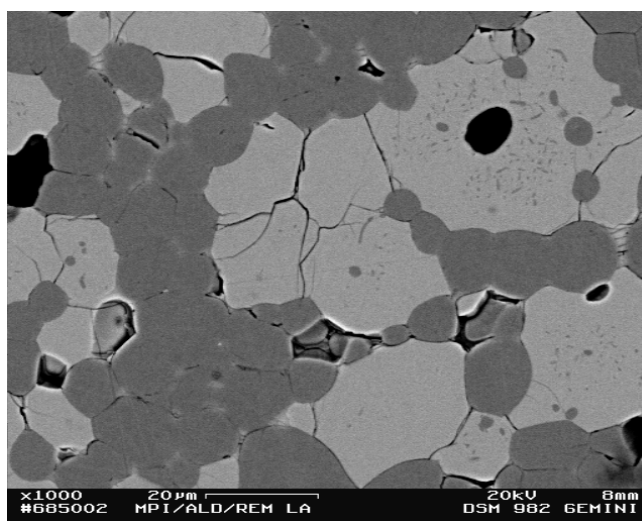


Figure 5-3. The SEM back scattered electron image ($\times 1000$) of the sample containing 10 mol% $\text{NdO}_{1.5}$ heat treated at 1600°C for 72h (the grey areas are the monoclinic phase formed from the tetragonal phase during cooling, and the white ones are the fluorite phase).

5.2.3. The fluorite + pyrochlore phase equilibrium

The order-disorder transition between the fluorite and pyrochlore phases presents complex characters according to the present experimental work. In the ZrO_2 -rich region, 10 samples with compositions from 30 to 40 mol% $\text{NdO}_{1.5}$ (without 31 mol%) with the step of each 1 mol% were prepared, and heat treated at different temperatures. Clear superstructure peaks of pyrochlore with different intensities can be found for all the compositions. Up to 1600°C , the XRD peaks of all those samples do not show visibly separated peaks for the fluorite and pyrochlore phases. Probably the samples are not completely ordered at those temperatures. The XRD results of the samples heat treated at 1700°C confirm this point. At this temperature separated peaks of fluorite and pyrochlore can be found for the compositions

from 32 to 34 mol% $\text{NdO}_{1.5}$. Fig. 5-4 shows the lattice parameters determined in this work by XRD using Si and Al_2O_3 powder as internal standard and those data collected from literature. The fluorite + pyrochlore two-phase region obtained from the difference of the lattice parameters is very narrow (around 30 to 36 mol% $\text{NdO}_{1.5}$).

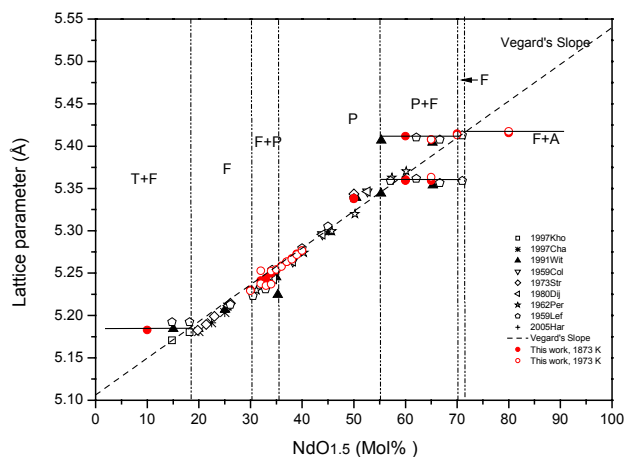


Figure 5-4. The lattice parameters of fluorite and pyrochlore in the $\text{ZrO}_2 - \text{NdO}_{1.5}$ system determined by this work and those data collected from literature.

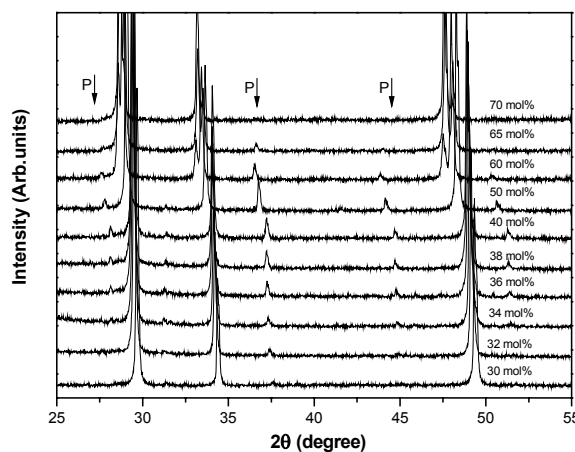


Figure 5-5. The XRD patterns for the $\text{ZrO}_2 - \text{NdO}_{1.5}$ samples (30-70 mol% $\text{NdO}_{1.5}$) heat treated at 1600°C .

Some selected XRD patterns for the samples heat treated at 1600°C are shown in Fig. 5-5. The intensities of the superstructure peaks of pyrochlore phases gradually enhance with increasing the $\text{NdO}_{1.5}$ content up to 50 mol%, and then reduce at higher $\text{NdO}_{1.5}$ contents due to the increase of the amount of the fluorite phase. The sample containing 70 mol% $\text{NdO}_{1.5}$ consists of almost pure fluorite. In the $\text{NdO}_{1.5}$ -rich region, the XRD peaks of the fluorite and pyrochlore phases are easily separated after the heat treatment at 1600°C even for a short time (Fig. 5-5). Combining the XRD measurements with EDX analysis, the determined compositions for the fluorite + pyrochlore equilibrium at $\text{NdO}_{1.5}$ -rich side are given in Table 5-3, and also marked in Fig. 5-4 by the lattice parameter measurement. However, the homogeneity range of pyrochlore at the ZrO_2 -rich side is much larger than that at the $\text{NdO}_{1.5}$ -rich side according to present experimental data. Considering the difference of the ordering kinetics of the pyrochlore phase in different regions, it is reasonable to conclude that the ordering of pyrochlore at the ZrO_2 -rich side should be a long-time process, and it is even difficult to reach complete thermodynamic equilibrium at 1700°C after 36 h, while it is much easier for the samples in the $\text{NdO}_{1.5}$ -rich region. Thus, the data on the two-phase region in ZrO_2 -rich obtained from XRD measurements are thought to be still in metastable state.

Finally, different phase regions are divided according to the change of lattice parameters in Fig. 5-4, assuming that the pyrochlore phase has the symmetric homogeneity range. The Vegard's slope is constructed based on the lattice parameter of pure zirconia in literature [1992Yas], which assessed this value from abundant ZrO_2 -based systems. However, it seems that the lattice parameter of completely ordered pyrochlore at 50 mol% $NdO_{1.5}$ doesn't fit onto this slope.

5.2.4. The fluorite + A- Nd_2O_3 and pyrochlore + A- Nd_2O_3 phase equilibria

Fig. 5-6 is the SEM photograph for the fluorite + A-type Nd_2O_3 microstructure of the sample 80 mol% $NdO_{1.5}$ heat treated at 1873 K for 72h, where the grey areas are the fluorite phase, and the white ones are the A- Nd_2O_3 phase with lathy morphology. According to the XRD measurements, the samples with the compositions 60-80 mol% $NdO_{1.5}$ heat treated at 1673 K presents the pyrochlore and A- Nd_2O_3 structure. This result is consistent with the invariant reaction $F \Leftrightarrow P + A-Nd_2O_3$ which occurs at 1713 K reported by [1971Rou]. The measured compositions of the fluorite phase and the A- Nd_2O_3 phase are given in Table 5-3. The composition of the fluorite phase of fluorite + A- Nd_2O_3 phase equilibrium at 1873 K is rather close to that of fluorite + pyrochlore phase equilibrium, and indicates that the fluorite phase will decompose at some lower temperature in this region.

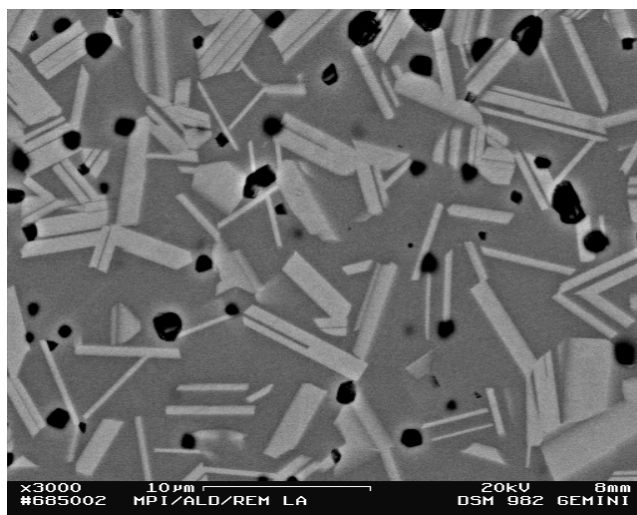


Figure 5-6. The SEM back scattered electron image ($\times 3000$) of the sample with 80 mol% $NdO_{1.5}$ heat treated at 1600°C for 72h (the grey areas are the fluorite phase, and the white ones are the A-type Nd_2O_3).

5.3. Selected experimental data for optimization

The liquidus data and the invariant reactions at the $\text{NdO}_{1.5}$ -rich side reported by [1971Rou], the phase boundary data of tetragonal + fluorite, fluorite + pyrochlore, and fluorite + A- Nd_2O_3 phase equilibria obtained in this work and those of [1995Kat, 1999Tab] are accepted as phase diagram data.

The heat content data for pyrochlore determined by [1997Bol, 2005Sed] and in this work are consistent and are taken for the optimization of thermodynamic properties, as well as those data for 30 mol% $\text{NdO}_{1.5}$ obtained in this work. Furthermore, the heat capacity data for the 50 mol% $\text{NdO}_{1.5}$ pyrochlore measured by [2003Lut1, 2003Lut2] are also considered for the optimization. The enthalpy of formation of pyrochlore reported by [1971Kor] is considered, but not given much weight in the assessment, due to the proved uncertainty in the $\text{ZrO}_2 - \text{LaO}_{1.5}$ system.

5.4. Optimization procedure

As the first step, the phase equilibria without the ordered pyrochlore phase were roughly optimized by adopting the liquidus, tetragonal + fluorite phase boundary data and the heat content data for the ZrO_2 -30 mol% $\text{NdO}_{1.5}$ sample, with limited number of parameters. Then, by treating the pyrochlore phase as the stoichiometric compound, a further assessment was done by adding the heat content and enthalpy of formation data of the pyrochlore phase. Finally, a full assessment is carried out by simultaneously using all selected data.

For the fluorite phase, a $T \ln T$ contribution to zeroth order interaction parameter was applied to fit the experimental enthalpy increment data. For the tetragonal, X-, H- and A-type phases, only one interaction parameter was adopted because they are only stable at a limited range of composition and temperature. No any interaction parameter was used for the monoclinic phase because of its negligible homogeneity range.

The optimized thermodynamic parameters for all phases are given in **Appendix**.

5.5. Calculated results and discussion

The calculated $\text{ZrO}_2 - \text{NdO}_{1.5}$ phase diagram is presented in Fig. 5-7, compared with the experimental data. The invariant reactions obtained in the calculation are listed in Table 5-1 together with the experimental results.

Due to a wide tetragonal + fluorite two-phase region, the fluorite phase can not be completely stabilized to low temperature. It decomposes into the tetragonal and pyrochlore phases at 1487 K and 23.4 mol% $\text{NdO}_{1.5}$ according to the present calculation. The calculated

invariant reaction $T \Leftrightarrow M + P$ occurs at 1326 K and 1.0 mol% $\text{NdO}_{1.5}$, which is consistent with the composition reported by [1995And]. However, the temperature (1153 K) suggested for the reaction by [1995And] is much lower, and is actually the temperature of the martensitic transformation, which is not corresponding to this invariant reaction. The calculated T_0 line for the monoclinic and tetragonal phases in Fig. 5-8 reproduces well the data of [1995And, 1993Yas]. For the diffusionless fluorite to tetragonal transition, the present calculation gives the prediction that the T' phase can be only obtained for the compositions less than 12 mol% $\text{NdO}_{1.5}$.

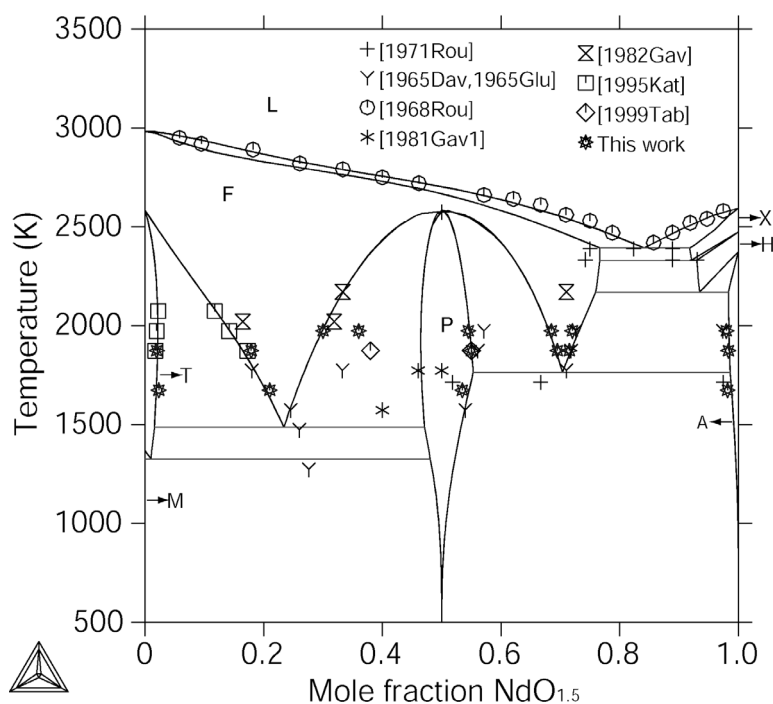


Figure 5-7. The calculated $\text{ZrO}_2 - \text{NdO}_{1.5}$ phase diagram compared with the experimental data.

The experimental data on the fluorite + pyrochlore phase equilibrium are reproduced well within the experimental limits. To fit the phase boundary of the fluorite phase at the $\text{NdO}_{1.5}$ -rich side, the congruent transition temperature has to be elevated by 11 K with respect to 2573 K estimated by [1971Rou]. Compared to the $\text{ZrO}_2 - \text{LaO}_{1.5}$ system, the homogeneity range of the pyrochlore phase in the $\text{ZrO}_2 - \text{NdO}_{1.5}$ system is considerably larger. The temperature of the invariant reaction $F \Leftrightarrow P + A\text{-Nd}_2\text{O}_3$ is calculated to be 1763 K, which is 50 K higher than the result reported in [1971Rou], while the calculated compositions of the fluorite and pyrochlore phases show deviation with the experimental data [1971Rou] within 5 mol% $\text{NdO}_{1.5}$. The present results are thought to be more reasonable than the data obtained by XRD measurements in [1971Rou], because they are optimized from the more reliable phase

boundary data obtained in this work. The calculated invariant reactions $L \Leftrightarrow F + X\text{-Nd}_2\text{O}_3$ and $X\text{-Nd}_2\text{O}_3 \Leftrightarrow H\text{-Nd}_2\text{O}_3 + F$ show reasonable agreement with the experimental data of [1971Rou] except some deviations on the compositions of the terminal solutions. Considering the large experimental error in this region, the present calculations are reasonably acceptable. At high temperatures, the calculated invariant reactions $L \Leftrightarrow F + X\text{-Nd}_2\text{O}_3$ (2393 K, L: 84.1 mol% $\text{NdO}_{1.5}$) and $X\text{-Nd}_2\text{O}_3 \Leftrightarrow F + H\text{-Nd}_2\text{O}_3$ (2330 K, X: 92.1 mol% $\text{NdO}_{1.5}$) are considerably consistent with those data reported by Rouanet [1971Rou] within the limits of uncertainties. The reaction $H\text{-Nd}_2\text{O}_3 \Leftrightarrow F + A\text{-Nd}_2\text{O}_3$ is predicted at 2169 K in this work.

The enthalpies of formation of fluorite and pyrochlore (per mole of cations) of ZrO_2 -50 mol% $\text{NdO}_{1.5}$ at 298 K calculated in this work are $-8029 \text{ J}\cdot\text{mol}^{-1}$ and $-18169 \text{ J}\cdot\text{mol}^{-1}$, respectively, which are comparable to those data of the $\text{ZrO}_2 - \text{LaO}_{1.5}$ system. Fig. 5-9 and Fig. 5-10 present the experimental and calculated heat content for the composition 30 mol% $\text{NdO}_{1.5}$ and 50 mol% $\text{NdO}_{1.5}$, respectively. For the 30 mol% $\text{NdO}_{1.5}$ sample with fluorite structure, the calculation shows some deviation with the experimental data at high temperatures. A better fit can be reached if a larger value for the $T \ln T$ part of the interaction parameter is used. However, finally this value is selected to be -32 by taking the other $\text{ZrO}_2 -$

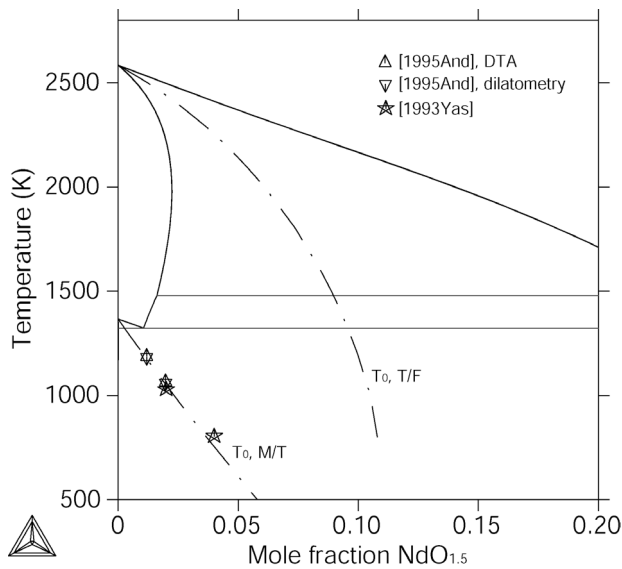


Figure 5-8. The calculated $\text{ZrO}_2 - \text{NdO}_{1.5}$ partial phase diagram, and T_0 lines for monoclinic + tetragonal and tetragonal + fluorite equilibria together with experimental data.

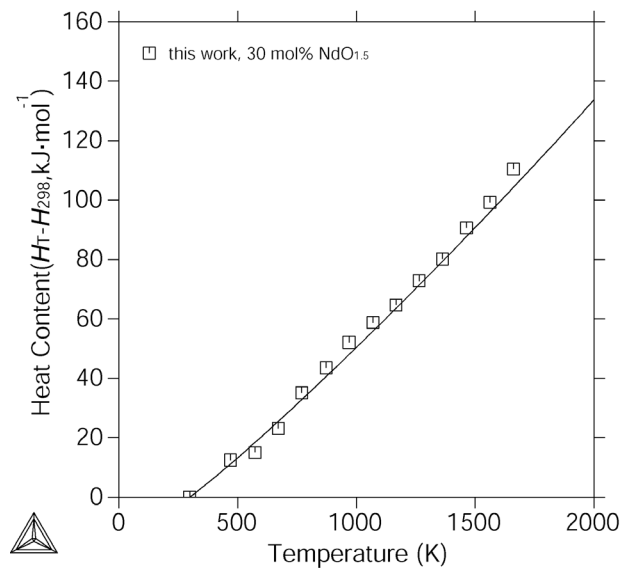


Figure 5-9. The calculated heat content ($H_T - H_{298}$) of the sample ZrO_2 -30 mol% $\text{NdO}_{1.5}$ together with experimental data.

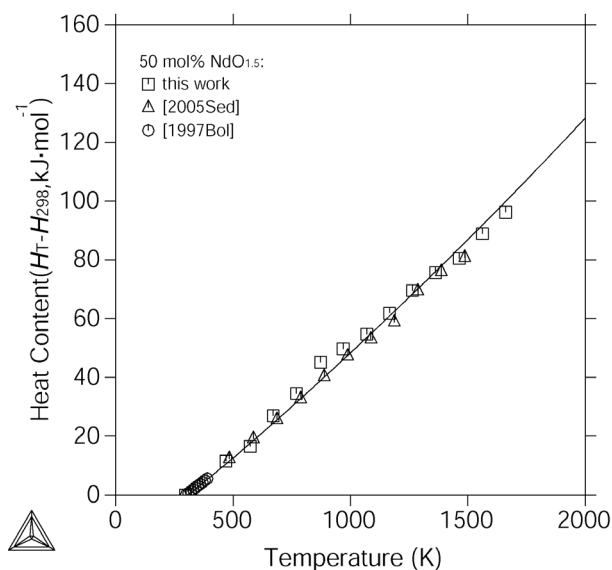


Figure 5-10. The calculated enthalpy increment ($H_T - H_{298}$) of the ZrO_2 -50 mol% $NdO_{1.5}$ sample together with experimental data.

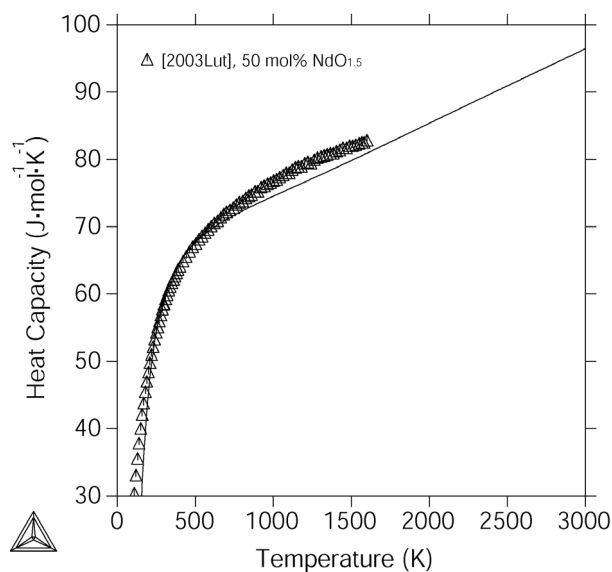


Figure 5-11. The calculated heat capacity of stoichiometric pyrochlore in $ZrO_2 - NdO_{1.5}$ system together with the experimental data.

$REO_{1.5}$ system into account, and also because a coefficient with larger value for this $T \ln T$ part can question the reasonability of thermodynamic properties. For the pyrochlore at 50 mol% $NdO_{1.5}$, good consistency is found between present experimental data and those of [2005Sed, 1997Bol], and the calculation reproduces experimental well except slight discrepancy at high temperatures. This is caused by the effort to obtain the agreement with the experimental heat capacity data, which is shown in Fig. 5-11. In view of the experimental uncertainties, the present calculations on both heat content and heat capacity are reasonably acceptable.

Table 5-1. The invariant reactions in the $ZrO_2 - NdO_{1.5}$ system.

Reaction	Type	Reference	Temperature (K)	Composition of phases (mol% $NdO_{1.5}$)		
$L \Leftrightarrow F + X$	eutectic	[1971Rou]	2388	82.3	75	89
		This work	2393	84.1	76.7	91.8
$X \Leftrightarrow H + F$	eutectoid	[1971Rou]	2333	89	93.1	74.2
		This work	2330	92.1	93	76.7
$H \Leftrightarrow F + A$	eutectoid	This work	2169	93.5	76	98.3
$F \Leftrightarrow P + A$	eutectoid	[1971Rou]	1713	66.7	51.9	97.4
		This work	1763	70.3	55.3	98.6
$F \Leftrightarrow P$	congruent	[1971Rou]	2573	50	50	–
		This work	2584	50	50	–

$F \Leftrightarrow T + P$	eutectoid	This work	1487	23.4	1.6	47.1
$T \Leftrightarrow M + P$	eutectoid	[1995And]	1153	1.0	–	–
		This work	1326	1.0	0.03	48.1

Table 5-2. The composition of the samples investigated in the $ZrO_2 - NdO_{1.5}$ system and observed phases.

No.	NdO _{1.5} (mol%)	Observed phases		
		1400 °C	1600 °C	1700 °C
1	10	F + M	F + M	F + M
2	30	P	F	F
3	32	P	P	F + P
4	33	P	P	F + P
5	34	P	P	F + P
6	35	P	P	P
7	36	P	P	P
8	37	P	P	P
9	38	P	P	P
10	39	P	P	P
11	40	P	P	P
12	50	P	P	P
13	60	P + A	P + F	P + F
14	65	P + A	P + F	P + F
15	70	P + A	F	F
16	80	P + A	F + A	F + A

Table 5-3. Measured phase composition data (mol% NdO_{1.5}) for different phase equilibria in the $ZrO_2 - NdO_{1.5}$ system at different temperatures.

Temperature (K)	T + F		P + F		F (P) + A	
	T	F	P	F	F (P)	A
1673	2.3 ± 0.5	21 ± 1	–	–	54 ± 1.5	98 ± 1
1873	2.0 ± 0.5	17.9 ± 1	55 ± 1	69.5 ± 1	71.5 ± 1	98 ± 1
1973	–	–	54.5 ± 1	68.5 ± 1		98 ± 1

Chapter 6

Experimental study and thermodynamic modeling of the $\text{ZrO}_2 - \text{SmO}_{1.5}$ system

6.1. Literature review

6.1.1. Phase equilibria

The phase equilibria of the $\text{ZrO}_2 - \text{Sm}_2\text{O}_3$ system were experimentally investigated by [1962Per, 1968Rou2, 1971Rou, 1981Gav, 1982Zoz, 1995And, 1999Tab].

[1962Per] firstly studied the phase relations of the $\text{ZrO}_2 - \text{Sm}_2\text{O}_3$ system in the temperature range 1000-2500°C. However, most of the phase boundaries and reactions were given by dashed lines, which were thought to be less precise. A detailed determination was done by [1968Rou2, 1971Rou] above 1800°C using HTXRD measurements. The liquidus curve was well determined and the solidus was accordingly estimated. A continuous transition $C_1 \Leftrightarrow C_2$ was reported like in some other systems they studied. However, this was shown to be not correct according to the recent experimental work on the $\text{ZrO}_2 - \text{GdO}_{1.5}$ system [2005Zin]. The invariant reaction $L \Leftrightarrow F + X\text{-Sm}_2\text{O}_3$ was shown occurring at 2190°C and 75 mol% Sm_2O_3 . Three other reactions $X\text{-Sm}_2\text{O}_3 \Leftrightarrow F + \text{H-Sm}_2\text{O}_3$, $\text{H-Sm}_2\text{O}_3 \Leftrightarrow F + \text{A-Sm}_2\text{O}_3$, and $\text{A-Sm}_2\text{O}_3 + F \Leftrightarrow \text{B-Sm}_2\text{O}_3$ were only estimated in the work of [1968Rou2, 1971Rou]. In the ZrO_2 -rich region of the system, the phase boundary of $F / F + T$ was determined by HTXRD. A fluorite + pyrochlore two-phase region was proposed by dashed lines. [1999Tab] confirmed this two-phase region beyond 55 mol% $\text{SmO}_{1.5}$ by XRD measurements, but, in the ZrO_2 -rich region, no two-phase region could be detected.

The stoichiometric pyrochlore \Leftrightarrow fluorite transition was determined at 1920°C by [1982Zoz] using DTA. The melting point for this composition was found to be at $2497 \pm 10^\circ\text{C}$. The pyrochlore \Leftrightarrow fluorite transformation temperature was measured to be about 100 K lower than the value reported by [1971Rou] (2025°C). The composition range of the pyrochlore phase reported by [1965Col] extended from 37.4 to 60.1 mol% $\text{SmO}_{1.5}$ at 1450°C, which was very similar to the range shown by [1962Per]. [1981Gav] reported the fluorite / fluorite + pyrochlore phase boundary in ZrO_2 -rich region to be at 25 mol% Sm_2O_3 . [1999Tab] determined the extent of the pyrochlore solid solution in the range from 38.5 to 55 mol% $\text{SmO}_{1.5}$ at 1500°C by XRD method.

At the ZrO_2 -rich side, the eutectoid point of the invariant reaction $T \Leftrightarrow M + F$ was determined at 865°C and 1.5 mol% Sm_2O_3 by [1995And], together with a tentative phase

diagram for the ZrO_2 -rich region. However, the samples investigated were far from equilibrium condition according to the heat treatment route, resulting in rather large solubility of Sm_2O_3 (3-6 mol%) in the tetragonal phase at $1170^\circ C$. With the help of lattice parameter measurements, [1981Gav] found the minimum amount of Sm_2O_3 to stabilize the zirconia in the cubic fluorite structure to be 6 mol% at 2170 K and 9.5 mol% at 2020 K. The phase boundaries of the tetragonal + fluorite equilibrium were experimentally examined by [1995Kat] in the temperature range $1600-1800^\circ C$.

All the experimental data on the invariant reactions are listed in Table 6-1.

6.1.2. Thermodynamic data

[1971Kor] determined the enthalpy of formation (from oxides) of the stoichiometric pyrochlore phase by combustion in a bomb calorimeter. The measured value was $-26673 \text{ J}\cdot\text{mol}^{-1}$ (per mole of cations) at 298.15 K. Recently [2005Nav] reported a less negative value ($-14629 \text{ J}\cdot\text{mol}^{-1}$, per mole of cations).

The entropy of the pyrochlore phase $Sm_2Zr_2O_7$ ($65.1 \text{ J}\cdot\text{mol}^{-1}\cdot\text{K}^{-1}$, 298.15 K, per mole of cations) was estimated by the method of ground-state degeneracy in the work of [2004Lut].

6.2. Experimental results and discussion

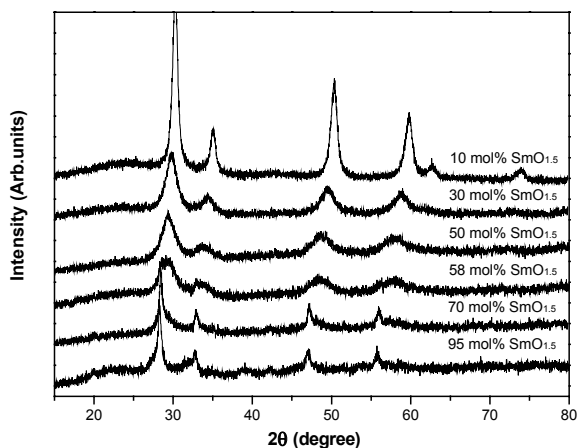


Figure 6-1. The XRD patterns of the as-pyrolysed $ZrO_2 - SmO_{1.5}$ samples at $700^\circ C$ for 3h.

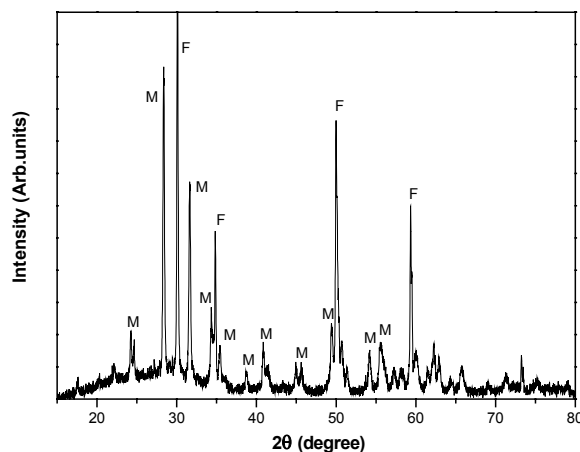


Figure 6-2. The XRD patterns of the ZrO_2 -10 mol% $SmO_{1.5}$ sample heat treated at $1400^\circ C$ for 168h.

6.2.1. The as-pyrolysed state

Totally thirteen samples with different compositions were prepared in this work. The prepared compositions together with the observed microstructures at different temperatures

are listed in Table 6-2. The XRD patterns of several pyrolysed samples are given in Fig. 6-1. It is clear that the compositions of 50 and 58 mol% $\text{SmO}_{1.5}$ have wider fluorite peaks which correspond to finer powder particles. Samples in the ZrO_2 -rich region show peaks of the tetragonal phase, while in $\text{SmO}_{1.5}$ -rich samples some weak peaks of the B-type Sm_2O_3 are present.

6.2.2. The tetragonal + fluorite phase equilibrium

The XRD patterns (Fig. 6-2) of the sample containing 10 mol% $\text{SmO}_{1.5}$ heat treated in the temperature range 1400-1700°C show well developed monoclinic and fluorite structures. The SEM back scattered electron image ($\times 1000$) of the ZrO_2 -10 mol% $\text{SmO}_{1.5}$ sample heat treated at 1600°C for 72h is shown in Fig. 6-3, where the light areas are the fluorite phase, and the dark areas are the monoclinic phase which formed from the tetragonal phase during cooling. The obvious cracks at the grain boundaries are caused by the considerable volume change during the tetragonal-to-monoclinic martensitic transformation. Table 6-3 gives the determined tetragonal + fluorite phase boundary data at different temperatures. Present measured data agree with those of [1995Kat] very well within small experimental uncertainties.

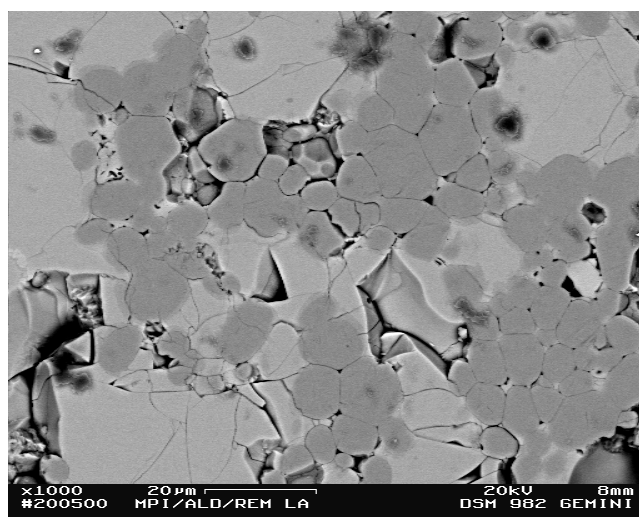


Figure 6-3. The SEM back scattered electron image ($\times 1000$) of the ZrO_2 -10 mol% $\text{SmO}_{1.5}$ sample heat treated at 1600°C for 72h (the light areas are the fluorite phase, and the dark ones are the monoclinic phase).

6.2.3. The fluorite + pyrochlore phase equilibrium

It has been already inferred from the work on the $\text{ZrO}_2 - \text{NdO}_{1.5}$ system that the samples in the fluorite + pyrochlore two-phase region at the ZrO_2 -rich side could not reach

equilibrium even after 36h at 1700°C. For the $\text{ZrO}_2 - \text{SmO}_{1.5}$ system, the samples with 36, 37, 38, 39 and 40 mol% $\text{SmO}_{1.5}$ heat treated at both 1600°C for 72h and 1700°C for 36h do not show any visible separate peaks of fluorite and pyrochlore. In the $\text{SmO}_{1.5}$ -rich region, the strong separated peaks of fluorite and pyrochlore can be found on the XRD patterns for the sample with 58 mol% $\text{SmO}_{1.5}$, though there is only a small difference on the 2θ angles. The XRD patterns of the samples 36, 37, 38, 39, 40, 50 and 58 mol% $\text{SmO}_{1.5}$ heat treated at 1600°C for 72h are shown in Fig. 6-4. With increasing the $\text{SmO}_{1.5}$ content, the intensities of the superstructure peaks become stronger gradually up to 50 mol%, and then decrease until the composition 58 mol% $\text{SmO}_{1.5}$. The same compositions heat treated at 1700°C for 36h do not show any difference on the XRD patterns. According to the intensities of the superstructure peaks, it is inferred in this work that the composition of the fluorite / fluorite + pyrochlore phase boundary is around 35 mol% $\text{SmO}_{1.5}$ in the temperature range studied. The lattice parameters of the fluorite and pyrochlore phases were determined by using the Si powder as the internal standard, and are plotted in Fig. 6-5, together with literature data. The lattice parameter of the 50 mol% $\text{SmO}_{1.5}$ sample does not seem to fit into the Vegard's slope constructed from the data of the fluorite phase. Based on the XRD and EDX results of the ZrO_2 -58 mol% $\text{SmO}_{1.5}$ sample, the fluorite + pyrochlore phase boundaries are around 55 and 69 mol% $\text{SmO}_{1.5}$, respectively, at 1600°C, which can be seen in Table 6-3.

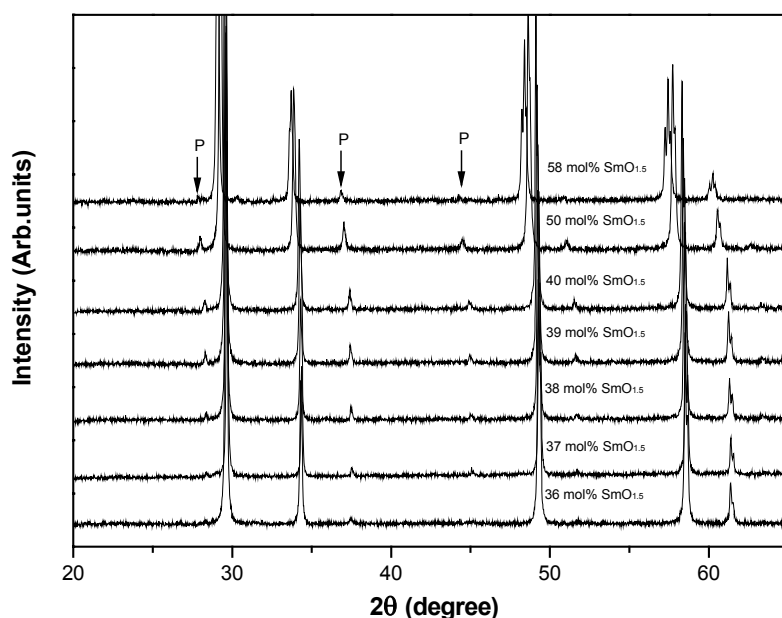


Figure 6-4. The XRD patterns of the $\text{ZrO}_2 - \text{SmO}_{1.5}$ samples with the pyrochlore peaks (1600°C, 72h).

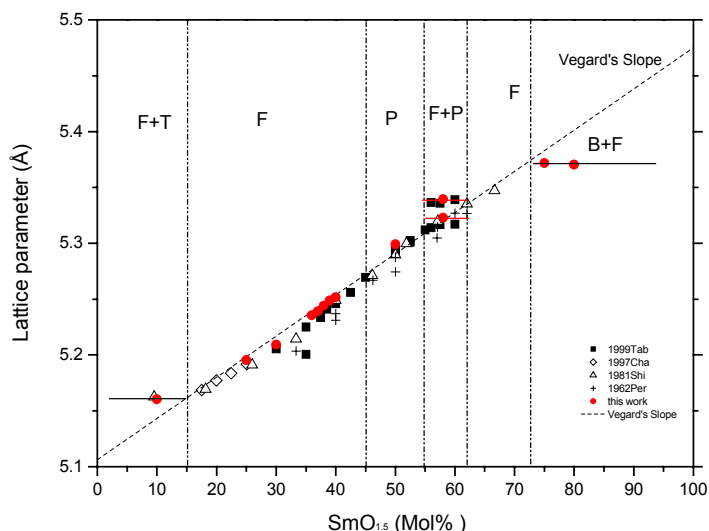


Figure 6-5. The lattice parameters of the fluorite and pyrochlore phases in the $ZrO_2 - SmO_{1.5}$ system determined in this work and in the literature.

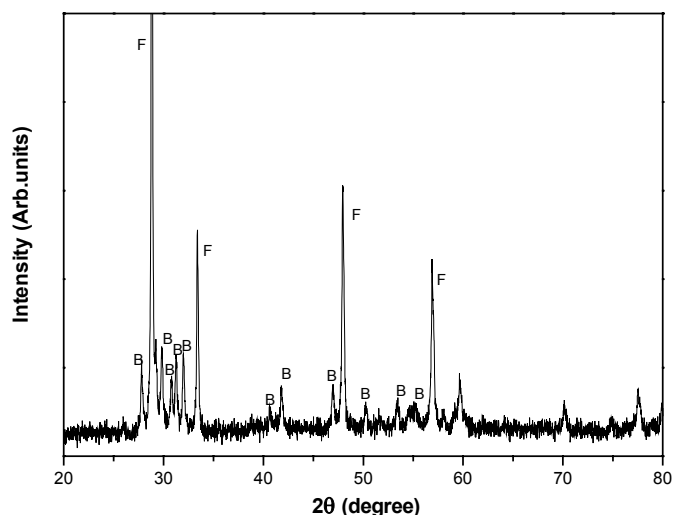


Figure 6-6. The XRD patterns of the ZrO_2 -80 mol% $SmO_{1.5}$ sample after heat treatment at $1400^\circ C$.

6.2.4. The fluorite + B- Sm_2O_3 phase equilibrium

According to XRD measurements, the sample ZrO_2 -80 mol% $SmO_{1.5}$ heat treated between $1400^\circ C$ - $1700^\circ C$ presents the fluorite and the B- Sm_2O_3 structure (Fig. 6-6). The measured phase boundary data for the fluorite + B- Sm_2O_3 phase equilibrium are listed in Table 6-3. With increasing temperature, the solubility range of the fluorite phase extends to higher $SmO_{1.5}$ contents, and the solubility of ZrO_2 in B- Sm_2O_3 also increases. Fig. 6-7 is the SEM back scattered electron image ($\times 3000$) of the sample ZrO_2 -80 mol% $SmO_{1.5}$ heat treated at $1700^\circ C$ for 36h, showing a very homogeneous microstructure. The grey areas are the fluorite phase, and the white areas with the lathy morphology are the B- Sm_2O_3 phase.

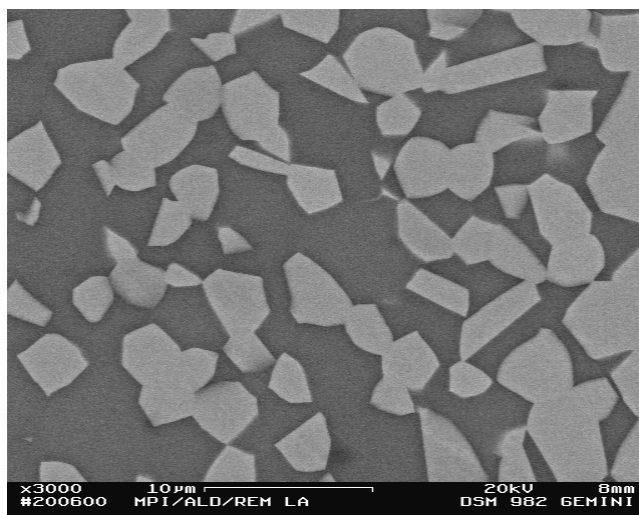


Figure 6-7. The SEM back scattered electron image ($\times 3000$) of the sample ZrO_2 -80 mol% $\text{SmO}_{1.5}$ heat treated at 1700°C for 36h (the grey areas are the fluorite phase, and the white ones are the B-type Sm_2O_3 phase).

6.3. Selected experimental data for optimization

The phase boundary data obtained in this work on the tetragonal + fluorite, fluorite + pyrochlore, and the fluorite + B- Sm_2O_3 phase equilibria together with those of [1995Kat], the temperatures of the $\text{P} \leftrightarrow \text{F}$ transformation, the liquidus and the invariant reactions measured by [1968Rou2, 1971Rou] as well as the homogeneity range data of the pyrochlore phase reported by [1999Tab] are accepted for the optimization.

The enthalpy of formation of the pyrochlore phase reported by [2005Nav] is taken as a start value, while the data from [1971Kor] on the enthalpy of formation of the fluorite phase are rejected due to a too negative value. The average values of the heat capacities of $\text{Nd}_2\text{Zr}_2\text{O}_7$ and $\text{Eu}_2\text{Zr}_2\text{O}_7$ [2004Lut] are accepted as reference data for $\text{Sm}_2\text{Zr}_2\text{O}_7$. The heat content data of ZrO_2 -30 mol% $\text{SmO}_{1.5}$ and ZrO_2 -50 mol% $\text{SmO}_{1.5}$ samples determined in this work are adopted for assessment of the thermodynamic properties.

6.4. Optimization procedure

As a first step, a preliminary phase diagram without the ordered pyrochlore phase was roughly assessed based on the liquidus, tetragonal + fluorite, fluorite + B- Sm_2O_3 phase boundary data and the heat content data for the ZrO_2 -30 mol% $\text{SmO}_{1.5}$ sample, by using a limited number of parameters. Secondly, further optimization was done by treating the pyrochlore phase as a stoichiometric compound, using the heat content and enthalpy of formation data. Finally, a full assessment was carried out by simultaneously taking all selected data into account.

For the fluorite phase, a $T \ln T$ contribution into the zeroth order interaction parameter was applied to fit the experimental heat content data. For the phases T, X, H, A and B, only one interaction parameter was adopted due to their limited composition and or temperature range. No any interaction parameter was applied for the monoclinic phase and the low-temperature C-type phase because of their negligible or unknown homogeneity ranges.

The optimized thermodynamic parameters are summarized in **Appendix**.

6.5. Calculated results and discussion

The calculated $\text{ZrO}_2 - \text{SmO}_{1.5}$ phase diagram is shown in Fig. 6-8, together with the experimental data. The phase equilibria data obtained in this work and those of [1971Rou, 1995Kat, 1999Tab] are well reproduced. The calculated invariant reactions are given in Table 6-1.

It can be seen in Fig. 6-8 that the calculated tetragonal + fluorite two-phase region is well consistent with the experimental data of this work and of [1995Kat]. Compared with the $\text{ZrO}_2 - \text{NdO}_{1.5}$ system, this two-phase region of the $\text{ZrO}_2 - \text{SmO}_{1.5}$ system is a little bit narrower. The calculated invariant reaction $T \Leftrightarrow M + F$ is 1315 K, at which the solubility of $\text{SmO}_{1.5}$ in the tetragonal phase is only 1.3 mol%, and the homogeneity range of the monoclinic phase is negligible. Fig. 6-9 is the calculated ZrO_2 -rich partial phase diagram including the calculated T_0 lines for the monoclinic + tetragonal and tetragonal + fluorite phase equilibria and experimental data. The results of [1993Yas, 1995And] on the T_0 line of the former one are well reproduced.

The calculated pyrochlore + fluorite equilibrium fit the phase boundary data obtained in this work and by [1999Tab], as well as the transformation temperature reported by [1971Rou]. Two invariant reactions involving the pyrochlore phase are calculated at 1115 K ($F \Leftrightarrow M + P$) and 1520 K ($F \Leftrightarrow P + \text{B-Sm}_2\text{O}_3$), respectively. At the $\text{SmO}_{1.5}$ -rich side, the phases pyrochlore, $\text{B-Sm}_2\text{O}_3$ and $\text{C-Sm}_2\text{O}_3$ are in equilibrium at low temperatures. Since it is not possible to equilibrate samples at such conditions, there is no experimental evidence for this, where the solubility range of the $\text{C-Sm}_2\text{O}_3$ phase is neglected.

The experimental data obtained in this work are taken into account to optimize the phase boundaries of the fluorite + $\text{B-Sm}_2\text{O}_3$ phase equilibrium. A good agreement with the calculation is obtained. This agreement makes the calculations get less consistency with the experimental compositions of the fluorite phase for invariant reactions reported by [1971Rou] at higher temperatures. However, owing to the large uncertainties of the HTXRD data of [1971Rou], present calculations are thought to be more reasonable by fitting the reliable phase

boundary data. The reported temperatures of the invariant reactions $L \rightleftharpoons F + X$ and $X \rightleftharpoons H + F$ by [1971Rou] are reproduced well. The temperatures of the reactions $H \rightleftharpoons A + F$ and $A + F \rightleftharpoons B$ were calculated as 2252 K and 2181 K, respectively.

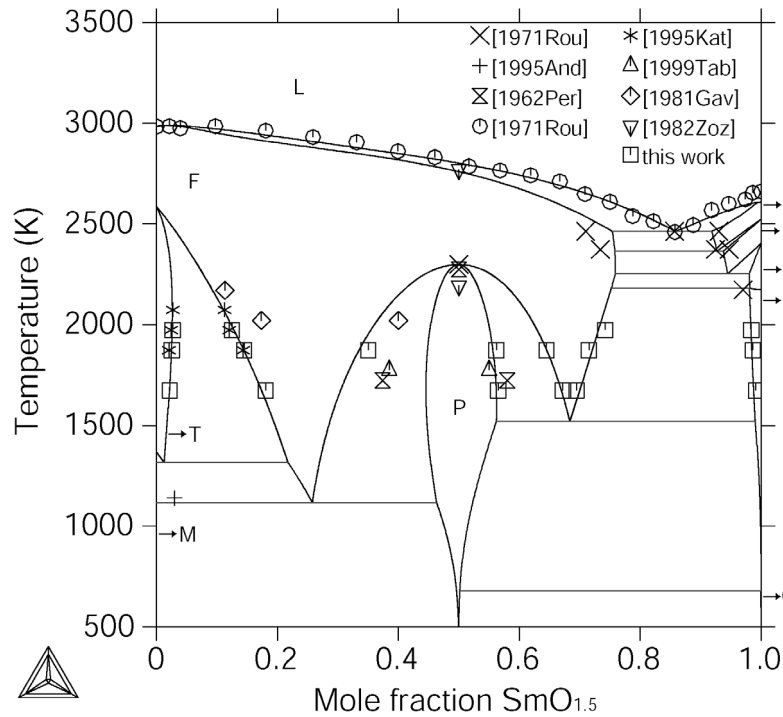


Figure 6-8. The calculated $ZrO_2 - SmO_{1.5}$ phase diagram together with experimental data.

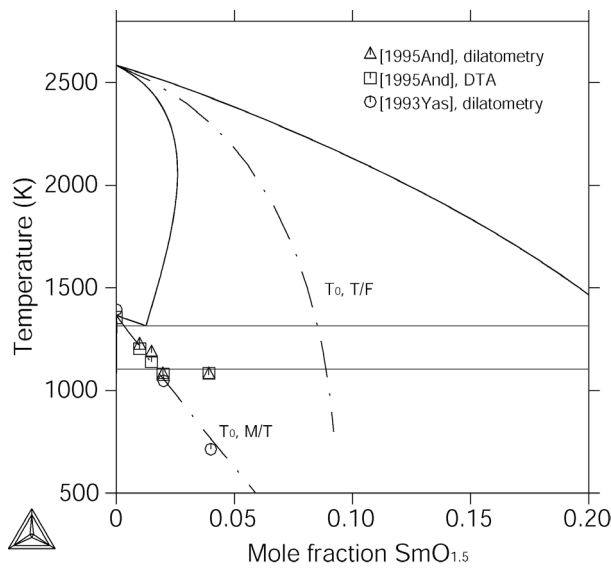


Figure 6-9. The calculated $ZrO_2 - SmO_{1.5}$ partial phase diagram together with the calculated T_0 lines for the monoclinic + tetragonal and tetragonal + fluorite phase equilibria and experimental data.

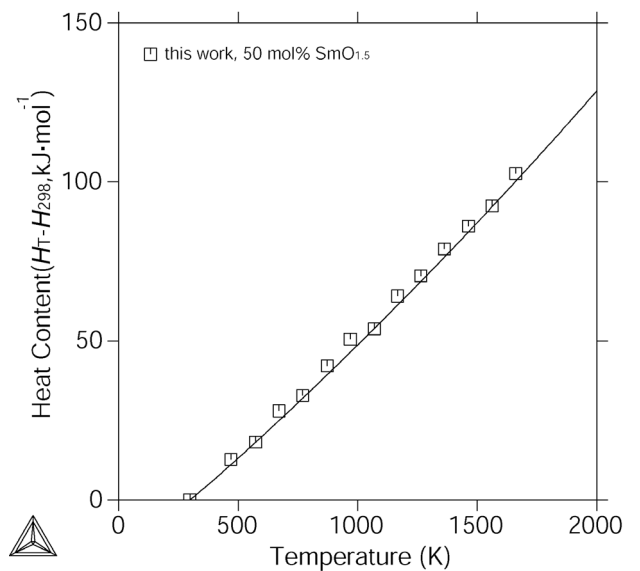


Figure 6-10. The calculated heat content ($H_T - H_{298}$) of the ZrO_2 -50 mol% $SmO_{1.5}$ sample together with experimental data.

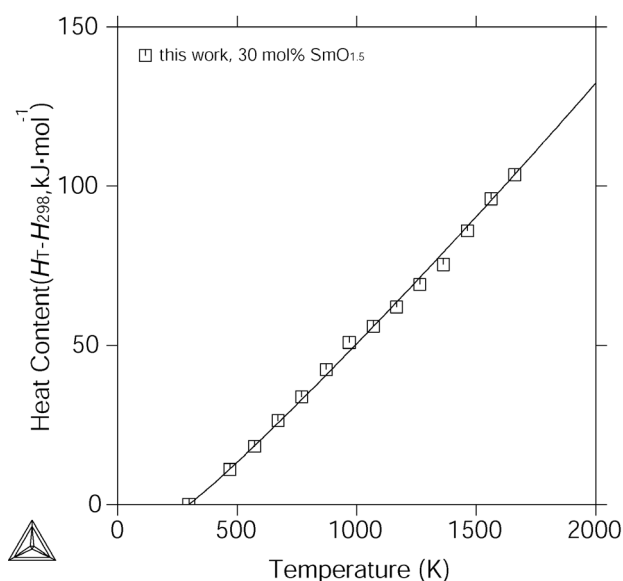


Figure 6-11. The calculated heat content ($H_T - H_{298}$) of the ZrO_2 -30 mol% $SmO_{1.5}$ sample together with experimental data.

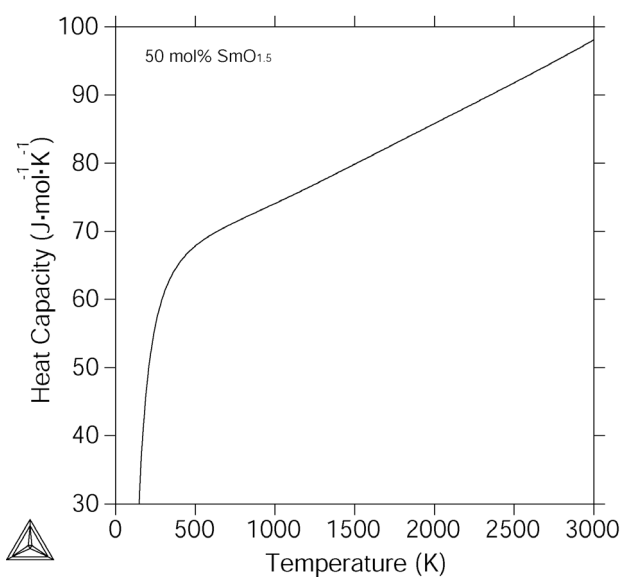


Figure 6-12. The calculated heat capacity of the ZrO_2 -50 mol% $SmO_{1.5}$ pyrochlore phase.

The enthalpies of formation of the fluorite and the pyrochlore phases finally obtained in this work are $-9023 \text{ J}\cdot\text{mol}^{-1}$ and $-16049 \text{ J}\cdot\text{mol}^{-1}$ (per mole of cations), respectively, which are comparable to those data for the $ZrO_2 - NdO_{1.5}$ system. Fig. 6-10 and Fig. 6-11 show the experimental and calculated heat contents of the samples containing 50 mol% $SmO_{1.5}$ and 30 mol% $SmO_{1.5}$, respectively. Good agreements are obtained. The calculated heat capacity of the stoichiometric pyrochlore phase is shown in Fig. 6-12. The value at 298.15 K is $60.51 \text{ J}\cdot\text{mol}^{-1}\cdot\text{K}^{-1}$.

Table 6-1 The invariant reactions in the $ZrO_2 - SmO_{1.5}$ system.

Reaction	Type	Reference	Temperature (K)	Composition of phases (mol% $SmO_{1.5}$)		
$L \Leftrightarrow F + X$	eutectic	[1971Rou]	2463	85.7	71	93
		This work	2463	85.8	75.4	91.8
$X \Leftrightarrow H + F$	eutectoid	[1971Rou]	2373	92.5	94.7	73.4
		This work	2365	92.7	93.8	75.8
$H \Leftrightarrow A + F$	eutectoid	This work	2252	94.4	98	75.9
$A + F \Leftrightarrow B$	eutectoid	[1971Rou]	2173	—	—	—
		This work	2181	98.1	75.2	98.06
$F \Leftrightarrow P + B$	eutectoid	This work	1520	68.3	56.2	98.9
$T \Leftrightarrow M + F$	eutectoid	[1995And]	1138	1.5	—	—
		This work	1315	1.3	0.02	21.7

F ⇌ M + P	eutectoid	This work	1115	25.8	~0	46.3
F ⇌ P	congruent	[1971Rou]	2298	50	50	–
		[1982Zoz]	2193	50	50	–
		This work	2299	50	50	–

Table 6-2. The compositions of the samples investigated in the ZrO₂ – SmO_{1.5} system and observed phases.

No.	SmO _{1.5} (mol%)	Observed phases		
		1400 °C	1600 °C	1700 °C
1	10	F + M	F + M	F + M
2	25	F	F	F
3	30	F	F	F
4	36	P	P	P
5	37	P	P	P
6	38	P	P	P
7	39	P	P	P
8	40	P	P	P
9	50	P	P	P
10	58	P + F	P + F	P + F
11	75	F + B	F	F
12	80	F + B	F + B	F + B
13	95	F + B	F + B	F + B

Table 6-3. Measured phase compositions data (mol% SmO_{1.5}) for different phase equilibria in the ZrO₂ – SmO_{1.5} system at different temperatures.

Temperature (K)	T + F		F + P		F + B	
	T	F	F	P	F	B
1673	2.2 ± 0.5	18.1 ± 1	67.2 ± 1	56.5 ± 1	69.5 ± 1	99.2 ± 0.5
1873	2.5 ± 0.5	14.5 ± 0.5	64.5 ± 1	56.2 ± 1	71.5 ± 1	98.6 ± 0.5
1973	2.7 ± 0.5	12.5 ± 0.5	–	–	74.2 ± 1	98.4 ± 0.5

Chapter 7

Experimental study and thermodynamic modeling of the $\text{ZrO}_2 - \text{GdO}_{1.5}$ system

7.1. Literature review

7.1.1. Phase equilibria

Phase diagram studies of the system $\text{ZrO}_2 - \text{GdO}_{1.5}$ have been performed by [1962Per, 1963Lef, 1964Lin1, 1968Rou2, 1971Rou, 1972Neg, 1978Sco, 1987Ueh] by using X-Ray diffraction and thermal analysis. In addition, some particular phase equilibria have been investigated in limited temperature and/or composition ranges using XRD, Raman and Mössbauer spectroscopy, petrographic analysis as well as EPMA [1980Dij, 1990Mor, 1991Leu, 1994Li, 1995Bha, 1995Kat, 1996Kar, 1999Kar, 2001Fei, 2003Wan, 2003Dut, 2004Nak].

The monoclinic structure of ZrO_2 was found to dissolve negligible amounts of gadolinia. The tetragonal phase is known to dissolve up to 3 mol% $\text{GdO}_{1.5}$ [1991Leu, 1995Kat]. The eutectoid decomposition of the tetragonal phase $T \Leftrightarrow M + F$ was found to occur at 1140 - 1145 °C [1972Neg]. The cubic fluorite-type phase is stabilized in a wide range of compositions and temperatures [1962Per, 1963Lef, 1971Rou, 1978Sco, 1991Leu, 1995Kat]. It coexists with the solid solution based on C-type modification of Gd_2O_3 at the gadolinia-rich side [1978Sco, 2001Fei]. The minimum amount of gadolinia needed to stabilize the single fluorite phase increases with decreasing temperature. The $\text{GdO}_{1.5}$ -rich phase boundary shifts from 69.9 to 76.5 mol% $\text{GdO}_{1.5}$ with increasing temperature (1450 to 1800 °C). The solubility of ZrO_2 in the monoclinic B-type modification of $\text{GdO}_{1.5}$ does not exceed 2 mol% [1962Per, 1971Rou, 2001Fei]. The literature data on the phase boundaries $T / T + F$, $T + F / F$, $F / F + \text{C-Gd}_2\text{O}_3$, and $\text{C-Gd}_2\text{O}_3 + \text{B-Gd}_2\text{O}_3 / \text{B-Gd}_2\text{O}_3$ are in good agreement.

Rouanet and Foex studied the phase diagram of the $\text{ZrO}_2 - \text{GdO}_{1.5}$ system from 1800 °C up to the liquidus temperatures [1968Rou2, 1971Rou]. The hexagonal ordered polymorph of Gd_2O_3 (H) dissolves up to 7 mol% ZrO_2 . It forms through the peritectic reaction at about 2350 °C and decomposes eutectoidally at 2050 °C. The liquidus temperatures are gradually decreasing down to the eutectic point at 2260 °C and 86.7 mol% $\text{GdO}_{1.5}$, where the liquid solidifies into the F and H- Gd_2O_3 phases. A lower temperature (2175°C) was reported for this eutectic reaction by [1964Lin1] with a similar eutectic composition (87.3 mol% $\text{GdO}_{1.5}$). The high temperature X-phase exists only in the vicinity of pure gadolinia. Karaulov and Zoz detected the melting point of the cubic solid solution $\text{Zr}_{0.5}\text{Gd}_{0.5}\text{O}_{1.75}$ at 2570 ± 14 °C

[1999Kar], which is consistent with the liquidus proposed by Rouanet [1971Rou], considering the possible large experimental error at high temperatures.

Serious disagreement exists in the literature with respect to the homogeneity range of the pyrochlore phase. The smallest one (45-55 mol% $\text{GdO}_{1.5}$) has been reported in Refs. [1962Per, 1980Dij, 2003Wan]. [1999Kar] determined the F / P phase boundary at 38 mol% $\text{GdO}_{1.5}$. It is worth noting that the majority of works [1962Per, 1976Mic, 1980Dij, 1999Kar] are mutually consistent with respect to the P / F phase boundary and the temperature of the order-disorder transition (1530 - 1550 °C), while [1987Ueh] suggested a considerably larger homogeneity range of the pyrochlore phase (31 - 61 mol% $\text{GdO}_{1.5}$) and a higher disordering temperature (> 1600 °C), while indicating two types of pyrochlore phase with sharp and broad superstructure reflections, respectively. A microdomain structure with antiphase boundaries was found in the composition ranges 33 - 43 and 57 - 60 mol% $\text{GdO}_{1.5}$ at 1500 °C and 46 - 54 mol% $\text{GdO}_{1.5}$ or wider at 1600 °C resulting in broad superstructure peaks of the pyrochlore phase accompanying sharp fundamental peaks of the fluorite structure [1987Ueh].

Also, phase equilibria involving C-type Gd_2O_3 phase are not well established. [1962Per] stated that a phase transition $\text{F} \Leftrightarrow \text{C-Gd}_2\text{O}_3$ is of first and second order at low and high temperatures, respectively and indicated the existence of the miscibility gap within the C-type phase domain from 71 to 87 mol% $\text{GdO}_{1.5}$ at 1500 °C, which closes above 1800 °C. [1968Rou2, 1971Rou] stated that the $\text{F} \Leftrightarrow \text{C-Gd}_2\text{O}_3$ transition appears to be continuous with a theoretical boundary at the composition of 50 mol% $\text{GdO}_{1.5}$. In contrast, [1978Sco] found in XRD study that samples with 80 mol% $\text{GdO}_{1.5}$ annealed at 1450 - 1850 °C contain F and C- Gd_2O_3 phases. However, the samples equilibrated at 1850 °C did show, in addition to the sharp fluorite and C-type reflections, some weak, diffuse reflections corresponding to a second C-type phase, and also contained a trace of B- Gd_2O_3 phase.

Two hexagonal intermediate phases H_2 and H_3 , which do not form two-phase fields had been observed between 1450 and 1800 °C by [1962Per]. From the large values of the lattice parameters it can be inferred that they are probably ordered superstructures of the Mn_2O_3 -type cubic solid solution (C-type phase). However, none of the subsequent studies of the $\text{ZrO}_2 - \text{GdO}_{1.5}$ system confirmed the existence of H_2 - or H_3 -phase. On the one hand, they are probably metastable phases. On the other hand, a very long heat treatment is typically necessary, e.g., 1 months at 1400 °C for the pyrochlore-type phase [1976Mic] to allow the ordered structure to form.

All the reported invariant reactions are compiled in Table 7-1.

7.1.2. Thermodynamic data

[1971Kor] determined the enthalpies of formation of the fluorite phase at 50 mol% $\text{GdO}_{1.5}$ by combustion of a mixture of Zr and Gd_2O_3 in a bomb calorimeter under an oxygen pressure of 25 atm. By using high temperature oxide melt solution calorimetry, [2001Hel] measured the enthalpies of formation of three compositions in this binary system: 50 mol% $\text{GdO}_{1.5}$ (pyrochlore), 45.6 mol.% $\text{GdO}_{1.5}$ (pyrochlore), and 53.5 mol.% $\text{GdO}_{1.5}$ (fluorite). These results are compiled in Table 7-2.

[2003Lut] determined the heat capacity of stoichiometric pyrochlore in the temperature range from 20 K to 1400 K by using adiabatic calorimetry and differential scanning calorimetry, while [2003Lec] measured the heat capacity of the sample with 20.4 mol% $\text{GdO}_{1.5}$.

7.2. Experimental results and discussion

7.2.1. The as-pyrolysed state

Totally samples with twenty eight different compositions were prepared for the $\text{ZrO}_2 - \text{GdO}_{1.5}$ system. Fig. 7-1 shows the XRD patterns of some as-pyrolysed samples after 450°C for 3h. The sample with 10 mol% $\text{GdO}_{1.5}$ shows clear patterns of the tetragonal phase, while the other samples are poorly crystallized. For the sample with 98 mol% $\text{GdO}_{1.5}$, the XRD patterns present probably the peaks of both the B- and C-type Gd_2O_3 phases. The prepared compositions together with the observed microstructures at different temperatures are listed in Table 7-3.

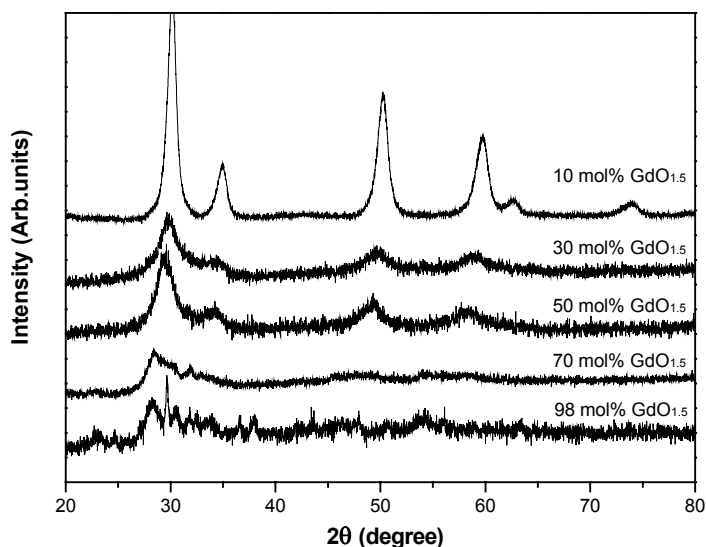


Fig. 7-1. The XRD patterns for the as-pyrolysed $\text{ZrO}_2 - \text{GdO}_{1.5}$ samples after 450°C for 3h.

7.2.2. The fluorite / pyrochlore phase transition

XRD patterns of the samples containing 41 to 59 mol% $\text{GdO}_{1.5}$ are presented in Fig. 7-2. It can be seen that at the composition of 44 mol% $\text{GdO}_{1.5}$ fluorite transforms into pyrochlore, which has the superstructure reflections denoted by "P". With increasing $\text{GdO}_{1.5}$ content the superstructure peaks grow until the stoichiometric composition (50 mol% $\text{GdO}_{1.5}$) is reached and then decrease. At the composition of 55 mol% $\text{GdO}_{1.5}$, the pyrochlore superstructure disappears and the fluorite phase is stable again. The homogeneity range of the pyrochlore phase at 1400 °C obtained in this work by XRD is thus around 44-54 mol% $\text{GdO}_{1.5}$ and it is well consistent with the literature data (45-55 mol% $\text{GdO}_{1.5}$) [1962Per, 1980Dij, 2003Wan]. It is, however, not possible to judge from the XRD patterns, whether two-phase regions between F and P exist, because the strongest peaks of fluorite and pyrochlore phases overlap.

The lattice parameters of fluorite and pyrochlore determined by using the Si-standard powder as well as those from the literature are shown in Fig. 7-3. The majority of reports present mutually consistent values and results of the present study are in line with the general trend. According to the composition dependence of lattice parameters, the phase boundaries T + F / F and F / F + C- Gd_2O_3 are clearly seen. The values obtained in this study (16 and 68 mol% $\text{GdO}_{1.5}$, respectively) are in good agreement with the available literature data for the temperature of 1400°C. At the same time, there is no any plateau in between indicating the absence of two-phase regions, where the structures of fluorite and pyrochlore coexist. An interesting observation is the marked deviation from Vegard's slope. It is evident that the lattice parameter is smaller than predicted one in the composition range from 25 to 45 mol% $\text{GdO}_{1.5}$ (Fig. 7-3). Furthermore, results obtained in this work indicate (see inset) that the lattice parameter slightly exceeds theoretical value between 45 and 62 mol% $\text{GdO}_{1.5}$.

Similar observations were reported by two groups of authors [1980Dij, 1987Ueh], who mentioned the existence of a bend on the curve representing the composition dependence of the lattice parameter of $\text{Zr}_{1-x}\text{Gd}_x\text{O}_{2-0.5x}$ solid solutions at $x = 0.33 - 0.35$. Around the same composition, the maximum activation enthalpy for ionic conductivity was found [1980Dij]. The observed discontinuity was interpreted as the onset of the ordering of oxygen vacancies [1980Dij] or even F / P phase boundary [1987Ueh]. In addition, an abrupt change of the relative absorption area and line width in Mössbauer spectra was detected between $x = 0.30$ and 0.35 [2004Nak]. However, more extensive compilation of the literature data as well as the results obtained in this work (Fig. 7-3) indicate that not just a bend, but a smooth S-shaped curve characterizes the composition dependence of the lattice parameter in the $\text{ZrO}_2 - \text{GdO}_{1.5}$ system. Such sigmoidal curve can be understood as the intermediate case between random

solution and phase separation, i.e., the ordering of the fluorite phase, which occurs in a wide composition range, from 25 to 62 mol% $\text{GdO}_{1.5}$. In fact, the existence of ordering in the sample with 25 mol% $\text{GdO}_{1.5}$, which has been quenched from 1600 °C was confirmed by electron diffraction [1991Wit]. Note that the unit cell parameter in the range of 18 - 25 mol% $\text{GdO}_{1.5}$ does obey Vegard's law (Fig. 7-3).

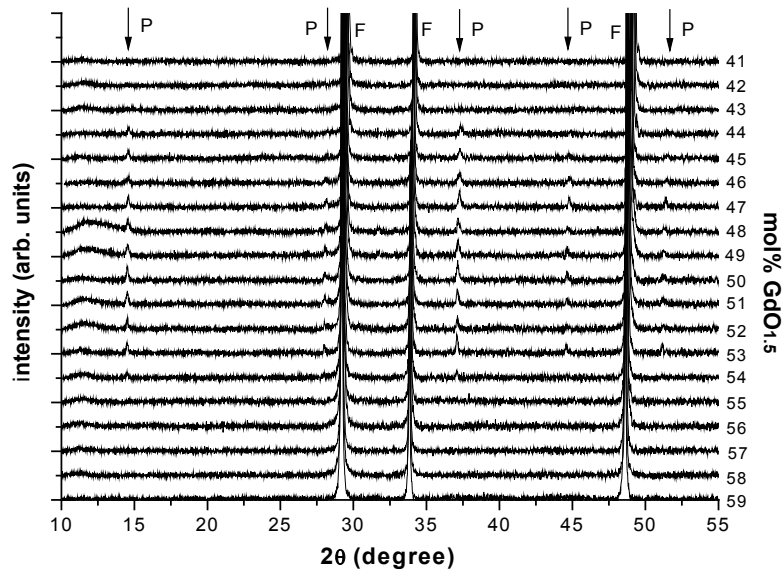


Fig. 7-2. XRD patterns of $\text{ZrO}_2 - \text{GdO}_{1.5}$ samples in the composition range from 41 to 59 mol% $\text{GdO}_{1.5}$. The letters P and F show the positions of superstructure reflections of the pyrochlore phase and fundamental reflections of the fluorite subcell, respectively.

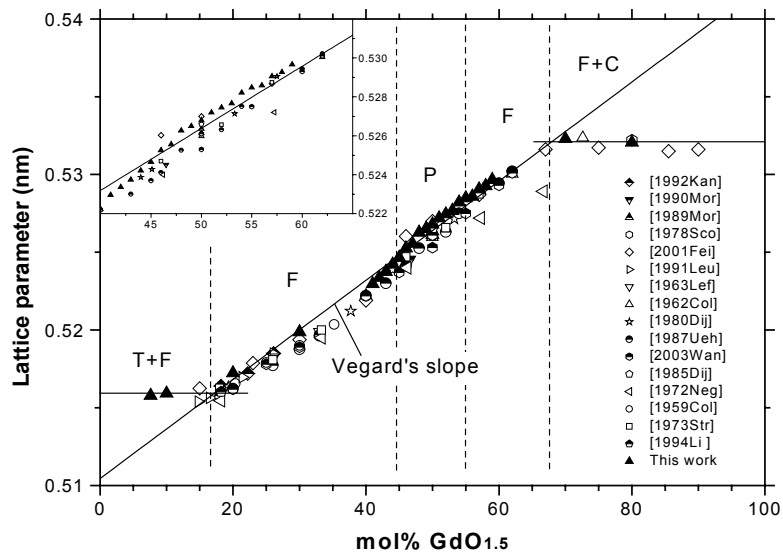


Fig. 7-3. Lattice parameters of the fluorite and pyrochlore phases of the $\text{ZrO}_2 - \text{GdO}_{1.5}$ system determined in this work and in literature.

Fig. 7-4 shows a bright field TEM micrograph of the typical microstructure found among the samples studied. The compositions of about 150 individual grains were analysed. The major quantity of these grains indicates a Zr:Gd ratio close to the nominal composition. However, partitioning at the nanometer level was detected and some of the grains exhibited very different $\text{GdO}_{1.5}$ contents. Selected examples of SAED patterns from all the samples are shown in Fig. 7-5.

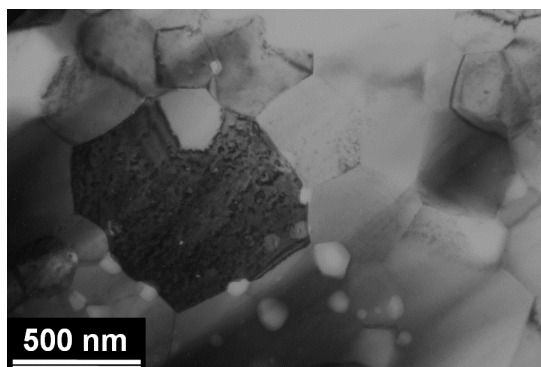


Fig. 7-4. Bright field TEM micrograph showing the typical polycrystalline microstructure found among the $\text{ZrO}_2 - \text{GdO}_{1.5}$ samples studied.

Fig. 7-5(a) presents a SAED pattern registered in the $[101]$ zone axis of a monoclinic grain with a composition close to pure ZrO_2 . Fig. 7-5(b) shows the diffraction pattern associated with one of the tetragonal grains in the $[110]$ zone axis. Note that the more intense reflections can also be indexed as cubic (fluorite-type) structure and there is a possibility that both the F and T phases contributed to the formation of this pattern. In fact, this kind of SAED patterns was observed in the grains with an average composition of 10-15 mol% $\text{GdO}_{1.5}$. In this range of trivalent cations doping, either grains with low solute tetragonal domains oriented into a cubic matrix (colony structure) or supersaturated tetragonal grains (T') could create patterns with the shown features [1988Heu]. Figs. 7-5 (c-e) show the SAED patterns registered along the $[110]$ zone axis for the stoichiometric pyrochlore (50 mol% $\text{GdO}_{1.5}$), fluorite and $\text{GdO}_{1.5}$ -rich pyrochlore grains, respectively. Fig. 7-5(f) shows the $[110]$ SAED pattern taken from one of the grains with a composition close to pure gadolinia, where reflections associated with the cubic network are labeled. Note that as in the case of pyrochlore, some superstructure reflections appear. In Figs. 7-5(e) and (f), these are diffuse elongated reflections at half distances between the (111) reflections of the reciprocal cubic network.

Figs. 7-6(a-h) show a series of SAED patterns registered from different grains among all the samples studied, where the content of $\text{GdO}_{1.5}$ measured by EDX increase from (a) to (h). In order to distinguish the fluorite and pyrochlore phase, $[110]$ zone axis was used since (111) and (002) satellite reflections of the pyrochlore structure clearly appear in this orientation. Furthermore, this orientation is most suitable for investigating of transitional structures, since the shape of diffuse scattering in these patterns changes most sensitively with composition [1985Suz]. This scattering is caused by vacancies on the oxygen sublattice (or oxygen vacancy clusters), acting as scattering centers of the incoming electron beam [1988Rüh].

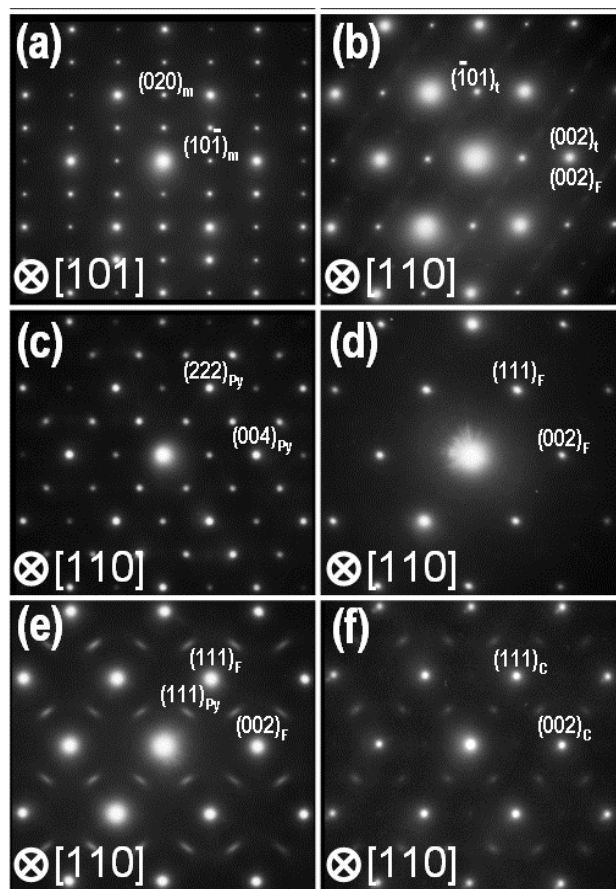


Fig. 7-5. SAED patterns of the monoclinic phase (a), tetragonal phase (b), stoichiometric pyrochlore (c), fluorite (d), $\text{GdO}_{1.5}$ -rich pyrochlore (e) and C- Gd_2O_3 (f) of the $\text{ZrO}_2 - \text{GdO}_{1.5}$ system.

Starting from the sample containing around 43 mol% $\text{GdO}_{1.5}$ the brightness of the superstructure reflections continuously increases as the composition approaches 50 mol% $\text{GdO}_{1.5}$ and then gradually decreases upon further increasing of the $\text{GdO}_{1.5}$ content. It is evident that a continuous transformation of the fluorite structure into pyrochlore one and then

again into fluorite (without any phase separation) takes place. Note that satellite spots are hardly visible in Fig. 7-6(a), while the SAED pattern shown in Fig. 7-6(h) corresponds to disordered fluorite phase. Thus, with respect to the homogeneity range of the pyrochlore phase, TEM observations are consistent with XRD measurements (Fig. 7-2). Also the sharpness and shape of the superstructure reflections change in a systematic way. Cubic grains in the ZrO_2 -rich region, presented sharp satellite spots Figs. 7-6(a-c). In the $\text{GdO}_{1.5}$ -rich grains, typical diffraction features of cubic (fluorite-type) structures, plus a subnetwork of diffuse and elongated (111) superstructure reflections are observed, Figs. 7-6(e-g). The extra diffuse scattered reflections are the proof of the existence of a partial pyrochlore character in these grains. They are largely perpendicular to the local $\langle 111 \rangle$ reciprocal space direction and seem to smear out as grains contain more $\text{GdO}_{1.5}$, since the same trend towards the appearance of single fluorite reflections is observed (Fig. 7-6(h)).

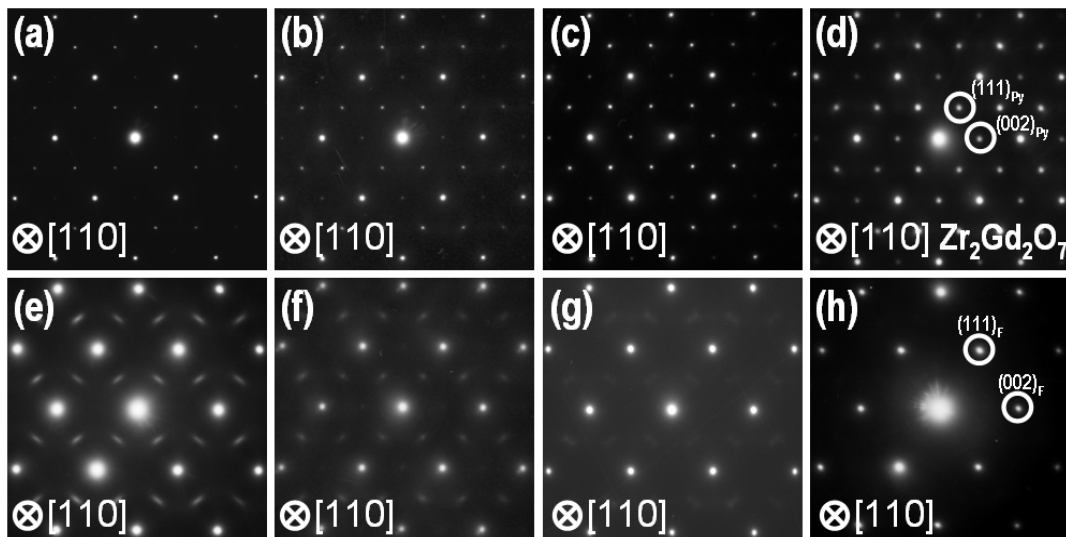


Fig. 7-6. Series of [110] SAED patterns from grains with compositions (mol% $\text{GdO}_{1.5}$): 43 - 45 (a), 45 - 47 (b), 47 - 49 (c), 50 (d), 51-53 (e), 53-55 (f), 55-57 (g), 60-66 (h) in the $\text{ZrO}_2 - \text{GdO}_{1.5}$ system.

In general, results obtained in the present work by TEM are consistent with the observations of Withers and co-workers [1991Wit] for a number of the $\text{ZrO}_2 - \text{REO}_{1.5}$ systems, where different superstructure patterns and/or diffuse scattering were found within the fluorite solid solution field depending on composition. From Figs. 7-6(a, b) it is evident that for ZrO_2 -rich grains the expected (002) satellite reflections of the pyrochlore structure are very weak. This is a characteristic feature of the "honeycomb pattern" [1991Wit], which was identified at 25 mol% $\text{LnO}_{1.5}$. At the same time, the SAED pattern of the sample containing

50 mol% $\text{GdO}_{1.5}$, which has been annealed at 1600 °C [1991Wit] looks very similar to Fig. 7-6(e). Such kind of ordering of the fluorite phase has been classified as "pyrochlore-like" [1991Wit]. Finally, the transition from "pyrochlore-like" to "C-type-related" ordering appears to be smooth [1991Wit], what is also evident from Figs. 7-5(e, f).

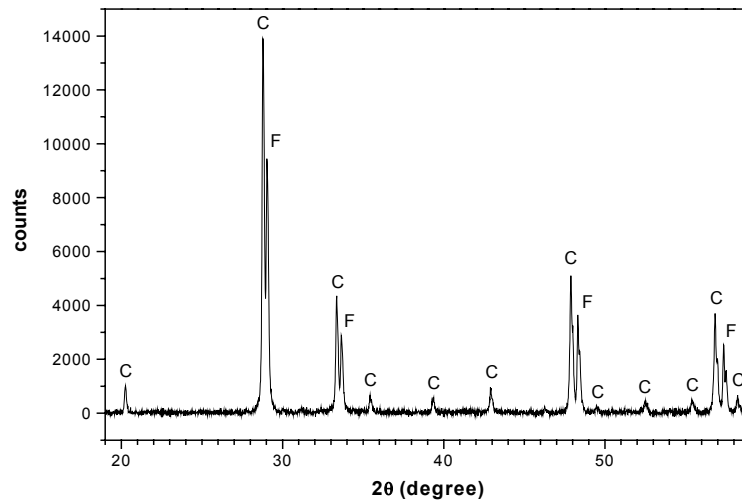


Fig. 7-7. XRD pattern of the sample ZrO_2 -80 mol% $\text{GdO}_{1.5}$ heat treated at 1400 °C for 240 h. The letters C and F denote the reflections, which belong to C- Gd_2O_3 and fluorite, respectively.

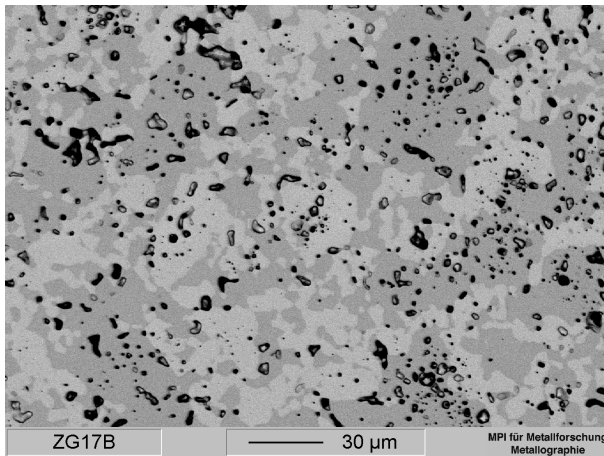


Fig 7-8. SEM micrograph of the sample containing ZrO_2 -80 mol% $\text{GdO}_{1.5}$ heat treated at 1700 °C for 36 h (the grey areas are the fluorite phase, and the white ones are C- Gd_2O_3).

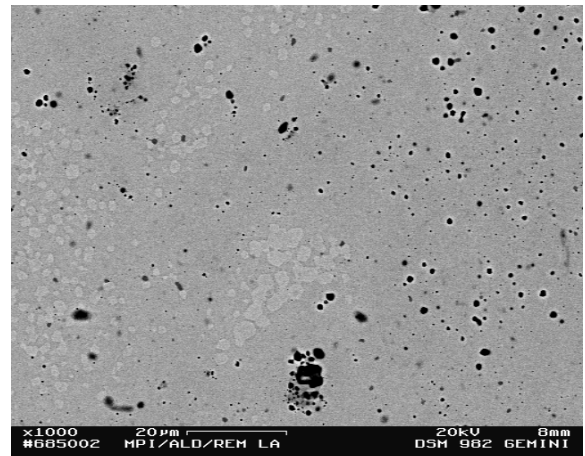


Fig. 7-9. SEM micrograph of the sample containing 95 mol% $\text{GdO}_{1.5}$ heat treated at 1600 °C for 72 h (the matrix is C- Gd_2O_3 , and the white areas are B- Gd_2O_3).

7.2.3. The fluorite + C- Gd_2O_3 and C- Gd_2O_3 + B- Gd_2O_3 phase equilibria

As an example, Fig. 7-7 shows the XRD pattern of the specimen containing 80 mol% $\text{GdO}_{1.5}$, which was heat treated at 1400 °C. Only the phases F and C- Gd_2O_3 are

observed. Fig. 7-8 shows the SEM micrograph of this sample, which was heat treated at 1700 °C. A very homogenous phase distribution can be seen, where the white areas correspond to C-Gd₂O₃ solid solution and the grey areas correspond to the fluorite phase. Very similar XRD and SEM results were obtained for the whole temperature range (1400 - 1700 °C). Also, the sample containing 70 mol% GdO_{1.5} was found to consist of two phases (F + C-Gd₂O₃) after annealing at 1400 - 1600 °C, although it becomes single-phase fluorite at 1700 °C. Fig. 7-9 shows a C-Gd₂O₃ + B-Gd₂O₃ two-phase microstructure in the sample containing 95 mol% GdO_{1.5}, where the matrix is C-Gd₂O₃. The lighter area corresponds to the monoclinic B-GdO_{1.5}. The measured phase boundary data for the F + C-Gd₂O₃ and C-Gd₂O₃ + B-Gd₂O₃ equilibria are compiled in Table 7-4. The values for F + C-Gd₂O₃ phase region are consistent with the data of [1978Sco]. The solubility of ZrO₂ in B-Gd₂O₃ was found to be around 1 mol%, in agreement with the literature data [1962Per, 1971Rou]. The composition of the C-Gd₂O₃ phase in equilibrium with B-Gd₂O₃ was established for the first time.

Thus, the present work shows that the phase transition $F \Leftrightarrow C$ is of first order and a wide two-phase region exists. Neither the hexagonal phases H₂ and H₃ nor the miscibility gap within C-Gd₂O₃ reported elsewhere [1962Per] can be confirmed.

7.2.4. The martensitic transformation temperatures of the tetragonal phase

The martensitic transformation temperatures of the ZrO₂ – GdO_{1.5} samples with 1 and 2 mol% GdO_{1.5} were determined by DTA up to the temperature of 1400°C. The detailed data on the temperatures of A_s , A_f , M_s and M_f are compiled in Table 7-5, together with the calculated T_0 temperatures.

7.3. Selected experimental data for optimization

7.3.1. Phase diagram data

The tetragonal + fluorite phase equilibrium data measured by [1991Leu, 1995Kat] are accepted because the samples were equilibrated for a long time and their compositions were supposed to be highly precise. For the order-disorder phase boundary between fluorite and pyrochlore, the results determined in this work and those of [2005Lec] are considered for optimization. Since at the GdO_{1.5}-rich side the results obtained in this work are quite consistent with those of [1978Sco, 2001Fei], all these data are included in the assessment of the fluorite + C-Gd₂O₃ phase boundaries. At high temperatures, the only available data from [1971Rou] are accepted for the optimization.

7.3.2. Thermodynamic data

Among the data on the enthalpy of formation of pyrochlore, the results obtained by [1971Kor] are much more negative than those of [2001Hel]. In view of the comparability of the data of the $\text{ZrO}_2 - \text{GdO}_{1.5}$ and $\text{ZrO}_2 - \text{YO}_{1.5}$ systems [2003Lee], the data of [2001Hel] are accepted to optimize the stability of the pyrochlore and fluorite phases.

The heat capacity data measured by [2003Lut] and in this work for pyrochlore, and by [2003Lec] for fluorite (20.4 mol% $\text{GdO}_{1.5}$), as well as heat content data determined in this work for samples with 30 and 50 mol% $\text{GdO}_{1.5}$ are taken for the optimization of thermodynamic properties.

7.4. Optimization procedure

In the first step, the phase diagram was roughly assessed by using phase equilibria and thermodynamic data without regarding the pyrochlore phase. In a second step, the pyrochlore phase was added to the assessment. The enthalpy of formation and heat capacity data were employed to obtain a preliminary Gibbs energy function for the stoichiometric composition of pyrochlore. Finally, a set of self-consistent thermodynamic parameters is determined to fit most of the experimental data.

By keeping all the parameters of other phases obtained in above steps, the system was assessed using the order-disorder model for pyrochlore phase. Only two more parameters describing the ordered pyrochlore were finally introduced to reproduce the second-order phase transition boundary.

The optimized thermodynamic parameters are given in **Appendix**.

7.5. Calculated results and discussion

7.5.1. The phase diagram without pyrochlore ordering

The calculated $\text{ZrO}_2 - \text{GdO}_{1.5}$ phase diagram without considering the pyrochlore phase is shown in Fig. 7-10. Most of the experimental data are well consistent with the calculated phase diagram. The calculated invariant reactions are given in Table 7-1.

The experimentally derived temperatures of [1971Rou] on the liquidus, and the reactions $\text{L} \Leftrightarrow \text{F} + \text{H-Gd}_2\text{O}_3$ and $\text{H-Gd}_2\text{O}_3 \Leftrightarrow \text{F} + \text{B-Gd}_2\text{O}_3$ are well reproduced, except the calculated solubility of $\text{GdO}_{1.5}$ in the fluorite phase for the reaction $\text{L} \Leftrightarrow \text{F} + \text{H-Gd}_2\text{O}_3$, which is about 4 mol% larger and that for the reaction $\text{H-Gd}_2\text{O}_3 \Leftrightarrow \text{F} + \text{B-Gd}_2\text{O}_3$, which is about 4 mol% less than the experimental data. The calculated phase compositions of the fluorite + C-

Gd₂O₃ phase equilibrium shows good agreement with the experimental data of [1978Sco, 2001Fei] and this work. The reaction F + B-Gd₂O₃ ⇌ C-Gd₂O₃ is extrapolated to occur at 2275 K, which is thought to be reasonable. The solubility of ZrO₂ in C-type Gd₂O₃ reaches a maximum value near 1873 K, and decreases at higher temperatures. The compositions of the fluorite phase of the invariant reactions reported by [1971Rou] were not fitted well because these data obtained by HTXRD could be less precise. The enthalpy of formation of the fluorite phase has to be increased in order to make a better fit for the phase compositions of the invariant reactions, while the agreement with the experimental data of the present work on both fluorite + C-Gd₂O₃ and fluorite + tetragonal phase equilibria would become worse.

The calculated decomposition of the tetragonal phase into the monoclinic phase and fluorite occurs at 1309 K and 1.4 mol% GdO_{1.5}. The calculated phase boundaries for the fluorite + tetragonal equilibrium agree well with the experimental data of [1995Kat]. An enlarged phase diagram of the ZrO₂-rich side of the system together with the experimental data of the T_0 lines are shown in Fig. 7-11. The calculated T_0 temperatures against compositions are given by dashed lines. There is a difference of about 3 mol% GdO_{1.5} between the T_0 data for tetragonal + fluorite equilibrium evaluated by [1991Leu] and the current calculation. A better fit would badly influence the phase diagram in other areas. The T_0 data obtained in this work by DTA measurements for the composition 1 and 2 mol% GdO_{1.5} are plotted in Fig. 7-11, and the present calculation reproduces them well within the experimental uncertainty.

7.5.2. Calculated results by the pyrochlore model $(Zr^{+4}, Gd^{+3})_2(Gd^{+3}, Zr^{+4})_2(O^{2-}, Va)_6(O^{2-})_1(Va, O^{2-})_1$

The phase diagram with the pyrochlore phase is shown in Fig. 7-12, where the pyrochlore is modeled as an independent compound resulting in a fluorite + pyrochlore two-phase region. The calculated phase boundaries are in good agreement with the experimental data of [2005Lec] and of this work. The data of [1999Kar, 1962Per] on the pyrochlore / pyrochlore + fluorite phase boundary are questionable because it will be almost impossible to determine this boundary at such low temperatures.

The calculated eutectoid point of the invariant reaction F ⇌ C-Gd₂O₃ + P is at 1145 K and 63 mol% GdO_{1.5}. This is reasonable, because according to [2005Lec], there is considerable single fluorite phase region at 1200°C in the GdO_{1.5}-rich region. In the ZrO₂-rich region, according to the present calculation, the fluorite phase extends to room temperature.

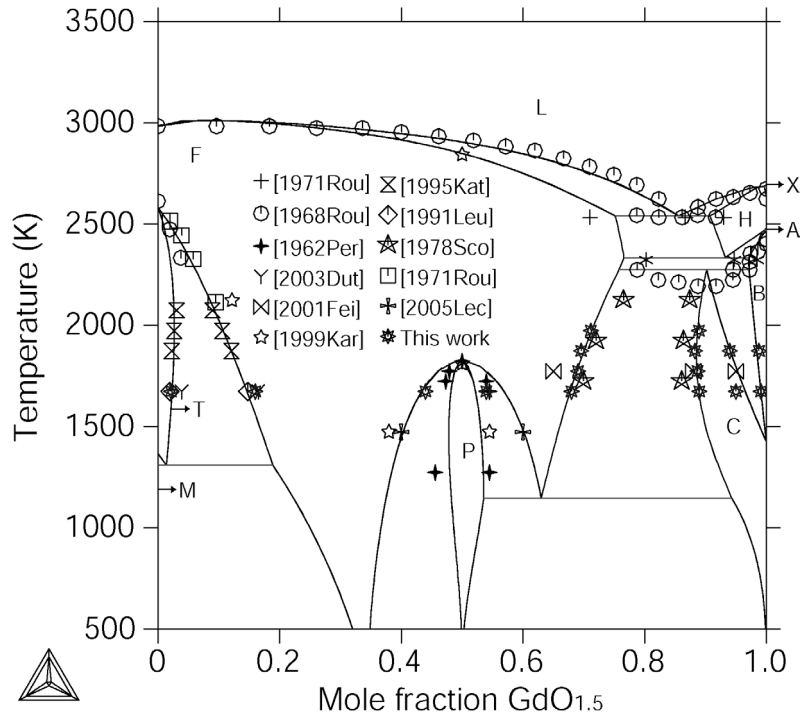


Figure 7-12. The calculated ZrO₂ – GdO_{1.5} phase diagram with the pyrochlore / fluorite modeled as a first order phase transition.

7.5.3. Calculated results by the pyrochlore model (Zr⁺⁴, Gd⁺³)₂(Gd⁺³, Zr⁺⁴)₂(O⁻², Va)₈

The calculated phase diagram using the order-disorder model for the pyrochlore phase is shown in Fig. 7-13. The second order pyrochlore / fluorite phase transition boundary is denoted by a dashed line. The experimental data of [2005Lec] and this work are well reproduced. The data [1962Per, 1999Kar] are not considered due to their less reliability. In accordance with experimental data, a phase transition boundary symmetric to 50 mol% GdO_{1.5} is obtained. At lower temperatures, the pyrochlore / fluorite phase boundary extends into the two-phase regions in both the ZrO₂ and GdO_{1.5}-rich region. It means at low temperatures the pyrochlore phase will be in equilibrium with both terminal solid solutions instead of the fluorite phase. The phase diagram modified in accordance with thermodynamic rules is shown in Fig. 7-14. At low temperatures, the phase boundaries of M + P and P + C-Gd₂O₃ two-phase equilibria are only slightly shifted, due to the small difference between the Gibbs energies of ordered pyrochlore and fluorite. It has to be mentioned that this phase diagram only gives the phase relations at the thermodynamically equilibrium state, and it doesn't mean that such two-phase regions can really occur under the condition of sluggish diffusion and the low driving force.

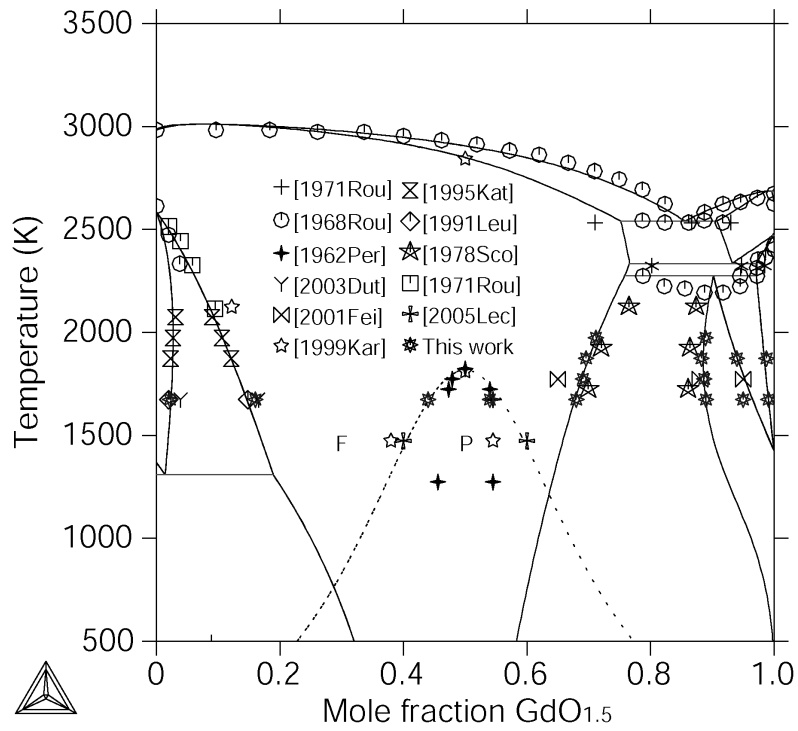


Figure 7-13. The calculated $\text{ZrO}_2 - \text{GdO}_{1.5}$ phase diagram including a second order pyrochlore-fluorite transition boundary.

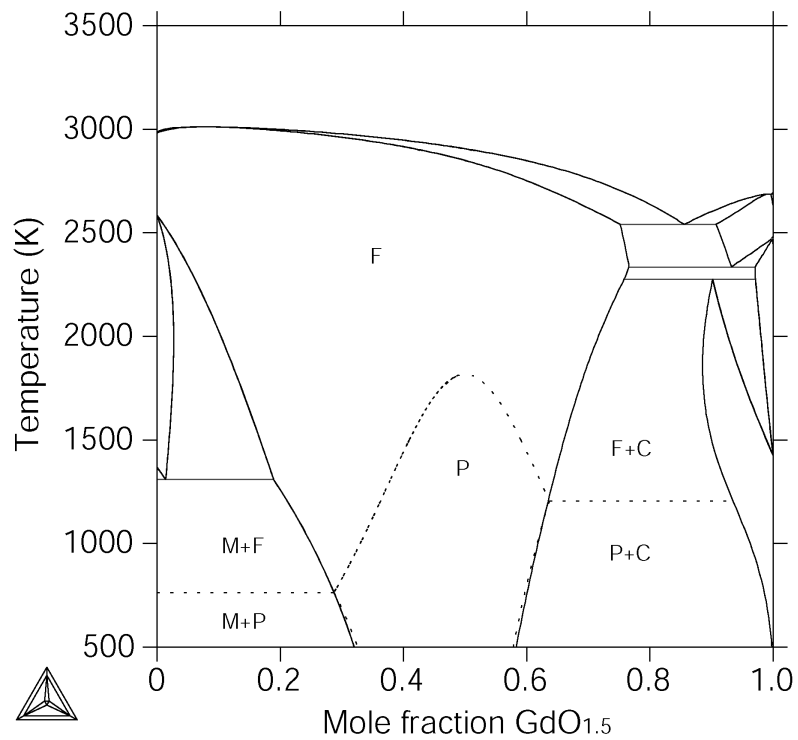


Figure 7-14. The calculated $\text{ZrO}_2 - \text{GdO}_{1.5}$ phase diagram modeled with a second order pyrochlore-fluorite phase transition. The related phase boundaries are shown by dashed lines.

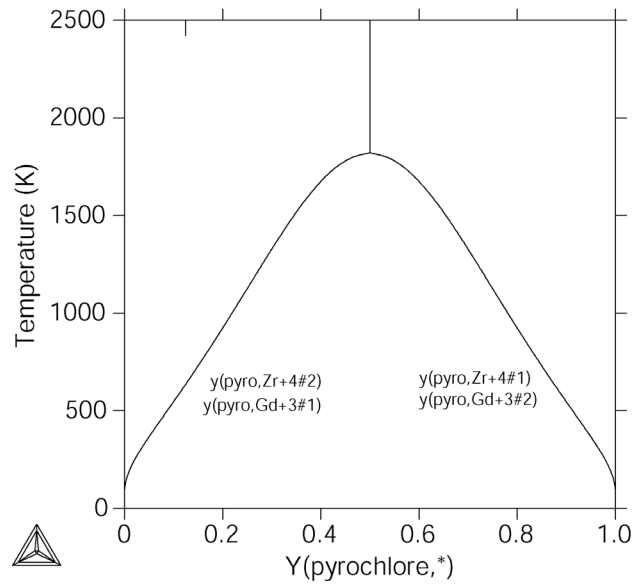


Figure 7-15. The calculated site fractions of the Zr^{+4} and Gd^{+3} species in the sublattice 1 and 2 for the composition ZrO_2 -50 mol% $GdO_{1.5}$ at different temperatures. With increasing temperature, the degree of order decreases.

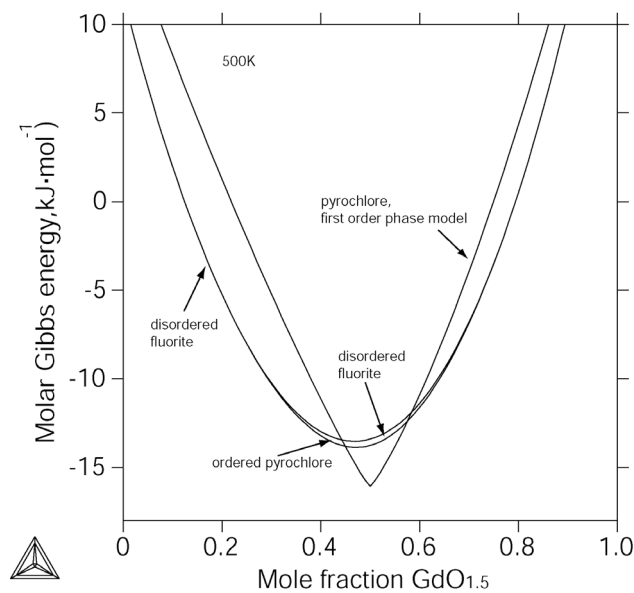


Figure 7-16. The calculated molar Gibbs energy curves of the fluorite and pyrochlore phases in the $ZrO_2 - GdO_{1.5}$ system at 500 K using two different models for the pyrochlore phase. (Reference state: monoclinic ZrO_2 and C-type $GdO_{1.5}$).

The site fractions of the Zr^{+4} and Gd^{+3} species in the sublattice 1 and 2 for the composition 50 mol% $GdO_{1.5}$ at different temperatures are calculated (Fig. 7-15). It can be seen that the completely ideal ordering only occurs at very low temperatures. With increasing the temperature, the ordering degree decreases gradually, and all the species fractions become identical at the temperature where the pyrochlore transforms into fluorite phase.

7.4.4. Thermodynamic properties

The experimental and calculated enthalpies of formation of pyrochlore and fluorite with different compositions are given in Table 7-2. Present calculations reproduce the data of [2001Hel] very well, whereas the result of [1971Kor] is too negative compared with this work. The enthalpy of formation of the pyrochlore phase calculated by the first order phase model is about $2000 \text{ J}\cdot\text{mol}^{-1}$ more negative than that calculated by the second order phase model. Fig. 7-16 presents the calculated molar Gibbs energy curves for both models of pyrochlore and that of the fluorite at 500 K (Reference state: monoclinic ZrO_2 and C-type $\text{GdO}_{1.5}$). At 50 mol% $\text{GdO}_{1.5}$ the energy difference between the fluorite and pyrochlore described by the first order phase model is more than $3000 \text{ J}\cdot\text{mol}^{-1}$, while the difference is greatly decreased by using the second order phase model. Beyond the compositions of second order phase transition, the Gibbs energy curves of the disordered fluorite and ordered pyrochlore will merge into a single curve.

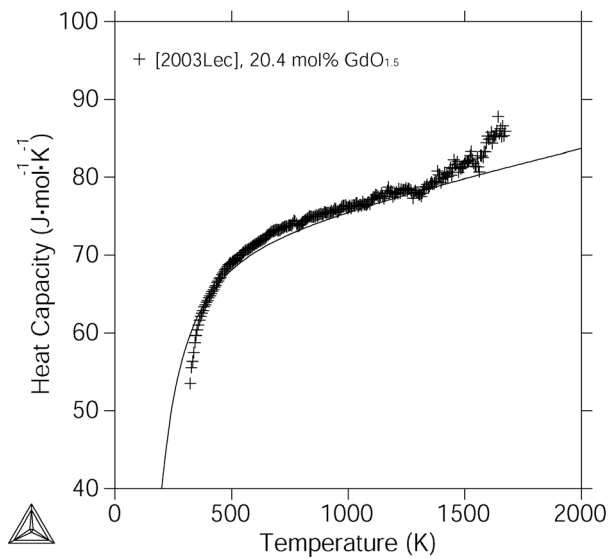


Figure 7-17. The calculated heat capacity for the sample ZrO_2 -20.4 mol% $\text{GdO}_{1.5}$ together with the experimental data [2003Lec].

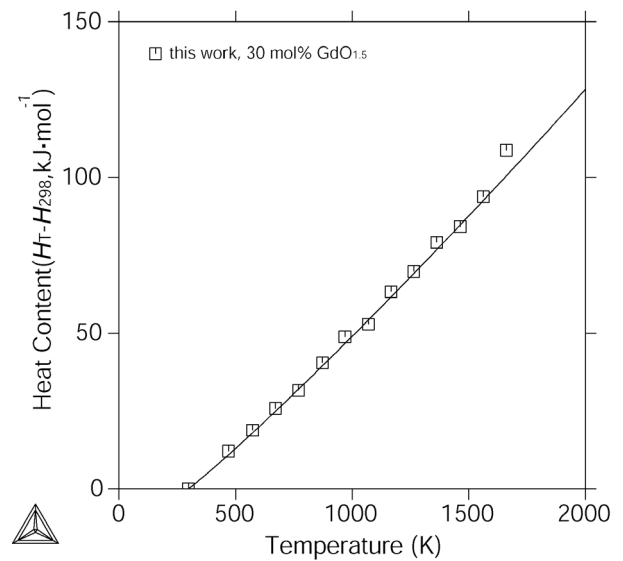


Figure 7-18. The calculated heat content for the sample ZrO_2 -30 mol% $\text{GdO}_{1.5}$ together with the experimental data.

Fig. 7-17 and Fig. 7-18 present the calculated and experimental heat capacity (20.4 mol% $\text{GdO}_{1.5}$) and heat content (30 mol% $\text{GdO}_{1.5}$) of fluorite. To fit the enthalpy increment and the heat capacity data, a $T \ln T$ contribution was used for zeroth order interaction parameter of the fluorite phase. The reasonable agreement of present calculations also demonstrates the consistency of the heat capacity and heat content data. The calculated and experimental heat capacity and heat content for the pyrochlore phase at 50 mol% $\text{GdO}_{1.5}$ are shown in Fig. 7-19

and Fig. 7-20, respectively, using two different pyrochlore models. The calculation by the first order phase model fits the heat capacity data well, while the result calculated by the second order phase model shows some deviation within the limits of experimental uncertainty. At the temperature of the pyrochlore-to-fluorite transition, the heat capacity calculated by the second order phase model indicates a discontinuity, since the pyrochlore phase becomes completely disordered. For the calculated heat content, however, a better fit with the experimental data is obtained using the order-disorder model. For the experimental heat capacity and heat content data, it can be seen that a good fit with one set of data will always cause a worse fit with other sets of data by using both models. This discrepancy originates from the uncertainties of the experimental data.

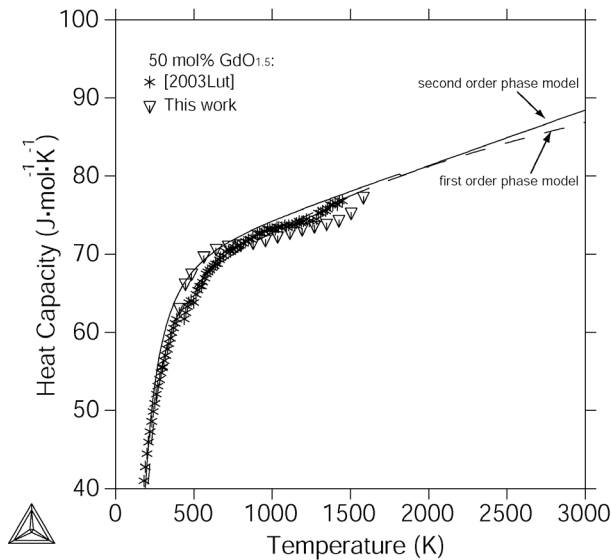


Figure 7-19. The calculated heat capacity for the sample ZrO_2 -50 mol% $GdO_{1.5}$ together with the experimental data with the two pyrochlore models used for assessments.

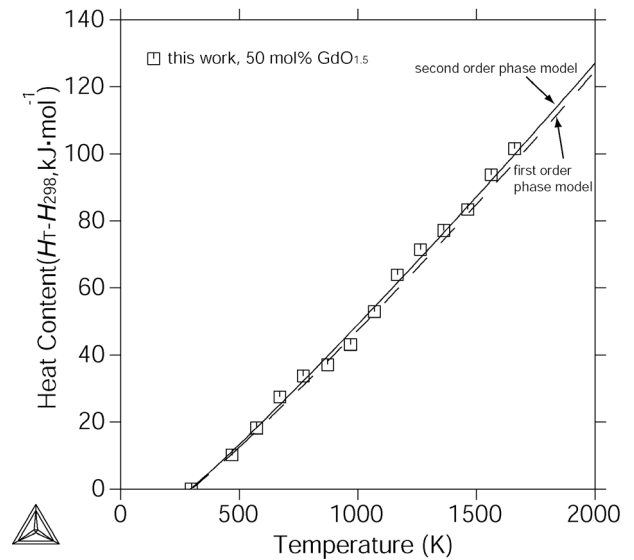


Figure 7-20. The calculated heat content for the sample ZrO_2 -50 mol% $GdO_{1.5}$ together with the experimental data with the two pyrochlore models used for assessments.

Table 7-1. The invariant reactions in the $ZrO_2 - GdO_{1.5}$ system.

Reaction	Type	Reference	Temperature (K)	Composition of phases (mol% $GdO_{1.5}$)		
$L \leftrightarrow F + H$	eutectic	[1964Lin1]	2448	87.3	—	—
		[1971Rou]	2533	86.7 ± 1	71	93

		This work	2518	85.7	75.4	91
H ⇌ F + B	eutectoid	[1971Rou]	2323	94.7	80.2	98.5
		This work	2335	93.2	76.6	97.1
L + X ⇌ H	peritectic	[1971Rou]	2623	96	99	97
		This work	2687	99.6	100	99.7
F + B ⇌ C	peritectoid	This work	2275	75.8	97.1	90.2
F ⇌ C + P	eutectoid	This work	1145	63	94.3	53.6
P ⇌ F	congruent	[1962Per]	1813 ± 10	50	50	–
		[1974Mic]	1803	50	50	–
		[1982Zoz]	1816	50	50	–
		[1989Mor]	1823	50	50	–
		This work	1823	50	50	–
T ⇌ M + F	eutectoid	[1972Neg]	1415	–	–	–
		This work	1309	1.4	0.02	18.9

Table 7-2. Experimental and calculated enthalpies of formation in the ZrO₂ – GdO_{1.5} system.

Compositions	Experimental data (J.mol ⁻¹)*	Calculated results (J.mol ⁻¹)*
50 mol.% GdO _{1.5} , P	-13050 ± 1200 [2001Hel]	-14752 (first order phase model) -12790 (second order phase model)
50 mol.% GdO _{1.5} , F	-18925 ± 2000 [1971Kor]	-11731
45.6 mol.% GdO _{1.5} , P	-12725 ± 825 [2001Hel]	-14849 (first order phase model) -12273 (second order phase model)
53.5 mol.% GdO _{1.5} , F	-11600 ± 850 [2001Hel]	-11292

*per mole of cations

Table 7-3. The compositions of the samples investigated in the ZrO₂ – GdO_{1.5} system and observed phases.

No.	GdO _{1.5} (mol%)	Observed phases		
		1400 °C	1600 °C	1700 °C
1	1	M		
2	2	M		
3	7.6	M + F		
4	10	M + F	M + F	M + F
5	20	F	F	
6	30	F	F	
7	41	F		
8	42	F		
9	43	F		
10	44	P		

11	45	P		
12	46	P		
13	47	P		
14	48	P		
15	49	P		
16	50	P	F	F
17	51	P		
18	52	P		
19	53	P		
20	54	P		
21	55	F		
22	56	F		
23	57	F		
24	58	F		
25	59	F		
26	70	F + C	F + C	F
27	80	F + C	F + C	F + C
28	95	C + B	C + B	C + B

Table 7-4. Measured phase compositions data (mol% GdO_{1.5}) for different phase equilibria in the ZrO₂ – GdO_{1.5} system at different temperatures.

Temperature (K)	F + C		C + B	
	F	C	C	B
1673	68.0 ± 1	89.0 ± 1	95.0 ± 1	99.1 ± 1
1773	69.0 ± 1	88.7 ± 1		
1873	69.6 ± 1	88.3 ± 1	94.0 ± 1	98.8 ± 1
1973	71.2 ± 1	88.9 ± 1		

Table 7-5. The DTA results of the martensitic transformation in the ZrO₂ – GdO_{1.5} system.

Composition (mol% GdO _{1.5})	On heating		On cooling		$T_0, (A_s+M_s)/2$ (K)	$T_0', (A_f+M_f)/2$ (K)
	A_s (K)	A_f (K)	M_s (K)	M_f (K)		
1	1251	1324	1142	1108	1197	1216
2	1075	1155	1003	928	1039	1042

Chapter 8

Experimental study and thermodynamic modeling of the $\text{ZrO}_2 - \text{DyO}_{1.5}$ system

8.1. Literature review

The phase equilibria of the $\text{ZrO}_2 - \text{Dy}_2\text{O}_3$ system were experimentally investigated by several groups [1962Per, 1970Tho, 1971Rou, 1980Pas, 1981Gav].

Perez [1962Per] firstly studied the phase relations in the temperature range 1000-2500°C. A $C_1 \Leftrightarrow C_2$ continuous phase transition was found in the Dy_2O_3 -rich region, and two metastable compounds H_2 and H_3 were reported. Furthermore, the C_2 phase based on the C-type Dy_2O_3 could form a miscibility gap in the composition range around 55-65 mol% Dy_2O_3 according to their paper. However, most of the phase boundaries and reactions were given by dashed lines, which were thought to be less precise.

[1970Tho] reported three intermediate phases in the $\text{ZrO}_2 - \text{DyO}_{1.5}$ system called α_1 , α_2 and σ in the temperature range 1000-1350°C. After heat treatment at 1050°C for 20 days, α_1 was considered to be stable in the composition range 21-29 mol% $\text{DyO}_{1.5}$, and corresponded to the fluorite phase because it could coexist with the monoclinic phase. With increasing the $\text{DyO}_{1.5}$ content, α_2 was stable in the composition range 53-59 mol% $\text{DyO}_{1.5}$. After heat treatment at 1350°C for 5 days, the σ phase was found beyond the composition of 85 mol% $\text{DyO}_{1.5}$, and was probably the C-type terminal solution. However, no more detailed information on the structures of these phases was given in this paper.

A detailed determination of the system above 1800°C was done by [1971Rou] using HTXRD measurements. The liquidus curve was well determined and the solidus was accordingly estimated. A continuous transition $C_1 \Leftrightarrow C_2$ was also reported like in the work of [1962Per]. This seems to be unreasonable according to the present experimental work on the $\text{ZrO}_2 - \text{GdO}_{1.5}$ system. The eutectic point of the invariant reaction $L \Leftrightarrow F + H\text{-Dy}_2\text{O}_3$ was determined at 2270°C and 80 mol% Dy_2O_3 . At 2150°C, the $H\text{-Dy}_2\text{O}_3$ phase (95 mol% Dy_2O_3) was found to decompose into C_2 and $B\text{-Dy}_2\text{O}_3$ phase by a eutectoid reaction.

[1980Pas] studied the $\text{ZrO}_2 - \text{Dy}_2\text{O}_3$ phase diagram over the whole composition range from 1150 to 2000°C. From 0 to 10 mol% Dy_2O_3 , the HTXRD measurement was conducted between room temperature and 1500°C, and a high-temperature dilatometry was employed to obtain the thermal expansion data from room temperature to 1300°C. By determining the lattice parameter, the minimum solubility of Dy_2O_3 in the fluorite phase was found to be ~8.5

mol% at 500°C, 7 mol% at 1200°C, 6.3 mol% at 1450°C, 5 mol% at 1765°C and ~2 mol% at ~2000°C. The maximum solubility of Dy₂O₃ in fluorite was found to be 53 mol% at 1765°C and 59 mol% at 2000°C. The eutectoid point of the invariant reaction $T \Leftrightarrow M + F$ was reported to occur at around 500°C and 4 mol% Dy₂O₃ based on the results of HTXRD and dilatometry measurements. The $C_1 \Leftrightarrow C_2$ continuous transition reported by [1962Per, 1971Rou] was not confirmed in their work, because the phase separation into fluorite and the C-type phases could be detected after the samples in the composition range 50 to 70 mol% Dy₂O₃ were annealed at ~1800°C. A F + C-Dy₂O₃ two-phase region was found by [1980Pas] in the composition ranges 53-67 mol% Dy₂O₃ at 1765°C and 59-73 mol% Dy₂O₃ at ~2000°C. Below 1765°C, two ordered hexagonal phases were detected in the Dy₂O₃-rich region. The M₇O_{11.5}-type H₂ phase was found to exist at the temperatures below 1700°C at a composition of 55 mol% Dy₂O₃. In the composition range from 65 to 90 mol% Dy₂O₃, another hexagonal M₇O₁₁-type H₃ phase was found. Both H₂ and H₃ were also reported previously by [1962Per] giving the same structure information. Neither the pyrochlore phase Dy₂Zr₂O₇ nor δ -Dy₄Zr₃O₁₂ was found in the work of [1980Pas]. Some invariant reactions involving fluorite, H₂, H₃, and C-type phases are not clear yet according to the experimental work of [1980Pas].

In the work of [1981Gav], the authors found the composition range of fluorite from 7 to 50 mol% Dy₂O₃ at 2020 K.

All the experimental data on the invariant reactions are listed in Table 8-1.

No any thermodynamic information concerning the ZrO₂ – DyO_{1.5} system is available in literature.

8.2. Experimental results and discussion

8.2.1. The as-pyrolysed state

Totally ten samples with different compositions were prepared in this work. The XRD patterns of the pyrolysed samples are given in Fig. 8-1. At the ZrO₂-rich side, a sample presents clear tetragonal peaks, while the XRD patterns of samples in DyO_{1.5}-rich region already show weak peaks of the C-type structure. For the sample containing 50 mol% DyO_{1.5}, wide XRD peaks indicate that it is poorly crystallized at this temperature. The compositions of all the samples and information about the observed structure after heat treatment at different temperatures are given in Table 8-2.

8.2.2. The tetragonal + fluorite phase equilibrium

The XRD patterns in Fig. 8-2 show clear a fluorite + monoclinic two-phase structure for the sample with 7 mol% DyO_{1.5} after heat treatment. Fig. 8-3 is a SEM image of the sample containing 7 mol% DyO_{1.5} heat treated at 1700°C for 36h. The grey areas are the monoclinic phase transformed from the tetragonal phase during cooling, and the light ones are the fluorite phase. Compared with the ZrO₂ – GdO_{1.5} system, in the ZrO₂ – DyO_{1.5} system the tetragonal + fluorite two-phase region is narrower, and the solubility range of the tetragonal phase is larger (Table 8-3).

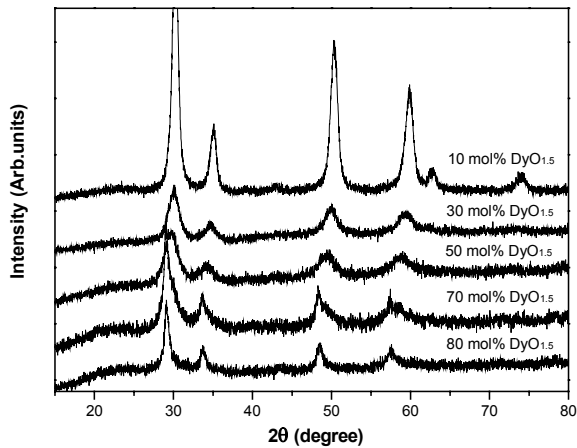


Figure 8-1. The XRD patterns of the as-lysed ZrO₂ – DyO_{1.5} samples at 700°C for 3h.

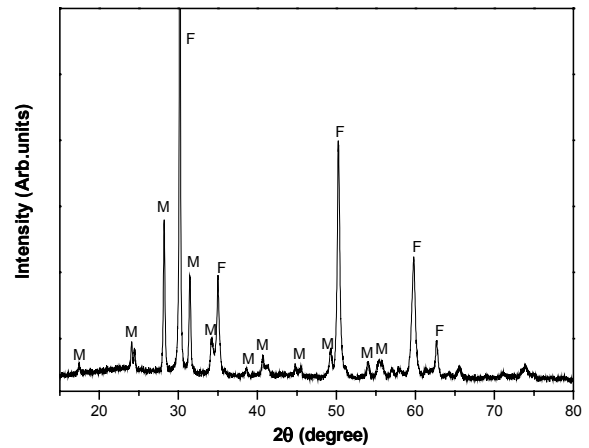


Figure 8-2. The XRD patterns of the sample ZrO₂-7 mol% DyO_{1.5} heat treated at 1400°C for 240h.

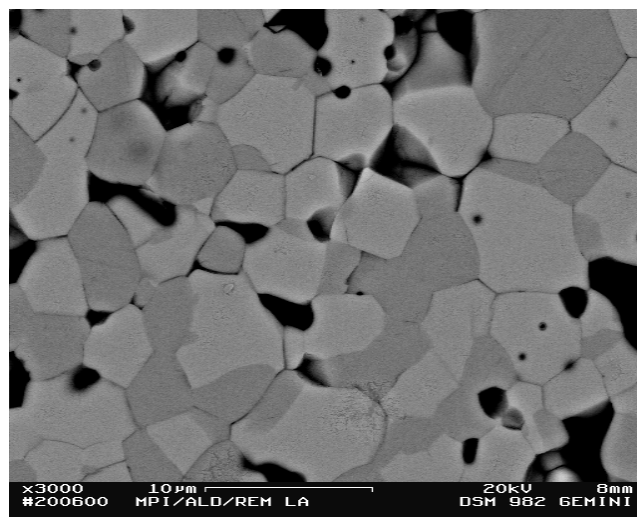


Figure 8-3. The SEM back scattered electron image (×3000) of the sample ZrO₂-7 mol% DyO_{1.5} heat treated at 1700°C for 36h (the grey areas are the monoclinic phase transformed from the tetragonal phase, and the light ones are fluorite).

8.2.3. The martensitic transformation temperatures of the tetragonal phase

The martensitic transformation temperatures of the samples containing 1 and 2 mol% DyO_{1.5} were measured by DTA up to 1400°C. The detailed temperature data of A_s , A_f , M_s and M_f are compiled in Table 8-4, together with the calculated T_0 temperatures.

8.2.4. The fluorite + C-Dy₂O₃ phase equilibrium

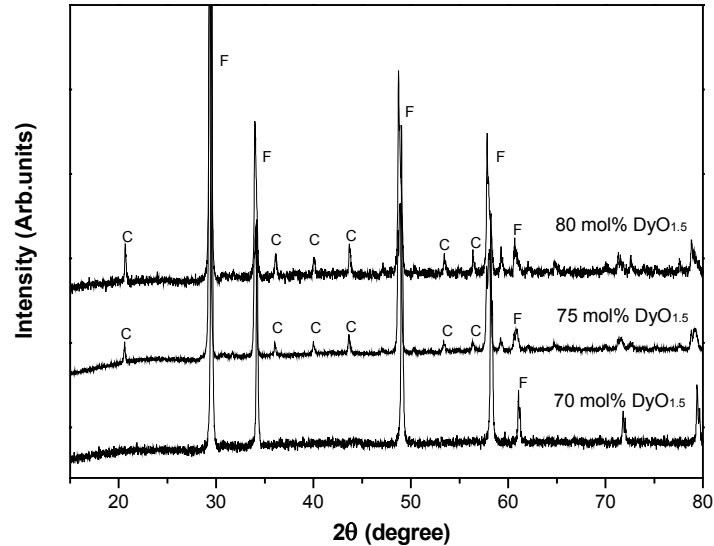


Figure 8-4. The XRD patterns of the ZrO₂ – DyO_{1.5} samples with 70, 75, and 80 mol% DyO_{1.5} heat treated at 1600°C for 72h.

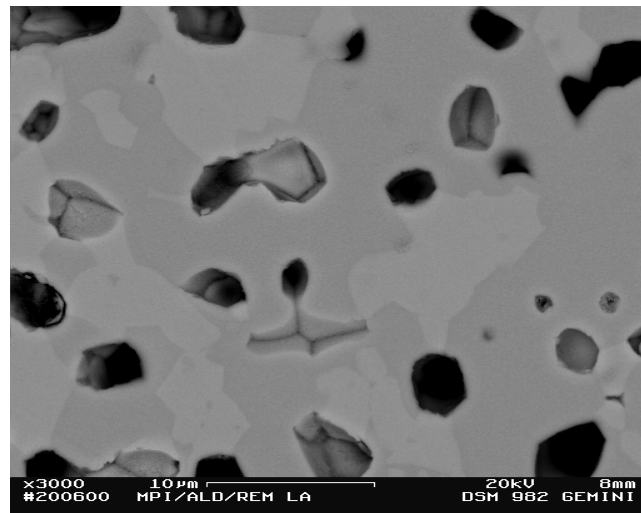


Figure 8-5. The SEM back scattered electron image (×3000) of the sample ZrO₂-75 mol% DyO_{1.5} heat treated at 1700°C for 36h (the grey areas are fluorite, and the light ones are C-type Dy₂O₃).

Neither pyrochlore nor the δ -type phase is found according to the XRD results in the investigated temperature range. This is consistent with the literature reports. Thus, the fluorite phase is only in equilibrium with the C-Dy₂O₃ phase beyond the composition of 50 mol%

DyO_{1.5}. Fig. 8-4 includes the XRD patterns of the samples with 70, 75 and 80 mol% DyO_{1.5} after heat treatment at 1600°C, 72h. The sample with 70 mol% DyO_{1.5} only shows fluorite peaks, and both the samples with 75 and 80 mol% DyO_{1.5} present the superstructure peaks of C-type phase. SEM-EDX analysis reveals that a narrow fluorite + C-Dy₂O₃ two-phase region exists in this region. The two-phase region is not easy to be identified by using the XRD measurements due to the overlapping of the strong peaks of fluorite and the C-type phases. Fig. 8-5 is a SEM image of the sample with 75 mol% DyO_{1.5} after heat treatment at 1700°C for 36h. The width of this two-phase region is only around 10 mol% according to the EDX data (Table 8-3). With increasing the temperature, the solubility of ZrO₂ in C-type phase reduces.

8.3. Selected experimental data for optimization

The experimental data on the tetragonal + fluorite and fluorite + C-Dy₂O₃ phase equilibria obtained in this work are adopted in the optimization, together with the high temperature liquidus data and invariant reactions reported by [1971Rou].

The heat content data of the samples with 30 and 50 mol% DyO_{1.5} in the range 473-1673 K measured in this work are accepted to assess the thermodynamic properties of the fluorite phase. For the enthalpy of formation of the fluorite phase, since there are no any experimental data, it is assumed that it should be slightly more negative than the value in the ZrO₂ – GdO_{1.5} system.

8.4. Optimization procedure

By using a limited number of parameters, in a first step the phase diagram was roughly assessed from the experimental phase equilibria data. In a second step, the optimization of the fluorite phase was improved by taking also the thermodynamic data of heat content into account. Finally, a full adjustment of the parameters of all phases was carried out in order that all the reliable experimental data could be well reproduced. To optimize the experimental heat content data, a $T \ln T$ contribution was added to the zeroth order interaction parameter of the fluorite phase. The optimized parameters are given in **Appendix**.

8.5. Calculated results and discussion

The calculated ZrO₂ – DyO_{1.5} phase diagram is shown in Fig. 8-6, together with the experimental data. The experimental phase boundary data obtained in this work and the

liquidus data of [1971Rou] are well reproduced. The calculated invariant reactions by this work are compiled in Table 8-1.

A reasonable tetragonal + fluorite two-phase region is calculated based on the present experimental data. The XRD results of [1980Pas, 1981Gav] show some deviation with this work, due to their less accuracy. The calculated eutectoid point of the invariant reaction $T \leftrightarrow F + M$ occurs at 1233 K and 3.2 mol% $DyO_{1.5}$. This temperature is much higher than the value 773 K reported by [1980Pas]. The present result is thought to be more reasonable, because the temperature of [1980Pas] obtained by dilatometry measurement is actually corresponding to the martensitic transformation temperature, rather than to the invariant reaction. Fig. 8-7 presents the calculated T_0 lines for the monoclinic + tetragonal and tetragonal + fluorite equilibria, agreeing well with the experimental data obtained in this work.

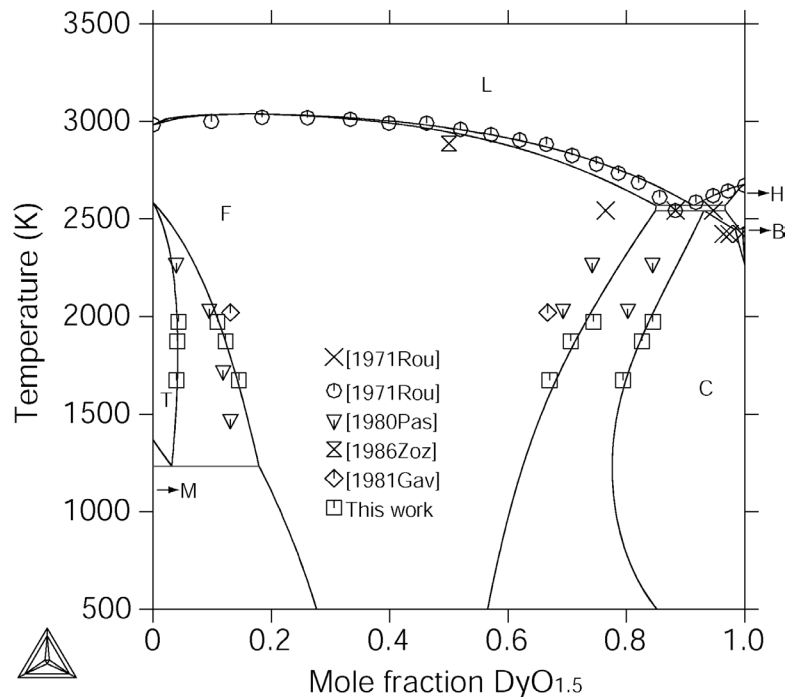


Figure 8-6. The calculated $ZrO_2 - DyO_{1.5}$ phase diagram together with experimental data.

The data on the fluorite + C- Dy_2O_3 phase equilibrium reported by [1980Pas, 1981Gav] are not consistent with but close to present calculations. With elevating the temperature, the solubility of ZrO_2 in C-type phase reduces in the temperature range studied. Two invariant reactions involving the C-type phase are calculated: $H-Dy_2O_3 + F \leftrightarrow C-Dy_2O_3$ at 2543 K and $H-Dy_2O_3 \leftrightarrow B-Dy_2O_3 + C-Dy_2O_3$ at 2445 K, for which the temperature is consistent with the experimental value 2423 K for this reaction reported by [1971Rou]. The temperature of the eutectic reaction $L \leftrightarrow F + H-Dy_2O_3$ calculated in this work is 2569 K,

which is close to the experimental data 2543 K of [1971Rou], while the calculated composition of each phase shows large discrepancies with those reported by [1971Rou]. However, the temperature of the reaction $\text{H-Dy}_2\text{O}_3 + \text{F} \Leftrightarrow \text{C-Dy}_2\text{O}_3$ predicted by the present calculation well reproduces the value of 2543 K for $\text{L} \Leftrightarrow \text{F} + \text{H-Dy}_2\text{O}_3$ reported by [1971Rou]. In view of the large experimental uncertainties and the reliable fluorite + C-Dy₂O₃ phase equilibrium data obtained in this work, the results of the present calculations are accepted as more reasonable.

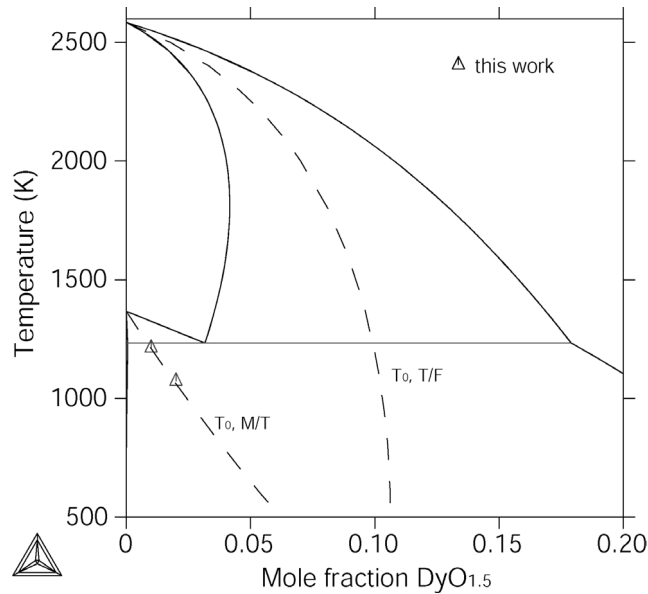


Figure 8-7. The calculated T_0 lines for the monoclinic + tetragonal and tetragonal + fluorite equilibria of the $\text{ZrO}_2 - \text{DyO}_{1.5}$ system, together with experimental data.

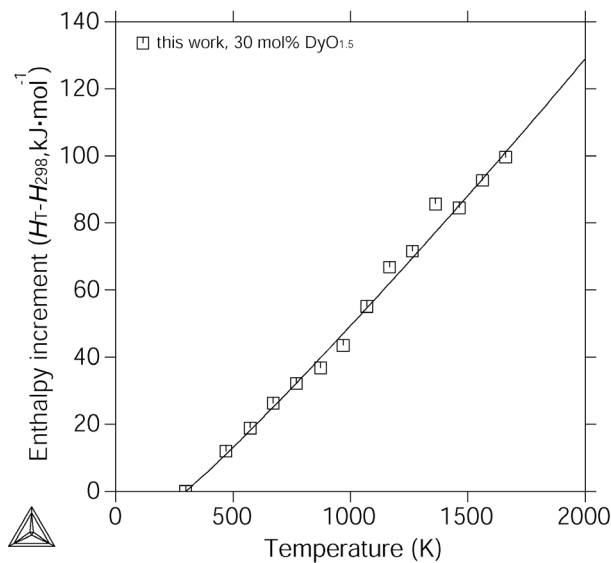


Figure 8-8. The experimental and calculated heat content ($H_T - H_{298}$) for the composition ZrO_2 -30 mol% $\text{DyO}_{1.5}$.

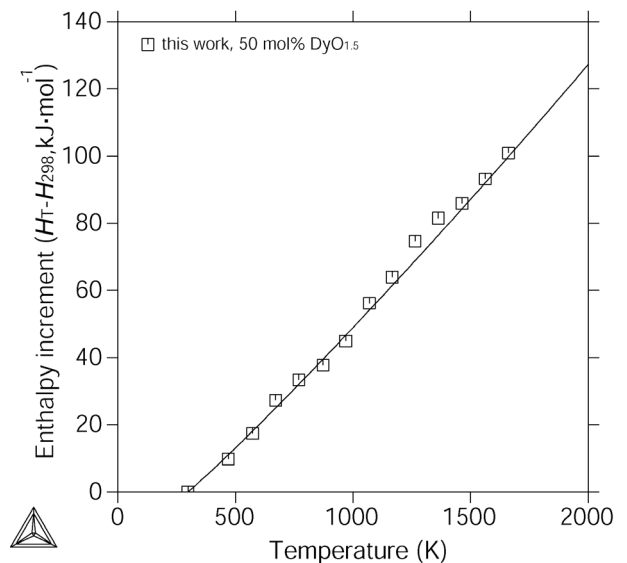


Figure 8-9. The experimental and calculated heat content ($H_T - H_{298}$) for the composition ZrO_2 -50 mol% $\text{DyO}_{1.5}$.

The experimental heat content data determined in this work for the samples containing 30 and 50 mol% DyO_{1.5} are given in Fig. 8-8 and Fig. 8-9 together with the calculated results. Though some data are scattered at high temperatures, the agreements are quite well after a $T \ln T$ contribution is adopted for the interaction parameter of the fluorite phase.

Table 8-1. The invariant reactions in the ZrO₂ – DyO_{1.5} system.

Reaction	Type	Reference	Temperature (K)	Compositions of phases (mol% DyO _{1.5})		
L ⇌ F + H	eutectic	[1971Rou]	2543	88.3	76.5	94.7
		This work	2569	91.3	85	96.7
H ⇌ C + B	eutectoid	[1971Rou]	2423	–	–	–
		This work	2445	99.2	98.4	99.6
H + F ⇌ C	peritectoid	This work	2543	96.7	84.9	93.1
T ⇌ M + F	eutectoid	[1980Pas]	773	4.0	–	–
		This work	1233	3.2	0.06	17.9

Table 8-2. The compositions of the samples investigated in the ZrO₂ – DyO_{1.5} system and observed phases.

No.	DyO _{1.5} (mol%)	Observed phases		
		1400 °C	1600 °C	1700 °C
1	1	M	–	–
2	2	M	–	–
3	7	F + M	F + M	F + M
4	10	F + M	F + M	F + M
5	30	F	F	F
6	50	F	F	F
7	60	F	F	F
8	70	F	F	F
9	75	F + C	F + C	F + C
10	80	C	C	C

Table 8-3. Measured phase compositions data (mol% DyO_{1.5}) for different phase equilibria in the ZrO₂ – DyO_{1.5} system at different temperatures.

Temperature (K)	T + F		F + C	
	T	F	F	C
1673	3.95 ± 0.5	14.5 ± 1	67 ± 1	79.4 ± 1
1873	4.1 ± 0.5	12.3 ± 1	70.6 ± 1	82.6 ± 1
1973	4.3 ± 0.5	10.9 ± 1	74.4 ± 1	84.5 ± 1

Table 8-4. The DTA results of martensitic transformation in the ZrO₂ – DyO_{1.5} system.

Composition (mol% DyO _{1.5})	On heating		On cooling		$T_{0s}, (A_s+M_s)/2$ (K)	$T_{0'f}, (A_f+M_f)/2$ (K)
	A_s (K)	A_f (K)	M_s (K)	M_f (K)		
1	1272	1318	1153	1117	1212.5	1217.5
2	1123	1186	1018	975	1073	1080.5

Chapter 9

Experimental study and thermodynamic modeling of the $\text{ZrO}_2 - \text{YbO}_{1.5}$ system

9.1. Literature review

The phase equilibria of the $\text{ZrO}_2 - \text{YbO}_{1.5}$ system were experimentally investigated by the several groups [1968Rou1, 1970Tho, 1971Rou, 1982Zoz, 1984Stu, 1987Ste, 1993Gon, 1999Kar].

[1968Rou1, 1971Rou] studied the phase relations above 1800°C by thermal analysis and HTXRD measurements. A congruent melting point of the fluorite phase was determined at 2825°C and 25 mol% Yb_2O_3 . The liquidus curve was well defined and the solidus was estimated according to the liquidus data. An invariant eutectic reaction in the Yb_2O_3 -rich region was detected to occur at around 2420°C . At lower temperatures, a continuous second-order transition from the fluorite phase to a cubic Tl_2O_3 -type phase was reported, and actually not correct according to the present experimental results on the $\text{ZrO}_2 - \text{GdO}_{1.5}$ and $\text{ZrO}_2 - \text{DyO}_{1.5}$ systems.

The ordered compound $\text{Yb}_4\text{Zr}_3\text{O}_{12}$ (δ) was reported by Thornber et al. [1970Tho]. By plotting the unit-cell volumes of fluorite and C-type Yb_2O_3 at 1600°C , they found that the fluorite phase extends up to 50 mol% $\text{YbO}_{1.5}$. Beyond this composition, it was in equilibrium with the δ phase which formed near the composition of 57.14 mol% $\text{YbO}_{1.5}$. At the $\text{YbO}_{1.5}$ -rich side, there was a two-phase region between δ and the C-type Yb_2O_3 solid solution phases up to the composition of 70 mol% $\text{YbO}_{1.5}$.

The phase relations below 2150°C were proposed by [1984Stu] based on the experiments in the composition range 0-60 mol% Yb_2O_3 using XRD measurements. The tetragonal + fluorite two-phase region was established and the invariant reaction $\text{T} \Leftrightarrow \text{F} + \text{M}$ was determined at around 520°C with low reliability, while the temperature of the phase transition between fluorite and the δ phase was measured as $1637 \pm 12^\circ\text{C}$. In the Yb_2O_3 -rich region, three hexagonal phases H_1 , H_2 , and H_3 reported by [1962Per] were not confirmed by the phase relations determined by [1984Stu], and thus were thought as metastable phases. A sharp boundary between the ordered δ phase and fluorite was shown in their work, together with a similar result on the $\text{ZrO}_2 - \text{Y}_2\text{O}_3$ system. In the Yb_2O_3 -rich region, the reaction $\text{F} \Leftrightarrow \delta + \text{C-Yb}_2\text{O}_3$ occurs at 1612°C where the eutectoid composition of fluorite is very close to the composition of δ phase. [1987Ste] studied the phase formation in the $\text{ZrO}_2 - \text{Yb}_2\text{O}_3$ system by

using XRD measurements. Samples in the composition range of 2 to 90 wt.% Yb_2O_3 were heat treated at 1400°C-1600°C for both 96h and 192h. Similar results to [1984Stu] were obtained on the phase evolution with increasing the Yb_2O_3 content. However, no any quantitative result was given on the phase boundaries.

The tetragonal + fluorite two-phase region was studied by [1993Gon] in the range of 0-10 mol% Yb_2O_3 with 0.5 mol% composition increments using dilatometry and XRD measurements. The samples were heat treated at four temperatures: 1700°C for 4h, 1640°C for 24h, 1290°C for 336h, and 840°C for 1000h. Compared with the result of [1984Stu], Gonzalez et al. [1993Gon] presented a narrower tetragonal + fluorite two-phase region. The tetragonal zirconia solution can dissolve up to 3 mol% Yb_2O_3 . The lower limit of the fluorite phase was established to be 7 mol% Yb_2O_3 at 840°C, 6 mol% Yb_2O_3 at 1290°C, 5 mol% Yb_2O_3 at 1640°C, and 4.8 mol% Yb_2O_3 at ~1700°C. The eutectoid point of the invariant reaction $T \Leftrightarrow F + M$ was determined at $400 \pm 20^\circ\text{C}$ and 2.3 mol% Yb_2O_3 by high-temperature dilatometry. However, this result is highly questionable and may be incorrect because the dilatometry actually only gives the $T \Leftrightarrow M$ martensitic transformation temperature. The compound $\text{Yb}_4\text{Zr}_3\text{O}_{12}$ was confirmed in their work, and the determined disordering temperature $1630 \pm 10^\circ\text{C}$ was well consistent with the result of [1984Stu]. The same result, 1630°C was also reported by [1999Kar].

The melting point of the sample ZrO_2 -50 mol% $\text{YbO}_{1.5}$ was measured at $2697 \pm 14^\circ\text{C}$ by [1982Zoz], and was consistent with the liquidus data determined by [1968Rou1]. Karaulov and Zoz [1999Kar] determined the homogeneity range of the compound $\text{Yb}_4\text{Zr}_3\text{O}_{12}$ in the temperature range 1200-1900°C. However, its composition range of 37-45 mol% Yb_2O_3 was given without an exact temperature.

A thermodynamic assessment of the $\text{ZrO}_2 - \text{YbO}_{1.5}$ system was done by Jacobson et al. [2002Jac] only based on the experimental data of [1968Rou1, 1984Stu] and a phase diagram with a less reliable fluorite + tetragonal two-phase region was presented.

No any experimental thermodynamic data are available in literature for the $\text{ZrO}_2 - \text{YbO}_{1.5}$ system.

All the experimental data on the invariant reactions are listed in Table 9-1.

9.2. Experimental results and discussion

9.2.1. The as-pyrolysed state

Totally seven samples with different compositions were prepared for the $\text{ZrO}_2 - \text{YbO}_{1.5}$ system: 6.5, 10, 30, 50, 57.14, 65 and 75 mol% $\text{YbO}_{1.5}$. The XRD patterns of the

samples after pyrolysis at 700°C for 3h are shown in Fig. 9-1. With increasing the content of $\text{YbO}_{1.5}$, the peaks become wider, and their number decreases, while revealing poorly crystallized microstructures. The observed phases of all samples after heat treatments by XRD measurement are summarized in Table 9-2.

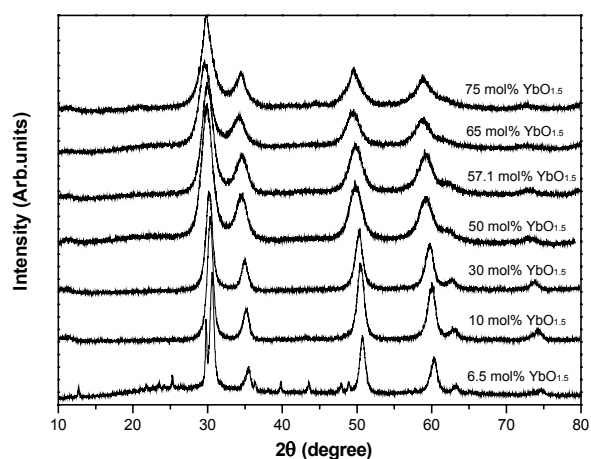


Figure 9-1. The XRD patterns of the $\text{ZrO}_2 - \text{YbO}_{1.5}$ samples as-pyrolysed at 700°C for 3h.

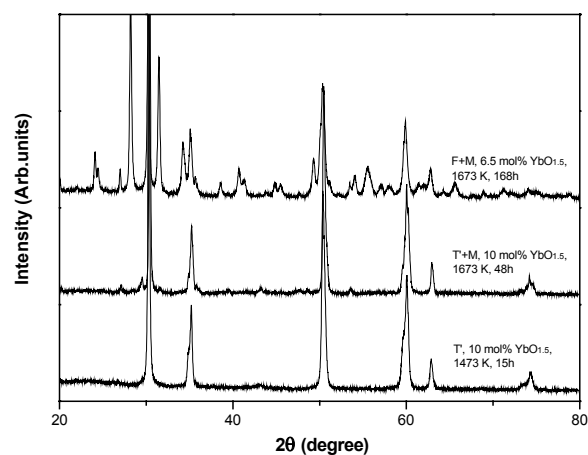


Figure 9-2. The XRD patterns of $\text{ZrO}_2 - \text{YbO}_{1.5}$ samples with 6.5 mol% and 10 mol% $\text{YbO}_{1.5}$ after different heat treatments.

9.2.2. The tetragonal + fluorite phase equilibrium

The tetragonal + fluorite phase equilibrium was determined by heat treating a sample with 6.5 mol% $\text{YbO}_{1.5}$, while the sample with 10 mol% $\text{YbO}_{1.5}$ heat treated at 1400°C has only a small amount of the monoclinic phase, and is not appropriate for composition analysis. The XRD patterns for these two samples heat treated at 1200°C and 1400°C are given in Fig. 9-2. The patterns of the sample containing 10 mol% $\text{YbO}_{1.5}$ present mainly the T' phase, which diffusionlessly transforms from fluorite during cooling, while those of the sample containing 6.5 mol% $\text{YbO}_{1.5}$ indicate clear the monoclinic and fluorite structure. Fig. 9-3 is the SEM back-scattered electron image ($\times 3000$) of the sample with 6.5 mol% $\text{YbO}_{1.5}$ heat treated at 1700°C for 36h. It shows a very homogeneous microstructure, in which the grey areas are the monoclinic phase transformed from the tetragonal phase during cooling, and the white areas are the fluorite phase. The measured data on the phase boundaries are listed in the Table 9-3. Present results agree better with the data of [1993Gon] than with those of [1984Stu]. The solubility of $\text{YbO}_{1.5}$ in the tetragonal phase exceeds 4 mol%, and increases at elevated temperatures. This is consistent with the results of [1995Kat] on some other systems. The solubility limit of the fluorite phase in the ZrO_2 -rich region reaches a low value compared with the other $\text{ZrO}_2 - \text{REO}_{1.5}$ system, and accordingly the fluorite + tetragonal two-phase

region is very narrow with a width of only around 6 mol% $\text{YbO}_{1.5}$ in the studied temperature range.

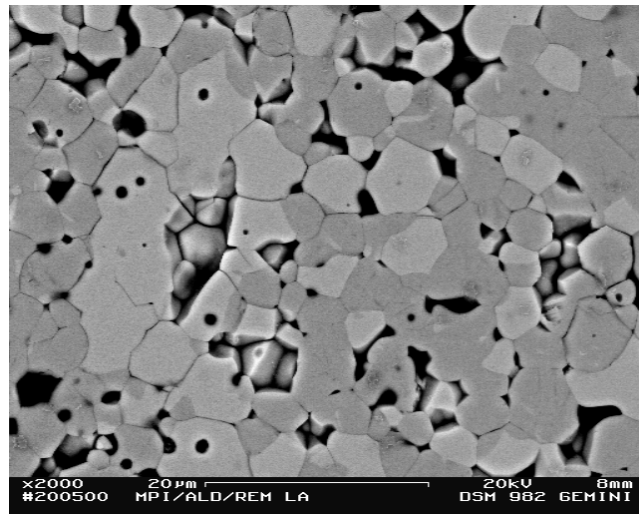


Figure 9-3. The SEM back scattered electron image ($\times 3000$) of the sample ZrO_2 -6.5 mol% $\text{YbO}_{1.5}$ heat treated at 1700°C for 36h (the grey areas are the monoclinic phase transformed from the tetragonal phase, and the white ones are fluorite).

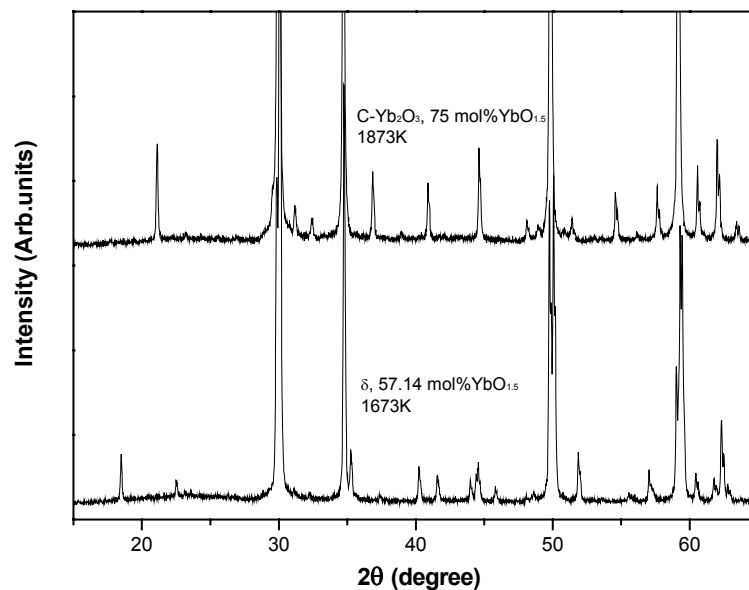


Figure 9-4. The XRD patterns of the δ phase and C-type Yb_2O_3 in the $\text{ZrO}_2 - \text{YbO}_{1.5}$ system.

9.2.3. The phase equilibria involving δ and C- Yb_2O_3

As the ordered structure of the fluorite phase, the δ phase is the only compound found in this work. The phase relations involving δ phase reported by [1984Stu, 1987Ste] are confirmed by the XRD measurements. Fig. 9-4 includes the XRD patterns of δ and C- Yb_2O_3 . Because δ and C- Yb_2O_3 are both ordered structures of the fluorite phase, the strong peaks of δ

always overlap with the peaks of fluorite. As a result, the $\delta + \text{C-Yb}_2\text{O}_3$ and $\text{F} + \text{C-Yb}_2\text{O}_3$ two-phase regions are hardly to be identified by the XRD measurements.

Fig. 9-5 is the SEM image of the microstructure of the sample containing 65 mol% $\text{YbO}_{1.5}$ consisting of δ and $\text{C-Yb}_2\text{O}_3$. The average grain size of the δ phase is less than $5 \mu\text{m}$ even after the heat treatment at 1600°C for 72h. The measured compositions of δ , $\text{C-Yb}_2\text{O}_3$ and fluorite of the $\delta + \text{C-Yb}_2\text{O}_3$ and $\text{F} + \text{C-Yb}_2\text{O}_3$ two-phase equilibria are summarized in Table 9-3.

Present XRD and SEM results are consistent with those of the $\delta \leftrightarrow \text{F}$ transformation and the reaction $\text{F} \leftrightarrow \delta + \text{C}$ reported by [1984Stu]. However, narrower $\delta + \text{C-Yb}_2\text{O}_3$ and $\text{F} + \text{C-Yb}_2\text{O}_3$ two-phase regions are obtained in this work by precise determination of the phase boundary data.

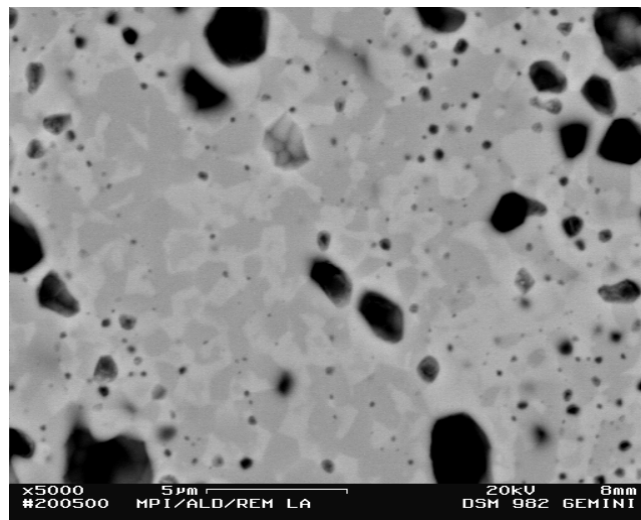


Figure 9-5. The SEM back scattered electron image ($\times 5000$) of the sample ZrO_2 -65 mol% $\text{YbO}_{1.5}$ heat treated at 1600°C for 72h (the grey areas are the fluorite phase, and the light ones are $\text{C-Yb}_2\text{O}_3$).

9.3. Selected experimental data for optimization

Due to the limited literature data on the phase diagram, the phase boundary data obtained in this work on the tetragonal + fluorite, $\delta + \text{C-Yb}_2\text{O}_3$, and fluorite + $\text{C-Yb}_2\text{O}_3$ phase equilibria, the temperatures for the $\delta \leftrightarrow \text{F}$ transformation and the reaction $\text{F} \leftrightarrow \delta + \text{C}$ found by [1984Stu, 1999Kar], the homogeneity range data of the δ phase reported by [1999Kar], and the liquidus data determined by [1968Rou1] together with the temperature of the invariant reaction involving liquid, $\text{C-Yb}_2\text{O}_3$, and $\text{H-Yb}_2\text{O}_3$ are adopted for the optimization of the phase diagram.

The heat content data of the samples with 30 mol% $\text{YbO}_{1.5}$ and 57.14 mol % $\text{YbO}_{1.5}$ in the temperature range 473-1673 K measured in this work are adopted for modeling. The enthalpy of formation of the fluorite phase in the $\text{ZrO}_2 - \text{YO}_{1.5}$ system [2003Lee] is adopted as a start value, in view of the similarities of these two systems.

9.4. Optimization procedure

In a first step, the phase diagram was roughly assessed by using liquidus and tetragonal + fluorite phase boundary data, without taking account of the ordered δ phase. Then, further optimization was done by treating the δ phase as a stoichiometric compound, and using the experimental heat content data. Finally, a full assessment is carried out by using all selected data simultaneously and introducing homogeneity range for the δ phase.

For the fluorite phase, a $T \ln T$ contribution to zeroth order interaction parameter was applied to fit the experimental heat content data. The Neumann-Kopp rule was adopted for the δ phase since it reproduces the experimental heat content data well, and the entropy of formation of the δ phase with respect to monoclinic ZrO_2 and C-type Yb_2O_3 was arbitrarily given $0.5 \text{ J} \cdot \text{mol}^{-1} \cdot \text{K}^{-1}$ in this work.

The optimized thermodynamic parameters for all phases are given in **Appendix**.

9.5. Calculated results and discussion

The calculated $\text{ZrO}_2 - \text{YbO}_{1.5}$ phase diagram is shown in Fig. 9-6, together with the experimental data, while the calculated invariant reactions are given in Table 9-1.

The assessed tetragonal + fluorite two-phase region shows good agreement with the phase equilibria data obtained in this work and those data on the composition limits of the tetragonal phase by [1984Stu, 1993Gon]. As for the fluorite phase, the data reported by [1993Gon] agree with current results well at high temperatures, and indicates discrepancy at low temperatures due to the experimental uncertainties. The phase boundary data of fluorite phase obtained in the work of [1984Stu] are less accurate, partly because the phase transformation character in this region is complicated and XRD cannot correctly record the phase transformation temperatures. Likewise, the temperatures of decomposition of the tetragonal phase into fluorite and the monoclinic phase [1984Stu, 1993Gon] seem to be too low compared to that of the equilibrium state. Presently calculated eutectoid point of the invariant reaction $\text{T} \Leftrightarrow \text{M} + \text{F}$ is at 1215 K and 3.6 mol% $\text{YbO}_{1.5}$, while the related composition of the fluorite phase is 15.6 mol% $\text{YbO}_{1.5}$, and the solubility of $\text{YbO}_{1.5}$ in monoclinic phase is only around 0.1 mol%.

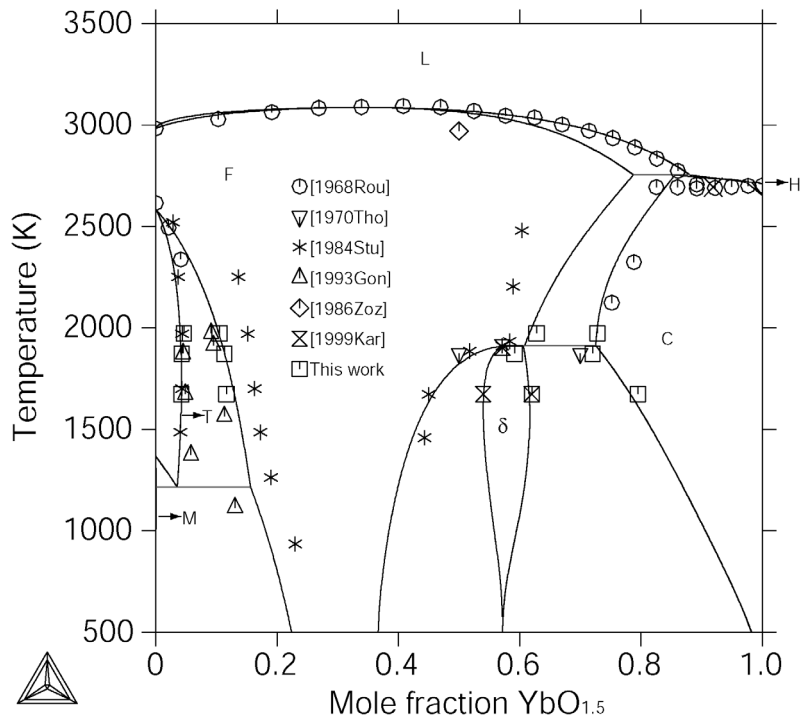


Figure 9-6. The calculated $ZrO_2 - YbO_{1.5}$ phase diagram together with experimental data.

The calculated liquidus show reasonable agreement with the experimental data considering their large uncertainties at such high temperatures. The congruent melting point of the fluorite phase calculated in this work is at 3085 K and 33.6 mol% $YbO_{1.5}$, which temperature is close to 3093 K reported by [1971Rou], but shows some discrepancy with respect to the composition (40 mol% $YbO_{1.5}$). Considering the smooth liquidus temperatures in a wide composition range and the large experimental uncertainties, the present calculated result is acceptable. At low temperatures, the calculated temperature 1908 K for the invariant reaction $F \Leftrightarrow \delta + C$ agrees well with the experimental data, while the temperature for the $F \Leftrightarrow \delta$ transition is only 1 K lower. The experimental results of [1999Kar] on the homogeneity range of the δ phase as well as those obtained in the present work are reproduced well by the calculation. However, the phase boundaries of the δ phase at both sides are not symmetrical to the composition 57.14 mol% $YbO_{1.5}$, and the calculated congruent composition for the $F \Leftrightarrow \delta$ transition is at 59.7 mol% $YbO_{1.5}$. These are thought to be reasonable by taking account of the possible larger solubility of $YbO_{1.5}$ in the δ phase in view of the difference of the Zr^{4+} and Yb^{3+} . The solubility of ZrO_2 in C-type Yb_2O_3 reaches its maximum value at this invariant reaction, and decreases at elevated temperatures. The $F / F + C$ - Yb_2O_3 phase boundary data of [1984Stu] show large discrepancy with the calculations and present experimental data. The literature data are less reliable because it is very difficult to study the $F + C$ - Yb_2O_3 two-phase region only by XRD according to the experience gathered in the present work due to the

overlapping of the XRD peaks of F and C-Yb₂O₃. In the Yb₂O₃-rich region, two calculated invariant reactions involving liquid phase are $L \Leftrightarrow C\text{-Yb}_2\text{O}_3 + H\text{-Yb}_2\text{O}_3$ at 2717 K, and $L + F \Leftrightarrow C\text{-Yb}_2\text{O}_3$ at 2754 K. In view of the large experimental uncertainties in this region, the present calculations provide at least a topologically reasonable phase diagram.

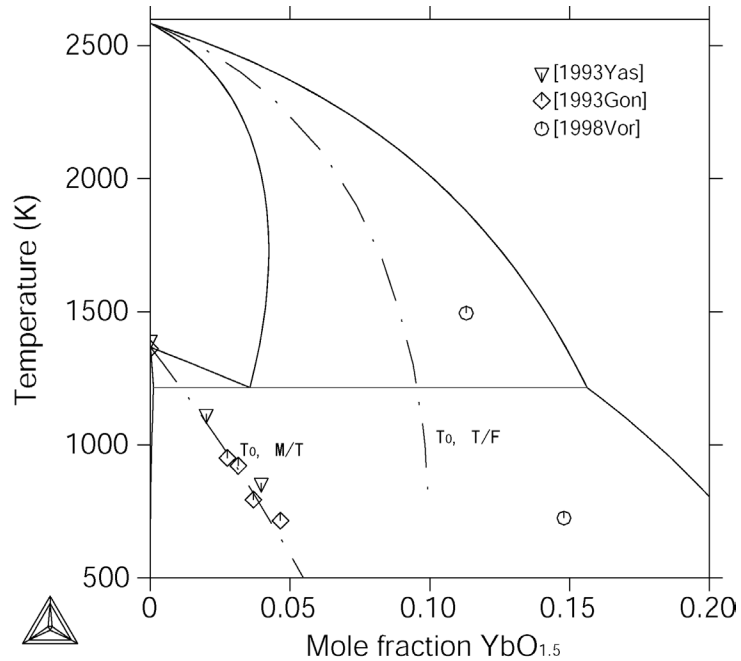


Figure 9-7. The calculated partial ZrO₂ – YbO_{1.5} phase diagram and the T_0 lines for the monoclinic + tetragonal and tetragonal + fluorite phase equilibria, together with the experimental data.

Fig. 9-7 presents the calculated T_0 lines for the monoclinic + tetragonal and tetragonal + fluorite phase equilibria, in which the experimental T_0 data are well reproduced. However, the estimated T_0 data [1998Vor] for the transition between fluorite and T', do not agree well with the present calculation. Since the calculation based on the equilibrium thermodynamics only gives the T_0 for the fluorite and tetragonal phase, and it is not clear yet if the Gibbs energy of metastable T' phase has exact the same behavior as the stable tetragonal phase. Thus, a better fit with the experimental data is not necessary and will make the phase diagram worse.

The enthalpy of formation (per mole of cations) of fluorite at 50 mol% YbO_{1.5} calculated in this work ($-16094 \text{ J}\cdot\text{mol}^{-1}$) is more negative than the value ($-6700 \text{ J}\cdot\text{mol}^{-1}$) reported by [2003Lee] for the ZrO₂ – YO_{1.5} system, however agrees with those data optimized by the CALPHAD method in the references [2004Chen, 2004Fab]. This is consistent with the results obtained for the other ZrO₂ – REO_{1.5} systems and that there is a tendency that with decreasing the ionic radius of RE⁺³, the stability of fluorite will increase. The calculated heat

contents of samples with 30 mol% $\text{YbO}_{1.5}$ and 57.14 mol% $\text{YbO}_{1.5}$ are plotted in Fig. 9-8 and Fig. 9-9, respectively, together with the experimental data obtained in this work. Though the experimental data show scattering due to the experimental uncertainties, the agreements with the calculations are still good enough. It can be seen from these two figures that the heat content of the fluorite phase changes faster than that of the δ phase, and a higher heat capacity can be deduced for the fluorite phase.

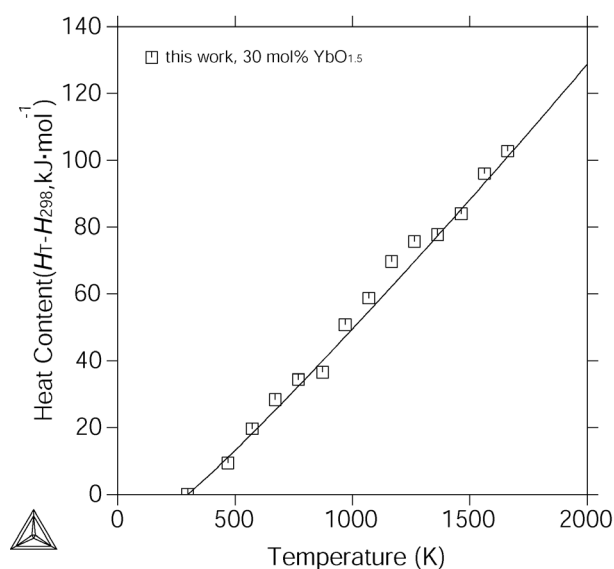


Figure 9-8. The experimental and calculated heat content ($H_T - H_{298}$) of fluorite with 30 mol% $\text{YbO}_{1.5}$.

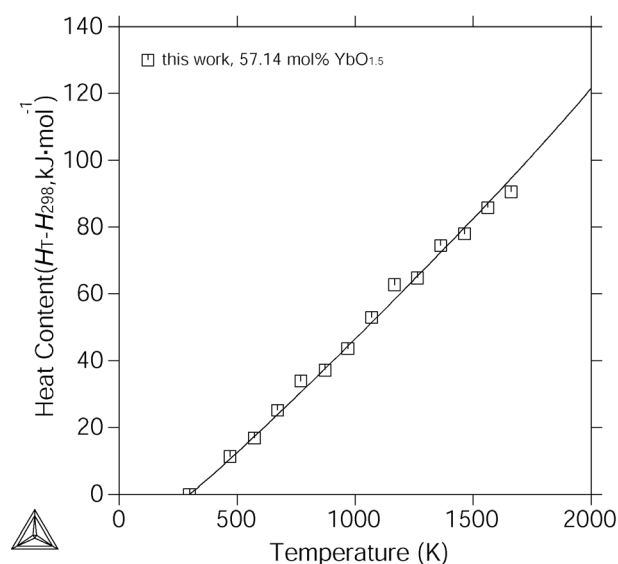


Figure 9-9. The experimental and calculated heat content ($H_T - H_{298}$) of δ with 57.14 mol% $\text{YbO}_{1.5}$.

Table 9-1. The invariant reactions in the $\text{ZrO}_2 - \text{YbO}_{1.5}$ system.

Reaction	Type	Reference	Temperature (K)	Compositions of phases (mol% $\text{YbO}_{1.5}$)		
$L \Leftrightarrow C + H$	eutectic	[1971Rou]	2693	92	—	—
		This work	2717	98.1	97.3	98.3
$L + F \Leftrightarrow C$	peritectic	This work	2754	88.1	78.8	85.6
$F \Leftrightarrow \delta + C$	eutectoid	[1984Stu]	1885	—	—	—
		This work	1907	60.8	60.6	72.5
$\delta \Leftrightarrow F$	congruent	[1984Stu]	1910	57.14	57.14	—
		[1993Gon]	1903	—	—	—
		[1999Kar]	1903	—	—	—
		This work	1908	59.7	59.7	—

T ⇌ M + F	eutectoid	[1993Gon]	673	4.5	3.1	15.6
		[1984Stu]	793	–	–	–
		This work	1215	3.6	0.1	15
F ⇌ L	congruent	[1971Rou]	3098	40	40	–
		This work	3085	33.6	33.6	–

Table 9-2. The compositions of the samples investigated in the ZrO₂ – YbO_{1.5} system and observed phases.

No.	YbO _{1.5} (mol%)	Observed phases		
		1400 °C	1600 °C	1700 °C
1	6.5	F + M	F + M	F + M
2	10	T' + M	T' + M	T' + M
3	30	F	F	F
4	50	F + δ	F	F
5	57.14	δ	δ	F
6	65	δ + C	δ + C	F + C
7	75	δ + C	C	C

Table 9-3. Measured phase compositions data (mol% YbO_{1.5}) for different phase equilibria in the ZrO₂ – YbO_{1.5} system at different temperatures.

Temperature (K)	T + F		δ + C		F + C	
	T	F	δ	C	F	C
1673	4.2 ± 0.5	11.7 ± 1	62.0 ± 1	79.5 ± 1.5	–	–
1873	4.3 ± 0.5	11.3 ± 1	59.2 ± 1	72.1 ± 1.5	–	–
1973	4.7 ± 0.5	10.5 ± 1	–	–	62.8 ± 1	72.8 ± 1

Chapter 10

Experimental study and calculation of the $\text{ZrO}_2 - \text{GdO}_{1.5} - \text{YO}_{1.5}$ system

10.1. Calculations and experimental results

The parameters for the $\text{ZrO}_2 - \text{YO}_{1.5}$ and $\text{GdO}_{1.5} - \text{YO}_{1.5}$ systems are taken from a recent assessment [2005Fab] for present calculations. No any further assessment is done for the $\text{ZrO}_2 - \text{GdO}_{1.5} - \text{YO}_{1.5}$ system. The calculated ternary isothermal sections at 1200, 1400 and 1600°C are presented in Fig. 10-1 (a-c). The projection of the liquidus surface is shown in Fig. 10-2. There is only one invariant reaction in this system $\text{C} + \text{L} \rightleftharpoons \text{H} + \text{F}$ at a temperature of 2316°C and a liquid composition of 8.6 mol% ZrO_2 and 61.3 mol% $\text{GdO}_{1.5}$. The univariant reaction $\text{L} \rightleftharpoons \text{H} + \text{X}$ is practically degenerated and proceeds in the $\text{GdO}_{1.5} - \text{YO}_{1.5}$ system from 70 to 99.9 mol% $\text{GdO}_{1.5}$.

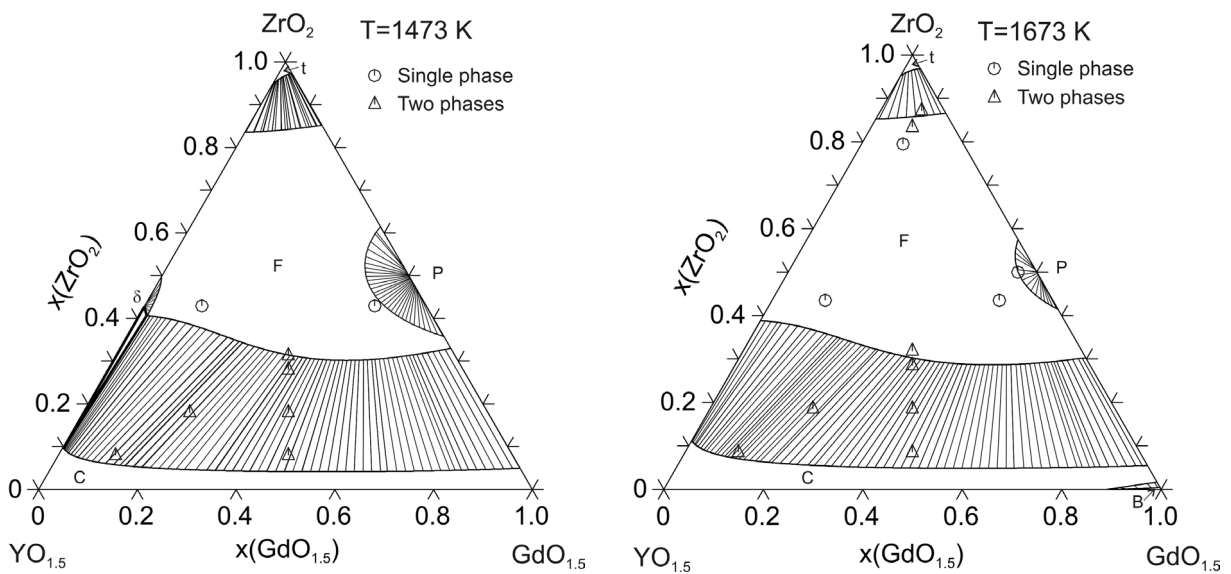


Figure 10-1 (a). Isothermal section at 1200°C

Figure 10-1 (b). Isothermal section at 1400°C

Selected XRD analysis of the samples annealed at 1400°C are presented in Fig. 10-3 and a summary of the phases identified in Table 10-1. No ternary compounds or three-phase regions were detected, as originally anticipated. In the ZrO_2 -rich region, the XRD analysis showed mainly the peaks of the fluorite and monoclinic phases. The monoclinic phase is not stable at 1400°C but results from martensitic transformation of the tetragonal phase during cooling. Fluorite is stable as a single phase in a wide composition range. At 1400°C, at least 5 mol% $\text{GdO}_{1.5}$ can be substituted by $\text{YO}_{1.5}$ in the pyrochlore structure. However, the XRD analysis could not conclusively ascertain if there is only pyrochlore or a pyrochlore + fluorite

phase assemblage in the region nominally denoted as a two-phase equilibrium in the thermodynamic model. The C-type phase is continuous along the $\text{GdO}_{1.5}$ - $\text{YO}_{1.5}$ binary for the temperature range of interest. With increasing ZrO_2 content a two-phase assemblage fluorite + C becomes stable across the entire range. The maximum concentration of ZrO_2 in the C-type phase does not exceed 10 mol%. In the temperature range 1200-1600°C, the phase boundaries F / F + C and C / F + C appear not to change very much with temperature.

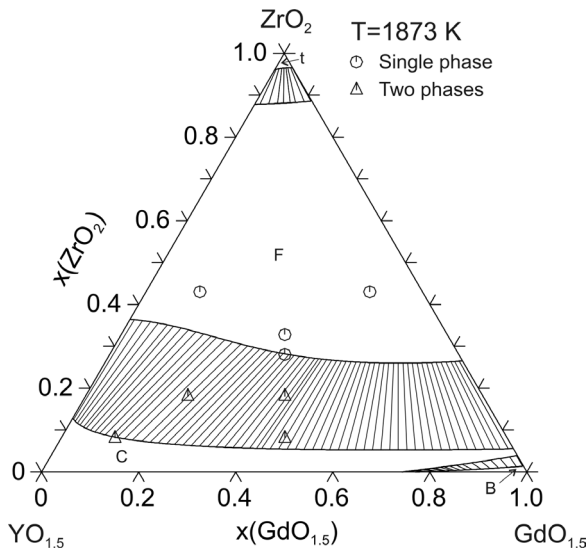


Figure 10-1 (c). Isothermal section at 1600°C

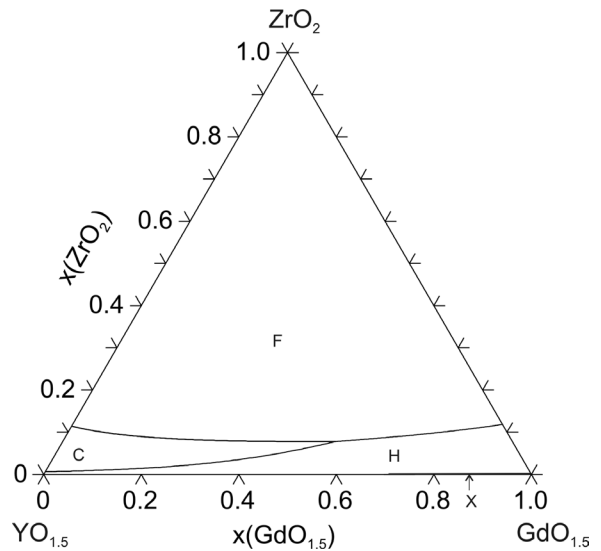


Figure 10-2. Calculated liquidus projection

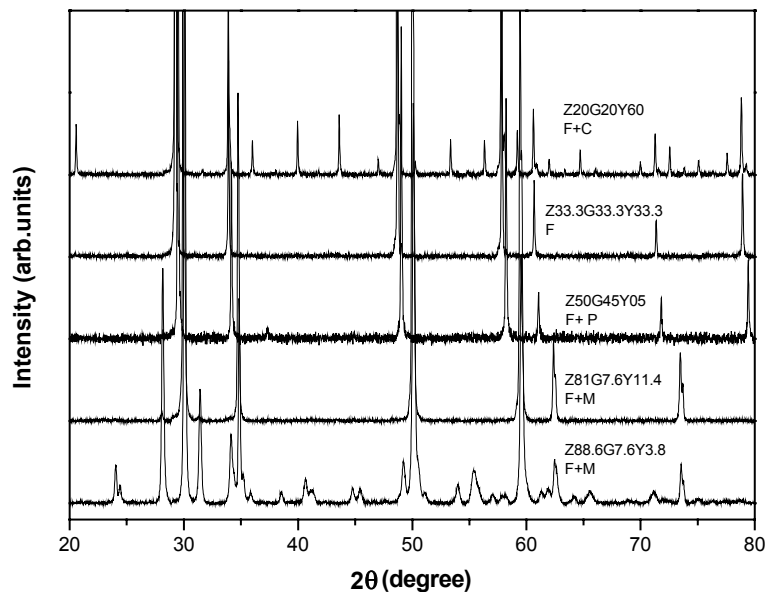


Figure 10-3. XRD patterns for the samples in the $\text{ZrO}_2 - \text{GdO}_{1.5} - \text{YO}_{1.5}$ system heat treated at 1400°C (Z, G, Y represent mol% of ZrO_2 , $\text{GdO}_{1.5}$ and $\text{YO}_{1.5}$ respectively).

10.2. Discussions

The experimental results show good agreement with the calculated sections in Figs. 10-1(a-c) indicating that the reassessment of the thermodynamic parameters for the ternary is not necessary and the database derived from the binaries properly represents the behavior of the system in this temperature range.

The similar behavior of the $\text{ZrO}_2 - \text{YO}_{1.5}$ and $\text{ZrO}_2 - \text{GdO}_{1.5}$ systems is reflected in the extension of the common fields across the entire ternary diagram, with the stability range of the ordered phases limited to the near vicinity of the corresponding binaries. It is well established that the ionic radius of Y^{+3} is too small to form a pyrochlore phase with ZrO_2 , so the de-stabilization of the pyrochlore with Y substitution for Gd is anticipated. A similar behavior is observed when Zr is substituted for Ti in the $\text{Y}_2\text{Ti}_2\text{O}_7$ pyrochlore. At the same time, substitution of the larger Gd cation for Y is also bound to readily de-stabilize the δ structure. The isothermal section at 1473 K in Fig. 10-1(a) gives confidence to the approach of using an intermediate layer of 7YSZ to control the interaction between $\text{Gd}_2\text{Zr}_2\text{O}_7$ and the protective Al_2O_3 in a TBC system, as discussed earlier. Incorporation of Y into $\text{Gd}_2\text{Zr}_2\text{O}_7$ induces disorder but it is not expected to change significantly the thermal isolation benefits of the latter [2002Wu].

Table 10-1. Summary of the XRD analysis of the samples in the $\text{ZrO}_2 - \text{GdO}_{1.5} - \text{YO}_{1.5}$ system heat treated at 1200-1600° C.

No.	Composition (mol%)			Observed phases		
	ZrO_2	$\text{GdO}_{1.5}$	$\text{YO}_{1.5}$	1200° C	1400° C	1600° C
1	88.6	7.6	3.8	–	F + M	–
2	88.6	3.8	7.6	–	F + M	–
3	84.8	7.6	7.6	–	F + M	–
4	81.0	7.6	11.4	–	F	–
5	50.0	45.0	5.0	–	P	–
6	45.0	45.0	10.0	F	F	F
7	45	10	45	F	F	F
8	33	33	33	F + C	F	F
9	30	35	35	F + C	F + C	F
10	20	20	60	C + F	C + F	C + F
11	20	60	20	–	C + F	–
12	20	40	40	C + F	C + F	C + F
13	10	10	80	C + F	C + F	C + F
14	10	45	45	C + F	C + F	C + F

Chapter 11

Characteristic changes in the $\text{ZrO}_2 - \text{REO}_{1.5}$ systems

11.1. The evolutions of the phase relations in the $\text{ZrO}_2 - \text{REO}_{1.5}$ systems

The rare earth oxides present similar physical and chemical properties, and show some trends with changing the ionic radius and molecular weight of the rare earth elements. As a matter of course, the phase relations in all the $\text{ZrO}_2 - \text{REO}_{1.5}$ systems also reveal similar characteristics and evolve with the change of the ionic radius or molecular weight.

For each $\text{ZrO}_2 - \text{REO}_{1.5}$ system except those with Dy and Sc, there is only one intermediate compound which is the ordered structure of the ZrO_2 -based cubic fluorite-type phase. From La to Gd, the pyrochlore phase at stoichiometric composition (50 mol% $\text{REO}_{1.5}$) is the stable compound, and from Ho to Yb, the ordered structure is the δ phase with the stoichiometry of 57.14 mol% $\text{REO}_{1.5}$. In the case of Dy, no any compound was found in this work. In the case of Sc, besides the δ phase, two other ordered compounds were also reported in literature [1970Spi, 1970Tho, 1977Ruh]. Fig. 11-1 collects the phase transition temperatures of the ordered phases in those systems. It is clear that the pyrochlore phase is preferably stable for the larger ionic radius of RE^{+3} , while the δ phase is preferably stable for the smaller ionic radius of RE^{+3} . With decreasing the ionic radius from La^{+3} to Dy^{+3} or increasing the ionic radius from Yb^{+3} to Dy^{+3} , both the pyrochlore and δ are less stable, and that is why no any ordered compound is found in the $\text{ZrO}_2 - \text{DyO}_{1.5}$ system. This is consistent with the fact that the pyrochlore is only stable when the $r_{A^{3+}} / r_{B^{4+}}$ ratio is between 1.46 and 1.80 [1983Sub]. On the other hand, even if the ordered structure can be thermodynamically stable, it will be kinetically very difficult to form at such low temperature.

As can be seen in Fig. 11-2, the solubility of $\text{REO}_{1.5}$ in tetragonal ZrO_2 at 1600°C increases when the ionic radius of RE reduces, and an approximate linear relation can be found for the solubility against ionic radius. At the same time, the fluorite phase field also extends towards lower solubility limits in the ZrO_2 -rich region when the RE^{+3} has a smaller ionic radius. As a result, the width of the tetragonal + fluorite two-phase region becomes narrower with decreasing the ionic radius. Furthermore, the decomposition temperature of the tetragonal phase (i.e. $\text{T} \Leftrightarrow \text{F} + \text{M}$ or $\text{T} \Leftrightarrow \text{P} + \text{M}$) is strongly influenced by the solubility limits of the tetragonal phase. Fig. 11-3 shows the calculated ZrO_2 -rich partial phase diagrams of the systems studied in this work without the pyrochlore phase. The clear trends for the change can be seen. Although some neighboring boundaries intersect each other in some temperature

ranges, reasonable characteristic changes are given by the present calculations within the limits of uncertainties.

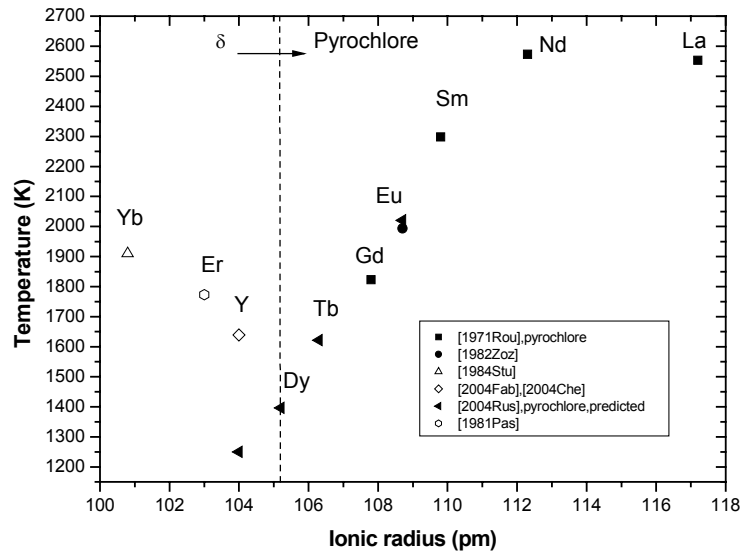


Fig. 11-1. The phase transformation temperatures of the ordered phases in the $ZrO_2 - REO_{1.5}$ systems.

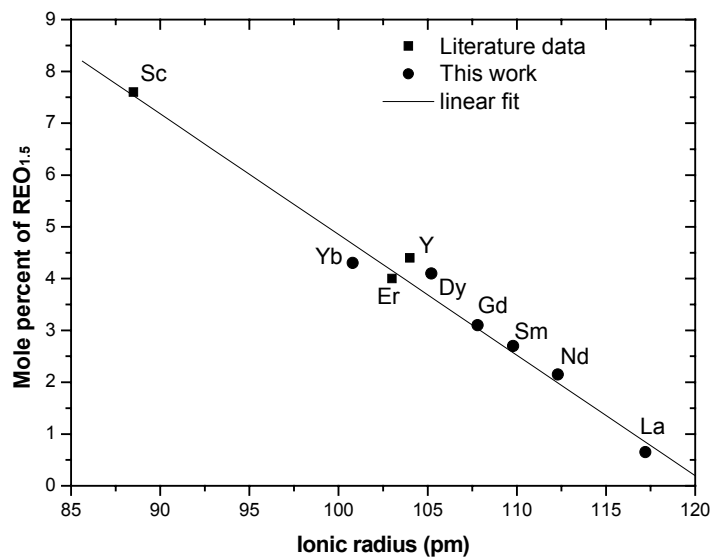


Figure 11-2. The average solubility of $REO_{1.5}$ in tetragonal ZrO_2 .

The linear functions of the lattice parameters of the fluorite phase constructed by Vegard's law for different systems are compiled in Fig. 11-4, in which the stable fluorite phase region at $1700^\circ C$ is lined out. With decreasing the lattice parameter of $REO_{1.5}$, some fluctuations are present on the width of the fluorite phase region due to the influence of the structural evolution of $REO_{1.5}$. The solubility of ZrO_2 in C-type $REO_{1.5}$ phase becomes larger when the radius of RE^{+3} decreases.

The phase equilibria are also related to the degree of lattice mismatch between different phases. According to the measured lattice parameters of the fluorite and pyrochlore phases in the $\text{ZrO}_2 - \text{NdO}_{1.5}$, $\text{ZrO}_2 - \text{SmO}_{1.5}$ and $\text{ZrO}_2 - \text{GdO}_{1.5}$ systems, the interface between the disordered and ordered phases should be more coherent and have less lattice mismatch with decreasing the radius of RE^{+3} . This trend can be also applied to the equilibria between fluorite and the $\text{REO}_{1.5}$ terminal solution phase. The two phases in equilibrium form a narrower two-phase region when they are more coherent at interface. This is consistent with the XRD observations on the overlapping of the strong peaks of the fluorite and C-type phase in the $\text{ZrO}_2\text{-DyO}_{1.5}$ and $\text{ZrO}_2\text{-YbO}_{1.5}$ systems. The large difference in SEM morphology between the two equilibrium phases (F + A equilibrium in the $\text{ZrO}_2 - \text{NdO}_{1.5}$ system and F + B equilibrium in the $\text{ZrO}_2 - \text{SmO}_{1.5}$ system) is also caused by the larger lattice mismatch for the case of larger RE^{+3} , while for the systems with F + C equilibrium and smaller RE^{+3} , the morphologies of fluorite and C-type phases do not show evident difference due to the more coherent interface.

At high temperatures, as it has been investigated by [1971Rou], the $\text{ZrO}_2 - \text{REO}_{1.5}$ system with smaller ionic radius of RE^{+3} has higher temperatures of liquidus. At the same time, the temperatures for the invariant reactions involving liquid and fluorite phases in $\text{REO}_{1.5}$ -rich side are also elevated.

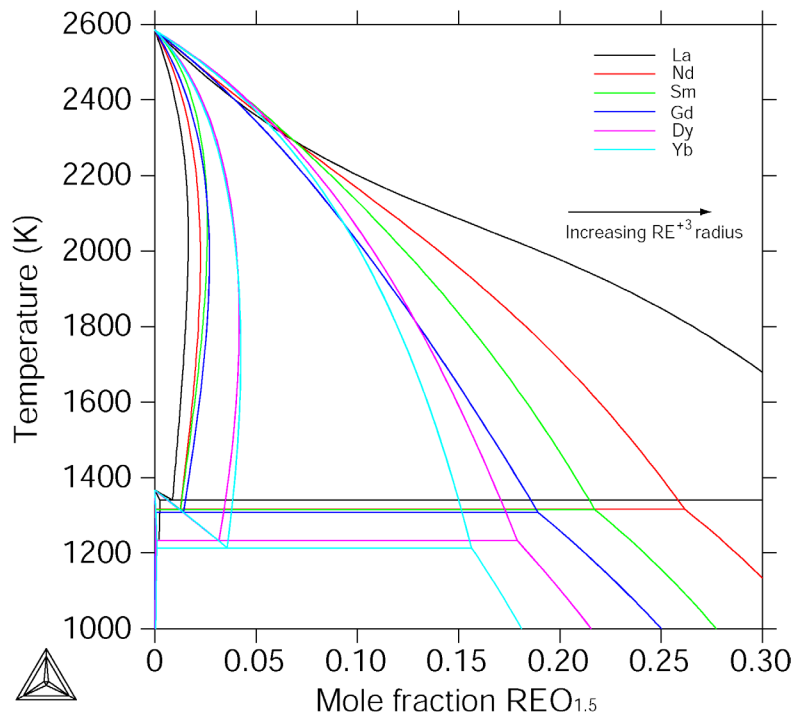


Figure 11-3. The calculated ZrO_2 -rich partial phase diagrams of different doping RE elements.

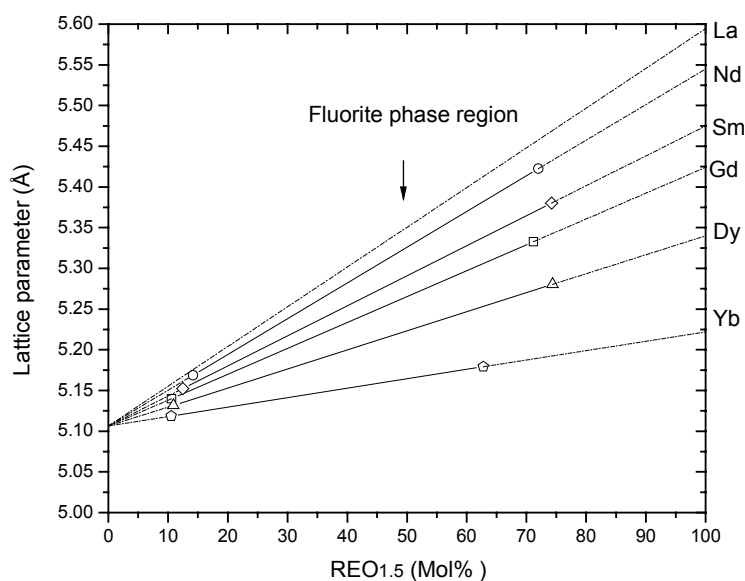


Figure 11-4. The lattice parameters of fluorite phases in all $ZrO_2 - REO_{1.5}$ systems constructed by Vegard's law (the solid lines give the stable fluorite phase region at $1700^\circ C$).

11.2. The evolutions of the thermodynamic properties in the $ZrO_2 - REO_{1.5}$ systems

The phase relations are essentially determined by the thermodynamic properties of phases. With the change of the ionic radius of RE^{+3} , it is found and confirmed in this work that some thermodynamic properties of different phases change towards a single trend.

Fig. 11-5 presents the enthalpy of formation of the fluorite and pyrochlore phases, which are the most important thermodynamic data for the $ZrO_2 - REO_{1.5}$ systems. The experimental data of [1971Kor] indicate that both fluorite and pyrochlore phases are more stable with decreasing the ionic radius of RE^{+3} . The experimental data reported by [2001Hel, 2003Lee, 2005Nav] are shown together with the fitted blue line, and it is interesting that all the data hold a single linear function, and the fluorite phase in the system with smaller RE^{+3} ionic radius is less stable. Present calculated results are given by the red symbols, in which the values for the pyrochlore phases are consistent with those of [2005Nav] within the experimental limits. However, present calculations on the enthalpies of formation of fluorite show complete different trends from those of [1971Kor, 2001Hel, 2003Lee]. With decreasing the RE^{+3} ionic radius, the enthalpy of formation of the fluorite phase becomes more negative. This is consistent with the phase relations that the tetragonal + fluorite two-phase region becomes gradually narrower with decreasing the radius of RE^{+3} . Moreover, it can be seen from Fig. 11-5 that the difference between the enthalpies of fluorite and pyrochlore becomes gradually larger with increasing the radius of RE^{+3} , and this tendency also agrees with the phase diagram that in case of a larger ionic radius of RE^{+3} there is a wider fluorite +

pyrochlore two-phase field, which is corresponding to larger difference between the Gibbs energies of fluorite and pyrochlore. Therefore, in view of those agreements with the evolution of phase relations, the present calculations on the enthalpies of formation of fluorite and pyrochlore are undoubtedly more reasonable than those experimental data.

From La to Yb, the stable structure of rare earth oxides at ambient temperature changes from A-type to C-type. With the change of the ionic radius of RE^{+3} , the enthalpies of transformation between those stable structures at ambient temperature to metastable fluorite structure are plotted in Fig. 11-6 together with the experimental and extrapolated data on the ZrO_2 - $YO_{1.5}$ system. Following the energetic trends established for the structural transformations among the A, B, C, H and X-type structures [2006Zin], present calculations show the increasing values on the enthalpy of the $A \Rightarrow F$ or $C \Rightarrow F$ transformation towards the larger ionic radius of RE^{+3} , and the linear functions can be constructed accordingly. So far, there is no reliable reference data on the enthalpy or entropy of those transformations for any system. Because such data cannot be obtained directly from experiments, some assumptions had to be made in the present work.

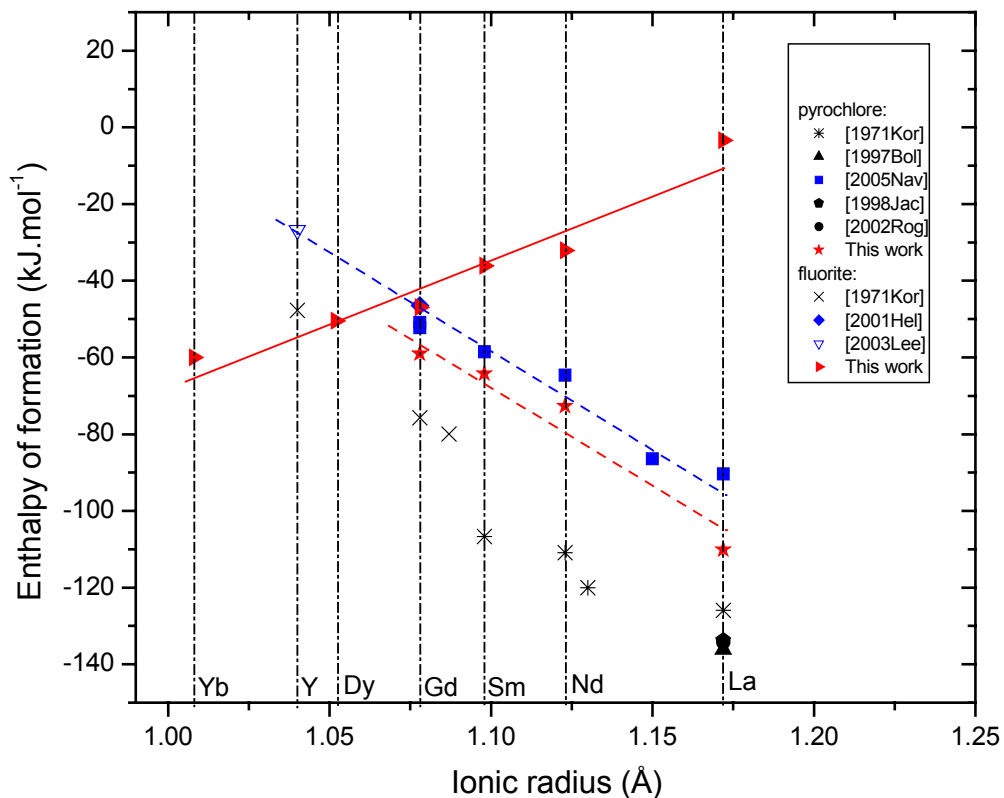


Figure 11-5. The experimental and calculated enthalpies of formation of pyrochlore and fluorite (per four moles of cations, reference state: the monoclinic ZrO_2 and the stable structure of $REO_{1.5}$ at room temperature, for the composition at 50 mol% $REO_{1.5}$).

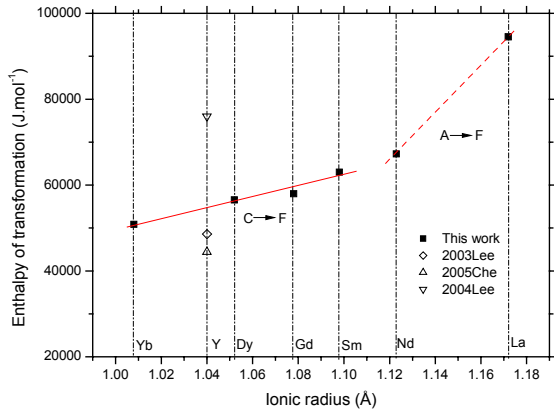


Figure 11-6. The calculated enthalpies of the $A \Rightarrow F$ (RE=La, Nd) and $C \Rightarrow F$ (RE=Sm, Gd, Dy, Y, Yb) transformations in RE_2O_3 compounds.

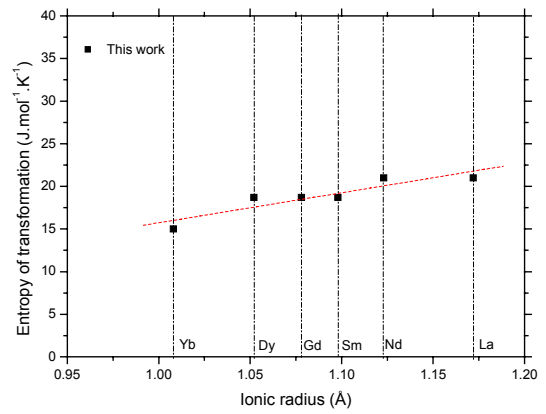


Figure 11-7. The calculated entropies of the $A \Rightarrow F$ (RE=La, Nd) and $C \Rightarrow F$ (RE=Sm, Gd, Dy, Yb) transformations in RE_2O_3 compounds.

For the corresponding entropies of transformation, it was assumed that those of $C \Rightarrow F$ for RE=Sm, Gd, Dy are identical, and so do those of $A \Rightarrow F$ for RE=La, Nd. However, for the transformation $C \Rightarrow F$, when RE=Yb, a lower entropy was selected during optimization. Fig. 11-7 shows an approximate increasing trend of the entropies against the ionic radius. Further experimental investigations are necessary to confirm the trends found in present calculations.

11.3. The mechanism of the pyrochlore ordering

The pyrochlore-type ordering occurs in the systems $ZrO_2 - REO_{1.5}$ when RE=La–Gd. As mentioned above, the changes of the thermodynamic properties of the fluorite and pyrochlore phases result in the different characters of phase diagrams. Taking the nature of the structural relation between pyrochlore and fluorite phases into account, the Gibbs energies of these two phases are also related, and can be separated into the disordered part and ordered part, in which the former can be stable before the ordering occurs. In this section, the mechanism for the pyrochlore ordering will be proposed from thermodynamic point of view to explain some experimental results obtained in this work for different systems.

Fig. 11-8 qualitatively shows the Gibbs energy curves at different states, in which the black and blue curves represent the completely disordered and ordered phases, respectively, while a given nonequilibrium state during the ordering is shown by the red dashed line. Since the ordering is a kinetically long process, it is reasonable to assume that there are many different intermediate configurational states which correspond to their own Gibbs energy curves. After a heat treatment for a certain time, the Gibbs energy curve of the ordered phase

may correspond to the red dashed line in Fig. 11-8. At the same time, the ordering kinetics may be different in different composition ranges. For example, the experimental results in the $\text{ZrO}_2 - \text{NdO}_{1.5}$ system already showed that the sample with 65 mol% $\text{NdO}_{1.5}$ is much easier to separate into well ordered pyrochlore phase, while for the samples in ZrO_2 -rich region they are much more difficult to reach a complete ordered state. The sluggish ordering kinetics in ZrO_2 -rich materials is mainly caused by the fact that more oxygen atoms are taking part in the process. However, those problems do not contradict the present assumption, because for a given composition, the Gibbs energy will actually undergo such a process from the curve F to the curve P in Fig. 11-8.

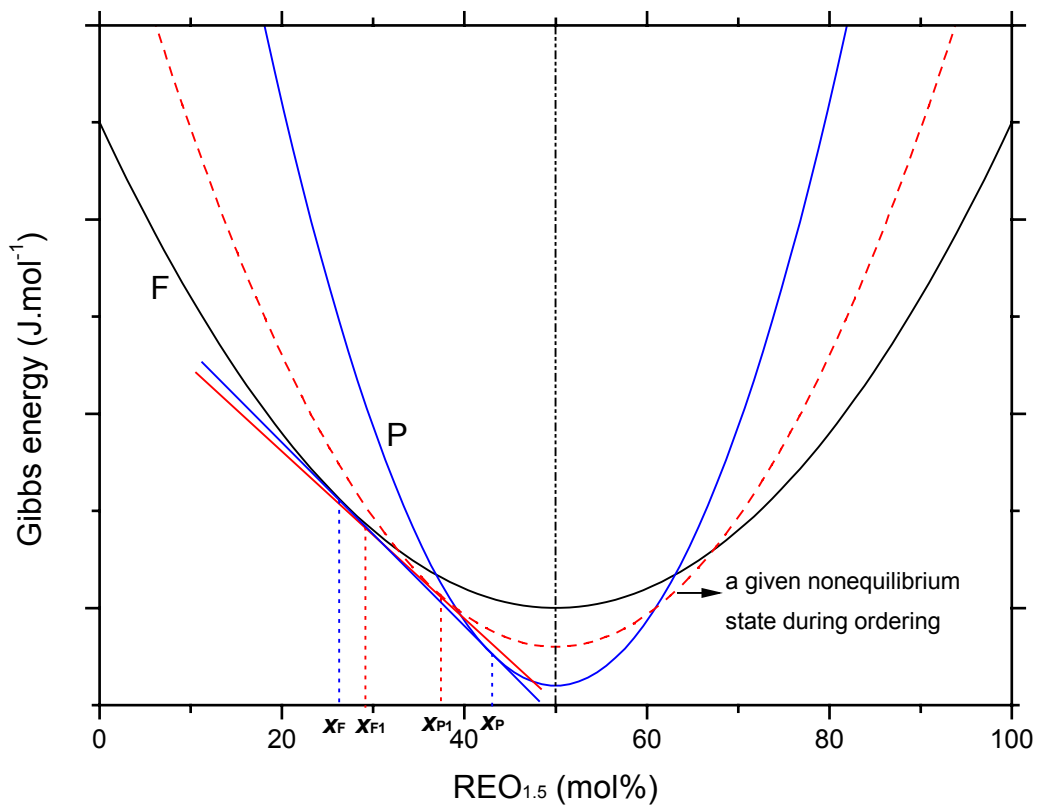


Figure 11-8. The Gibbs energy curves of fluorite and pyrochlore, together with that of a given non-equilibrium state during ordering.

Since the ordering in $\text{REO}_{1.5}$ -rich region can be approached more easily, it will be more interesting to discuss the ordering at the ZrO_2 excess side. Two common tangents are constructed based on the three Gibbs energy curves in Fig. 11-8. The blue one which connects the curve F and curve P determines the x_F and x_P , which represent the compositions of the fluorite and pyrochlore phases at equilibrium state, and the red one which connects the Gibbs energy curves of fluorite and the given state determines the x_{F1} and x_{P1} , which represent the

compositions of the fluorite and pyrochlore phases at a given nonequilibrium state. Suppose a sample, which will finally be fluorite + pyrochlore mixture after complete ordering, is now under the state given by the red dashed line. It can be seen that the two-phase region under this non-equilibrium state is smaller than that of the equilibrium case. This can elucidate the apparent large homogeneity range of the pyrochlore phase and the narrow two-phase region obtained from XRD measurements in the ZrO_2 -rich region of the $\text{ZrO}_2 - \text{NdO}_{1.5}$ system. For the systems such as $\text{ZrO}_2 - \text{SmO}_{1.5}$ and $\text{ZrO}_2 - \text{GdO}_{1.5}$, due to the smaller difference of the Gibbs energies of fluorite and completely ordered pyrochlore, the ordering will take longer time because of lower driving force and ordering kinetics. In fact, the heat treatment of the samples of the $\text{ZrO}_2 - \text{SmO}_{1.5}$ system at 1700°C does not present separate XRD peaks for fluorite and pyrochlore like in the $\text{ZrO}_2 - \text{NdO}_{1.5}$ system. At the same time, for the $\text{ZrO}_2 - \text{NdO}_{1.5}$ system, the XRD results of the samples heat treated at 1600°C do not show separate fluorite and pyrochlore peaks, although the samples heat treated at 1700°C do. It reveals that the phase partition only occurs when the ordering process approaches a certain configurational state. Based on the available experimental data in this work, it is not easy to judge the fluorite-to-pyrochlore ordering is of first- or second-order. The second-order transition may firstly occur in the ZrO_2 -rich region due to the limited driving force for the long distance diffusion, and then the transition becomes first-order type only when a certain configurational state has been reached to offer the necessary driving force for the long-distance diffusion. For the system such as $\text{ZrO}_2 - \text{GdO}_{1.5}$ which has very small difference between the Gibbs energies of fluorite and completely ordered pyrochlore, it will probably never turn into first-order transition. Furthermore, as it has been experimentally found and modeled in this work, even in the $\text{REO}_{1.5}$ -rich region for $\text{RE}=\text{Gd}$, the transition can also be possibly of second-order type when the Gibbs energies of fluorite and pyrochlore are very close. As a conclusion, from a thermodynamic point of view, it may be not possible to distinguish if the fluorite to pyrochlore transition is first- or second-order for some systems, and the classification of this transition probably depends on the kinetic process.

Zusammenfassung

ZrO₂-basierte Materialien sind wegen ihrer niedrigen Wärmeleitfähigkeit, ihrer hohen Hochtemperaturbeständigkeit und ausgezeichneten Grenzflächenkompatibilität als Wärmedämmschichten (WDS) für Hochtemperaturgasturbinen praktisch wichtig. Forschungen an Phasengleichgewichten, Phasenumwandlungen und der Thermodynamik von ZrO₂-basierten Systemen können die notwendigen grundlegenden Kenntnisse zur Verfügung stellen, um die nächste Generation von WDS Materialien zu entwickeln. In dieser Dissertation werden die Systeme ZrO₂ – HfO₂, Zr – O, Hf – O, ZrO₂ – LaO_{1.5}, ZrO₂ – NdO_{1.5}, ZrO₂ – SmO_{1.5}, ZrO₂ – GdO_{1.5}, ZrO₂ – DyO_{1.5}, ZrO₂ – YbO_{1.5} und ZrO₂ – GdO_{1.5} – YO_{1.5} experimentell und rechnerisch untersucht.

Probenpräparation und experimentelle Methoden

Die Proben werden durch chemische Fällung aus wässrigen Lösungen von Zr(CH₃COO)₄, HfO(NO₃)₂, und RE(NO₃)₃·xH₂O (RE=La, Nd, Sm, Gd, Dy, Yb) hergestellt. Unterschiedliche experimentelle Methoden wie Röntgendiffraktometrie (XRD), Rasterelektronenmikroskopie (SEM), Elektronenstrahlmikroanalyse (EPMA: electron probe microanalysis), Transmissionselektronenmikroskopie (TEM), Differentialthermoanalyse (DTA) und Hochtemperaturkalorimetrie werden benutzt, um die Phasenumwandlungen und Phasengleichgewichte zwischen 1400 und 1700°C sowie die Enthalpie und Wärmekapazität der Materialien zu untersuchen.

Experimentelle Resultate

Erstens wurden die thermodynamischen Gleichgewichtstemperaturen (T_θ , bei denen die freien Enthalpien der monoklinen und tetragonalen Phase identisch sind) für reines ZrO₂ (1367 ± 5 K) und HfO₂ (2052 ± 5 K) durch die DTA Untersuchung des Systems ZrO₂ – HfO₂ überprüft und extrapoliert. Die direkt durch die DTA-Messungen erhaltenen Temperaturen (A_s , A_f , M_s , M_f) bei der Martensitumwandlung der Materialien des Systems ZrO₂ – HfO₂ stimmen mit den berechneten Temperaturen T_θ sehr gut überein.

In dieser Dissertation werden das Tetragonal + Fluorit (oder das Tetragonal + Pyrochlor für RE=La) Zweiphasengebiet, das Phasengleichgewicht zwischen der ungeordneten Fluorit- und der geordneten Pyrochlorphase (oder δ Phase für RE=Yb) und das Phasengleichgewicht zwischen Fluorit und REO_{1.5} Phasen für ZrO₂ – REO_{1.5} (RE=La, Nd, Sm, Gd, Dy, Yb) Systeme gut etabliert und die Enthalpie von Materialien mit 30 mol%

$\text{REO}_{1.5}$ und 50 mol% $\text{REO}_{1.5}$ (57.14 mol% für $\text{RE}=\text{Yb}$) werden im Temperaturbereich von 200-1400°C bestimmt. Außerdem werden die isothermen Schnitte von $\text{ZrO}_2 - \text{GdO}_{1.5} - \text{YO}_{1.5}$ System bei der Temperatur 1200-1600°C durch XRD-Messungen experimentell untersucht.

Thermodynamisches Modellieren

Auf der Basis von erzielten DTA-Ergebnissen und Literaturdaten von Umwandlungstemperaturen von Monoklin \Leftrightarrow Tetragonal, Tetragonal \Leftrightarrow Kubisch and Kubisch \Leftrightarrow Flüssig, und der Thermodynamik von unterschiedlichen Strukturen werden die thermodynamischen Parameter von reinem ZrO_2 und HfO_2 eingeschätzt und das $\text{ZrO}_2 - \text{HfO}_2$ Phasendiagramm wird ohne Anpassungsparameter berechnet.

Auf der Basis von in dieser Arbeit und in der Literatur erhaltenen experimentellen Daten werden die Systeme $\text{Zr} - \text{O}$, $\text{Hf} - \text{O}$, $\text{ZrO}_2 - \text{REO}_{1.5}$ ($\text{RE}=\text{La}$, Nd , Sm , Gd , Dy , Yb) mit der CALPHAD (CALculation of PHase Diagram) Methode thermodynamisch optimiert. Die Lösungsphasen werden durch Untergitter-Modell beschrieben. Das Modell $(\text{Zr}^{+4}, \text{RE}^{+3})_2(\text{RE}^{+3}, \text{Zr}^{+4})_2(\text{O}^{-2}, \text{Va})_6(\text{O}^{-2})_1(\text{Va}, \text{O}^{-2})_1$ für Pyrochlorphase und das $(\text{Zr}^{+4})_1(\text{RE}^{+3}, \text{Zr}^{+4})_6(\text{O}^{-2}, \text{Va})_{12}(\text{Va}, \text{O}^{-2})_2$ für δ -Phase werden in der $\text{ZrO}_2 - \text{REO}_{1.5}$ Systemen erfolgreich verwendet. Darüberhinaus wird das Modell $(\text{Zr}^{+4}, \text{RE}^{+3})_2(\text{RE}^{+3}, \text{Zr}^{+4})_2(\text{O}^{-2}, \text{Va})_8$ auch für die mögliche Umwandlung zweiter Ordnung zwischen Fluorit- und Pyrochlorphase im $\text{ZrO}_2 - \text{GdO}_{1.5}$ System eingesetzt. Die meisten experimentellen Daten sind gut reproduzierbar und die selbstkonsistenten thermodynamischen Parameter sind für alle Systeme abgeleitet. Weil die experimentellen isothermen Schnitte des $\text{ZrO}_2 - \text{GdO}_{1.5} - \text{YO}_{1.5}$ Systems nur durch Extrapolation von binären Systemen gut reproduzierbar sind, wird keine weitere Optimierung durchgeführt.

Charakteristische Änderung der Systeme $\text{ZrO}_2 - \text{REO}_{1.5}$

Schließlich, basierend auf Untersuchungen und Berechnungen dieser Arbeit lassen sich charakteristische Änderungen in der $\text{ZrO}_2 - \text{REO}_{1.5}$ Systemen als Funktion des Ionenradius des dotierten Element RE^{+3} .

1). Die Löslichkeit von $\text{REO}_{1.5}$ in tetragonaler Phase steigt fast linear mit abnehmendem RE^{+3} Radius, gleichzeitig erweitert sich der Homogenitätsbereich der Fluoritphase in die Richtung ZrO_2 . Diese Änderungen haben einen schmalen Tetragonal + Fluorit zweiphasigen Bereich für das $\text{ZrO}_2 - \text{REO}_{1.5}$ System mit kleinem RE^{+3} zur Folge.

2). Es wurde bestätigt, dass die Pyrochlorstruktur nur dann stabil ist, wenn RE^{+3} Radius größer als der von Dy^{+3} ist. Der Homogenitätsbereich der Pyrochlorphase nimmt

allmählich von RE=La auf Gd zu, während die Umwandlungstemperatur von Fluorit \leftrightarrow Pyrochlor abnimmt. Im $\text{ZrO}_2 - \text{DyO}_{1.5}$ system findet man keine geordnete Verbindung, während die δ Phase im $\text{ZrO}_2 - \text{YbO}_{1.5}$ System geordnete Fluoritstruktur hat. Davon wird abgeleitet, dass die δ Phase nur dann stabil ist, wenn RE^{+3} Radius kleiner als der von Dy^{+3} ist, und die Umwandlungstemperatur von $\delta \leftrightarrow$ Fluorit mit sinkendem Ionradius RE^{+3} steigt.

3). Die Bildungsenthalpie der Fluoritphase hat negativere Werte bei kleineren RE^{+3} , während die geordnete Pyrochlorphase die umgekehrte Tendenz zeigt. Dies hat zur Folge, dass die Energiedifferenz zwischen Fluorit- und Pyrochlorphase bei kleinerem RE^{+3} kleiner wird, und deshalb das Fluorit + Pyrochlor Zweiphasengebiet schmaler wird.

4). Die komplette Ordnungseinstellung der Pyrochlor-phase mit ZrO_2 -Überschuß braucht sehr lange, besonders für Systeme mit kleinem RE^{+3} . Die Ordnung von Pyrochlor mit $\text{REO}_{1.5}$ -Überschuß geschieht viel schneller, weil wenige Sauerstoffatome an dem Prozess teilnehmen. Nach den XRD-Ergebnissen teilen sich die Proben im ZrO_2 -reichen Bereich nach 36 Stunden Wärmebehandlung bei 1700°C deutlich in eine 2-Phasen struktur auf, wohingegen die Probe nach Wärmebehandlung bei niedrigerer Temperatur dieses Verhalten nicht zeigt. Ähnliches Verhalten wird auch bei Proben mit ZrO_2 Überschuß im $\text{ZrO}_2 - \text{SmO}_{1.5}$ und $\text{ZrO}_2 - \text{GdO}_{1.5}$ System beobachtet. Diese Beobachtungen zeigen, dass die Fluorit \leftrightarrow Pyrochlor Phasenumwandlung in Materialien mit ZrO_2 Überschuß ein kinetisch langsamer Prozess ist. Er kann zuerst von zweiter Ordnung sein und dann von erster Ordnung, wenn eine bestimmte Konfiguration der geordneten Struktur erreicht wird und damit genügend Triebkraft für die langreichweitige Diffusion angeboten werden kann.

Appendix: The thermodynamic parameters obtained in this work

Ionic liquid: $(\text{Hf}^{+4}, \text{Zr}^{+4})_{\text{P}}(\text{O}^{-2}, \text{Va})_{\text{Q}}$
 $(\text{Dy}^{+3}, \text{Gd}^{+3}, \text{La}^{+3}, \text{Nd}^{+3}, \text{Sm}^{+3}, \text{Yb}^{+3}, \text{Zr}^{+4})_{\text{P}}(\text{O}^{-2}, \text{Va})_{\text{Q}}$

$$\begin{aligned}
 {}^0G_{\text{Hf}^{+4}, \text{O}^{-2}}^{\text{liq}} &= 2 \cdot \text{GHFO2L} & {}^0G_{\text{Hf}^{+4}, \text{Va}^{-4}}^{\text{liq}} &= \text{GHFLIQ} \\
 {}^0G_{\text{Zr}^{+4}, \text{O}^{-2}}^{\text{liq}} &= 2 \cdot \text{GZRO2L} & {}^0G_{\text{Zr}^{+4}, \text{Va}^{-4}}^{\text{liq}} &= \text{GZRLIQ} \\
 {}^0G_{\text{Dy}^{+3}, \text{O}^{-2}}^{\text{liq}} &= \text{GDY2O3L} & {}^0G_{\text{Gd}^{+3}, \text{O}^{-2}}^{\text{liq}} &= \text{GGD2O3L} \\
 {}^0G_{\text{La}^{+3}, \text{O}^{-2}}^{\text{liq}} &= \text{GLA2O3L} & {}^0G_{\text{Nd}^{+3}, \text{O}^{-2}}^{\text{liq}} &= \text{GND2O3L} \\
 {}^0G_{\text{Sm}^{+3}, \text{O}^{-2}}^{\text{liq}} &= \text{GSM2O3L} & {}^0G_{\text{Yb}^{+3}, \text{O}^{-2}}^{\text{liq}} &= \text{GYB2O3L} \\
 {}^0L_{\text{Hf}^{+4}, \text{O}^{-2}, \text{Va}^{-4}}^{\text{liq}} &= 368630.5 - 115.0386\text{T} & {}^1L_{\text{Hf}^{+4}, \text{O}^{-2}, \text{Va}^{-4}}^{\text{liq}} &= 55969 \\
 {}^0L_{\text{Zr}^{+4}, \text{O}^{-2}, \text{Va}^{-4}}^{\text{liq}} &= 75166 - 55.2382\text{T} & {}^1L_{\text{Zr}^{+4}, \text{O}^{-2}, \text{Va}^{-4}}^{\text{liq}} &= 39057.5 \\
 {}^0L_{\text{Dy}^{+3}, \text{Zr}^{+4}, \text{O}^{-2}}^{\text{liq}} &= -160886 & {}^1L_{\text{Dy}^{+3}, \text{Zr}^{+4}, \text{O}^{-2}}^{\text{liq}} &= -40724.6 \\
 {}^0L_{\text{Gd}^{+3}, \text{Zr}^{+4}, \text{O}^{-2}}^{\text{liq}} &= -76968 & {}^1L_{\text{Gd}^{+3}, \text{Zr}^{+4}, \text{O}^{-2}}^{\text{liq}} &= -248789.5 + 80\text{T} \\
 {}^0L_{\text{La}^{+3}, \text{Zr}^{+4}, \text{O}^{-2}}^{\text{liq}} &= -171356 & {}^1L_{\text{La}^{+3}, \text{Zr}^{+4}, \text{O}^{-2}}^{\text{liq}} &= -34723 \\
 {}^0L_{\text{Nd}^{+3}, \text{Zr}^{+4}, \text{O}^{-2}}^{\text{liq}} &= -173257 & {}^1L_{\text{Nd}^{+3}, \text{Zr}^{+4}, \text{O}^{-2}}^{\text{liq}} &= -33251 \\
 {}^0L_{\text{Sm}^{+3}, \text{Zr}^{+4}, \text{O}^{-2}}^{\text{liq}} &= -122143 & {}^1L_{\text{Sm}^{+3}, \text{Zr}^{+4}, \text{O}^{-2}}^{\text{liq}} &= -51808 \\
 {}^0L_{\text{Yb}^{+3}, \text{Zr}^{+4}, \text{O}^{-2}}^{\text{liq}} &= -85702 & {}^1L_{\text{Yb}^{+3}, \text{Zr}^{+4}, \text{O}^{-2}}^{\text{liq}} &= -28822
 \end{aligned}$$

Bcc: $(\text{Hf}, \text{Zr})_1(\text{O}, \text{Va})_1$

$$\begin{aligned}
 {}^0G_{\text{Hf}: \text{O}}^{\text{bcc}} &= \text{GHSEROO} + \text{GHSERHF} - 5000 \\
 {}^0G_{\text{Zr}: \text{O}}^{\text{bcc}} &= \text{GHSEROO} + \text{GHSERZR} - 513959.73 + 100\text{T} \\
 {}^0G_{\text{Hf}: \text{Va}}^{\text{bcc}} &= \text{GHFBCC} & {}^0G_{\text{Zr}: \text{Va}}^{\text{bcc}} &= \text{GZRBCC} \\
 {}^0L_{\text{Hf}: \text{O}, \text{Va}}^{\text{bcc}} &= -336506.062 & {}^0L_{\text{Zr}: \text{O}, \text{Va}}^{\text{bcc}} &= -79547.224
 \end{aligned}$$

Hcp: $(\text{Hf}, \text{Zr})(\text{O}, \text{Va})_{0.5}$

$$\begin{aligned}
 {}^0G_{\text{Hf}: \text{O}}^{\text{hcp}} &= 0.5 \cdot \text{GHSEROO} + \text{GHSERHF} - 273475.246 + 43.223\text{T} \\
 {}^0G_{\text{Zr}: \text{O}}^{\text{hcp}} &= 0.5 \cdot \text{GHSEROO} + \text{GHSERZR} - 286427.91 + 43.223\text{T} \\
 {}^0G_{\text{Hf}: \text{Va}}^{\text{hcp}} &= \text{GHSERHF} & {}^0G_{\text{Zr}: \text{Va}}^{\text{hcp}} &= \text{GHSERZR} \\
 {}^0L_{\text{Hf}: \text{O}, \text{Va}}^{\text{hcp}} &= -30160.306 + 3.303\text{T} & {}^1L_{\text{Hf}: \text{O}, \text{Va}}^{\text{hcp}} &= -2820.874 \\
 {}^0L_{\text{Zr}: \text{O}, \text{Va}}^{\text{hcp}} &= -37876.66 + 17.2915\text{T} & {}^1L_{\text{Zr}: \text{O}, \text{Va}}^{\text{hcp}} &= -4471.39
 \end{aligned}$$

Monoclinic: $(\text{Hf}^{+4}, \text{Zr}^{+4})_2(\text{O}^{-2}, \text{Va})_4$
 $(\text{Dy}^{+3}, \text{Gd}^{+3}, \text{La}^{+3}, \text{Nd}^{+3}, \text{Sm}^{+3}, \text{Yb}^{+3}, \text{Zr}^{+4})_2(\text{O}^{-2}, \text{Va})_4$

$$\begin{aligned}
 {}^0G_{\text{Hf}^{+4}, \text{O}^{-2}}^{\text{M}} &= 2 \cdot \text{GHFO2M} & {}^0G_{\text{Zr}^{+4}, \text{O}^{-2}}^{\text{M}} &= 2 \cdot \text{GZRO2M} \\
 {}^0G_{\text{Zr}^{+4}, \text{Va}}^{\text{M}} &= 2 \cdot \text{GZRO2M} - 4 \cdot \text{GHSEROO} \\
 {}^0G_{\text{Dy}^{+3}, \text{O}^{-2}}^{\text{M}} &= \text{GDY2O3C} + \text{GHSEROO} + 18.702165\text{T} + 65000 \\
 {}^0G_{\text{Dy}^{+3}, \text{Va}}^{\text{M}} &= \text{GDY2O3C} - 3 \cdot \text{GHSEROO} + 18.702165\text{T} + 65000 \\
 {}^0G_{\text{Gd}^{+3}, \text{O}^{-2}}^{\text{M}} &= \text{GGD2O3B} + \text{GHSEROO} + 18.702165\text{T} + 150000
 \end{aligned}$$

$${}^0G_{Gd^{+3},Va}^m = GGD2O3B - 3 \cdot GHSEROO + 18.702165T + 150000$$

$${}^0G_{La^{+3},O^{-2}}^m = GLA2O3A + GHSEROO + 18.702165T + 130000$$

$${}^0G_{La^{+3},Va}^m = GLA2O3A - 3 \cdot GHSEROO + 18.702165T + 130000$$

$${}^0G_{Nd^{+3},O^{-2}}^m = GND2O3A + GHSEROO + 18.702165T + 160000$$

$${}^0G_{Nd^{+3},Va}^m = GND2O3A - 3 \cdot GHSEROO + 18.702165T + 160000$$

$${}^0G_{Sm^{+3},O^{-2}}^m = GSM2O3B + GHSEROO + 18.702165T + 150000$$

$${}^0G_{Sm^{+3},Va}^m = GSM2O3B - 3 \cdot GHSEROO + 18.702165T + 150000$$

$${}^0G_{Yb^{+3},O^{-2}}^m = GYB2O3C + GHSEROO + 18.702165T + 30000$$

$${}^0G_{Yb^{+3},Va}^m = GYB2O3C - 3 \cdot GHSEROO + 18.702165T + 30000$$

Tetragonal: $(Hf^{+4}, Zr^{+4})_2(O^{-2}, Va)_4$
 $(Dy^{+3}, Gd^{+3}, La^{+3}, Nd^{+3}, Sm^{+3}, Yb^{+3}, Zr^{+4})_2(O^{-2}, Va)_4$

$${}^0G_{Hf^{+4},O^{-2}}^T = 2 \cdot GHFO2T \qquad {}^0G_{Zr^{+4},O^{-2}}^T = 2 \cdot GZRO2T$$

$${}^0G_{Zr^{+4},Va}^T = 2 \cdot GZRO2T - 4 \cdot GHSEROO$$

$${}^0G_{RE^{+3},O^{-2}}^T = GRE2O3T + GHSEROO + 18.702165T$$

$${}^0G_{RE^{+3},Va}^T = GRE2O3T - 3 \cdot GHSEROO + 18.702165T$$

$${}^0L_{Dy^{+3},Zr^{+4},O^{-2}} = {}^0L_{Dy^{+3},Zr^{+4},Va} = -103339.5$$

$${}^0L_{Gd^{+3},Zr^{+4},O^{-2}} = {}^0L_{Gd^{+3},Zr^{+4},Va} = -29296$$

$${}^0L_{La^{+3},Zr^{+4},O^{-2}} = {}^0L_{La^{+3},Zr^{+4},Va} = +20000$$

$${}^0L_{Nd^{+3},Zr^{+4},O^{-2}} = {}^0L_{Nd^{+3},Zr^{+4},Va} = -16304$$

$${}^0L_{Sm^{+3},Zr^{+4},O^{-2}} = {}^0L_{Sm^{+3},Zr^{+4},Va} = -25000$$

$${}^0L_{Yb^{+3},Zr^{+4},O^{-2}} = {}^0L_{Yb^{+3},Zr^{+4},Va} = -171196 + 40T$$

Fluorite: $(Hf^{+2}, Hf^{+4}, Zr^{+2}, Zr^{+4})_2(O^{-2}, Va)_4$
 $(Dy^{+3}, Gd^{+3}, La^{+3}, Nd^{+3}, Sm^{+3}, Yb^{+3}, Zr^{+4})_2(O^{-2}, Va)_4$

$${}^0G_{Hf^{+4},O^{-2}}^f = 2 \cdot GHFO2F \qquad {}^0G_{Zr^{+4},O^{-2}}^f = 2 \cdot GZRO2F$$

$${}^0G_{Hf^{+4},Va}^f = 2 \cdot GHFO2F - 4 \cdot GHSEROO \qquad {}^0G_{Zr^{+4},Va}^f = 2 \cdot GZRO2F - 4 \cdot GHSEROO$$

$${}^0G_{Hf^{+2},O^{-2}}^f = 2 \cdot GHSERHf + 4 \cdot GHSEROO - 875527.46 + 106.942T$$

$${}^0G_{Zr^{+2},O^{-2}}^f = 2 \cdot GHSEZR + 4 \cdot GHSEROO - 817859.56 + 106.942T$$

$${}^0G_{Hf^{+2},Va}^f = 2 \cdot GHSERHf - 875527.46 + 106.942T$$

$${}^0G_{Zr^{+2},Va}^f = 2 \cdot GHSEZR - 817859.56 + 106.942T$$

$${}^0L_{Hf^{+2},Hf^{+4},O^{-2}}^f = -11487.45 + 25T \qquad {}^1L_{Hf^{+2},Hf^{+4},O^{-2}}^f = -80000 + 20T$$

$${}^0L_{Hf^{+2},Hf^{+4},Va}^f = -11487.45 + 25T \qquad {}^1L_{Hf^{+2},Hf^{+4},Va}^f = -80000 + 20T$$

$${}^0L_{Zr^{+2},Zr^{+4},O^{-2}}^f = -211148.18 + 76.2T \qquad {}^1L_{Zr^{+2},Zr^{+4},O^{-2}}^f = -99968.54 + 23.58T$$

$${}^0L_{Zr^{+2},Zr^{+4},Va}^f = -211148.18 + 76.2T \qquad {}^1L_{Zr^{+2},Zr^{+4},Va}^f = -99968.54 + 23.58T$$

$${}^0G_{RE^{+3},O^{-2}}^f = GRE2O3F + GHSEROO + 18.702165T$$

$${}^0G_{RE^{+3},Va}^f = GRE2O3F - 3 \cdot GHSEROO + 18.702165T$$

$$\begin{aligned}
 {}^0L_{La^{+3},Zr^{+4};O^{-2}} &= {}^0L_{La^{+3},Zr^{+4};Va} = -259855 + 39.811T \\
 {}^1L_{La^{+3},Zr^{+4};O^{-2}} &= {}^1L_{La^{+3},Zr^{+4};Va} = -143201 \\
 {}^0L_{Nd^{+3},Zr^{+4};O^{-2}} &= {}^0L_{Nd^{+3},Zr^{+4};Va} = -269134.9 + 299.193T - 32T\ln T \\
 {}^1L_{Nd^{+3},Zr^{+4};O^{-2}} &= {}^1L_{Nd^{+3},Zr^{+4};Va} = -54416 \\
 {}^2L_{Nd^{+3},Zr^{+4};O^{-2}} &= {}^2L_{Nd^{+3},Zr^{+4};Va} = +35213 \\
 {}^0L_{Sm^{+3},Zr^{+4};O^{-2}} &= {}^0L_{Sm^{+3},Zr^{+4};Va} = -268887 + 246.6T - 25T\ln T \\
 {}^1L_{Sm^{+3},Zr^{+4};O^{-2}} &= {}^1L_{Sm^{+3},Zr^{+4};Va} = -23987.7 - 25.33T \\
 {}^0L_{Gd^{+3},Zr^{+4};O^{-2}} &= {}^0L_{Gd^{+3},Zr^{+4};Va} = -280478.5 + 271.7T - 25T\ln T \\
 {}^1L_{Gd^{+3},Zr^{+4};O^{-2}} &= {}^1L_{Gd^{+3},Zr^{+4};Va} = -21424 \\
 {}^0L_{Dy^{+3},Zr^{+4};O^{-2}} &= {}^0L_{Dy^{+3},Zr^{+4};Va} = -280272.6 + 200.08T - 20T\ln T \\
 {}^1L_{Dy^{+3},Zr^{+4};O^{-2}} &= {}^1L_{Dy^{+3},Zr^{+4};Va} = 20890 - 25T \\
 {}^0L_{Yb^{+3},Zr^{+4};O^{-2}} &= {}^0L_{Yb^{+3},Zr^{+4};Va} = -301096 + 267574T - 25T\ln T \\
 {}^1L_{Yb^{+3},Zr^{+4};O^{-2}} &= {}^1L_{Yb^{+3},Zr^{+4};Va} = 103435 - 50T
 \end{aligned}$$

A-RE₂O₃: (Dy⁺³, Gd⁺³, La⁺³, Nd⁺³, Sm⁺³, Yb⁺³, Zr⁺⁴)₂(O⁻²)₃(O⁻², Va)₁

$$\begin{aligned}
 {}^0G_{RE^{+3};O^{-2};Va}^A &= GRE2O3A & {}^0G_{RE^{+3};O^{-2};O^{-2}}^A &= GRE2O3A + GHSEROO \\
 {}^0G_{Zr^{+4};O^{-2};Va}^A &= 2 \cdot GZRO2F - GHSEROO + 50000 & {}^0G_{Zr^{+4};O^{-2};O^{-2}}^A &= 2 \cdot GZRO2F + 50000 \\
 {}^0L_{La^{+3},Zr^{+4};O^{-2};O^{-2}} &= {}^0L_{La^{+3},Zr^{+4};O^{-2};Va} = +20000 \\
 {}^0L_{Nd^{+3},Zr^{+4};O^{-2};O^{-2}} &= {}^0L_{Nd^{+3},Zr^{+4};O^{-2};Va} = +10000 \\
 {}^0L_{Sm^{+3},Zr^{+4};O^{-2};O^{-2}} &= {}^0L_{Sm^{+3},Zr^{+4};O^{-2};Va} = +15000
 \end{aligned}$$

B-RE₂O₃: (Dy⁺³, Gd⁺³, La⁺³, Nd⁺³, Sm⁺³, Yb⁺³, Zr⁺⁴)₂(O⁻²)₃(O⁻², Va)₁

$$\begin{aligned}
 {}^0G_{RE^{+3};O^{-2};Va}^B &= GRE2O3B & {}^0G_{RE^{+3};O^{-2};O^{-2}}^B &= GRE2O3B + GHSEROO \\
 {}^0G_{Zr^{+4};O^{-2};Va}^B &= 2 \cdot GZRO2M - GHSEROO + 20000 & {}^0G_{Zr^{+4};O^{-2};O^{-2}}^B &= 2 \cdot GZRO2M + 20000 \\
 {}^0L_{Sm^{+3},Zr^{+4};O^{-2};O^{-2}} &= {}^0L_{Sm^{+3},Zr^{+4};O^{-2};Va} = +45000 \\
 {}^0L_{Gd^{+3},Zr^{+4};O^{-2};O^{-2}} &= {}^0L_{Gd^{+3},Zr^{+4};O^{-2};Va} = +51000 \\
 {}^0L_{Dy^{+3},Zr^{+4};O^{-2};O^{-2}} &= {}^0L_{Dy^{+3},Zr^{+4};O^{-2};Va} = +5000
 \end{aligned}$$

C-RE₂O₃: (Dy⁺³, Gd⁺³, La⁺³, Nd⁺³, Sm⁺³, Yb⁺³, Zr⁺⁴)₂(O⁻²)₃(O⁻², Va)₁

$$\begin{aligned}
 {}^0G_{RE^{+3};O^{-2};Va}^C &= GRE2O3C & {}^0G_{RE^{+3};O^{-2};O^{-2}}^C &= GRE2O3C + GHSEROO \\
 {}^0G_{Zr^{+4};O^{-2};Va}^C &= 2 \cdot GZRO2F - GHSEROO + 5000 & {}^0G_{Zr^{+4};O^{-2};O^{-2}}^C &= 2 \cdot GZRO2F + 5000 \\
 {}^0L_{Gd^{+3},Zr^{+4};O^{-2};O^{-2}} &= {}^0L_{Gd^{+3},Zr^{+4};O^{-2};Va} = -78798 + 21.2367T \\
 {}^1L_{Gd^{+3},Zr^{+4};O^{-2};O^{-2}} &= {}^1L_{Gd^{+3},Zr^{+4};O^{-2};Va} = +30000 \\
 {}^2L_{Gd^{+3},Zr^{+4};O^{-2};O^{-2}} &= {}^2L_{Gd^{+3},Zr^{+4};O^{-2};Va} = +30000 \\
 {}^0L_{Dy^{+3},Zr^{+4};O^{-2};O^{-2}} &= {}^0L_{Dy^{+3},Zr^{+4};O^{-2};Va} = -109928 \\
 {}^1L_{Dy^{+3},Zr^{+4};O^{-2};O^{-2}} &= {}^1L_{Dy^{+3},Zr^{+4};O^{-2};Va} = +30000
 \end{aligned}$$

$${}^2L_{Dy^{+3},Zr^{+4};O^{-2};O^{-2}} = {}^2L_{Dy^{+3},Zr^{+4};O^{-2};Va} = + 12910$$

$${}^0L_{Yb^{+3},Zr^{+4};O^{-2};O^{-2}} = {}^0L_{Yb^{+3},Zr^{+4};O^{-2};Va} = - 124356 + 20.914T$$

$${}^1L_{Yb^{+3},Zr^{+4};O^{-2};O^{-2}} = {}^1L_{Yb^{+3},Zr^{+4};O^{-2};Va} = 32000$$

H-RE₂O₃: (Dy⁺³, Gd⁺³, La⁺³, Nd⁺³, Sm⁺³, Yb⁺³, Zr⁺⁴)₂(O⁻²)₃(O⁻², Va)₁

$${}^0G_{RE^{+3};O^{-2};Va}^H = \text{GRE2O3H}$$

$${}^0G_{RE^{+3};O^{-2};O^{-2}}^H = \text{GRE2O3H} + \text{GHSEROO}$$

$${}^0G_{Zr^{+4};O^{-2};Va}^H = 2 \cdot \text{GZRO2F} - \text{GHSEROO} + 10000$$

$${}^0G_{Zr^{+4};O^{-2};O^{-2}}^H = 2 \cdot \text{GZRO2F} + 10000$$

$${}^0L_{La^{+3},Zr^{+4};O^{-2};O^{-2}} = {}^0L_{La^{+3},Zr^{+4};O^{-2};Va} = - 31179$$

$${}^0L_{Nd^{+3},Zr^{+4};O^{-2};O^{-2}} = {}^0L_{Nd^{+3},Zr^{+4};O^{-2};Va} = - 27000$$

$${}^0L_{Sm^{+3},Zr^{+4};O^{-2};O^{-2}} = {}^0L_{Sm^{+3},Zr^{+4};O^{-2};Va} = - 4188$$

$${}^0L_{Gd^{+3},Zr^{+4};O^{-2};O^{-2}} = {}^0L_{Gd^{+3},Zr^{+4};O^{-2};Va} = 17367$$

$${}^0L_{Dy^{+3},Zr^{+4};O^{-2};O^{-2}} = {}^0L_{Dy^{+3},Zr^{+4};O^{-2};Va} = - 30828$$

$${}^0L_{Yb^{+3},Zr^{+4};O^{-2};O^{-2}} = {}^0L_{Yb^{+3},Zr^{+4};O^{-2};Va} = - 8253$$

X-RE₂O₃: (Dy⁺³, Gd⁺³, La⁺³, Nd⁺³, Sm⁺³, Y⁺³, Yb⁺³, Zr⁺⁴)₂(O⁻²)₃(O⁻², Va)₁

$${}^0G_{RE^{+3};O^{-2};Va}^X = \text{GRE2O3X}$$

$${}^0G_{RE^{+3};O^{-2};O^{-2}}^X = \text{GRE2O3X} + \text{GHSEROO}$$

$${}^0G_{Zr^{+4};O^{-2};Va}^X = 2 \cdot \text{GZRO2F} - \text{GHSEROO} + 10000$$

$${}^0G_{Zr^{+4};O^{-2};O^{-2}}^X = 2 \cdot \text{GZRO2F} + 10000$$

$${}^0L_{La^{+3},Zr^{+4};O^{-2};O^{-2}} = {}^0L_{La^{+3},Zr^{+4};O^{-2};Va} = - 38254$$

$${}^0L_{Nd^{+3},Zr^{+4};O^{-2};O^{-2}} = {}^0L_{Nd^{+3},Zr^{+4};O^{-2};Va} = - 35763$$

$${}^0L_{Sm^{+3},Zr^{+4};O^{-2};O^{-2}} = {}^0L_{Sm^{+3},Zr^{+4};O^{-2};Va} = - 14857$$

Pyrochlore: (Zr⁺⁴, RE⁺³)₂(RE⁺³, Zr⁺⁴)₂(O⁻², Va)₆(O⁻²)₁(Va, O⁻²)₁. The suffixes RE define the corresponding functions (see below).

$${}^0G_{RE^{+3};RE^{+3};O^{-2};O^{-2};O^{-2}}^P = 2 \cdot \text{GPYRORE} + 2 \cdot \text{GHSEROO} - \text{GPYROZR} + \text{GANCARE} + \text{GREC1} + \text{GREC2} + \text{GREC3}$$

$${}^0G_{Zr^{+4};RE^{+3};O^{-2};O^{-2};O^{-2}}^P = \text{GPYRORE} + \text{GHSEROO} + \text{GREC2}$$

$${}^0G_{RE^{+3};Zr^{+4};O^{-2};O^{-2};O^{-2}}^P = \text{GPYRORE} + \text{GHSEROO} + \text{GANCARE} - \text{GREC1} + \text{GREC2} + \text{GREC3} + \text{GREC4}$$

$${}^0G_{Zr^{+4};Zr^{+4};O^{-2};O^{-2};O^{-2}}^P = \text{GPYROZR}$$

$${}^0G_{RE^{+3};RE^{+3};Va;O^{-2};O^{-2}}^P = 5 \cdot \text{GPYROZR} - 10 \cdot \text{GPYRORE} + 6 \cdot \text{GPYRORE2O3} - 4 \cdot \text{GHSEROO} - 5 \cdot \text{GANCARE} + 134.8548T - 5 \cdot \text{GREC1} + \text{GREC2} + \text{GREC3} + \text{GREC5} + \text{GREC8} + \text{GREC9}$$

$${}^0G_{Zr^{+4};RE^{+3};Va;O^{-2};O^{-2}}^P = 6 \cdot \text{GPYROZR} - 11 \cdot \text{GPYRORE} + 6 \cdot \text{GPYRORE2O3} - 5 \cdot \text{GHSEROO} - 6 \cdot \text{GANCARE} + 134.8548T - 6 \cdot \text{GREC1} + \text{GREC2} + \text{GREC5} + \text{GREC8}$$

$${}^0G_{RE^{+3};Zr^{+4};Va;O^{-2};O^{-2}}^P = 6 \cdot \text{GPYROZR} - 11 \cdot \text{GPYRORE} + 6 \cdot \text{GPYRORE2O3} - 5 \cdot \text{GHSEROO} - 5 \cdot \text{GANCARE} + 134.8548T - 6 \cdot \text{GREC1} + \text{GREC5} + \text{GREC8} + \text{GREC10}$$

$${}^0G_{Zr^{+4};Zr^{+4};Va;O^{-2};O^{-2}}^P = 7 \cdot \text{GPYROZR} - 12 \cdot \text{GPYRORE} + 6 \cdot \text{GPYRORE2O3} - 6 \cdot \text{GHSEROO} - 6 \cdot \text{GANCARE} + 134.8548T - 6 \cdot \text{GREC1} + \text{GREC5} + \text{GREC8} + \text{GREC10}$$

$${}^0G_{RE^{+3};RE^{+3};O^{-2};O^{-2};Va}^P = 2 \cdot \text{GPYRORE} - \text{GPYROZR} + \text{GHSEROO} + \text{GANCARE} + \text{GREC1}$$

$$\begin{aligned}
 {}^0G_{Zr^{+4};RE^{+3};O^{-2};O^{-2};Va}^P &= \text{GPYRORE} \\
 {}^0G_{RE^{+3};Zr^{+4};O^{-2};O^{-2};Va}^P &= \text{GPYRORE} + \text{GANCARE} \\
 {}^0G_{Zr^{+4};Zr^{+4};O^{-2};O^{-2};Va}^P &= \text{GPYROZR} - \text{GHSEROO} \\
 {}^0G_{RE^{+3};RE^{+3};Va;O^{-2};Va}^P &= 6 \cdot \text{GPYRORE2O3} - 10 \cdot \text{GPYRORE} + 5 \cdot \text{GPYROZR} - 5 \cdot \text{GHSEROO} \\
 &\quad - 5 \cdot \text{GANCARE} + 134.8548\text{T} - 5 \cdot \text{GREC1} \\
 {}^0G_{Zr^{+4};RE^{+3};Va;O^{-2};Va}^P &= 6 \cdot \text{GPYRORE2O3} - 11 \cdot \text{GPYRORE} + 6 \cdot \text{GPYROZR} - 6 \cdot \text{GHSEROO} \\
 &\quad - 6 \cdot \text{GANCARE} + 134.8548\text{T} - 6 \cdot \text{GREC1} + \text{GREC5} + \text{GREC6} \\
 {}^0G_{RE^{+3};Zr^{+4};Va;O^{-2};Va}^P &= 6 \cdot \text{GPYRORE2O3} - 11 \cdot \text{GPYRORE} + 6 \cdot \text{GPYROZR} - 6 \cdot \text{GHSEROO} \\
 &\quad - 6 \cdot \text{GANCARE} + 134.8548\text{T} - 6 \cdot \text{GREC1} + \text{GREC7} \\
 {}^0G_{Zr^{+4};Zr^{+4};Va;O^{-2};Va}^P &= 6 \cdot \text{GPYRORE2O3} - 12 \cdot \text{GPYRORE} + 7 \cdot \text{GPYROZR} - 7 \cdot \text{GHSEROO} \\
 &\quad - 6 \cdot \text{GANCARE} + 134.8548\text{T} - 6 \cdot \text{GREC1} + \text{GREC5} + \text{GREC6}
 \end{aligned}$$

Pyrochlore: $(Zr^{+4}, Gd^{+3})_2(Gd^{+3}, Zr^{+4})_2(O^{-2}, Va)_8$ (has the disordered contribution from fluorite).

$$\begin{aligned}
 {}^0G_{Zr^{+4};Gd^{+3};Va}^P &= {}^0G_{Gd^{+3};Zr^{+4};Va}^P = {}^0G_{Zr^{+4};Gd^{+3};O^{-2}}^P = {}^0G_{Gd^{+3};Zr^{+4};O^{-2}}^P = -13.962\text{T} \\
 {}^0L_{Zr^{+4},Gd^{+3};Gd^{+3};O^{-2}} &= {}^0L_{Zr^{+4},Gd^{+3};Zr^{+4};O^{-2}} = +4844.5 \\
 {}^0L_{Zr^{+4},Gd^{+3};Gd^{+3};Va} &= {}^0L_{Zr^{+4},Gd^{+3};Zr^{+4};Va} = +4844.5 \\
 {}^0L_{Zr^{+4},Gd^{+3};Zr^{+4};O^{-2}} &= {}^0L_{Gd^{+3};Gd^{+3};Zr^{+4};O^{-2}} = +4844.5 \\
 {}^0L_{Zr^{+4},Gd^{+3};Zr^{+4};Va} &= {}^0L_{Gd^{+3};Gd^{+3};Zr^{+4};Va} = +4844.5
 \end{aligned}$$

δ ($RE_4Zr_3O_{12}$): $(Zr^{+4})_1(RE^{+3}, Zr^{+4})_6(O^{-2}, Va)_{12}(Va, O^{-2})_2$

$$\begin{aligned}
 {}^0G_{Zr^{+4};Zr^{+4};O^{-2};O^{-2}}^\delta &(\text{GZZOO}) = 7 \cdot \text{GZRO2F} + 175000 \\
 {}^0G_{Zr^{+4};Zr^{+4};O^{-2};Va}^\delta &= 7 \cdot \text{GZRO2F} - 2 \cdot \text{GHSEROO} + 175000 \\
 {}^0G_{Zr^{+4};Yb^{+3};O^{-2};Va}^\delta &= 1.5 \cdot \text{GDELTA} - 0.5 \cdot \text{GZZOO} + \text{GHSEROO} + 47.6278\text{T} \\
 {}^0G_{Zr^{+4};Yb^{+3};Va;Va}^\delta &= 12 \cdot \text{GDELTA1} - 16.5 \cdot \text{GDELTA} + 5.5 \cdot \text{GZZOO} - 11 \cdot \text{GHSEROO} - \\
 &\quad 180.5012\text{T} \\
 {}^0G_{Zr^{+4};Yb^{+3};O^{-2};O^{-2}}^\delta &= 1.5 \cdot \text{GDELTA} - 0.5 \cdot \text{GZZOO} + 3 \cdot \text{GHSEROO} + 47.6278\text{T} - \text{REC1} \\
 {}^0G_{Zr^{+4};Zr^{+4};Va;Va}^\delta &= 7 \cdot \text{GZZOO} - 14 \cdot \text{GHSEROO} - 18 \cdot \text{GDELTA} + 12 \cdot \text{GDELTA1} - 228.129\text{T} - \\
 &\quad \text{REC2} \\
 {}^0G_{Zr^{+4};Zr^{+4};O^{-2};Va}^\delta &= 7 \cdot \text{GZZOO} - 12 \cdot \text{GHSEROO} - 18 \cdot \text{GDELTA} + 12 \cdot \text{GDELTA1} - 228.129\text{T} - \\
 &\quad \text{REC2} - \text{REC3} \\
 {}^0G_{Zr^{+4};Yb^{+3};Va;O^{-2}}^\delta &= 12 \cdot \text{GDELTA1} - 16.5 \cdot \text{GDELTA} + 5.5 \cdot \text{GZZOO} - 9 \cdot \text{GHSEROO} - \\
 &\quad 180.5012\text{T} - \text{REC1} - \text{REC2} - \text{REC3} - \text{REC4}
 \end{aligned}$$

Functions:

GZRLIQ, GHSEZR, GZRBCC, and GHSEROO are the lattice stabilities for liquid, hcp-Zr, bcc-Zr and 1/2 O₂ gas from SGTE pure elements database [1991Din].

GHFO2M: $-1144228.5 + 446.1053\text{T} - 74.15647\text{TlnT} - 0.00297849\text{T}^2 + 630000\text{T}^{-1}$;

GHFO2T: $8208 - 4\text{T} + \text{GHFO2M}$;

GHFO2F: $19420 - 8\text{T} + \text{GHFO2M}$;

GHFO2L: $109073 - 37.1743\text{T} + \text{GHFO2M}$;

GZRO2M: $-1126163.5 + 424.8908\text{T} - 69.38751\text{TlnT} - 0.0037588\text{T}^2 + 683000\text{T}^{-1}$;

GZRO2T: $5468 - 4\text{T} + \text{GZRO2M}$;

GZRO2F: $15804 - 8T + \text{GZRO2M}$;
GZRO2L: $102831 - 37.1743T + \text{GZRO2M}$;
GPYROZR: $4 \cdot \text{GZRO2F} + 10000 + 16T$

ZrO₂ – LaO_{1.5} system:

GLA2O3A: $-1833257 + 692.9664T - 120.629T \ln(T) - 0.006854T^2 + 808000T^{-1} - 1.0E+07T^{-2}$
GLA2O3C: $\text{GLA2O3A} + 8337 + 7.788T$
GLA2O3B: $\text{GLA2O3A} + 4139 + 2.215T$
GLA2O3H: $\text{GLA2O3A} + 32350 - 13.986T$
GLA2O3X: $\text{GLA2O3A} + 43192 - 18.555T$
GLA2O3L: $\text{GLA2O3A} + 141329 - 56.622T$
GLA2O3F: $\text{GLA2O3A} + 73630.5 - 11T$
GLA2O3T: $\text{GLA2O3F} + 10000$
GPYROLA: $-4194070 + 1531.07053T - 260.811T \ln(T) - 0.00891455T^2 + 1898400T^{-1}$
GPYROLA2O3: $2 \cdot \text{GLA2O3A} + 160000$
GREC2= 140000
GANCALA= 400000

ZrO₂ – NdO_{1.5} system:

GND2O3A: $-1847329 + 637.4243T - 116.358T \ln(T) - 0.014677T^2 + 711000T^{-1} - 10000000T^{-2}$
GND2O3C: $\text{GND2O3A} - 1311 + 6.550T$
GND2O3B: $\text{GND2O3A} - 399 + 1.684T$
GND2O3H: $\text{GND2O3A} + 33189 - 13.986T$
GND2O3X: $\text{GND2O3A} + 44489 - 18.555T$
GND2O3L: $\text{GND2O3A} + 143621 - 56.785T$
GND2O3F: $\text{GND2O3A} + 63285.47 - 19.33T$
GND2O3T: $\text{GND2O3F} + 10000$
GPYROND: $-4175068 + 1561.884T - 270.0852T \ln(T) + 1894137.6T^{-1} - 0.01561361T^2$
GPYROND2O3: $2 \cdot \text{GND2O3A} + 98491.2 - 10T$
GREC2= 160000
GANCAND= 300000

ZrO₂ – SmO_{1.5} system:

GSM2O3C: $-1875835 + 780.6356T - 135.618T \ln(T) - 0.006896T^2 + 1191000T^{-1}$
GSM2O3B: $-1871213 + 751.7711T - 132.137T \ln(T) - 0.008367T^2 + 1405000T^{-1} - 40000000T^{-2}$
GSM2O3A: $\text{GSM2O3B} + 3324 - 1.5295T$
GSM2O3H: $\text{GSM2O3B} + 36932 - 15.515T$
GSM2O3X: $\text{GSM2O3B} + 48460 - 20.084T$
GSM2O3L: $\text{GSM2O3B} + 154133 - 60.603T$
GSM2O3F: $\text{GSM2O3C} + 63018.408 - 18.7T$
GSM2O3T: $\text{GSM2O3F} + 10000$
GPYROSM: $-4186073 + 1590.2918T - 273.4902T \ln(T) + 1700000T^{-1} - 0.01142041T^2$
GPYROSM2O3: $2 \cdot \text{GSM2O3C} + 158810 - 39T$
GREC2= 20000
GREC6= - 250000
GANCASM= 250000

ZrO₂ – GdO_{1.5} system:

GGD2O3C: $-1868812 + 660.0623T - 119.1688T\ln(T) - 0.006438T^2 + 772000T^{-1}$
GGD2O3B: $-1858111 + 620.0992T - 114.534T\ln(T) - 0.007203T^2 + 540000T^{-1}$
GGD2O3A: $GGD2O3B + 6300 - 2.579T$
GGD2O3H: $GGD2O3B + 41000 - 16.565T$
GGD2O3X: $GGD2O3B + 53031 - 21.134T$
GGD2O3L: $GGD2O3B + 124733 - 47.759T$
GGD2O3F: $GGD2O3C + 57983.8 - 18.7T$
GGD2O3T: $GGD2O3F + 10000$
GPYROGD: $-4186033 + 1593.9449T - 271.805T\ln T + 2454000T^{-1} - 0.0098325T^2$
GPYROGD2O3: $2 \cdot GGD2O3C + 100000$
GREC6= -250000
GANCAGD= 200000

ZrO₂ – DyO_{1.5} system:

GDY2O3C: $-1902316 + 679.1313T - 122.593T\ln(T) - 0.006971T^2 + 59000T^{-1}$
 $+ 40000000T^{-2}$
GDY2O3B: $GDY2O3C + 9255 - 4.09T$
GDY2O3A: $GDY2O3C + 15637 - 5.546T$
GDY2O3H: $GDY2O3C + 43703 - 18.076T$
GDY2O3X: $GDY2O3B + 55825 - 22.645T$
GDY2O3L: $GDY2O3B + 134876 - 52.131T$
GDY2O3F: $GDY2O3C + 56553.6 - 18.7T$
GDY2O3T: $GDY2O3F + 10000$

ZrO₂ – YbO_{1.5} system:

GYB2O3C: $-1853511 + 702.7502T - 123.821T\ln(T) - 0.004567T^2 + 50000000T^{-2}$
GYB2O3B: $GYB2O3C + 15345 - 3.725T$
GYB2O3A: $GYB2O3C + 25165 - 5.293T$
GYB2O3H: $GYB2O3C + 25612 - 9.654T$
GYB2O3X: $GYB2O3B + 38391 - 14.223T$
GYB2O3L: $GYB2O3B + 107451 - 39.875T$
GYB2O3F: $GYB2O3C + 50837.64 - 15T$
GYB2O3T: $GYB2O3F + 10000$
GDELTA: $2 \cdot GYB2O3C + 3 \cdot GZRO2C - 183993 + 3.5T$
GDELTA1: $3 \cdot GYB2O3C + GZRO2C - 21000 - 14T$
GREC1= 400000

References:

- [1925Hen] F. Henning, "The melting point of hafnium-oxide", *Naturwiss.*, 13 (1925) 661.
- [1932Cla] P. Clausing, "The melting points of zirconium oxide and hafnium oxide", *Z. Anorg. Allgem. Chem.*, 204 (1932) 33-39.
- [1932Rot] W. A. Roth, and L. Becker, "Atomic number and heat of formation", *Z. Phys. Chem. A*, 159 [1] (1932) 1-26.
- [1934Jae] F. M. Jaeger, W. A. Veenstra, "The exact measurement of the specific heats of solid substances at high temperatures. VII. The calorimetric behaviour of zirconium", *Recl. Trav. Chim*, 53 (1934) 917-932.
- [1937War] H.V. Wartenberg, K. Eckhardt, "Schmelzdiagramme höchstfeuerfester Oxyde. VIII. (System mit CeO₃)", *Z. Anorg. Allgem. Chem.*, 232(1937) 179-187.
- [1944Kel] K. K. Kelley, "Specific heat of ZrO₂ at low temperatures", *Journal of Industrial and Engineering Chemistry (Washington, D. C.)*, 36 (1944) 377.
- [1948Red] O. Redlich, A. T. Kister, *Ind. Eng. Chem.*, 40 (1948) 345.
- [1950Art] J. S. Arthur, "The specific heats of MgO, TiO₂, and ZrO₂ at high temperatures", *J. Appl. Phys.*, 21 [8] (1950) 732-733.
- [1950Cou] J. P. Coughlin, E. G. King, High-temperature heat contents of some zirconium-containing substances, *J. Am. Chem. Soc.*, 72 [5] (1950) 2262-2265.
- [1953Hum] G. L. Humphrey, "Heats of formation of hafnium oxide and hafnium nitride", *J. Am. Chem. Soc.*, 75 [12] (1953) 2806-2807.
- [1953Orr] R. L. Orr, "High temperature heat contents of hafnium dioxide and hafnium tetrachloride", *J. Am. Chem. Soc.*, 75 [5] (1953) 1231-1232.
- [1953Tod] S. S. Todd, "Heat capacities at low temperatures and entropies at 298.16K of hafnium dioxide and hafnium tetrachloride", *J. Am. Chem. Soc.*, 75 [12] (1953) 3035-3036.
- [1954Cur] C. E. Curtis, L. M. Doney, J. R. Johnson, "Some properties of hafnium oxide, hafnium silicate, calcium hafnate, and hafnium carbide", *J. Am. Ceram. Soc.*, 37 [10] (1954) 458-465.
- [1954Dom] R. F. Domagala, D. J. Mcpherson, "System zirconium-oxygen", *Trans. AIME*, 200 (1954) 238-246.
- [1955Bro] F.H. Brown, JR., P. Duwez, "The Systems Zirconia-Lanthana and Zirconia-Neodymia", *J. Am. Ceram. Soc.*, 38 (1955) 95-101.
- [1956Rot] R. S. Roth, "Pyrochlore-type compounds containing double oxides of trivalent and tetravalent", *Journal of Research of the National Bureau of Standards*, 56 [1] (1956) 17-25.
- [1959Col] J. Lefevre, R. Collongues, M. Perez y Jorba, "Sur l'existence d'une transition continue de la structure quadratique a la structure cubique les systems zircone-oxyde de terre rare", *C. R. Acad. Sci. (France)*, 249 (1959) 2329-2331 .
- [1959Lef] J. Lefevre, M. Perez, R. Collongues, "On the equilibrium diagrams of ZrO₂ with rare earth oxides", *Bull.Soc.Chim.France*, 5 (1959) 1969-1971.
- [1961Col] R. Collongues, "Phase diagrams of zirconia-rare earth oxide systems", *Bulletin de la societe chim. De France*, (1961) 70-74.
- [1961Geb] E. Gebhardt, H. D. Seghezzi, W. Dürschnabel, "Untersuchungen in system zirkonium-sauerstoff. 2. Untersuchungen zur kinetik der reaktion zwischen zirkonium und

- sauerstoff, sowie über die konstitution des systems zirkonium-sauerstoff”, *J. Nucl. Mater.*, 4 (1961) 255-268
- [1961Hol] B. Holmberg, T. Dagerham, “X-ray studies on solid solutions of oxygen in α -zirconium”, *Acta Chem. Scand.*, 15 (1961) 919-925.
- [1961Jor] M. P. y Jorba, F. Queyroux, R. Collongues, “Existence of a continuous transition between the fluorite structure and the Tl_2O_3 typical structure in the rare earth zirconium oxide systems”, *Compt. Rend.*, 253 (1961) 670-672.
- [1961Kel] K. K. Kelley, E. G. King, “Data on theoretical metallurgy. XIV. Entropies of the elements and inorganic compounds”, *Bulletin - United States, Bureau of Mines*, No. 592 (1961) 1-149.
- [1962Col] R. Collongues, F. Queyroux, M. Perez y Jorba, J. Lefevre, “Sur l'apparition de differents etats ordonnes dans les phase non stoechiometriques refractaires”, *Bull. Soc. Chim. Fr.*, 1 (1962) 149-155.
- [1962Kom] K. L. Komarek, M. Silver, Proc. Symp. on Thermodynamics of Nuclear Materials, International Atomic Energy Agency, Vienna, May 1962, 749.
- [1962Per] M. Perez Y Jorba, “Contribution a letude des systems zircone-oxydes de terres rares”, *Ann. Chim.*, t. 7 [7-8] (1962) 479-511.
- [1962Smi] D. K. Smith, C.F. Cline, “Verification of existence of cubic zirconia at high temperature”, *J. Am. Ceram. Soc.*, 45 [5] (1962) 249-250.
- [1963Bau] W. L. Baun, “Transformation at high temperatures of hafnia and zirconia”, *Science*, 140 [3573] (1963) 1330-1331.
- [1963Lef] J. Lefevre, “Contribution a l'etude-de diffenentes modifications structurales des phases de type floutine dans les systems a base de zircone ou doxyde de hafnium”, *Ann. Chim.* 8 [1-2] (1963) 117-149.
- [1963Pea] C. D. Pears, D. Osment, “The Thermal Properties of Twenty-Six Solid Materials to 5000 °F or Their Destruction Temperatures”, *Technical Documentary Report No. ASD-TDR 62-765*, Southern Research Institute, Birmingham, AL, 1963.
- [1963Rud] E. Rudy, P. Stecher, “The constitution diagram of the hafnium-oxygen system”, *J. Less-common Metals*, 5 [1] (1963) 78-89.
- [1963Sil] M. D. Silver, P. A. Farrar, K. L. Komarek, “Thermodynamic properties and lattice parameters of hafnium-oxygen alloys”, *Trans. Metall. Soc. AIME*, 227 (1963) 876-884.
- [1963Wol] G. M. Wolten, “Diffusionless phase transformations in zirconia and hafnia”, *J. Am. Ceram. Soc.*, 46 [9] (1963) 418-422.
- [1964Hub] E. Y. Huber, E. L. Head, C. E. Holly, “The heats of formation of zirconium diboride and dioxide”, *J. Phys. Chem.*, 68 [10] (1964) 3040-3042.
- [1964Lin] T.H.Lin, H.C.Yu, “Phase equilibria of systems Ln_2O_3 (Rare Earth Oxides)- ZrO_2 . I. phase equilibria of the binary system La_2O_3 - ZrO_2 ”, *J. Chin. Ceram. Soc.*, 3 (1964) 159-166.
- [1964Lin1] T. H. Lin, H. C. Yu, “Phase equilibria of systems Ln_2O_3 (Rare Earth Oxides)- ZrO_2 . II. phase equilibria of the binary system Gd_2O_3 - ZrO_2 ”, *J. Chin. Ceram. Soc.*, 3 (1964) 229-235.
- [1964Ohn] B. Ohnysty, F. K. Rose, “Thermal expansion measurements on thoria and hafnia to 4500°F”, *J. Am. Ceram. Soc.*, 47 [8] (1964) 398-400.

- [1965Bog] A. G. Boganov, V. S. Rudenko, and L. P. Makarov, "X-ray investigation of zirconium and hafnium oxides at temperatures up to 2750°C", *Proc. Acad. Sci. USSR, Chem. Sect.*, 160 (1965) 146-148.
- [1965Col] M. R. Collongues, M. F. Queyrous, M. Perez, Y. Jorba, and M. J-C. Gilles, Structures et propriétés des composés formés par les oxydes de terres rares avec les oxydes des éléments du groupe 4A, *Bull. Soc. Chim. France*, 4, (1965) 1141.
- [1965Dav] I. A. Davtyan, V. B. Glushkova, E. K. Keler, "A study of the Nd₂O₃-ZrO₂ system. Investigation of the regions rich in zirconium dioxide", *Inorg. Mater.*, 1 [5] (1965) 679-685.
- [1965Dom] R. F. Domagala, R. Ruh, "The hafnium-oxygen system", *ASM Trans. Quart.*, 58 [2] (1965) 164-175.
- [1965Glu] V. B. Glushkova, I. A. Davtyan, E. K. Keler, "Study of the system Nd₂O₃-ZrO₂. Investigation of regions rich in neodymium oxide", *Inorg. Mater.*, 1 [11] (1965), 1766-1774.
- [1965Lam] W. A. Lambertson, F. H. Genzel, USAEC Report AECD-3465 (1965).
- [1965Nog] T. Noguchi, M. Mizuno, T. Kozuka, M. Yoshida, T. Yamamoto, "High-temperature research in a solar furnace. IV. Measurement of spectral emissivity and freezing point of metal oxides", *Nagoya Kogyo Gijutsu Shikensho Hokoku* 14 [1] (1965) 28-38.
- [1965Sta] O. M. Stansfield, "Thermal expansion of polycrystalline HfO₂-ZrO₂ solid solutions", *J. Am. Ceram. Soc.*, 48 (1965) 436-437.
- [1965Tsa] D. Sh. Tsagareishvili, G. G. Gvelesiani, "Enthalpy and heat capacity of some rare earth oxides", *Russ. J. Inorg. Chem.*, 10 [2] (1965) 171-172.
- [1965Tsa1] D. Sh. Tsagareishvili, G. G. Gvelesiani, "Heat contents and heat capacities of oxides of europium, thulium, and ytterbium at high temperatures", *Trudy Gruz. Inst. Metall.*, 14 (1965) 187-198.
- [1965Vie] D. Viechnicki, V. S. Stubican, "Mechanism of decomposition of the cubic solid solutions in the system ZrO₂-MgO", *J. Am. Ceram. Soc.*, 48 [6] (1965) 292-297.
- [1966Kir] V. A. Kirillin, A. E. Sheindlin, V. Ya. Chekhovskoi, I. A. Zhukova, V. D. Tarasov, "Enthalpy and specific heat of zirconium oxide in the 100-2500°K temperature range", *Teplofiz. Vys. Temp.*, 4 [6] (1966) 878-879.
- [1966Nog1] T. Noguchi, M. Mizuno, T. Kozuka, "Freezing point measurement on metal oxides with a solar furnace", *Kogyo Kagaku Zasshi*, 69 (1966) 1705-9.
- [1966Nog2] T. Noguchi, T. Kozuka, "Heating curves of solids obtained by a solar furnace", *Solar Energy*, 10 (1966) 203-206.
- [1967Kor] A. N. Kornilov, I. M. Ushakova, S. M. Skuratov, "Standard heat of formation of zirconium dioxide", *Russ. J. Phys. Chem.*, 41 [1] (1967) 101-103.
- [1968Hub] E. J. Huber, C. E. Holley, "Enthalpy of formation of hafnium oxide", *J. Chem. Eng. Data*, 13 [2] (1968) 252-253.
- [1968Ruh] R. Ruh, H. J. Garrett, R. F. Domagala and N. M. Tallen, "The system zirconia-hafnia", *J. Am. Ceram. Soc.*, 51 [1] (1968) 23-27.
- [1968Rou1] A. Rouanet, "Solidification diagrams and high temperature phase diagrams of zirconia-erbium oxide, zirconia-yttrium oxide and zirconia-ytterbium oxide systems", *C. R. Acad. Sc. Paris, Ser. C*, t.267 [23] (1968) 1581-1583.

- [1968Rou2] A. Rouanet, M. Foex, "Study at high temperature of systems formed by zirconia with samarium and gadolinium sesquioxides", *C. R. Acad. Sc. Paris, Ser. C*, t.267 [15] (1968) 873-876.
- [1968Rou3] A. Rouanet, "Resistance and phase structures of lanthanum zirconium oxide systems at high temperatures", *C. R. Acad. Sc. Paris, Ser. C*, t.267 [5] (1968) 395-397.
- [1970Lat] R. E. Latta, E. C. Duderstadt, R. E. Fryxell, "Melting point of pure zirconia", *J. Nucl. Mater.*, 35 (1970) 345-346.
- [1970Pat] R. N. Patil, E. C. Subbarao, "Monoclinic-tetragonal phase transition in zirconia: mechanism, pretransformation and coexistence", *Acta Cryst.*, A26 (1970) 535-542.
- [1970Rou] A. Rouanet, "High temperature properties of zirconia-neodymium sesquioxide systems", *C. R. Acad. Sc. Paris, Ser. C*, t.270 [9] (1970) 802-805.
- [1970Spi] M. Spiridonov, L. N. Popova, R. Ya. Popil'skii, "On the phase relations and the electrical conductivity in the system ZrO_2 - Sc_2O_3 ", *J. Solid State Chem.*, 2 [3] (1970) 430-438.
- [1970Tho] M. R. Thornber, D. J. M. Bevan, E. Summerville, "Mixed oxides of the type MO_2 (fluorite) - M_2O_3 . V. Phase studies in the systems ZrO_2 - M_2O_3 (M=Sc, Yb, Er, Dy)", *J. Solid State Chem.*, 1, (1970) 545-553.
- [1971JAN] *JANAF Thermochemical Tables*, Edited by D. R. Stull and H. Prophet, National Bureau of Standards, U.S. Department of Commerce, Washington, 1971.
- [1971Kor] V. R. Korneev, V. B. Glushkova, E. K. Keler, "Heats of formation of rare earth zirconates", *Inorg. Mater.*, 7 (1971) 781-782.
- [1971Rou] A. Rouanet, "Contribution to study of zirconium-oxides systems of lanthanides close to melting point", *Rev. Int. Hautes Temp. Refract.*, 8 [2] (1971) 161-180.
- [1972Cab] F. Cabannes, J. Simonato, M. Foex, J. P. Coutures, "Utilisation des températures de fusion des eutectiques comme étalons secondaires de températures au-dessus de 2327 K", *High Temp. - High Press.*, 4 (1972) 589-596.
- [1972Hir] M. Hirabayashi, S. Yamaguchi, T. Arai, H. Asano, S. Hashimoto, "Interstitial order-disorder transformations in the Zr-O and Hf-O systems near the compositions $ZrO_{1/3}$ and $HfO_{1/6}$ ", *J. Phys. Soc. Japan*, 32 (1972) 1157.
- [1972Neg] A. Negro, I. Amato, "An investigation of the zirconia-gadolinia system", *J. Less-Common Met.*, 26 (1972) 81-88.
- [1972Por] K. I. Portnoi, N. I. Timofeeva, S. E. Salibekov, and I. V. Romanovich, "Synthesis and investigation of properties of complex oxides of rare earths and zirconium", *Inorg. Mater.*, 8 [2] (1972) 358-360.
- [1972Sta] D. W. Stacy, J. K. Johnstone, D. R. Wilder, "Axial thermal expansion of HfO_2 ", *J. Am. Ceram. Soc.*, 55 [9] (1972) 482-483.
- [1973Cla] F. Claisse, T. M. Giam, "Transformation in hcp zirconium-oxygen alloys", *J. Less-Common Met.*, 30 (1973) 377-385.
- [1973Hir] M. Hirabayashi, S. Yamaguchi, T. Arai, "Superstructure and order-disorder transformation of interstitial oxygen in hafnium", *J. Phys. Soc. Japan*, 35 (1973) 473-481.
- [1973Mit] T. Mitsuhashi, Y. Fujiki, "Phase transformation of monoclinic ZrO_2 single crystal", *J. Am. Ceram. Soc.*, 56 [9] (1973) 493.
- [1973Pal] S.F. Pal'guev, L. N. Fomina, V. N. Strekalovskii, "Thermal X-ray diffraction study of the reaction of zirconium dioxide and lanthanum oxide in the region of occurrence of

$\text{La}_2\text{Zr}_2\text{O}_7$ ”. *Tr. Inst. Elektrokhim., Ural. Nauchn. Tsentr. Akad. Nauk SSSR*, 19 (1973) 120-127.

[1973Ruh] R. Ruh, V. A. Patel, “Proposed phase relations in the HfO_2 -rich portion of the system Hf-HfO_2 ”, *J. Am. Ceram. Soc.*, 56 [11] (1973) 606-607.

[1973Str] V. I. Strakhov, Ya. V. Klucharov, G. G. Sergeev, “ ZrO_2 and Nd_2O_3 interactions in isothermal processing conditions”, *Zh. Prikl. Khim.*, 46 [9] (1973) 2083-2085.

[1974Bou] G. Boureau, P. Gerdanian, “Use of a Tian-Calvet microcalorimeter at 1300°C direct measurement of $h_{\text{O}_2}^M$ in the metal-oxygen systems”, *Canad. Metall. Quarter.*, 13 [2] (1974) 339-343.

[1974Hir] M. Hirabayashi, S. Yamaguchi, T. Arai, H. Asano, S. Hashimoto, “Order-disorder transformation of oxygen-atoms dissolved in zirconium studied by neutron-diffraction”, *Phys. Stat. Sol. (a)*, 23 (1974) 331-339.

[1974Kor] A. N. Kornilov, I. M. Ushakova, G. B. Shvejkin, “Thermochemistry of the hafnium-oxygen system”, *Russ. J. Phys. Chem.*, 48 [5] (1974) 779.

[1974Sub] E. C. Subbarao, H. S. Maiti, K. K. Srivastava, “Martensitic transformation in zirconia”, *Phys. Stat. Sol. (a)*, 21 (1974) 9-40.

[1974Mic] D. Michel, M. Perez y Jorba, and R. Collongues, “Order-disorder transformation of the fluorite structure to the pyrochlore structure for the phases $(1-x)$ zirconium oxide- x lanthanum oxide”, *Mat. Res. Bull.*, 9 [11] (1974) 1457-1468.

[1974Pap] Y. N. Paputskii, V. A. Krzhizhanovskaya, and V. B. Glushkova, “Enthalpy of formation of rare earth hafnates and zirconates”, *Inorg. Mater.*, 10 [8] (1974) 1338-1339.

[1974Str] K.K. Srivastava, R.N. Patil, C.B. Choudhary, K. V. G. K. Gokhale, E. C. Subbarao, “Revised phase diagram of the system $\text{ZrO}_2\text{-YO}_{1.5}$ ”, *Trans. J. Br. Ceram. Soc.* 73 (1974) 85-91.

[1974Vas] I. A. Vasil'eva, Zh. V. Granovskaya, “Thermodynamic properties of zirconium oxides”, *Russ. J. Phys. Chem.*, 48 [6] (1974) 902-904.

[1975Ack] R. J. Ackerman, E. G. Rauh, C. A. Alexander, “The thermodynamic properties of $\text{ZrO}_2(\text{g})$ ”, *High Temp. Sci.*, 7 (1975) 304-316.

[1975Ald] P. Aldebert, J. M. Badie, J. P. Traverse, J. L. Buevoz, and G. Roullet, “Application of a high temperature neutron diffraction apparatus to the study of refractory oxides”, *Rev. Int. Hautes Temp. Refract.*, 12 (1975) 307-319.

[1975Kor] A. N. Kornilov, I. M. Ushakova, E. J. Huber, C. E. Holley, “The enthalpy of formation of hafnium dioxide”, *J. Chem. Thermodynamics*, 7 (1975) 21-26.

[1975Sta] D. W. Stacy, D. R. Wilder, “The yttria-hafnia system”, *J. Am. Ceram. Soc.*, 58 [7-8] (1975) 285-288.

[1976Kuz] A. K. Kuznetsov, P. A. Tikhonov, M. V. Kravchinskaya, “The $\text{HfO}_2\text{-Pr}_2\text{O}_3$ system”, *Russ. J. Inorg. Chem.*, 21 [5] (1976) 718-720.

[1976Mic] D. Michel, M. Perez y Jorba, R. Collongues, “Study by raman spectroscopy of order-disorder phenomena occurring in some binary oxides with fluorite-related structures”, *J. Raman Spectr.*, 5 (1976) 163-180.

[1976Ros] H. J. Rossell, “Crystal structure of some fluorite-related M_7O_{12} compounds”, *J. Solid State Chem.*, 19 (1976) 103-111.

- [1976Rud] G. I. Ruda, V. V. Vavilova, I. I. Kornilov, L. E. Fykin, L. D. Panteleev, "Phase equilibrium and solid-state transitions in the system Hf-O", *Inorg. Mater.*, 12 [3] (1976) 396-400.
- [1976Ruh] R. Ruh, G. W. Hollenberg, "Phase relations and thermal expansion in the system HfO₂-TiO₂", *J. Am. Ceram. Soc.*, 59 [11-12] (1976) 495-498.
- [1977Ack] R. J. Ackermann, S. P. Garg, E. G. Rauh, "High-temperature phase-diagram for system Zr-O", *J. Am. Ceram. Soc.*, 60 [7-8] (1977) 341-345.
- [1977Luk] H. L. Lukas, E. Th. Henig, B. Zimmermann, "Optimization of phase diagrams by a least squares method using simultaneously different types of data", *Calphad*, 1 [3] (1977) 225-236.
- [1977Ruh] R. Ruh, H. J. Garrett, R. F. Domagala, V. A. Patel, "The system zirconia-scandia", *J. Am. Ceram. Soc.*, 60 [9-10] (1977) 399-403.
- [1977Sch] R. W. Scheiecher, D. R. Wilder, H. Moeller, "The system HfO₂-Eu₂O₃", *J. Am. Ceram. Soc.*, 60 [11-12] (1977) 501-504.
- [1977Sco] H. G. Scott, "The yttria-zirconia δ phase", *Acta Cryst.*, B33 (1977) 281-282.
- [1978Ack] R. J. Ackermann, S. P. Garg, E. G. Rauh, "The lower phase boundary of ZrO_{2-x}", *J. Am. Ceram. Soc.*, 61 [5-6] (1978) 275-276.
- [1978Sco] H. G. Scott, "On the continuous transition between two structure types in the zirconia-gadolinia system", *J. Mater. Sci.*, 13 (1978) 1592-1593.
- [1978Zoz] E. I. Zoz, A. M. Gavrish, N. V. Gul'ko, "Phase formation in the system ZrO₂(HfO₂)-La₂O₃", *Inorg. Mater.*, 14 [1] (1978) 84-86.
- [1979Ack] R. J. Ackermann, S. P. Garg, E. G. Rauh, "The thermodynamic properties of substoichiometric zirconium dioxide at the lower phase boundary", *High Temp. Sci.*, 11 (1979) 199-210.
- [1979Che] V. Ya. Chekhovskoi, I. A. Zhukova, V. D. Tarasov, "Enthalpy and heat capacity of zirconium dioxide in the temperature region 1100-2500°K", *Teplofiz. Vys. Temp.*, 17 [4], 754-758 (1979).
- [1980Dij] T. Van Dijk, K. J. De Vries, A. J. Burggraaf, "Electrical conductivity of fluorite and pyrochlore Ln_xZr_{1-x}O_{2-x/2} (Ln=Gd, Nd) solid solutions", *Phys. Stat. Sol. (a)*, 58 (1980) 115-125.
- [1980Pas] C. Pascual, P. Duran, "Phase relations and ordering in the dysprosia-zirconia system", *J. Mater. Sci.*, 15 (1980) 1701-1708.
- [1980Rau] E. G. Rauh, S. P. Garg, "The ZrO_{2-x} (cubic)-ZrO_{2-x} (cubic+tetragonal) phase boundary", *J. Am. Ceram. Soc.*, 63 [3-4] (1980) 239-240.
- [1981Gav] A. M. Gavrish, L. S. Alekseenko, L. A. Tarasova, G. P. Orekhova, "Structure and some properties of solid solutions in the systems ZrO₂-R₂O₃ (R=Sm, Dy)", *Inorg. Mater.*, 17 (1981) 1541-1544.
- [1981Gav1] A. M. Gavrish, N. V. Gul'ko, L. A. Tarasova, "X-ray diffraction and crystal-optical investigation of phase relations in the Nd₂O₃-ZrO₂ system", *Russ. J. Inorg. Chem.*, 26 (1981) 1785-1788.
- [1981Shi] K. Shinozaki, H. R. Sun, K. Uematsu, N. Mizutani, M. Kato, "Sintering of Sm₂O₃-ZrO₂ solid solution", *Nippon Kagaku Kaishi*, 9 (1981) 1454-1461.

- [1981Sub] E. C. Subbarao, "Zirconia - an overview", pp. 1-24 in *Advances in Ceramics*, Vol. 3, *Science and Technology of Zirconia*. Edited by A.H. Heuer, L.W. Hobbs, The American Ceramic Society, Columbus, OH, 1981.
- [1982Gav] A. M. Gavrish, L. S. Alekseenko, L. A. Tarasova, G. P. Orekhova, "Structure and electrical resistance of solid solutions in the $ZrO_2-Nd_2O_3$ system", *Inorg. Mater.*, 18 [2] (1982) 214-216.
- [1982Zoz] E. I. Zoz, E. N. Fomichev, A. A. Kalashnik, and G. G. Eliseeva, "The structure and properties of lanthanide zirconates and hafnates", *Russ. J. Inorg. Chem.*, 27 [1] (1982) 54-56.
- [1983Sen] G. B. Senft, V. S. Stubican, "Phase relations and ordering in the system HfO_2-CaO ", *Mater. Res. Bull.*, 18 [10] 1163-1170 (1983).
- [1983Sub] M. A. Subramanian, G. Aravamudan, G. V. Subba Rao, "Oxide pyrochlores-A review", *Prog. Solid St. Chem.*, 15 (1983) 55-143.
- [1984Bou] G. Boureau, P. Gerdanian, "High temperature thermodynamics of solutions of oxygen in zirconium and hafnium", *J. Phys. Chem. Solids*, 45 [2] (1984) 141-145.
- [1984Ruh] R. Ruh, K. S. Mazdiyasi, P. G. Valentine, H. O. Bielstein, "Phase relations in the system $ZrO_2-Y_2O_3$ at low Y_2O_3 contents", *J. Am. Ceram. Soc.*, 67 [9] (1984) C-190-C-192.
- [1984Stu] V. S. Stubican, G. S. Corman, J. R. Hellmann, G. Senft, "Phase relationships in some ZrO_2 systems", pp. 96-106 in *Advances in Ceramics*, Vol. 12, *Science and Technology of Zirconia II*. Edited by N. Claussen, M. Rühle, A. H. Heuer, The American Ceramic Society, Columbus, OH, 1984.
- [1985Ada] J. W. Adams, H. H. Nakamura, R. P. Ingel, R. W. Rice, "Thermal expansion behavior of single-crystal zirconia", *J. Am. Ceram. Soc.*, 68 [9] (1985) C-228-C-231.
- [1985Bel] A. N. Belov, G. A. Semenov, "Thermodynamics of binary solid solutions of zirconium, hafnium, and yttrium oxides from high-temperature mass spectrometry data", *Russ. J. Phys. Chem.*, 59 (1985) 342-344.
- [1985Dij] M. P. Van Dijk, A. J. Burggraaf, A. N. Cormack, C. R. A. Catlow, "Defect structures and migration mechanisms in oxide pyrochlores", *Solid State Ionics*, 17 (1985) 159-167.
- [1985Hil] M. Hillert, B. Jansson, B. Sundman, J. Agren, "A 2-sublattice model for molten solutions with different tendency for ionization", *Metall. Trans. A*, 16 [2] (1985) 261-266.
- [1985Per] C. H. Perry, D. -W. Liu, R. P. Ingel, "Phase characterization of partially stabilized zirconia by Raman spectroscopy", *J. Am. Ceram. Soc.*, 68 [8] (1985) C-184-C-187.
- [1985She] A. V. Shevchenko, L. M. Lopato, "TA method application to the highest refractory oxide systems investigation", *Thermochimica Acta*, 93, 537-540 (1985).
- [1985Sun] B. Sundman, B. Jansson, J-O. Andersson, "The thermo-calc databank system", *Calphad*, 9 (1985) 153-190.
- [1985Suz] S. Suzuki, M. Tanaka, M. Ishigame, "Structural studies on $ZrO_2-Y_2O_3$ system by electron-diffraction and electron microscopy-I", *Jap. J. Appl. Phys.*, 24 [4] (1985) 401-410.
- [1986Abr] J. P. Abriata, J. Garces, R. Versaci, "The O-Zr (oxygen-zirconium) system", *Bull. Alloy Phase Diagram*, 7 [2] (1986) 116-124.
- [1986Ban] M. J. Bannister, J. M. Barnes, "Solubility of TiO_2 in ZrO_2 ", *J. Am. Ceram. Soc.*, 69 [11] (1986) C-269-C-271.

- [1986Hil] M. Hillert, B. Jansson, "Thermodynamic model for nonstoichiometric ionic phases – application to CeO_{2-x} ", *J. Am. Ceram. Soc.*, 69 [10] (1986) 732-734.
- [1986Yam] T. Yamada, M. Yoshimura, S. Somiya, "Redetermination of the solidification points of Al_2O_3 , Y_2O_3 , and HfO_2 by digital pyrometry with an arc-imaging furnace", *High Temp. – High Press.*, 18 (1986) 377-388.
- [1986Yos] N. Yoshikawa, H. Eda, H. Suto, "On the cubic/tetragonal phase equilibrium of the ZrO_2 - Y_2O_3 system", *J. Jpn. Inst. Metals*, 50 [1] (1986) 113-118.
- [1986Yos1] N. Yoshikawa and H. Suto, "Transformation behaviour of Y_2O_3 -PSZ investigated by thermal dilatometry", *J. Jpn. Inst. Met.*, 50 [1] (1986) 108-113.
- [1987Cou] J. P. Coutures, J. Coutures, "The system HfO_2 - TiO_2 ", *J. Am. Ceram. Soc.*, 70 [6] (1987) 383-387.
- [1987She] A. V. Shevchenko, L. M. Lopato, V. D. Tkachenko, A. K. Ruban, "Reaction of hafnium and zirconium dioxide", *Inorg. Mater.*, 23 [2] (1987) 225-229.
- [1987Ste] S. Stecura, "New ZrO_2 - Yb_2O_3 plasma-sprayed coatings for thermal barrier applications", *Thin Solid Films*, 150 (1987) 15-40.
- [1987Ueh] T. Uehara, K. Koto, F. Kanamaru, H. Horiuchi, "Stability and antiphase domain structure of the pyrochlore solid solution in the ZrO_2 - Gd_2O_3 system", *Solid State Ionics*, 23 (1987) 137-143.
- [1988Ans] I. Ansara, B. Sundman, P. Willemin, "Thermodynamic modeling of ordered phases in the Ni-Al system", *Acta Metall.*, 36 [4] (1988) 977-982.
- [1988Bas] B. Bastide, P. Odier, J. P. Coutures, "Phase equilibrium and martensitic transformation in lanthana-doped zirconia", *J. Am. Ceram. Soc.*, 71 [6] (1988) 449-453.
- [1988Heu] A. H. Heuer, R. Chaim, V. Lanteri, "Phase Transformations and Micro-structural Characterization of Alloys in the System Y_2O_3 - ZrO_2 ", pp. 3-20 in *Advances in Ceramics*, Vol. 24, *Science and Technology of Zirconia III*. Edited by S. Somiya, N. Yamamoto, H. Yanagida, The American Ceramic Society, Westerville, Ohio, 1988.
- [1988Rüh] M. Rühle, L. T. Ma, W. Wunderlich, A. G. Evans, "TEM studies on phases and phase stabilities of zirconia ceramics", *Physica B*, 150 (1988) 86-98.
- [1988Sig] L. M. Sigalov, L. M. Lopato, "Study of the zirconia-hafnia system using radiant heating", *Geliotekhnika*, 4 (1988) 55-57.
- [1988Yam] T. Yamada, M. Mizuno, T. Ishizuka, T. Noguchi "Liquidus curve measurement in the system zirconia-hafnia", pp. 959-964 in *Advances in Ceramics*, Vol. 24, *Science and Technology of Zirconia III*. Edited by S. Somiya, N. Yamamoto, H. Yanagida, The American Ceramic Society, Westerville, Ohio, 1988.
- [1989Mor] T. Moriga, A. Yoshisa, F. Kanamaru, K. Koto, "Crystal structure analyses of the pyrochlore and fluorite-type $\text{Zr}_2\text{Gd}_2\text{O}_7$ and anti-phase domain structure", *Solid State Ionics*, 31 (1989) 319-328.
- [1990Dur] P. Duran, M. Gonzalez, C. Moure, J. R. Jurado, C. Pascual, "A new tentative phase equilibrium diagram for the ZrO_2 - CeO_2 system in air", *J. Mater. Sci.*, 25 (1990) 5001-5006.
- [1990Fre] F. Frey, H. Boysen, T. Vogt, "Neutron powder investigation of the monoclinic to tetragonal phase transformation in undoped zirconia", *Acta Cryst.*, B46 (1990) 724-730.
- [1990Mor] T. Moriga, S. Emura, A. Yoshisa, S. Kikkawa, F. Kanamaru, K. Koto, "X-ray and raman study on coordination states of fluorite- and pyrochlore-type compounds in the system ZrO_2 - Gd_2O_3 ", *Solid State Ionics*, 40/41 (1990) 357-361.

- [1990Nev] M. V. Nevitt, Y. Fang, S. K. Chan, "Heat capacity of monoclinic zirconia between 2.75 and 350K", *J. Am. Ceram. Soc.*, 73 [8] (1990) 2502-2504.
- [1990Ore] V. M. Orera, R. I. Merino, Y. Chen, R. Cases, P. J. Alonso, "Intrinsic electron and hole defects in stabilized zirconia single-crystals", *Phys. Rev. B*, 42 [16] (1990) 9782-9789.
- [1990Zhe] C. G. Zheng, A. R. West, "Phase equilibria and electrical properties in the system ZrO_2 - La_2O_3 - Nb_2O_5 ", *Br. Ceram. Trans. J.*, 89 (1990) 138-141.
- [1991Boy] H. Boysen, F. Frey, T. Vogt, "Neutron powder investigation of the tetragonal to monoclinic phase transformation in undoped zirconia", *Acta Cryst.*, B47 (1991) 881-886.
- [1991Din] A. T. Dinsdale, "SGTE data for pure elements", *Calphad*, 15 [4] (1991) 317-425.
- [1991Du] Y. Du, Z. P. Jin, P. Y. Huang, "Thermodynamic assessment of the ZrO_2 - $YO_{1.5}$ system", *J. Am. Ceram. Soc.*, 74 [7] (1991) 1596-1577.
- [1991Gul] D. D. Gulamova, S. N. Novoselova, "Polymorphism of zirconium and hafnium dioxides", *Russ. J. Inorg. Chem.*, 36 [5] 639-641 (1991).
- [1991Hil] M. Hillert, "Thermodynamic model of the cubic→tetragonal transition in nonstoichiometric zirconia", *J. Am. Ceram. Soc.*, 74 [8] (1991) 2005-2006.
- [1991Kom] D. Komyoji, A. Yoshiasa, T. Moriga, S. Emura, F. Kanamaru, and K. Koto, EXAFS study of the fluorite-type compounds in the systems $(1-x)ZrO_2$ - $xYbO_{1.5}$ ($x=0.18 \leq x \leq 0.5$) and $Zr_2Ln_2O_7$ ($Ln=Tb, Dy, Ho, Er, \text{ and } Yb$), *Solid State Ionics*, 50 (1992) 291-301.
- [1991Leu] D. K. Leung, C. J. Chan, M. Rühle, F. Lange, "Metastable crystallization, phase partitioning, and grain growth of ZrO_2 - Gd_2O_3 materials processed from liquid precursors", *J. Am. Ceram. Soc.*, 74 [11] (1991) 2786-2792.
- [1991Obo] T. V. Obolonchik, L. M. Lopato, G. I. Gerasimiyuk, A. V. Shevchenko, "interaction in the HfO_2 - ZrO_2 - Y_2O_3 system at 1250-1900°C", *Inorg. Mater.*, 27 [11] (1991) 2004-2007.
- [1991Red] V. P. Red'ko, L. M. Lopato, "Crystal structure of the compounds $M_4Zr_3O_{12}$ and $M_4Hf_3O_{12}$ (where M is a rare-earth element)", *Inorg. Mater.*, 27 [9] (1991) 1609-1614.
- [1991Wit] R. L. Withers, J.G. Thompson, P. J. Barlow, "An electron, and X-ray powder, diffraction study of cubic, fluorite-related phases in various ZrO_2 - Ln_2O_3 systems", *J. Solid State Chem.*, 94 [1] (1991) 89-105.
- [1992Col] R. Collongues, "Nonstoichiometry in oxides", *Prog. Crystal Growth and Charact.*, 25 [4] (1992) 203-240.
- [1992Du] Y. Du, Z. P. Jin, P. Y. Huang, "Thermodynamic calculation of the zirconia-calcia system", *J. Am. Ceram. Soc.*, 75 [11] (1992) 3040-3048.
- [1992Kan] T. K. Kang, T. Nagasaki, N. Igawa, K. I. Hiun, H. Ohno, "Electrical properties of cubic, stabilized, single ZrO_2 - Gd_2O_3 crystals", *J. Am. Ceram. Soc.*, 75 [8] (1992) 2297-2299.
- [1992Nis] T. Nishizawa, "Progress of CALPHAD", *Mater. Trans. JIM*, 33 [8] (1992) 713-722.
- [1992She] T. S. Sheu, T. Y. Tien, I. W. Chen, Cubic-to-tetragonal (t') transformation in zirconia-containing systems, *J. Am. Ceram. Soc.*, 75 [5] (1992) 1108-1116.
- [1992Wan] J. Wang, H. P. Li, R. Stevens, "Hafnia and hafnia-toughened ceramics", *J. Mater. Sci.*, 27 (1992) 5397-5430.

- [1992Yas] M. Yashima, N. Ishizawa, M. Yoshimura, "Application of an ion-packing model based on defect clusters to zirconia solid solutions: II, Applicability of Vegard's law", *J. Am. Ceram. Soc.*, 75 [6] (1992) 1550-1557.
- [1993Gon] M. Gonzalez, C. Moure, J. R. Jurado, P. Duran, "Solid-state reaction, microstructure and phase relations in the ZrO₂-rich region of the ZrO₂-Yb₂O₃ system", *J. Mater. Sci.*, 28 (1993) 3451-3456.
- [1993Yam] T. Yamada, M. Mizuno, "Liquidus curve measurement in the system HfO₂-ZrO₂", *Nagoya Kogyo Gijutsu Shikensho Hokoku*, 42 (1993) 236-245.
- [1993Yas] M. Yashima, N. Ishizawa, T. Noma, M. Yoshimura, "Tetragonal ↔ monoclinic phase transition temperature of rare-earth-doped zirconia prepared by Arc melting", *J. Ceram. Soc. Japan*, 101 [8] (1993) 871-876.
- [1993Zas] A. M. Zaslavskii, A. E. Slivinskaya, A. V. Mel'nikov, "Solid solutions in condensates of zirconia-dysprosia and hafnia-dysprosia systems", *Fizika i Khimiya Obrabotki Materialov*, 2 (1993) 111-115.
- [1994Li] P. Li, I. W. Chen, "Effect of dopants on zirconia stabilization—An X-ray absorption study: I, trivalent dopants", *J. Am. Ceram. Soc.*, 77 [1] (1994) 118-128.
- [1994Tch] F. Tcheliébou, A. Boyer, "microstructural and mechanical effects of oxide addition into thin ZrO₂ matrix", *Mater. Sci. Eng. B*, 26 (1994) 175-180.
- [1995And] E. R. Andrievsakaya, L. M. Lopato, "Influence of composition on the T→M transformation in the systems ZrO₂-Ln₂O₃ (Ln=La, Nd, Sm, Eu)", *J. Mater. Sci.*, 30 (1995) 2591-2596.
- [1995Bha] S. Bhattacharyya, D. C. Agrawal, "Preparation of tetragonal ZrO₂-Gd₂O₃ powder", *J. Mater. Sci.*, 30 (1995) 1495-1499.
- [1995Bol] M. Bolech, E. H. P. Cordfunke, F. J. J. G. Janssen, A. Navrotsky, "Standard enthalpy of formation of Lanthanum Zirconate", *J. Am. Ceram. Soc.*, 78 [8] (1995) 2257-2258.
- [1995Du] Y. Du, M. Yashima, T. Koura, M. Kakihana, M. Yoshimura, "Thermodynamic assessment of the ZrO₂-LaO_{1.5} system", *J. European Ceram. Soc.*, 15 (1995) 503-511.
- [1995Kat] J. Katamura, T. Seri, T. Sakuma, "The cubic-tetragonal phase equilibria in the ZrO₂-R₂O₃ (R=Y, Gd, Sm, Nd) systems", *J. Phase Equilib.*, 16 (1995) 315-319.
- [1995Kat1] T. Kato, T. Tsuji, "heat capacity measurements of hafnium-oxygen solid solutions at high temperatures", *Thermochim. Acta*, 267 (1995) 397-404.
- [1995Yas] M. Yashima, T. Mitsuhashi, H. Takashina, M. Kakihana, T. Ikegami, M. Yoshimura, "Tetragonal-monoclinic phase transition enthalpy and temperature of ZrO₂-CeO₂ solid solutions", *J. Am. Ceram. Soc.*, 78 [8] (1995) 2225-2228.
- [1995Tsu1] T. Tsuji, M. Amaya, "Study on order-disorder transition of Zr-O alloys (O/Zr=0–0.31) by heat capacity measurement", *J. Nucl. Mater.*, 223 (1995) 33-39.
- [1995Tsu2] T. Tsuji, M. Amaya, "Heat capacity measurement on ZrO_x (x=0–0.31) from 325 to 905 K. Part I. Heat capacity anomaly due to thermal non-equilibrium state at low temperature", *Thermochim. Acta*, 259 (1995) 1-12.
- [1996Hai] S. Haile, S. Meilicke, "The kinetics of ordering in gadolinium zirconate: an unusual oxygen ion conductor", *Mat. Res. Soc. Proc.*, 398 (1996) 599-604.

- [1996Kar] A. G. Karaulov, E. I. Zoz, T. M. Shlyakhova, "Structure and properties of refractories based on zirconia stabilized by gadolinium oxide", *Refract. Ind. Ceram.*, 37 (1996) 83-87.
- [1996Wil] D. B. Williams, C. B. Carter, *Transmission Electron Microscopy*, 1996, Plenum Press, New York, p. 599.
- [1996Yas] M. Yashima, M. Kakihana, M. Yoshimura, "Metastable-stable phase diagrams in the zirconium-containing systems utilized in solid-oxide fuel cell application", *Solid State Ionics*, 86-88 (1996) 1131-1149.
- [1996Yas2] M. Yashima, K. Ohtake, M. Kakihana, H. Arashi, M. Yoshimura, "Determination of tetragonal-cubic phase boundary of $Zr_{1-x}R_xO_{2-x/2}$ (R=Nd, Sm, Y, Er, and Yb) by Raman scattering", *J. Phys. Chem. Solids*, 57 (1996) 17-24.
- [1997And] E. R. Andrievskaya, L. M. Lopato, A. V. Shevchenko, V. P. Smirnov, "Phase equilibria in the HfO_2 - Eu_2O_3 system", *Inorg. Mater.*, 33 [7] (1997) 703-706.
- [1997Ans] I. Ansara, N. Dupin, H. L. Lukas, B. Sundman, "Thermodynamic assessment of the Al-Ni system", *J. Alloy. Compd.*, 247 (1997) 20-30.
- [1997Bol] M. Bolech, E. H. P. Cordfunke, A. C. G. Van Genderen, R. R. Van Der Laan, F. J. J. G. Janssen, J. C. Van Miltenburg, "The heat capacity and derived thermodynamic function of $La_2Zr_2O_7$ and $Ce_2Zr_2O_7$ from 4 to 1000K", *J. Phys. Chem. Solids*, 58 (1997) 433-439.
- [1997Cha] W. K. Chang, A. A. Wang, Y. H. Lee, "Oxygen-induced structural change of zirconia by adding rare earth oxides with solid state method", *J. Alloy Compd.*, 249 (1997) 251-255.
- [1997Kas] N. V. Kasper, I. O. Troyanchuk, "Dilatometric study of martensitic transformation in CeO_2 -stabilized ZrO_2 ", *Inorg. Mater.*, 33 [8] 820-822 (1997).
- [1997Kat] T. Kato, T. Tsuji, "Study on order-disorder transition of Hf-O alloys (O/Hf=0.11-0.22) by heat capacity measurement", *J. Nucl. Mater.*, 247 (1997) 98-102.
- [1997Kho] K. A. Khor, J. Yang, "Rapidly solidified neodymia-stabilized zirconia coatings prepared by DC plasma spraying", *Surf. Coat. Technol.*, 96 (1997) 313-322.
- [1998Che] P. Y. Chevalier, E. Fischer, "Thermodynamic modeling of the O-U-Zr system", *J. Nucl. Mater.*, 257 (1998) 213-255.
- [1998Hil] M. Hillert, *Phase equilibria, phase diagrams and phase transformations, their thermodynamic basis*, Cambridge university press, Cambridge, 1998.
- [1998Jac] K. T. Jacob, N. Dasgupta, Y. Waseda, "Composition-graded solid electrolyte for determination of the Gibbs energy of formation of lanthanum zirconate", *J. Am. Ceram. Soc.*, 81 [7] (1998) 1926-1930.
- [1998Mol] I. Molodetsky, A. Navrotsky, M. Lajavardi, A. Brune, "The energetics of cubic zirconia from solution calorimetry of yttria- and calcia-stabilized zirconia", *Zeit. Phys. Chem.*, 207 (1998) 59-65.
- [1998Ond] Phase equilibria diagram special volume, *Phase diagrams for zirconium and zirconia systems*, edited by Helen M. Ondik, Comp. in the Phase Equilibrium Diagrams Data Center, National Institute of Standards and Technology, Gaithersburg, Maryland, 1998.
- [1998Vor] Yu. K. Voron'ko, A. A. Sobol', L. I. Tsymbal, "Cubic-to-tetragonal phase transitions in ZrO_2 - Ln_2O_3 and HfO_2 - Ln_2O_3 solid solutions", *Inorg. Mater.*, 34 [4] (1998) 350-356.

- [1998Wil] P. J. Wilde, C. R. A. Catlow, "Defects and diffusion in pyrochlore structured oxides", *Solid State Ionics*, 112 (1998) 173-183.
- [1999Dup] N. Dupin, I. Ansara, "On the sublattice formalism applied to the B2 phase", *Z. Metallkd.*, 90 [1] (1999) 76-85.
- [1999Hay] M. Hayakawa, K. Nishio, J. Hamakita, T. Onda, "Isothermal and athermal martensitic transformations in a zirconia-yttria alloy", *Mater. Sci. Eng.*, A273-275 (1999) 213-217.
- [1999Kar] A. G. Karaulov, E. I. Zoz, "Phase formation in the ZrO_2 - HfO_2 - Gd_2O_3 and ZrO_2 - HfO_2 - Yb_2O_3 systems", *Refract. Ind. Ceram.*, 40 (1999) 479-483.
- [1999Low] J. E. Lowther, J. K. Dewhurst, J. M. Leger, and J. Haines, "Relative stability of ZrO_2 and HfO_2 structural phases", *Phy. Rev. B*, 60 [21] (1999) 14485.
- [1999Tab] Y. Tabira, R. L. Withers, "Structure and crystal chemistry as a function of composition across the wide range nonstoichiometric $(1-\epsilon)ZrO_2 \cdot \epsilon SmO_{1.5}$, $0.38 < \epsilon < 0.55$, oxide pyrochlore system", *J. Solid State Chem.*, 148 (1999) 205-214.
- [1999Tab1] Y. Tabira, R. Withers, J. Thompson, S. Schmid, "Structured diffuse scattering as an indicator of inherent cristobalite-like displacive flexibility in the rare earth zirconate pyrochlore $La_8Zr_{1-\delta}O_{2-\delta/2}$, $0.49 < \delta < 0.51$ ", *J. Solid State Chem.*, 142 (1999) 393-399.
- [1999Tho] J. B. Thomson, A. R. Armstrong, P. G. Bruce, "An oxygen-rich pyrochlore with fluorite composition", *J. Solid State Chem.*, 148 (1999) 56-62.
- [1999Toj] T. Tojo, T. Atake, T. Mori, H. Yamamura, "Heat capacity and thermodynamic function of zirconium and yttria-stabilized zirconium", *J. Chem. Thermodynamics*, 31 (1999) 831-845.
- [1999Wil] R. E. Willford, W. J. Weber, R. Devanathan, "Effects of cation disorder on oxygen vacancy migration in $Gd_2Ti_2O_7$ ", *J. Electroceramics*, 3 [4] (1999) 409-424.
- [2000Kat] S. Kato, K. Ozawa, K. Edamoto, S. Otani, "Photoelectron spectroscopy study of the oxidation of $ZrC(100)$ ", *Jpn. J. Appl. Phys.*, 39 [9A] (2000) 5217-5222.
- [2000Min] L. Minervini, R. W. Grimes, K. E. Sickafus, "Disorder in pyrochlore oxides", *J. Am. Ceram. Soc.*, 83 [8] (2000) 1873-1878.
- [2000Vas] R. Vassen, X. Q. Cao, F. Tietz, D. Basu, D. Stöver, "Zirconates as new materials for thermal barrier coatings", *J. Am. Ceram. Soc.*, 83 (2000) 2023-2028.
- [2001Fei] A. J. Feighery, J. T. S. Irvine, C. Zheng, "Phase relations at 1500°C in the ternary system ZrO_2 - Gd_2O_3 - TiO_2 ", *J. Solid State Chem.*, 160 (2001) 302-306.
- [2001Fuj] H. Fujimori, M. Yashima, M. Kakihana, M. Yoshimura, "In situ ultraviolet raman study on the phase transition of hafnia up to 2085K", *J. Am. Ceram. Soc.*, 84 [3] (2001) 663-665.
- [2001Kit] H. Kitaoka, K. Ozawa, K. Edamoto, S. Otani, "The interaction of water with oxygen-modified $ZrC(100)$ surfaces", *Solid State Commun.*, 118 [1] (2001) 23-26.
- [2001Hel] K. Helean, B. D. Begg, A. Navrotsky, B. Ebbinghaus, W. J. Weber, R. C. Ewing, "Enthalpies of formation of $Gd_2(Ti_{2-x}Zr_x)O_7$ pyrochlores", *Mat. Res. Soc. Proc.*, 663 (2001) 691-697.
- [2001Hil] M. Hillert, "The compound energy formalism", *J. Alloy. Compd.*, 320 (2001) 161-176.

- [2001Jer] D. A. Jerebtsov, G. G. Mikhailov, S. V. Sverdina, "Phase diagram of the system: $ZrO_2-Cr_2O_3$ ", *Ceramics Int.*, 27 (2001) 247-250.
- [2001Lia] P. Liang, N. Dupin, S. G. Fries, H. J. Seifert, I. Ansara, H. L. Lukas, F. Aldinger, "Thermodynamic assessment of the Zr-O binary system", *Z. Metallkd.*, 92 (2001) 747-756.
- [2001Mal] M.J. Maloney, "Thermal barrier coating systems and materials", U.S. Patent 6,177,200, (2001).
- [2001Pir] M. Pirzada, R. W. Grimes, L. Minervini, J. Maguire, K. E. Sickafus, "Oxygen migration in $A_2B_2O_7$ pyrochlores", *Solid State Ionics*, 140 (2001) 201-208.
- [2001Sch] P. K. Schelling, S. R. Ohillpot, D. Wolf, "Mechanism of the cubic-to-tetragonal phase transition in zirconia and yttria-stabilized zirconia by molecular-dynamics simulation", *J. Am. Ceram. Soc.*, 84 [7] (2001) 1609-1619.
- [2001Tab] Y. Tabira, R. L. Withers, J. C. Bary, L. Elcoro, "The Strain-Driven Pyrochlore to "Defect Fluorite" Phase Transition in Rare Earth Sesquioxide Stabilized Cubic Zirconias", *J. Solid State Chem.*, 159 (2001) 121-129.
- [2001Tan] H. Tanaka, S. Sawai, K. Morimoto, K. Hisano, "Measurement of spectral emissivity and thermal conductivity of zirconium by thermal radiation calorimetry", *J. Thermal Anal. Calor.*, 64 (2001) 867-872.
- [2001Wil] R. E. Willford, W. J. Weber, "Computer simulation of Pu^{3+} and Pu^{4+} substitutions in gadolinium zirconate", *J. Nucl. Mater.*, 299 (2001) 140-147.
- [2002Arr] R. Arroyave, L. Kaufman, T. W. Eagar, "Thermodynamic modeling of the Zr-O system", *Calphad*, 26 [1] (2002) 95-118.
- [2002Fos] A. S. Foster, F. L. Gejo, A. L. Shluger, M. Nieminen, "Vacancy and interstitial defects in hafnia", *Phy. Rev. B*, 65 (2002) 174117.
- [2002Jac] N. S. Jacobson, Z.-K. Liu, L. Kaufman, F. Zhang, "Calculation of phase equilibria in the $Y_2O_3-Yb_2O_3-ZrO_2$ system", *Electrochemical Society Proceedings*, 5 (2002) 1-8.
- [2002Lop] A. G. Lopez, J. M. Fernandez, A. D. Rodriguez, "Contribution to the study of the transition to a superstructure in high yttria content YCSZ", *J. Euro. Ceram. Soc.*, 22 (2002) 2821-2825.
- [2002Nic] J.R. Nicholls, K.J. Lawson, A. Johnstone, and D.S. Rickerby, "Methods to reduce the thermal conductivity of EB-PVD TBCs", *Surface and Coatings Technology*, 151-152 (2002) 383-391.
- [2002Pad] Padture N. P., Gell M, Jordan E. H., "Thermal barrier coatings for gas turbine engine applications", *Science*, 296 (2002) 280-284.
- [2002Rog] G.Rog, A. Kozłowska-Rog, "Determination of the standard molar Gibbs energy of formation of lanthanum zirconate by a galvanic cell involving lanthanum β -alumina electrolyte", *J. Chem. Thermodynamics*, 34 (2002) 1311-1315.
- [2002Sta] C. R. Stanek, L. Minervini, R. W. Grimes, "Nonstoichiometry in $A_2B_2O_7$ pyrochlores", *J. Am. Ceram. Soc.*, 85 [11] (2002) 2792-2798.
- [2002Wu] J. Wu, X. Wei, N. P. Padture, P. G. Klemens, M. Gell, E. Garcia, P. Miranzo, M. I. Osendi, "Low-thermal-conductivity rare-earth zirconates for potential thermal barrier coating applications", *J. Am. Ceram. Soc.*, 85 (2002) 3031-3035.
- [2003Deg] C. Degueldre, P. Tissot, H. Lartigue, M. Pouchon, "Specific heat capacity and Debye temperature of zirconium and its solid solution", *Thermochimica Acta*, 403, (2003) 267-273.

- [2003Dut] S. Dutta, S. Bhattacharya, D. C. Agrawal, “Electrical properties of ZrO_2 - Gd_2O_3 ceramics”, *Mater. Sci. Eng. B*, 100 (2003) 191-198.
- [2003Kan] J. Kang, E.-C. Lee, K. J. Chang, “First-principles study of the structural phase transformation of hafnia under pressure”, *Phy. Rev. B*, 68, 054106 (2003).
- [2003Lec] B. Leclercq, R. Mevrel, V. Liedtke, W. Hohenauer, “Thermal conductivity of zirconia-based ceramics for thermal barrier coating”, *Materialwiss. Werkstofftech.*, 34 [4] (2003) 406-409.
- [2003Lee] T. A. Lee, A. Navrotsky, I. Molodetsky, “Enthalpy of formation of cubic yttria-stabilized zirconia”, *J. Mater. Res.*, 18 [4] (2003) 908-918.
- [2003Lia] J. Lian, L. Wang, J. Chen, K. Sun, R. C. Ewing, J. Matt Framer, L. A. Boatner, “The order–disorder transition in ion-irradiated pyrochlore”, *Acta Mater.*, 51 [5] (2003) 1493-1502.
- [2003Lut] S. Lutique, PhD thesis, Universite Paris XI, 2003.
- [2003Lut1] S. Lutique, R. J. M. Konings, V. V. Rondinella, J. Somers, T. Wiss, “The thermal conductivity of $Nd_2Zr_2O_7$ pyrochlore and the thermal behaviour of pyrochlore-based inert matrix fuel”, *J. Alloy. Compd.*, 352 (2003) 1-5.
- [2003Lut2] S. Lutique, P. Javorsky, R. J. M. Konings, A. C. G. Van Genderen, J. C. van Miltenburg, F. Wastin, “Low temperature heat capacity of $Nd_2Zr_2O_7$ pyrochlore”, *J. Chem. Thermodynamics*, 35 (2003) 955-965.
- [2003Nag] M. Nagashima, T. Nakayama, S. Yamanaka, M. Fujikane, Y. Hayashi, T. Sekino, T. Kusunose, K. Niihara, “Fabrication of metastable ZrO_{2-x} single nano-sized particles”, *Mater. Lett.*, 57 (2003) 4023-4027.
- [2003Pet] L. Petit, A. Svane, Z. Szotek, W. M. Temmerman, “First-principle calculations of $PuO_{2\pm x}$ ”, *Science*, 301 (2003) 498-500.
- [2003Sim] D. Simeone, G. Baldinozzi, D. Gosset, M. Dutheil, A. Bulou, T. Hansen, “Monoclinic to tetragonal semireconstructive phase transition of zirconia”, *Phy. Rev. B*, 67 (2003) 064111.
- [2003Sur] A. Suresh, M. J. Mayo, W. D. Porter, “Thermodynamics of the tetragonal-to-monoclinic phase transformation in fine and nanocrystalline yttria-stabilized zirconium powders”, *J. Mater. Res.*, 18 [12] (2003) 2912-2921.
- [2003Wan] J. H. Wang, A. Nakamura, M. Takeda, “Structural properties of the fluorite- and pyrochlore-type compounds in the Gd_2O_3 - ZrO_2 system $xGdO_{1.5}-(1-x)ZrO_2$ with $0.18 \leq x \leq 0.62$ ”, *Solid State Ionics*, 164 (2003) 185-191.
- [2003Zhu] D. Zhu, Y.L. Chen, and R.A. Miller, “Defect clustering and nano-phase structure characterization of multi-component rare earth oxide doped zirconia-yttria thermal barrier coatings”, *Ceramic Engineering and Science Proceedings*, 24 (2003) 525-534.
- [2004Blu] G. D. Blundred, C. A. Bridges, M. J. Rosseinsky, “New oxidation states and defect chemistry in the pyrochlore structure”, *Angew. Chem. Int. Ed.*, 43 (2004) 3562-3565.
- [2004Che] P. Y. Chevalier, E. Fischer, B. Cheynet, “Progress in the thermodynamic modelling of the O–U–Zr ternary system”, *Calphad*, 28 [1] (2004) 15-40.
- [2004Chen] M. Chen, B. Hallstedt, L. J. Gauckler, “Thermodynamic modeling of the ZrO_2 - $YO_{1.5}$ system”, *Solid State Ionics*, 170 (2004) 255-274.
- [2004Fab] O. Fabrichnaya, F. Aldinger, “Assessment of thermodynamic parameters in the system ZrO_2 - Y_2O_3 - Al_2O_3 ”, *Z. Metallkd.*, 95 (2004) 27-39.

- [2004Jac] N. S. Jacobson, Z.-K. Liu, L. Kaufman, F. Zhang, “Thermodynamic modeling of the ZrO_2 - $YO_{1.5}$ system”, *J. Am. Ceram. Soc.*, 87 [8] (2004) 1559-1566.
- [2004Lee] T. A. Lee, A. Navrotsky, “Enthalpy of formation of cubic yttria-stabilized hafnia”, *J. Mater. Res.*, 19 [6] 1855-1861 (2004).
- [2004Lev] C. G. Levi, “Emerging materials and processes for thermal barrier systems”, *Curr. Opin. Solid State Mater. Sci.*, 8 (2004) 77-91.
- [2004Lut] S. Lutique, P. Javorsky, R. J. M. Konings, J. -C. Krupa, A. C. G. van Genderen, J. C. van Miltenburg, F. Wastin, “The low-temperature heat capacity of some lanthanide zirconates”, *J. Chem. Thermodynamics*, 36 (2004) 609-618.
- [2004Nak] A. Nakamura, H. Otake, J. Wang, M. Takeda, “ ^{155}Gd Mössbauer spectroscopic and X-ray diffraction study of the $Zr_{1-x}Gd_xO_{2-x/2}$ ($0 < x \leq 1.0$) system”, *J. Phys. Chem. Solids*, 66 [2-4] (2004) 356-363.
- [2004Pan] W. R. Panero, L. Stixrude, “First-principles calculation of defect-formation energies in the $Y_2(Ti,Sn,Zr)_2O_7$ pyrochlore”, *Phy. Rev. B*, 70 (2004) 054110.
- [2004Sun] B. Sundman, 2004, private communication.
- [2004Wan] C. Wang, M. Zinkevich and F. Aldinger, “On the thermodynamic modeling of the Zr-O system”, *Calphad*, 28 [4] 281-292 (2004).
- [2005Car] M. A. Caravaca, R. A. Casali, “ab initio localized basis set study of structural parameters and elastic properties of HfO_2 polymorphs”, *J. Phys: Condens. Matter*, 17 (2005) 5795-5811.
- [2005Har] E. J. Harvey, K. R. Whittle, G. R. Lumpkin, R. I. Smith, S. A. T. Redfern, “Solid solubilities of $(La, Nd)_2(Zr, Ti)_2O_7$ phases deduced by neutron diffraction”, *J. Solid State Chem.*, 178 (2005) 800-810.
- [2005Jaf] J. E. Jaffe, R. A. Bachorz, M. Gutowski, “Low-temperature polymorphs of ZrO_2 and HfO_2 : A density-functional theory study”, *Phy. Rev. B*, 72 (2005) 144107.
- [2005Lak] S. M. Lakiza, L. M. Lopato, “Phase diagram of the Al_2O_3 - ZrO_2 - La_2O_3 system”, *J. European Ceram. Soc.*, 25 (2005) 1373-1380.
- [2005Lec] R. M. Leckie, S. Kraemer, M. Ruhle, C. G. Levi, “Thermochemical compatibility between Alumina and ZrO_2 - $GdO_{3/2}$ thermal barrier coatings”, *Acta Mater.*, 53 (2005) 3281-3292.
- [2005Lug] V. Luggi, D. R. Clarke, “High temperature aging of YSZ coatings and subsequent transformation at low temperature”, *Surface & Coatings Technology*, 200 (2005) 1287-1291.
- [2005Nav] A. Navrotsky, “Thermochemical insights into refractory ceramic materials based on oxides with large tetravalent cations”, *J. Mater. Chem.*, 15[19] (2005) 1883-1890.
- [2005Nav1] A. Navrotsky, L. Benoist, H. Lefebvre, “Direct calorimetric measurement of enthalpies of phase transitions at 2000-2400°C in yttria and zirconia”, *J. Am. Ceram. Soc.*, 88 [10] (2005) 2942-2944.
- [2005Oht] H. Ohtani, S. Matsumoto, B. Sundman, T. Sakuma, M. Hasebe, “Equilibrium between fluorite and pyrochlore structures in the ZrO_2 - Nd_2O_3 system”, *Mater. Trans.*, 46 [6] (2005) 1167-1174.
- [2005Pit] M. W. Pitcher, S. V. Ushakov, A. Navrotsky, B. F. Woodfield, G. S. Li, J. Boerio-Goates, B. M. Tissue et al., “Energy crossovers in nanocrystalline zirconia”, *J. Am. Ceram. Soc.*, 88 [1] (2005) 160-167.

[2005Sed] D. Sedmidubsky, O. Benes, R. J. M. Konings, “High temperature heat capacity of $\text{Nd}_2\text{Zr}_2\text{O}_7$ and $\text{La}_2\text{Zr}_2\text{O}_7$ pyrochlores”, *J. Chem. Thermodynamics*, 37 (2005) 1098-1103.

[2005Ste] M. Sternik, K. Parlinski, “Lattice vibrations in cubic, tetragonal, and monoclinic phases of ZrO_2 ”, *J. Chem. Phys.*, 122 (2005) 064707.

[2005Zin] M. Zinkevich, Ch. Wang, F. M. Morales, M. Rühle, F. Aldinger, “Phase equilibria in the ZrO_2 – $\text{GdO}_{1.5}$ system at 1400–1700 °C”, *J. Alloy. Compd.*, 398[1-2] (2005) 261-268.

[2006Lak] S. Lakiza, O. Fabrichnaya, Ch. Wang, M. Zinkevich, F. Aldinger, “Phase Diagram of the ZrO_2 – Gd_2O_3 – Al_2O_3 System”, *J. Eur. Ceramic Soc.*, 26 (2006) 233-246.

[2006Mor] Y. Moriya, A. Navrotsky, “High-temperature calorimetry of zirconia: Heat capacity and thermodynamics of the monoclinic–tetragonal phase transition”, *J. Chem. Thermodynamics*, 38 [3] (2006) 211-223.

[2006Zin] M. Zinkevich, “Thermodynamics of rare earth sesquioxides”, *Prog. Mater. Sci.*, in press, 2006.

[2006Zin1] M. Zinkevich, D. Djurovic, F. Aldinger, “Thermodynamic modeling of cerium-oxygen system”, *Solid State Ionics*, 177 [11-12] (2006) 989-1001.

Curriculum Vitae (Lebenslauf)

Family name: **Wang**

First name: **Chong**

Gender: Male

Date of Birth: 20-07-1977

Place of Birth: Jingmen, Hubei province, P. R. China

Nationality: P. R. China

Education:

02.2003-Now: PhD student, Max-Planck-Institute for Metals Research, PML; University of Stuttgart, Institute for Advanced Ceramics, Stuttgart, Germany

Supervisor: Prof. Dr. Fritz Aldinger

Group Leader: Dr. Matvei Zinkevich

Thesis: Experimental and computational phase studies of the ZrO₂-based systems for thermal barrier coatings.

09.1998-07.2001: M.E, Materials Science, Central South University, Department of Materials Science and Engineering, Changsha, China

Supervisor: Prof. Zhanpeng Jin

Thesis: Computational thermodynamic studies of the borate systems.

09.1994-07.1998: B.E, Materials Science, Central South University of Technology, Department of Materials Science and Engineering, Changsha, China

09.1991-07.1994: Longquan High School, Jingmen, China

09.1988-07.1991: Shilipu Middle School, Jingmen, China

09.1987-07.1988: Shiniu Primary School, Jingmen, China

09.1983-07.1987: Linchang Primary School, Jingmen, China